NEES Nonstructural

ASSESSMENT OF FLOOR ACCELERATIONS IN YIELDING BUILDINGS

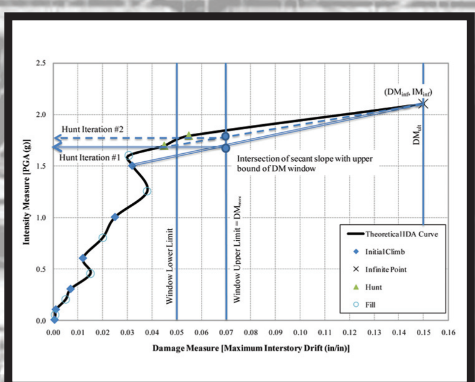

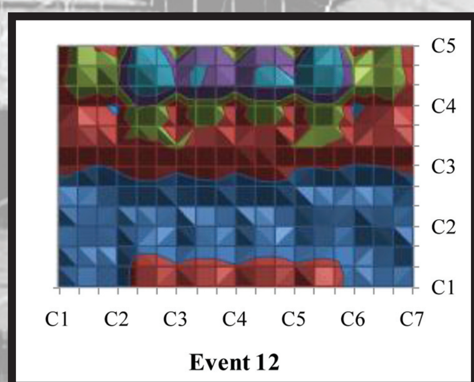

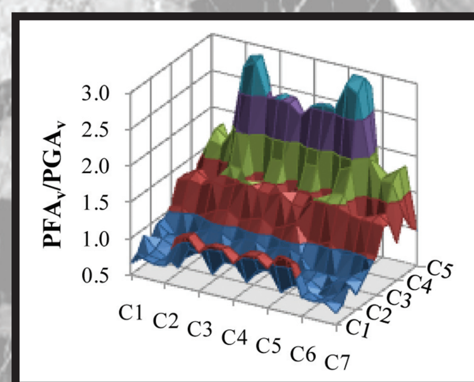

By

Joseph D. Wieser, Gokhan Pekcan, Arash E. Zaghi, Ahmad M. Itani and Emmanuel "Manos" Maragakis

Technical Report MCEER-12-0008 ■ October 5, 2012

This research was conducted at the University of Nevada, Reno and was supported by the National Science Foundation under Grant No. CMMI-0721399.

Sponsored by the
National Science Foundation
NSF Grant Number CMMI-0721399

Project Title
Simulation of the Seismic Performance of
Nonstructural Systems

Project Team
University of Nevada Reno
University at Buffalo, State University of New York
Georgia Institute of Technology
Rutherford & Chekene
University of California, San Diego
Consortium of Universities for Research in Earthquake Engineering (CUREE)

Web Site
http://www.nees-nonstructural.org

DISCLAIMER

Assessment of Floor Accelerations in Yielding Buildings

by

Joseph D. Wieser,[1] Gokhan Pekcan,[2] Arash E. Zaghi,[3] Ahmad M. Itani[4]
and Emmanuel "Manos" Maragakis[5]

Publication Date: October 5, 2012
Submittal Date: January 4, 2012

Technical Report MCEER-12-0008

NSF Grant Number CMMI-0721399

1 Graduate Student, Department of Civil and Environmental Engineering, University of Nevada, Reno
2 Associate Professor, Department of Civil and Environmental Engineering, University of Nevada, Reno
3 Assistant Professor, Department of Civil and Environmental Engineering, University of Connecticut
4 Professor, Department of Civil and Environmental Engineering, University of Nevada, Reno
5 Dean of College of Engineering, University of Nevada, Reno

MCEER
University at Buffalo, State University of New York
133A Ketter Hall, Buffalo, NY 14260
Phone: (716) 645-3391; Fax (716) 645-3399
E-mail: *mceer@buffalo.edu*; Website: *http://mceer.buffalo.edu*

Project Overview

NEES Nonstructural: Simulation of the Seismic Performance of Nonstructural Systems

Nonstructural systems represent 75% of the loss exposure of U.S. buildings to earthquakes, and account for over 78% of the total estimated national annualized earthquake loss. A very widely used nonstructural system, which represents a significant investment, is the ceiling-piping-partition system. Past earthquakes and numerical modeling considering potential earthquake scenarios show that the damage to this system and other nonstructural components causes the preponderance of U.S. earthquake losses. Nevertheless, due to the lack of system-level research studies, its seismic response is poorly understood. Consequently, its seismic performance contributes to increased failure probabilities and damage consequences, loss of function, and potential for injuries. All these factors contribute to decreased seismic resilience of both individual buildings and entire communities.

Ceiling-piping-partition systems consist of several components, such as connections of partitions to the structure, and subsystems, namely the ceiling, piping, and partition systems. These systems have complex three-dimensional geometries and complicated boundary conditions because of their multiple attachment points to the main structure, and are spread over large areas in all directions. Their seismic response, their interaction with the structural system they are suspended from or attached to, and their failure mechanisms are not well understood. Moreover, their damage levels and fragilities are poorly defined due to the lack of system-level experimental studies and modeling capability. Their seismic behavior cannot be dependably analyzed and predicted due to a lack of numerical simulation tools. In addition, modern protective technologies, which are readily used in structural systems, are typically not applied to these systems.

This project sought to integrate multidisciplinary system-level studies to develop, for the first time, a simulation capability and implementation process to enhance the seismic performance of the ceiling-piping-partition nonstructural system. A comprehensive experimental program using both the University of Nevada, Reno (UNR) and University at Buffalo (UB) NEES Equipment Sites was developed to carry out subsystem and system-level full-scale experiments. The E-Defense facility in Japan was used to carry out a payload project in coordination with Japanese researchers. Integrated with this experimental effort was a numerical simulation program that developed experimentally verified analytical models, established system and subsystem fragility functions, and created visualization tools to provide engineering educators and practitioners with sketch-based modeling capabilities. Public policy investigations were designed to support implementation of the research results.

The systems engineering research carried out in this project will help to move the field to a new level of experimentally validated computer simulation of nonstructural systems and establish a model methodology for future systems engineering studies. A system-level multi-site experimental research plan has resulted in a large-scale tunable test-bed with adjustable dynamic properties, which is useful for future experiments. Subsystem and system level experimental results have produced unique fragility data useful for practitioners.

An evaluation of the acceleration demands on nonstructural components in typical steel moment frame structures was performed in this study. The incremental dynamic analysis method was used to evaluate

the floor response of inelastic steel moment frame buildings subjected to all three components of a suite of 21 ground motions. A database of floor response motions was generated and used to identify the effect of variables such as structural period, structural yielding, relative height within the structure, nonstructural component damping ratio, and out-of-plane flexibility of the floor system on acceleration demands on nonstructural components. As a result of this study, a more realistic formulation of the peak floor acceleration response that accounts for the effect of structural period and ductility is proposed and may be used to improve current code estimations. In addition, the feasibility of using floor response motions from the database as drive motions for shake table testing of nonstructural components was assessed and is recommended for use in future experimental testing.

Project Management Committee

Manos Maragakis, Principal Investigator, University of Nevada Reno, Department of Civil Engineering, Reno, NV 89557; *maragaki@unr.edu.*

André Filiatrault, Co-Principal Investigator, University at Buffalo, State University of New York, Department of Civil, Structural and Environmental Engineering, Buffalo, NY 14260; *af36@buffalo.edu.*

Steven French, Co-Principal Investigator, Georgia Institute of Technology, College of Architecture, P.O. Box 0695, Atlanta, GA 30332; *Steve.French@ arch.gatech.edu*.

William Holmes, Rutherford & Chekene, 55 Second Street, Suite 600, San Francisco, CA 94105; *wholmes@ruthchek.com.*

Tara Hutchinson, Co-Principal Investigator, University of California, San Diego, Department of Structural Engineering, 9500 Gilman Drive, #0085, La Jolla, CA 92093; *tara@ucsd.edu*.

Robert Reitherman, Co-Principal Investigator, CUREE, 1301 S. 46th Street, Bldg. 420, Richmond, CA 94804; *reitherman@curee.org*.

ABSTRACT

The large investment in nonstructural components in buildings and severe damage to these components in recent earthquakes necessitates improved design provisions for these components. The present study uses the OpenSees finite element framework to develop full three-dimensional models of four steel moment frame buildings. The incremental dynamic analysis method is employed to evaluate the floor response of inelastic steel moment frame buildings subjected to all three components of a suite of 21 ground motions. To better understand the acceleration demands on nonstructural components, this study focuses on the influence of structural period, level of ductility of the structure, and relative height in the building on the horizontal and vertical floor acceleration response. The horizontal floor acceleration response is shown to decrease with increasing structural period and ductility while varying nonlinearly along the height of the building. In contrast, the vertical acceleration response was found to be independent of structural period, level of ductility, and relative height. Variation in the vertical acceleration response is primarily attributed to the out-of-plane flexibility of the floor system. Significant vertical acceleration amplification is only observed away from the column supports. As a result of this study, a more realistic formulation of the peak floor acceleration response accounting for the effect of structural period and ductility is proposed and may be used to improve current code estimations is proposed. In addition, a direct method for developing an envelope horizontal floor response spectrum is developed.

ACKNOWLEDGMENTS

Funding for this study was provided by the National Science Foundation under award number CMMI-0721399, "NEESR-GC: Simulation of the Seismic Performance of Nonstructural Systems." Any opinions, findings, and conclusions or recommendations expressed in this report are those of the authors, and do not necessarily reflect the views of the sponsoring organization.

TABLE OF CONTENTS

TABLE OF CONTENTS (CONT'D)

SECTION **TITLE** **PAGE**

TABLE OF CONTENTS (CONT'D)

TABLE OF CONTENTS (CONT'D)

LIST OF ILLUSTRATIONS

LIST OF ILLUSTRATIONS (CONT'D)

FIGURE TITLE **PAGE**

LIST OF ILLUSTRATIONS (CONT'D)

FIGURE TITLE **PAGE**

LIST OF ILLUSTRATIONS (CONT'D)

FIGURE TITLE **PAGE**

LIST OF ILLUSTRATIONS (CONT'D)

LIST OF TABLES

TABLE **TITLE** **PAGE**

SECTION 1
INTRODUCTION

1.1 Background Information

Nonstructural components are not part of the main gravity or lateral load-resisting system. They include architectural elements, mechanical systems, and building contents. These components represent 75% of the loss exposure of US buildings to earthquakes and account for over 78% of the future estimated national annualized earthquake loss (Maragakis et al., 2007). In several recent earthquakes, extensive damage and loss of functionality of buildings has resulted even when no structural damage has occurred. For example in the 1994 Northridge earthquake, the Olive View Medical Center in Sylmar, CA experienced essentially no structural damage yet was forced to shut down and evacuate patients due to water leakage from broken fire sprinkler piping systems (Reitherman and Sabol, 1995). This is an example of severe ground motion affecting a modern building that was designed under the California Hospital Seismic Safety Act to be more earthquake-resistant than most buildings. Buildings designed to lesser standards typically have a much lower level of attention paid to nonstructural components. It is also true that most nonstructural components are more damageable than the structure even at relatively low severities of shaking. Moderately intense shaking at a given site is much more likely than very intense shaking. These factors combine to make nonstructural damage more prevalent than structural damage.

Nonstructural components can be categorized by sensitivity into two classes, namely acceleration-sensitive or drift-sensitive. Components such as suspended ceilings, light fixtures, fire sprinkler piping, bookshelves, etc. are considered acceleration-sensitive because they are most susceptible to damage incurred from inertial forces. Whereas components such as partition walls, cladding, vertical riser pipes, etc. fall into the drift-sensitive classification because they are susceptible to damage due to interstory drift response of the supporting structure. Consequently, both the acceleration and drift response of the supporting structure impose the seismic demands on the nonstructural components within a building. Thus, enhancing the understanding of the building response to seismic events is critical in the seismic design of nonstructural components.

In light of the importance of protecting the integrity of nonstructural components during earthquakes, there is a need for additional research to develop reliable performance-based design criteria for nonstructural components. The presented study supports this field of research through the evaluation of floor acceleration and interstory drift responses of typical moment frame structures for the purpose of developing the seismic demands on nonstructural components throughout the building.

1.2 Literature Review

The seismic performance of nonstructural components has been the topic of research for critical facilities such as nuclear power plants for decades, but the design of nonstructural components in ordinary buildings has not received as much attention. Much of the research conducted by the nuclear industry is based on coupled models of the structural and nonstructural systems. This type of modeling is difficult and impractical to implement in the design of nonstructural components in ordinary buildings (Villaverde, 1997). As a result, researchers began searching for more economical methods of analysis. One of the first simplified methods of analysis of nonstructural components is the floor response spectrum method. In this method, a response history analysis of the building is performed and the floor acceleration time history response is used to generate a floor response spectrum which can be used to design the nonstructural component. While this method does not rigorously model dynamic interaction between the nonstructural components and the supporting structure, it has been shown to provide conservative estimates for the acceleration demands on nonstructural components (Villaverde, 1997).

Others have proposed methods to generate floor response spectra directly from the ground acceleration spectrum. Examples are the methods proposed by Biggs and Roesset (1970), Amin et al. (1971), and Singh (1974). These methods are either largely empirical or have complicated theoretical backgrounds of random vibration theory and spectral density functions. These proposed methods as well as the floor response spectrum method can become computationally expensive for implementation in practical design settings. Thus, recent research efforts have been aimed at the development of simple code equations to accurately determine the peak floor acceleration response of buildings. Accurate estimates of the peak floor accelerations can be used to provide minimum acceleration demands on nonstructural components located throughout the supporting structure.

Rodriguez et al. (2002) studied the influence of inelastic response of regular buildings on peak floor acceleration demands and proposed a new method for estimating the peak floor accelerations. This method was based on modal superposition and considered the nonlinear response and higher mode effects of the supporting structure (Rodriguez et al., 2002).

Taghavi and Miranda (2006) use a continuum model of a shear beam rigidly linked to a flexural beam. The relative shear stiffness to flexural stiffness ratio is used to model structures ranging from braced frames to moment frames. The influence of lateral load-resisting system, reduction of lateral stiffness, structural period, and structural nonlinearity on the peak floor accelerations and floor response spectra were studied.

Medina et al. (2006) analytically studied stiff moment-resisting frame buildings with periods designed to be equal to 0.1 times the number of stories and uniform lateral stiffness distribution over the height of the structures. Peak floor accelerations and floor response spectra were generated.

Most of these studies performed simple two-dimensional analysis to assess the horizontal floor accelerations throughout the building. This study expands on previous studies by generating three-dimensional models with explicitly modeled floor systems and incorporating vertical acceleration.

Pekcan et al. (2003) generated horizontal and vertical floor acceleration spectra for two elastically responding concrete buildings. They showed that the out-of-plane flexibility of the floor systems generate significant amplification of the vertical acceleration such that the vertical acceleration of nonstructural components may exceed the horizontal acceleration.

This study builds on the work of all of the previously mentioned research by providing quantitative information on the dependence of the acceleration response of elastically responding nonstructural components on ground motion characteristics and on structural properties of three-dimensional moment-resisting frame buildings, including explicitly modeled floor systems.

1.3 Objectives and Scope

The presented study has two primary motivations. The first is to determine the effect of building floor accelerations on the response of nonstructural components. In order to more accurately understand the seismic demand imposed on nonstructural components at different floor levels, an analytical study assessing the floor response characteristics of inelastically responding steel moment frame structures was performed. The second motivation of this investigation was to generate a set of motions appropriate for shake table testing of nonstructural components. The set of motions should include the acceleration demands on nonstructural components mounted on yielding structures because almost all buildings are designed using criteria that anticipates inelastic structural behavior in strong earthquake shaking. The following outlines the objectives and scope of this particular study.

- Develop a robust database of floor response histories
- Characterize floor level response in terms of acceleration spectra, interstory drift, and seismic energy content
- Review the current code requirements for seismic demands of nonstructural systems
- Select a set of floor motions from the developed database which are applicable for shake table testing of nonstructural components

In order to achieve these objectives, incremental dynamic analysis (IDA) using a suite of 21 historically recorded ground motions has been performed on a group of four representative steel special moment-resisting frame structures. Incremental dynamic analysis was selected in order to develop the robust database of structural responses, as this methodology requires numerous nonlinear dynamic analyses. The numerical models have been constructed such that the effects of geometric and material nonlinearities, out-of-plane floor flexibility, and vertical ground excitation are included. These effects increase the robustness of the database by allowing for the characterization of floor responses in terms of level of yielding within the structure, and location within the elevation as well as plan of the structure. From the developed database a thorough review of code requirements was completed. In addition, an ensemble of shake table input motions selected from the accumulated floor response database was generated for the purpose of evaluating the seismic performance of nonstructural components mounted in yielding structures.

SECTION 2
BUILDING DESCRIPTION

2.1 Introduction

This chapter provides descriptions of the building structures investigated in this study. The first part of the chapter discusses the geometry and design assumptions of the selected buildings including the dimensions, lateral load-resisting systems, structural steel sections, deck slabs, and material properties. The second part of the chapter focuses on the computational models of each building developed for this study wherein a brief overview of the OpenSees finite element platform is presented. The nonlinear material and element models as well as the boundary conditions are described in detail. Pushover analyses results and the dynamic characteristics of the structures are also presented in this chapter.

2.2 Building Design

A set of four steel special moment-resisting frame (SMRF) buildings were selected for this investigation. This set consists of a 3-story office building (B3), a 3-story hospital (H3), a 9-story office building (B9), and a 20-story office building (B20). While the office buildings were designed as a part of the SAC steel project (Gupta and Krawinkler, 1999), the hospital building was designed specifically for this project. The set contained a diverse range of heights and occupancies, while the lateral load-resisting system remained constant in order to provide a thorough investigation of steel SMRF buildings. Hence, the findings of this investigation are applicable to SMRF buildings which are commonly used on the west coast of the United States.

2.2.1 SAC Office Buildings

The three post-Northridge Los Angeles designs developed in the SAC steel project were used in this investigation (Gupta and Krawinkler, 1999). Moreover, the 1994 Uniform Building Code (ICBO, 1994) along with the improved connection details of the FEMA 267 Guidelines (FEMA, 1995) were used to design these SMRFs. Table 2-1 defines the loading assumptions provided by the SAC steel project. In addition to the strength design, the buildings were required to conform to a drift limit of $h/400$ (0.25%) under the design lateral loads, where h is the story height.

Table 2-1 SAC Loading Assumptions

Load Classification	Load Assumption
Steel Framing	as designed.
Floors and Roof	3 in metal decking with 2.5 in of normal weight concrete fill and fireproofing.
Roofing	7 psf average.
Ceilings and Flooring	3 psf average, including fireproofing.
Mechanical/Electrical	7 psf average for all floors, additionally 40 psf over penthouse area for equipment.
Partitions	as per code requirements (10 psf for seismic load, 20 psf for gravity design).
Exterior Wall	25 psf of wall surface average, including any penthouses. Assume 2 ft from perimeter column lines to edge of building envelope. Include 42 in parapet at main roof level, none at penthouse roof.
Live Load	typical code values for office or hospital occupancy.
Wind Load	as per code requirements, assuming congested area (Exposure B as per UBC '94 definition).
Seismic Load	as per code requirements.
Soil Type	stiff soil (UBC'94 = S2) (IBC'06 = Site Class D)

The base shear and equivalent lateral forces were obtained from the equations of Section 1628 of the 1994 UBC (ICBO, 1994). The Los Angeles area is located in Seismic Zone 4, thus for these equations, the seismicity factor, Z, was set equal to 0.4, the importance factor, I, for office structures was taken as 1.0, the soil type was assumed to be a stiff soil, S2, and the load reduction factor, R_w, for SMRFs was taken as 12. These seismic parameters produce design lateral loads that governed the design of the lateral load-resisting systems (Gupta and Krawinkler, 1999).

The design forces used in the design of the SAC buildings per the 1994 UBC were compared to the design seismic forces prescribed by the 2006 IBC. In order to generate a more fair comparison, the force reduction factors, R_w (UBC) and R (IBC), were each set to 1. The vertical distribution of the story forces generated by each code for the three SAC structures are compared in Figure 2-1, Figure 2-2, and Figure 2-3. Particularly worth noting is that the 1994 UBC uses a triangular distribution of base shear with an additional roof force to account for the higher mode effects, whereas the 2006 IBC uses a parabolic distribution. Though the force distributions are noticeably different, the story shear distributions follow a very similar pattern. The design base shear for the 3- and 20-story buildings is approximately 10% less using the 1994 UBC, however, the design base shear for the 9-story building is about 25% greater using the 1994 UBC.

The designs specify dual grade A36 Gr. 50 (nominal F_y = 50 ksi) steel for all members. The sections that follow introduce the buildings individually.

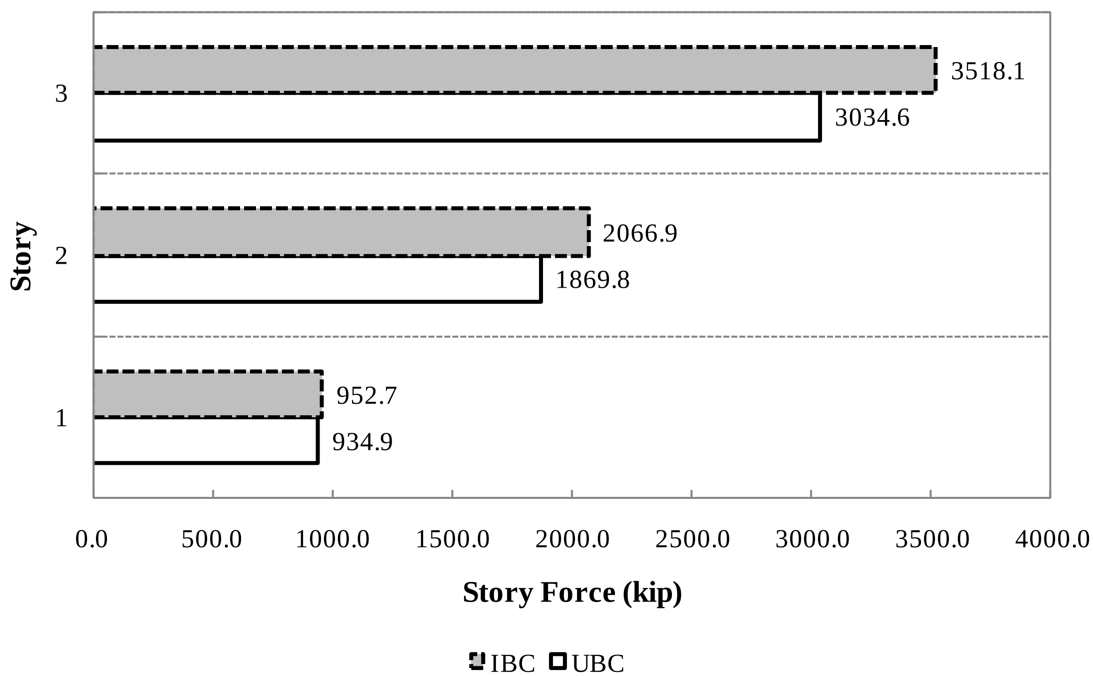

Figure 2-1 Story Force Comparison of Building B3

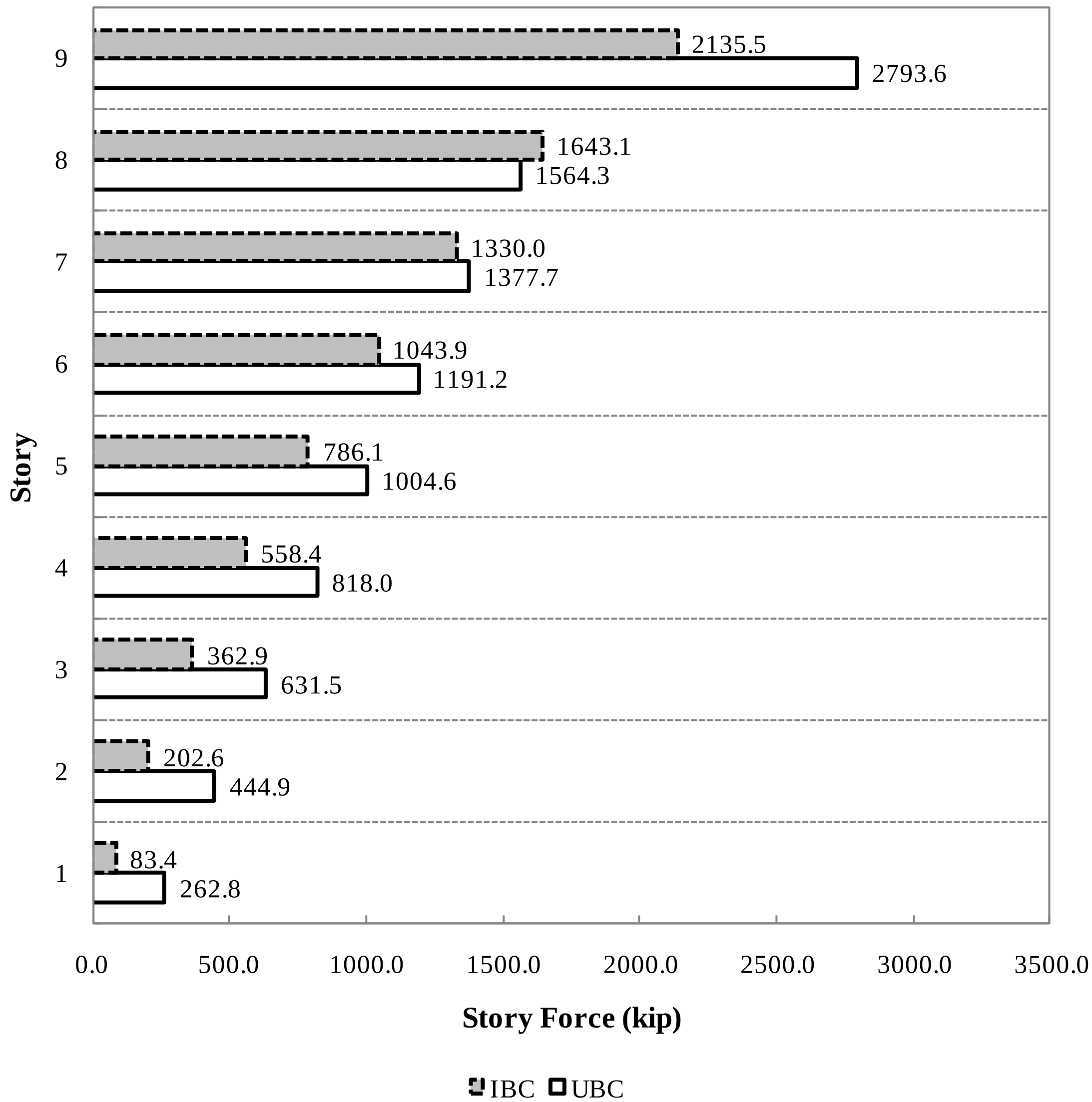

Figure 2-2 Story Force Comparison of Building B9

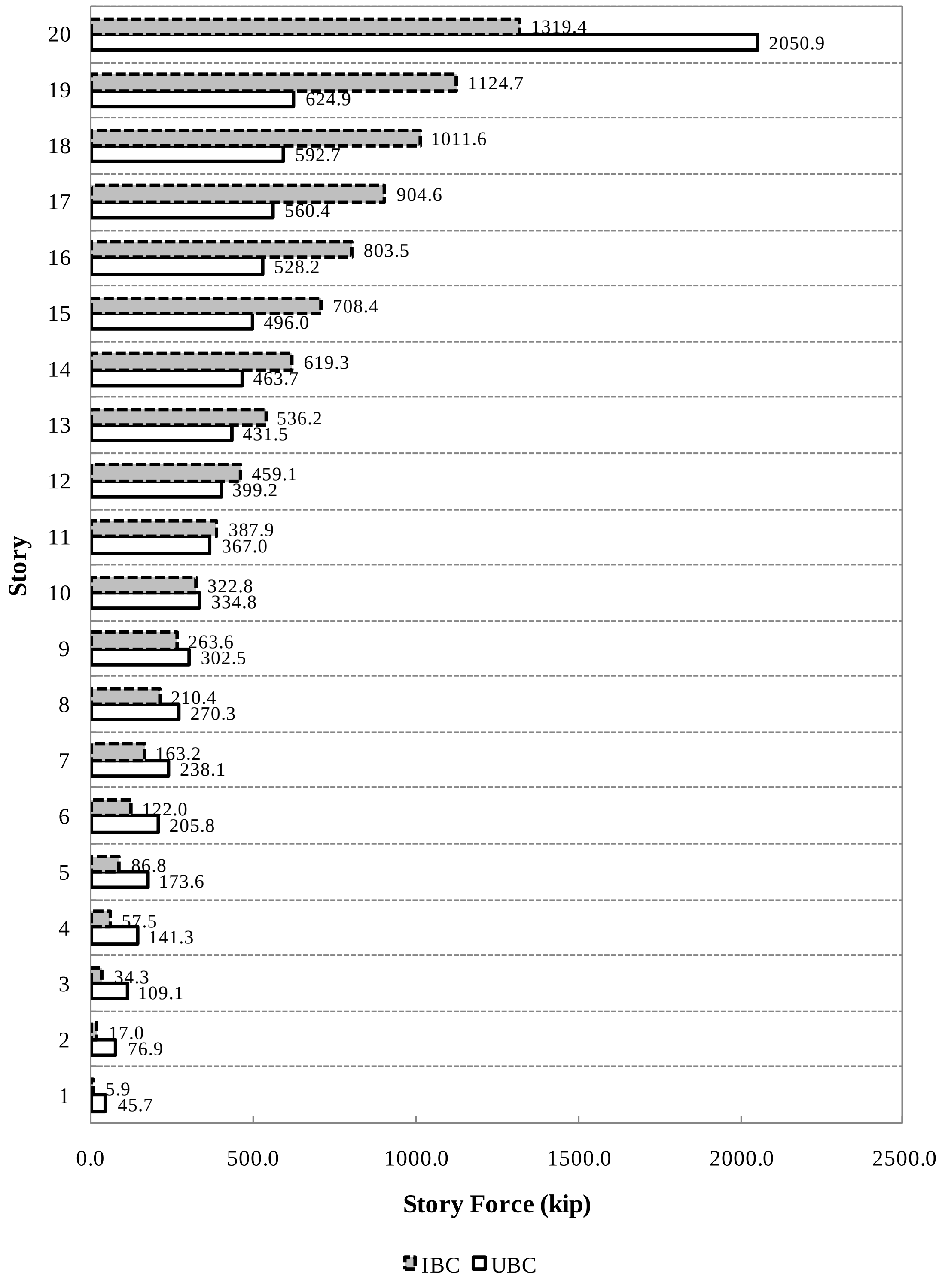

Figure 2-3 Story Force Comparison of Building B20

2.2.1.1 3-Story Office Building (Building B3)

Building B3 is the 3-story SAC office building. The plan and elevation views for this building are illustrated in Figure 2-4. It has plan dimensions of 180 ft by 120 ft which is divided into 6 equal 30 ft bays in the East-West direction (x-direction) and 4 equal 30 ft bays in the North-South direction (y-direction). The overall height of Building B3 is 39 feet with a constant story height of 13 feet. The lateral load-resisting SMRFs are shown in bold in Figure 2-4**.** The lateral design loads described in Section 2.2.1 were developed using elevation and seismic weights of Table 2-2. The structural steel sections are presented in Table 2-3.

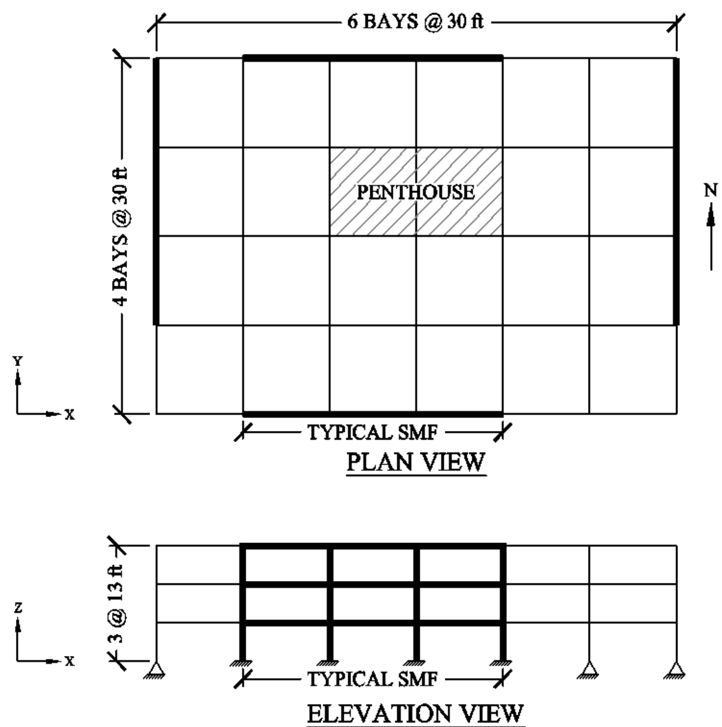

Figure 2-4 3-Story Office Building (Building B3)

Table 2-2 Elevation, Seismic Weight, and Design Story Forces of Building B3

Floor Level	**Elevation** *ft*	**Seismic Weight** *kip*	**Design Story Force** *kip*
2	13	2110	78
3	26	2110	156
Roof	39	2283	253
Total	-	6503	487

Table 2-3 Beam and Column Sections for Building B3

Story Level	Seismic Frame				Gravity Frame		
	Column		Girder		Column		Beam
	Interior	Exterior	SMRF	Collector	Penthouse	Other	
1	W14x311	W14x257	W30x116	W21x44	W14x82	W14x68	W16x26
2	W14x311	W14x257	W30x116	W21x44	W14x82	W14x68	W16x26
3	W14x311	W14x257	W24x62	W21x44	W14x82	W14x68	W14x22

2.2.1.2 9-Story Office Building (Building B9)

Building B9 is the 9-story SAC office building. The plan and elevation views are illustrated in Figure 2-5. It has plan dimensions of 150 ft by 150 ft which is divided into 5 equal 30 ft bays in the East-West direction (x-direction) and 5 equal 30 ft bays in the North-South direction (y-direction). Building B9 is 122 ft tall and includes a 12 ft basement, first story height of 18 ft, and 8 stories of 13 ft each. The lateral load resisting SMRFs are shown in bold in Figure 2-5. The beams in the last bay of SMRFs are pinned in order to decouple the orthogonal frames. The elevations and seismic weights of Building B9, defined in Table 2-4, were used to establish the design seismic lateral loads. The design sections are presented in Table 2-5.

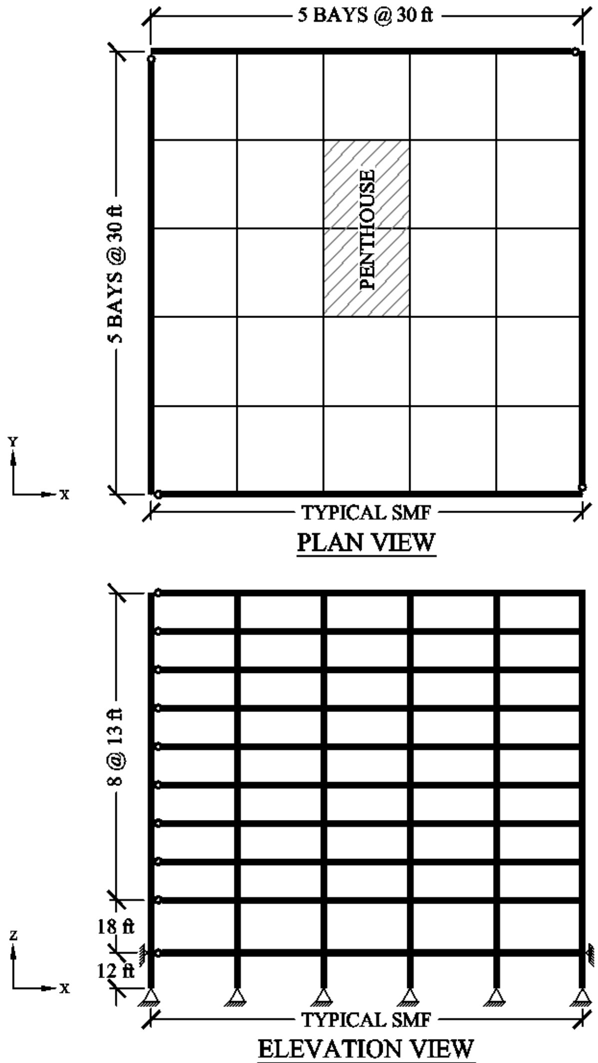

Figure 2-5 9-Story Office Building (Building B9)

Table 2-4 Elevation, Seismic Weight, and Design Story Forces of Building B9

Floor Level	Elevation *ft*	Seismic Weight *kip*	Design Story Force *kip*
2	18	2223	22
3	31	2185	37
4	44	2185	53
5	57	2185	68
6	70	2185	84
7	83	2185	99
8	96	2185	115
9	109	2185	130
Roof	122	2354	233
Total	-	19872	841

Table 2-5 Beam and Columns Sections for Building B9

Story Level	Seismic Frame			Gravity Frame		
	Column		Girder	Column		Beam
	Interior	Exterior	SMRF	Penthouse	Other	
-1	W14x500	W14x370	W36x150	W14x211	W14x193	W18x35
1	W14x500	W14x370	W36x150	W14x211	W14x193	W16x26
2	W14x500 W14x455	W14x370 W14x370	W36x150	W14x211 W14x159	W14x193 W14x145	W16x26
3	W14x455	W14x370	W33x141	W14x159	W14x145	W16x26
4	W14x455 W14x370	W14x370 W14x283	W33x141	W14x159 W14x120	W14x145 W14x109	W16x26
5	W14x370	W14x283	W33x141	W14x120	W14x109	W16x26
6	W14x370 W14x283	W14x283 W14x257	W33x130	W14x120 W14x90	W14x109 W14x82	W16x26
7	W14x283	W14x257	W27x102	W14x90	W14x82	W16x26
8	W14x283 W14x257	W14x257 W14x233	W27x94	W14x90 W14x61	W14x82 W14x48	W16x26
9	W14x257	W14x233	W24x62	W14x61	W14x48	W14x22

2.2.1.3 20-Story Office Building (Building B20)

Building B20 is the 20-story SAC office building. The plan and elevation views are illustrated in Figure 2-6. It has plan dimensions of 120 ft by 100 ft which is divided into 6 equal 20 ft bays in the East-West direction (x-direction) and 5 equal 20 ft bays in the North-South direction (y-direction). Building B20 is 265 ft tall and has two 12 ft basements, first story height of 18ft, and 19 stories 13 ft in height. The SMRFs are shown in bold in Figure 2-6. The corner columns are designed as box sections to carry biaxial moments. The elevations and seismic weights of Building B20 are defined in Table 2-6. The design sections of Building B20 are presented in Table 2-7.

2.2.2 Hospital Building

In order to broaden the scope of this study, an SMRF hospital building was included. Hospital structures are unique in that they typically have taller story heights, yet are required to comply with very stringent drift ratios, typically 1.0 - 1.5% under the design equivalent static lateral loads. The target seismic design performance of the hospital building is immediate occupancy as opposed to the life safety for the office and residential buildings. After a seismic event, hospitals are required to stay operational with minimal interruption. As a result, they are often designed with significantly more strength and are typically stiffer than office buildings. Hospital buildings also contain a large number of nonstructural components critical to the operation of the hospital. Thus, this study has included Building H3, a 3-story hospital building, to identify the differences in performance and response between hospital and office structures.

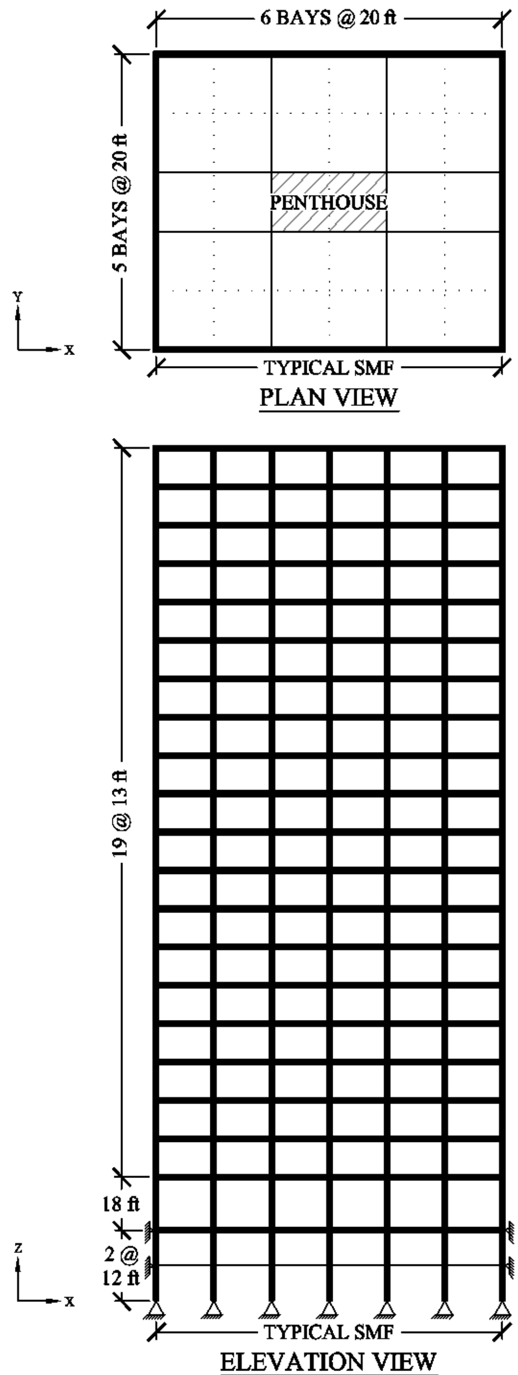

Figure 2-6 20-Story Office Building (Building B20)

Table 2-6 Elevation, Seismic Weight, and Design Story Forces of Building B20

Floor Level	Elevation *ft*	Seismic Weight *kip*	Design Story Force *kip*
2	18	1244	4
3	31	1216	6
4	44	1216	9
5	57	1216	12
6	70	1216	14
7	83	1216	17
8	96	1216	20
9	109	1216	23
10	122	1216	25
11	135	1216	28
12	148	1216	31
13	161	1216	33
14	174	1216	36
15	187	1216	39
16	200	1216	41
17	213	1216	44
18	226	1216	47
19	239	1216	49
20	252	1216	52
Roof	265	1290	171
Total	-	24422	701

Table 2-7 Beam and Column Sections for Building B20

Story Level	Seismic Frame			Gravity Frame		
	Column		Girder	Column	Beam	
	Interior	Exterior	SMRF		40 ft	20 ft
-2	W24x335	15x15x2.00	W14x22	W14x550	W18x40	W14x22
-1	W24x335	15x15x2.00	W30x99	W14x550	W24x55	W14x22
1	W24x335	15x15x2.00	W30x99	W14x550	W18x40	W14x22
2	W24x335 W24x335	15x15x2.00 15x15x1.25	W30x99	W14x550 W14x455	W18x40	W14x22
3	W24x335	15x15x1.25	W30x99	W14x455	W18x40	W14x22
4	W24x335	15x15x1.25	W30x99	W14x455	W18x40	W14x22
5	W24x335 W24x279	15x15x1.25 15x15x1.00	W30x108	W14x455 W14x370	W18x40	W14x22
6	W24x279	15x15x1.00	W30x108	W14x370	W18x40	W14x22
7	W24x279	15x15x1.00	W30x108	W14x370	W18x40	W14x22
8	W24x279 W24x279	15x15x1.00 15x15x1.00	W30x108	W14x370 W14x311	W18x40	W14x22
9	W24x279	15x15x1.00	W30x108	W14x311	W18x40	W14x22
10	W24x279	15x15x1.00	W30x108	W14x311	W18x40	W14x22
11	W24x279 W24x229	15x15x1.00 15x15x1.00	W30x99	W14x311 W14x257	W18x40	W14x22
12	W24x229	15x15x1.00	W30x99	W14x257	W18x40	W14x22
13	W24x229	15x15x1.00	W30x99	W14x257	W18x40	W14x22
14	W24x229 W24x162	15x15x1.00 15x15x0.75	W30x99	W14x257 W14x176	W18x40	W14x22
15	W24x162	15x15x0.75	W30x99	W14x176	W18x40	W14x22
16	W24x162	15x15x0.75	W30x99	W14x176	W18x40	W14x22
17	W24X162 W24x117	15x15x0.75 15x15x0.75	W27x84	W14x176 W14x108	W18x40	W14x22
18	W24x117	15x15x0.75	W27x84	W14x108	W18x40	W14x22
19	W24x117 W24x94	15x15x0.75 15x15x0.50	W24x62	W14x108 W14x43	W18x40	W14x22
20	W24x94	15x15x0.50	W21x50	W14x43	W18x35	W12x14

2.2.2.1 3-Story Hospital Building (Building H3)

Building H3 is a 3-story hospital building designed as a part of this investigation. This building was designed according to the 2006 International Building Code (ICC, 2006). The plan and elevation views are illustrated in Figure 2-7. The plan dimensions mimic that of Building B3 while the elevation was adjusted to be more representative of current hospital buildings. It has plan dimensions of 180 ft by 120 ft which is divided into 6 equal 30 ft bays in the East-West direction (x-direction) and 4 equal 30 ft bays in the North-South direction (y-direction). The first, second, and third story heights were adjusted to 20 ft, 16 ft and 16 ft, respectively, making the building 52 ft tall. The SAC gravity loading assumptions, defined in Table 2-1, were adopted for the design with the exception of the live load which was increased from 50 psf to 60 psf everywhere. The lateral load-resisting SMRFs are shown in bold in Figure 2-7. The 2006 IBC calculates the seismic base shear demand using a different equation than that used by the 1994 UBC. Among the differences, the most significance is the fact that the 2006 IBC equation for base shear is site-specific. To be representative of a large seismically active region, the site parameters were determined from the average of the California seismicity parameters according to the 2002 USGS seismicity maps (USGS, 2002). The maximum mapped MCE S_S and S_1 values of each zip code in California were used to obtain the mean S_S and its corresponding S_1 as well as the mean S_1 and its corresponding S_S. This was accomplished by selecting the S_S and S_1 values of the zip code, with the S_S value closest to the mean of the S_S values and similarly for S_1.

Table 2-8 summarizes these values. These two sets of parameters produced similar design spectra, thus either set may be considered representative. The mean S_S and its corresponding S_1 were selected for this study as the corresponding spectrum has a wider plateau, and thus is more conservative. The design seismic values S_{DS} and S_{D1} were calculated according to the provisions of the 2006 IBC, corresponding to two-thirds of the S_{MS} and S_{M1} values. It should be noted that these parameters correspond to a location in the San Francisco Bay area. This is different from the Los Angeles area used to design the original SAC buildings, however when the SAC buildings were designed these two locations had equivalent seismic design criteria, i.e. the seismic zone factors were equivalent under the 1994 UBC. A comparison of the 1994 UBC design spectrum and 2006 IBC design spectrum with the mean S_S and its corresponding S_1 seismicity parameters are compared in Figure 2-8. In comparing the spectra, it is noted that while the short period acceleration demand is comparable the wider plateau generates greater acceleration demands in the long period range. For the purpose of this study, the assumed seismicity parameters were considered acceptable.

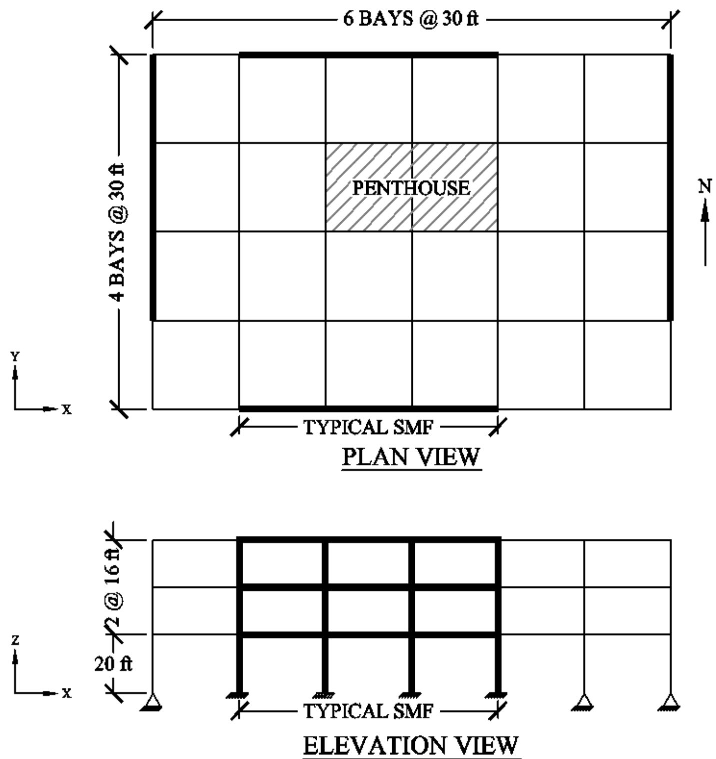

Figure 2-7 3-Story Hospital Building (Building H3)

Table 2-8 Site Location Seismicity Parameters for Building H3

	Based on S_S			**Based on S_1**	
	S_S (g)	S_1 (g)		S_S (g)	S_1 (g)
Mean	1.508	0.750		1.557	0.597
Median	1.523	0.617		1.845	0.600
Maximum	2.893	1.261		2.259	1.298
Minimum	0.211	0.139		0.211	0.139

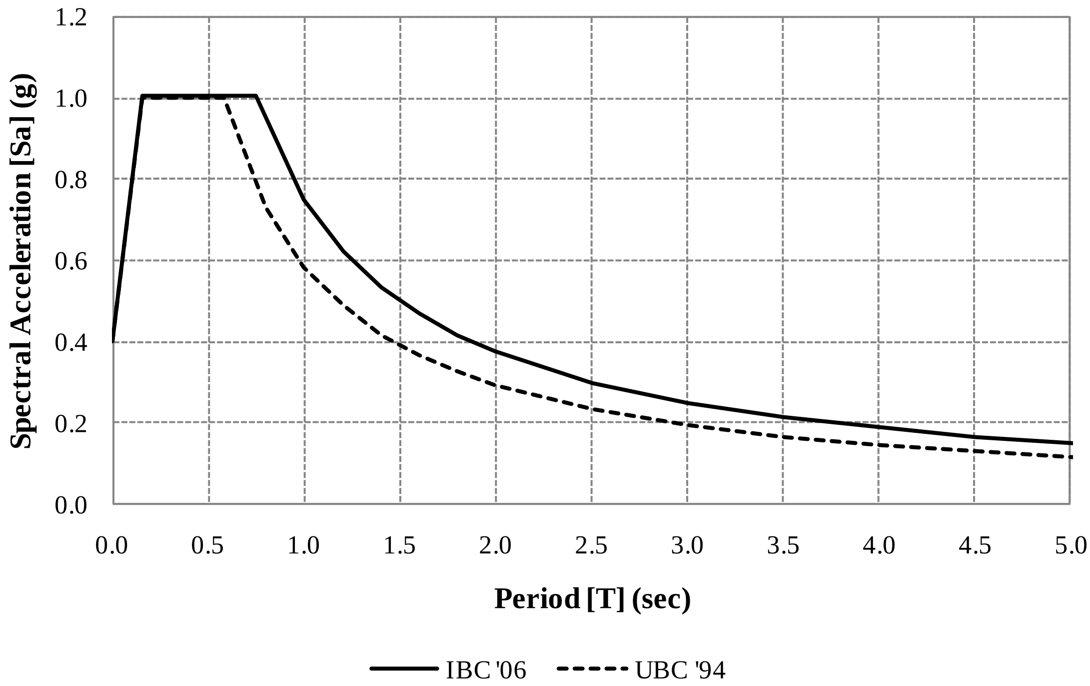

Figure 2-8 Design Acceleration Spectrum Comparison

Just as the seismic design forces differ between the 2006 IBC and 1994 UBC, so too do the drift limitations prescribed in each. As such, Building H3 was designed to conform to a drift limit of 0.015h (1.5%) under the design lateral loads per the 2006 IBC. The elevation and seismic weight of each floor derived from the loading assumptions are shown in Table 2-9 and the design sections are presented in Table 2-10. The AISC Steel Construction Manual (AISC, 2005) was used as the reference design specification along with SAP2000 software (CSI, 2007) to complete the design of Building H3.

Table 2-9 Elevation, Seismic Weight, and Design Story Forces of Building H3

Floor Level	**Elevation** *ft*	**Seismic Weight** *kip*	**Design Story Force** *kip*
2	20	2187	157
3	36	2157	316
Roof	52	2464	563
Total	-	6808	1036

Table 2-10 Beam and Column Sections for Building H3

Story Level	Seismic Frame				Gravity Frame		
	Column		Girder		Column		Beam
	Interior	Exterior	SMRF	Collector	Penthouse	Other	
1	W27x368	W27x368	W33x152	W21x68	W14x109	W14x109	W21x83
2	W27x368	W27x368	W33x152	W21x68	W14x109	W14x109	W21x83
3	W27x368	W27x368	W33x152	W21x68	W14x109	W14x109	W21x83

2.3 Computational Models

Once the details of the buildings were well defined, three-dimensional finite element models were developed using the OpenSees ver. 2.1.0 platform (Mazzoni et al., 2009). In the following sections, a brief overview of the OpenSees software framework is presented and is followed by a discussion of the modeling objectives and details.

2.3.1 OpenSees Framework

Developed by the Pacific Earthquake Engineering Research Center (PEER) and adopted as the simulation software for the George E. Brown Jr. Network for Earthquake Engineering Simulation (NEES), the Open System for Earthquake Engineering Simulation (OpenSees) is widely used in the field of performance-based earthquake engineering. As an open source framework used to analyze structural and geotechnical systems, the OpenSees software was selected for its extensive nonlinear analysis capability, computational speed, and availability (OpenSees, 2010). OpenSees has the capability to model large scale nonlinear structures through providing several beam-column element models as well as a wide variety of uniaxial material models. It also offers several analysis algorithms, and solution methods for solving nonlinear problems (OpenSees, 2010).

2.3.2 Modeling Objectives

Computational models of the four buildings included in this study were developed in view of the objectives and scope stated in Section 1.3, and summarized below:

1. To investigate the horizontal floor acceleration response characteristics in yielding SMRF structures.
2. To evaluate the interstory drift demands for the design of nonstructural components.
3. To investigate the vertical floor acceleration response characteristics in yielding SMRF structures with realistic floor details.

Objectives (1) and (3) defined the necessity for three-dimensional models. First, three-dimensional response history analyses are required to adequately assess the absolute acceleration response of a structure. Second, in order to capture out-of-plane flexibility of the floor decks, they must be modeled using shell elements in the horizontal floor planes. Nonlinearity of the structure must also be included in the model to achieve objectives (1) through (3). As a result, the models developed for this study were three-dimensional models that explicitly model the floor decks, gravity framing systems, and special moment frame systems.

2.3.3 Material Models

Two types of material models were used in the development of the structural finite element models: linear-elastic and nonlinear. For the purpose of this investigation the nonlinearity in the concrete deck elements was neglected, also the steel gravity frames were assumed to behave elastically, therefore linear-elastic material properties were assigned to these structural elements. Due to the large amount of yielding expected in the SMRF members, a nonlinear steel material was assigned to both the columns and beams of the SMRFs.

2.3.3.1 Elastic Materials

The elastic steel material was assumed to have an elastic modulus, E, equal to 29,000 ksi, a Poisson's ratio, v, equal to 0.3, and a shear modulus, G, equal to 11,154 ksi.

The concrete material was assumed to have an elastic modulus, E, of 3,605 ksi, based on a 4,000 psi concrete, determined from Section 8.5.1 of the ACI 318-08 (ACI, 2008). The Poisson's ratio, v, of the concrete was defined to be 0.2.

2.3.3.2 Nonlinear Steel Material

The material model implemented in the steel fiber sections of the seismic frame beams and columns a Giuffre-Menegotto-Pinto steel material with isotropic strain hardening (Mazzoni et al., 2009). The "steel02" command in OpenSees was used to generate the nonlinear steel material whose cyclic stress-strain relationship is shown in Figure 2-9. This command consists of six mandatory parameters: the yield stress, F_y, was set to 50 ksi; the initial modulus of elasticity, E_0, was set to 29,000 ksi; the strain hardening ratio (the ratio between the post-yield tangent and initial modulus of elasticity), b, was assumed to be 0.02; and the three parameters controlling the transition from the elastic region to the plastic region, R0, cR1, and cR2, were set to 10, 0.925, and 0.15, respectively as recommended per the OpenSees manual (Mazzoni et al., 2009). The five optional parameters controlling the isotropic hardening and initial stress were taken as default, in effect neglecting the effect of isotropic hardening.

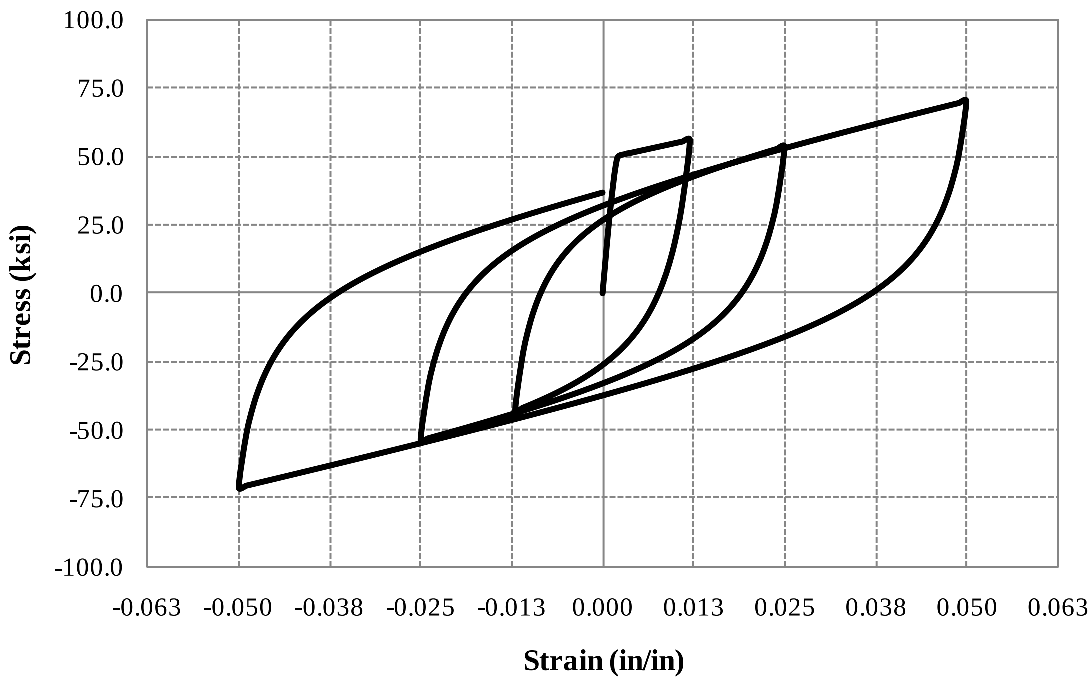

Figure 2-9 Steel Stress-Strain Relationship

2.3.4 Member Sections

2.3.4.1 Steel Sections

Fiber section modeling was used to consider the nonlinearity in the beam-column elements of the SMRFs. These sections are applied to both the beams and the columns of the SMRFs. The 16-

fiber box sections and 9-fiber W-shape sections were used to minimize the computational effort while still providing accurate nonlinear behavior and the generalized distribution of fibers for both the Box and W-shape sections can be seen in Figure 2-10. Results of a sensitivity analysis on the moment curvature relationship of the section were used to find the optimum number of fibers. Figure 2-11 shows the results of a moment curvature analysis and Figure 2-12 shows the error in the moment between sections with various numbers of fibers. The 9-fiber section provides a moment curvature relationship within 1% of the 45-fiber section. The 9-fiber section splits the flanges into three fibers in order to calculate the moment of inertia about the minor axis of the section, I_y and assure numerical stability. It is understood that biaxial yielding is not expected in W-Sections in SMRFs because of beam connectivity and base fixity. However, the box sections in the corner columns of the Building B20 model experience biaxial yielding. Thus, more fibers are included to help capture the biaxial actions on the corner columns. The fiber sections generated using the uniaxial material define nonlinear relationships for three of the four member degrees of freedom (axial, strong axis bending, and weak axis bending), while the fourth degree of freedom (torsion) is defined by a linear relationship. The slope of this linear relationship was defined as the shear modulus, *G*, of steel multiplied by the torsional constant, *J*, of the section. The section aggregator command was used to assemble the available four degrees of freedom. Shear deformations in the members were neglected.

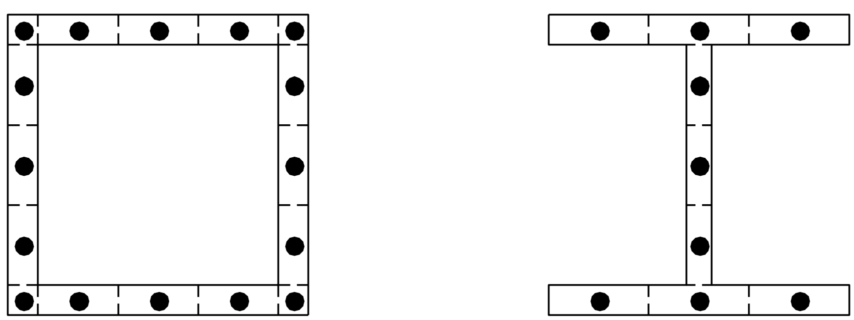

Figure 2-10 Typical Fiber Layouts for Steel Box and W-Shape Sections

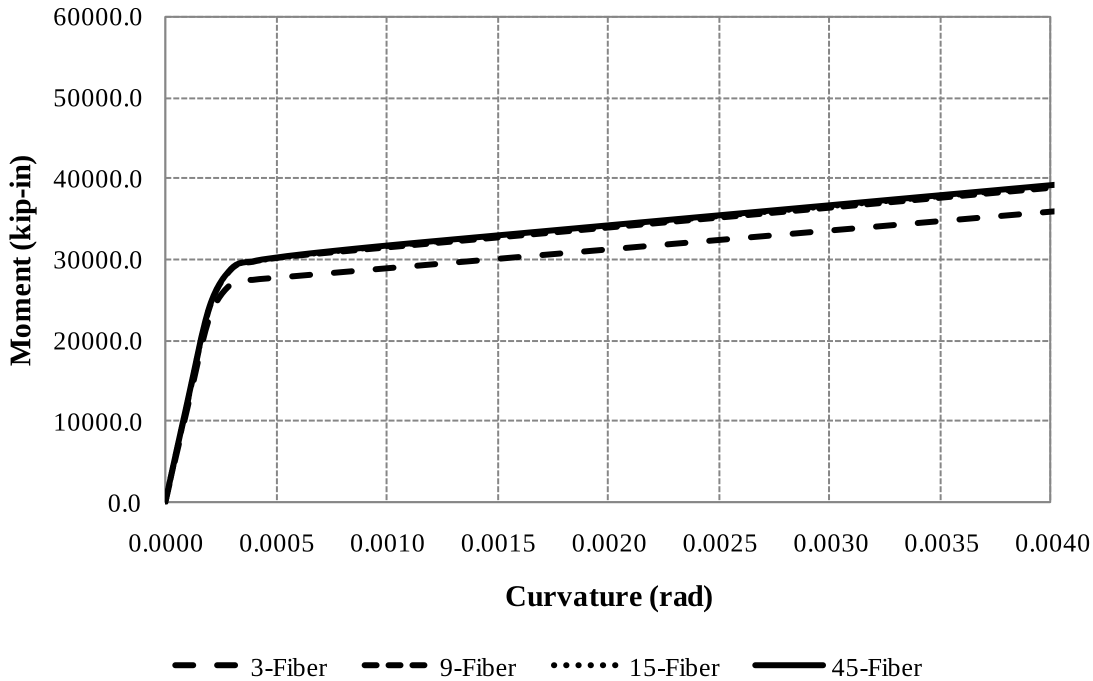

Figure 2-11 W-Section Moment Curvature Analysis

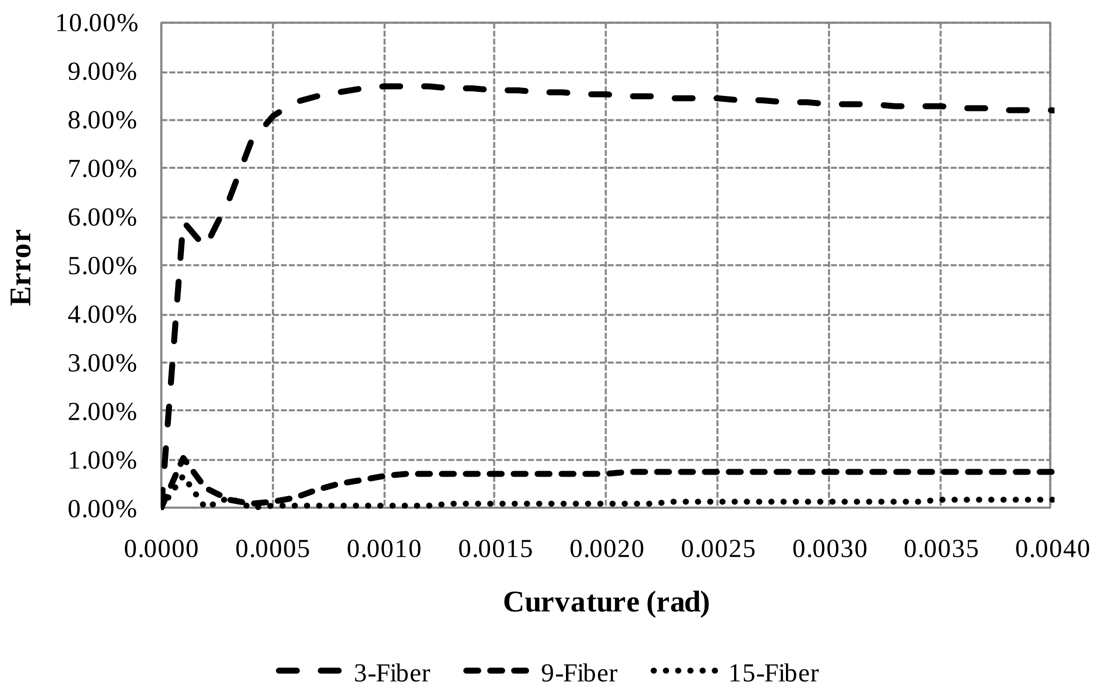

Figure 2-12 Error in Moment between Sections

2.3.4.2 Concrete Floor Deck Sections

The cross section of the shell elements used to model the floor decks were defined using the Elastic Plate Membrane Section command in OpenSees (Mazzoni et al., 2009). This command defines an isotropic section suitable for plate and shell analysis. The command calls for the elastic modulus of the material, E, the Poisson's ratio, v, the thickness of the section, t, and the mass density of the material, ρ. The thickness of the section, t, was modified from the actual concrete floor thickness, 5.5 in, to implicitly account for the rigidity of the secondary beams on the composite deck. This adjustment was used to represent the bending moment of inertia of the composite section. The thickness modification was calculated by considering the full composite action between the concrete and the secondary steel beams, as shown in Figure 2-13 and (2-1) through (2-3):

$$t = \left(\frac{12 I_{cg}}{b} \right)^{1/3} \tag{2-1}$$

$$I_{cg} = \left[\frac{1}{12} b t_c^3 + t_c b \left(y - \frac{t_c}{2} \right)^2 \right] + \left[n_d I_s + n_d A_s \left(y - \frac{2t_c + d_s}{2} \right)^2 \right] \tag{2-2}$$

$$y = \frac{\frac{b}{2} t_c^2 + n_d A_s \frac{2t_c + d_s}{2}}{t_c b + n_d A_s} \tag{2-3}$$

where:

t = the equivalent thickness of a concrete rectangular section

I_{cg} = the moment of inertia of the composite section about its neutral axis

y = the distance from the top of the composite section to its neutral axis

t_c = the thickness of the concrete deck

b = the spacing of the secondary beams

d_s = the depth of the secondary beam section

A_s = the area of the secondary beam section

I_s = the moment of inertia of the secondary beam section

n_d = the modular ratio of steel to concrete

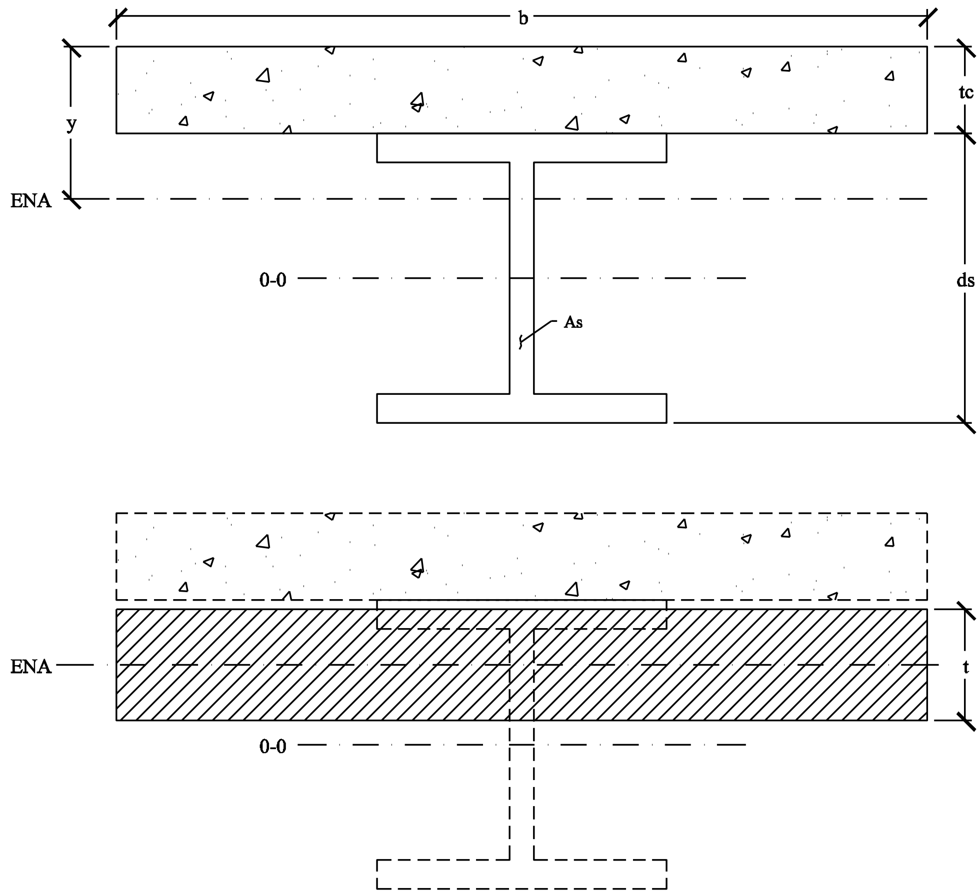

Figure 2-13 Composite Section Calculation

All four buildings have 5.5 in thick concrete slabs and secondary beam spacing of 10 ft. The modular ratio was taken as 6.25. A summary of the secondary beam sections and equivalent thickness for each of the floors of buildings is presented in Table 2-11. Modification of the thickness of the shell elements changes the in-plane rigidity as well as the out-of-plane rigidity, nevertheless, it was considered acceptable for two reasons. The first is that the out-of-plane rigidity is a function of t^3 while the in-plane rigidity is a function of t. Thus the in-plane effect of the modification is substantially less than the out-of-plane effect. For example, when the secondary beam is a W16x26, the equivalent thickness is 9.5 in. The thickness, t, increases by 73%, but the thickness cubed, t^3, increases by 415%. Secondly, it is standard practice that in-plane, the shell diaphragms are nearly rigid for regular buildings with aspect ratios close to 1.0, and hence this modification will have a negligible effect on the overall horizontal response of the building. The mass density, ρ, term was neglected as the mass was distributed manually to the nodes as described in Section 2.3.8.

Table 2-11 Floor Slab Equivalent Thickness

Building	Floor	Secondary Beam Section	Equivalent Thickness, t (*in*)
Building B3	Floor 2-3	W16x26	9.5
	Roof	W14x22	8.6
Building H3	Floor 2-3	W16x26	9.5
	Roof	W14x22	8.6
Building B9	Floor 2-9	W16x26	9.5
	Roof	W14x22	8.6
Building B20	Floor 2-20	W18x40	11.3
	Roof	W18x35	10.8

2.3.5 Element Types

The finite element models consist of a few different element types. For the gravity frame elements, Elastic Beam Column (Mazzoni et al., 2009) elements were used. Elastic Beam Column Elements are defined by the cross sectional area, A, the elastic modulus, E, the shear modulus, G, the torsional constant, J, the bending moment of inertia about both the local y and z axes, I_y and I_z, and the coordinate transformation defining the local axes of the element.

For the SMRFs, the beams and the columns were modeled with a Nonlinear Beam Column Element (this element was changed to Force Based Beam Column Element after ver. 2.0) (Mazzoni et al., 2009). This element by default implements the non-iterative force formulation, and considers the spread of plasticity along the element's length. The Gauss-Lobatto quadrature rule is used to integrate along the length of the element. Nonlinear Beam Column Elements are defined by the number of integration points along the length, a section tag of a previously defined section (i.e. fiber section), and the coordinate transformation defining the local axes of the element with respect to the global coordinates. For this study, all of the Nonlinear Beam Column Elements except the columns of the 3-story buildings are defined with 3 integration points. The columns of the 3-story buildings are defined with 5 integration points. The reason for using a smaller number of integration points is that all of the frame elements, except the columns of the 3-story buildings, are divided into segments to either conform to the mesh of the floor slab or to accommodate the location of column splices.

In addition to modeling the material nonlinearities, the geometric nonlinearities (P-Delta effects) were also considered. These effects are accounted for through the assignment of corotational geometric transformations to all of the column elements (Mazzoni et al., 2009). This type of transformation considers large displacements when accounting for the secondary effects. Linear transformations were assigned to the beam elements, as secondary effects are not commonly considered for beams due to small axial loads.

For the floor decks, the "block2D" command was implemented to define a mesh of shell elements. These shell elements use a bilinear isoparametric formulation in combination with a modified shear interpolation. This combination is implemented in order to improve thin-plate bending performance of the shell element (Mazzoni et al., 2009). The Elastic Membrane Plate Section defined in Section 2.3.4.2 was used to define the shell elements. Each floor panel was modeled using a three-by-three mesh of shell elements. The mesh size of the floor deck was calibrated based on the sensitivity analysis described in Section 2.3.9.

2.3.6 Element Connectivity

The beam-to-column connections within the models are assumed to perform in one of two ways: either the moment is constrained, as in the case of the SMRFs, or the moment is released, as for the pinned gravity frames. These connections are modeled using the "equalDOF" multipoint constraint command (Mazzoni et al., 2009) that imposes equivalent movement between the master node and the slave nodes. For the moment connections, all of the degrees of freedom of the beam end node were constrained to those of the column node. For the pinned connections, all of the degrees of freedom except for the rotation about the major bending axis of the beam were constrained to the column node. This simplified method neglects the partial fixity of the pinned connections.

The panel zones, end offsets, and effects of the top and bottom plates of the moment connections were neglected considering the following discussion. Several authors have compared two-dimensional models of the SAC buildings using various modeling techniques, (Foutch and

Seung-Yul, 2001); (Gupta and Krawinkler, 1999). It has been shown that using centerline models makes the frame weaker and more flexible than models that consider the clear dimensions. Foutch and Seung-Yul (2001) suggests that centerline models are adequate for design purposes and will provide conservative estimates of strength and lateral drift, but are not recommended to assess the seismic performance. Gupta and Krawinkler (1999) agree, stating that the use of centerline dimensions of the columns may provide an overestimation of the column contribution to lateral drift by a factor of two or more. Yet later, they report median global drift responses to a set of ground motions with 2% probability of exceedance in 50 years only differ by 2% between models considering the panel zones as opposed to centerline models. The period difference between models is reported to be within 7%. This being said, centerline models were used in this study because incorporating end offsets and shear deformations of the panel zone would have greatly added to the computational effort, which was of major concern with the shell element modeling of the floor decks. Also for this particular set of buildings the negligible difference in drift response under dynamic loads provided confidence that the effect of the end length offsets and panel zones would be small. This decision was made with the intent that these models would be used to assess global performance characteristics of the structures which are less affected by this underlying assumption. Considering the size of the models, this level of significance for neglecting the end offsets was deemed acceptable. Another concern presented was the significant difference in the strength of the centerline models compared to the end offset models at large drifts. Their results show a significant increase in the strength in the models that consider the offsets and a quick decline in the strength for the centerline models. By visual inspection of the pushover curves generated for this study, the quick decline in strength is not observed due to the presence of the floor shell elements. As a result, some of the loss of strength due to the centerline dimensions is compensated for through the presence of elastic shell elements modeling the floor slabs.

In an attempt to capture the one-way slab action, the shell elements were attached only to the beams running in the x-direction at a spacing determined by the floor mesh size. The connection used to attach the floor deck elements to the beam elements assumes a “pinned” condition in which the moments about both axes defining the horizontal plane were released. It was observed that “fixing” the slabs to the beams significantly increased the lateral stiffness and strength of the structure which would be the case if a sufficient number of studs were welded to the beams in the

SMRFs to provide a full composite action. However, since full composite action is not typical in building construction, this type of connection was provided to simulate the partial composite nature of the floor slab to the SMRF beams. This being said, a portion of the moment is transferred to the beam from the slab by maintaining continuity of the vertical deformations of the floor deck. The contribution of this moment to lateral stiffness is important and is controlled by the mesh size of the floor deck elements, as described in Section 2.3.9.

2.3.7 Boundary Conditions

The boundary conditions of the models were implemented in two different ways. For the buildings without basement levels (B3 and H3), the bases of the columns of the seismic frames were fixed along all the translational DOFs and about the strong axis, but were pinned about the weak axis. The bases of the gravity columns were pinned. This condition applies restraint to the nodes in all translational degrees of freedom, and the rotational degree of freedom about the vertical axis (the torsional degree of freedom of the column). These restraints were assigned using the “fix” command in OpenSees that assigns a single point boundary constraint to a node.

For the buildings with basement levels (B9 and B20), the boundary conditions were applied in a slightly different manner. The bases of all the columns were “pinned.” The rigid behavior of the basement floors was modeled through the implementation of axially rigid x-shaped trusses acting as a solid retaining wall all around the basement levels. These auxiliary braces provided lateral rigidity while retaining the continuity of the columns throughout the basement stories. The reason that restraints were not used for basement floors and the ground floor was to avoid assigning a restraint to a constrained node: because the column nodes of these floors were constrained to the floor slabs they could not also be restrained in OpenSees.

2.3.8 Seismic Mass and Gravity Load Distribution

The gravity loads and seismic masses described in Table 2-2, Table 2-4, Table 2-6, and Table 2-9 were evenly distributed over the nodes of the floor shell elements. The nodal masses are assigned to all three translational degrees of freedom. The nodal gravity loads were the force equivalent of the nodal masses assigned to the same nodes.

2.3.9 Model Verification and Sensitivity Analyses

To validate the modeling assumptions and details, the obtained fundamental periods were compared to previously published values in several other studies (Foutch and Seung-Yul, 2001); (Gupta and Krawinkler, 1999). Table 2-12 compares the fundamental period of the models developed for this study against those presented in previous works.

Table 2-12 Comparison of Fundamental Periods *(sec)*

Building	Current Study	Gupta et al., 1999	Foutch et al., 2001
B3	1.10	1.03	n/a
B9	2.39	2.34	2.49
B20	3.89	3.98	3.77

Similarly, it was critical to determine the appropriate mesh size for the floor diaphragms. A convergence test comparing the mesh size to the fundamental period of the structure was used to determine that a three-by-three mesh of shell elements per bay should be used. A convergence criterion of 5% difference in the fundamental period was used. The three-by-three per bay mesh size remained constant among each of the four building models.

2.4 Building Dynamic Characteristics

2.4.1 Building B3

Building B3 has a fundamental period of vibration of 1.10 sec. The fundamental mode is a translational mode in the y-direction. The fundamental mode accounts for 84% of the total mass participation in the y-direction. Table 2-13 describes the mode shapes and presents the modal mass participation factors of the significant modes of vibration. The significant modes are defined as the modes which accumulate at least 90% of the total mass.

Table 2-13 Building B3 Mode Shape Description and Mass Participation Factors

Mode	Period	Mass Participation Factor			Description
		X	Y	RZ	
	sec	%	%	%	
1	1.10	0.00%	83.84%	42.22%	First Y translational mode
2	1.08	83.99%	0.00%	18.76%	First X translational mode
3	0.67	0.00%	0.00%	22.83%	First torsional mode
4	0.33	13.15%	0.00%	2.86%	Second X translational mode
5	0.33	0.00%	13.43%	6.92%	Second Y translational mode
23	0.21	0.00%	0.00%	3.48%	Second torsional mode
Sum	--	97.14%	97.27%	97.07%	

2.4.2 Building H3

The fundamental period of Building H3 is 1.01 sec. This period is similar to that of Building B3 even though the sections are considerably larger because the story heights and the seismic mass have also been increased. The fundamental mode is a y-direction translational mode with a modal mass participation factor of 88 % of total mass. The mode shapes and mass participation factors of the significant modes of Building H3 are described in Table 2-14.

Table 2-14 Building H3 Mode Shape Description and Mass Participation Factors

Mode	Period	Mass Participation Factor			Description
		X	Y	RZ	
	sec	%	%	%	
1	1.01	0.00%	88.49%	44.61%	First Y translational mode
2	1.00	88.52%	0.00%	19.71%	First X translational mode
3	0.62	0.00%	0.00%	24.16%	First torsional mode
4	0.28	9.97%	0.00%	2.22%	Second X translational mode
7	0.28	0.00%	9.77%	4.92%	Second Y translational mode
54	0.17	0.00%	0.00%	2.69%	Second torsional mode
Sum	--	98.49%	98.26%	98.31%	

2.4.3 Building B9

Building B9 has a fundamental period of 2.39 sec. The fundamental mode shape is a y-direction translational mode. Approximately 81% of the y-direction total translational mass is participating in fundamental mode. Table 2-15 describes the significant mode shapes and mass participation factors of Building B9.

Table 2-15 Building B9 Mode Shape Description and Mass Participation Factors

Mode	Period	Mass Participation Factor			Description
		X	Y	RZ	
	sec	%	%	%	
1	2.39	0.02%	81.20%	28.62%	First Y translational mode
2	2.38	82.01%	0.02%	30.62%	First X translational mode
3	1.48	0.00%	0.00%	22.72%	First torsional mode
4	0.88	0.00%	11.43%	4.06%	Second X translational mode
5	0.88	11.15%	0.00%	4.13%	Second Y translational mode
6	0.55	0.00%	0.00%	2.99%	Second torsional mode
Sum	--	93.18%	92.65%	93.14%	

2.4.4 Building B20

The fundamental period of Building B20 is 3.89 sec. This period corresponds to the fundamental mode shape which is a y-direction translational mode. The fundamental mode accounts for 80% of the mass participation in the y-direction. The mass participation factors and mode shape descriptions for Building B20 are presented in Table 2-16.

Table 2-16 Building B20 Mode Shape Description and Mass Participation Factors

Mode	Period	Mass Participation Factor			Description
		X	Y	RZ	
	sec	%	%	%	
1	3.89	0.00%	80.49%	34.59%	First Y translational mode
2	3.47	81.17%	0.00%	24.22%	First X translational mode
3	2.18	0.00%	0.00%	22.44%	First torsional mode
4	1.37	0.00%	10.66%	4.58%	Second Y translational mode
5	1.22	10.48%	0.00%	3.13%	Second X translational mode
6	0.80	0.00%	3.51%	1.51%	Third Y translational mode
Sum	--	91.65%	94.66%	90.47%	

2.5 Building Strength Characteristics

2.5.1 Nonlinear Static Pushover Analysis

Nonlinear static (pushover) analyses were completed to assess the lateral strength of each building. The lateral load patterns were proportioned to the total weight using the ratio illustrated in (2-4) (ASCE, 2010).

$$F_x = \frac{w_x h_x^k}{\sum w_i h_i^k} W \tag{2-4}$$

where:

F_x = the story force at the x^{th} floor

w_x, w_i = the weight of the x^{th} and the i^{th} floor, respectively

h_x, h_i = the height of the x^{th} and i^{th} floors above the ground

k = an exponent related to the period of the building. The value of k shall be determined in accordance with Equation 12.8-12 of ASCE 7-05 (ASCE, 2010)

The k exponents were taken as 1.265, 1.225, 1.915, and 2.0 for Building B3, H3, B9, and B20, respectively. Displacement controlled analysis was used to develop the pushover curves. Base shear was normalized with respect to the total weight to represent relative the strength of each of the structures. Figure 2-14 and Figure 2-15 show the normalized base shear versus roof drift (roof displacement divided by total height). It is noted that the short buildings have considerably more strength than the taller buildings due to larger design base shear as a result of their small natural period.

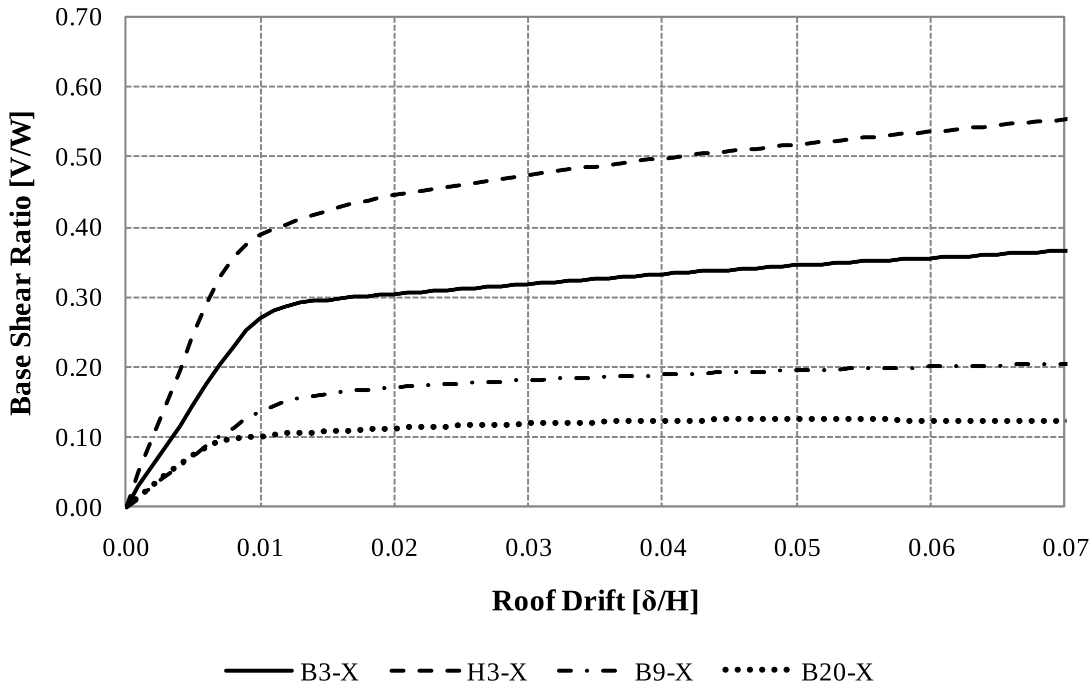

Figure 2-14 Nonlinear Static Pushover Curves for the Major Direction

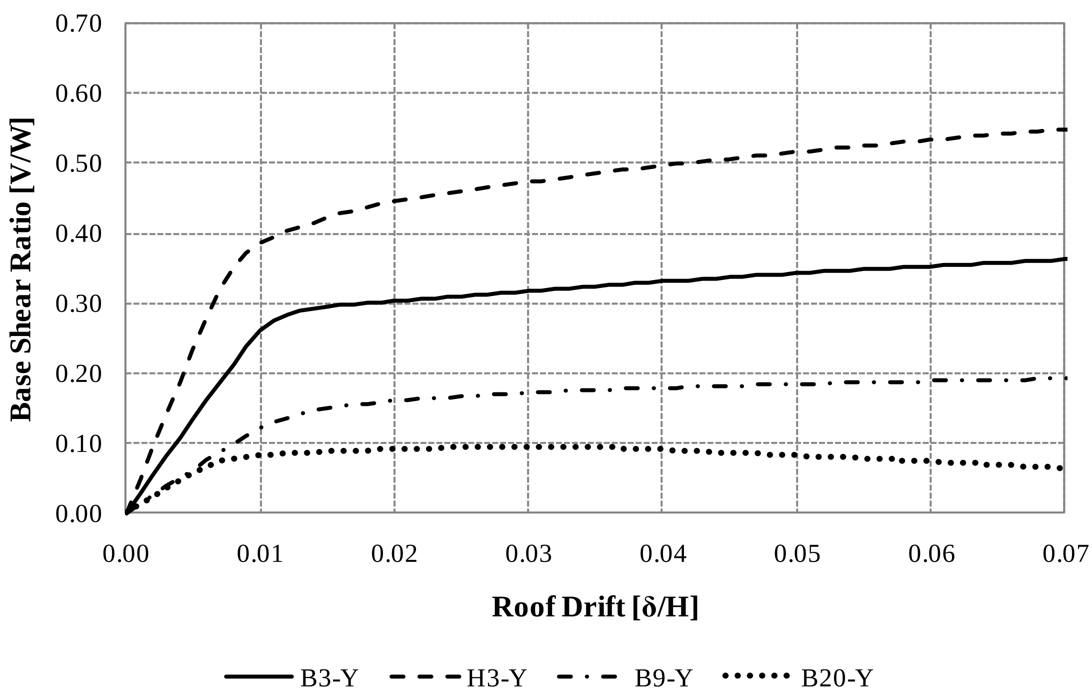

Figure 2-15 Nonlinear Static Pushover Curves for the Minor Direction

Base shear, *V*, was the quantity selected to compare the yield capacity to the design demand which was determined from the governing design code provisions. The yield base shear is determined from the idealized bilinear pushover curve as defined in FEMA 273 (FEMA, 1997b) and shown in Figure 2-16. The yield points for each of the buildings are shown in Table 2-17 and the pushover curves for each direction are compared in Figure 2-14 and Figure 2-15. The design base shear demand, yield base shear, and the demand to capacity ratios (D/C) are presented in Table 2-18. Observations of the data presented in tables and figures are further discussed below for each building.

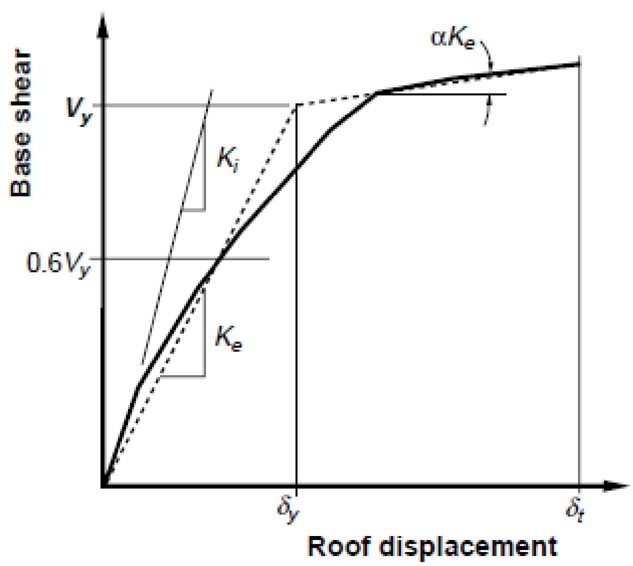

Figure 2-16 FEMA 273 Pushover Curve Bilinearization

Table 2-17 Nonlinear Static Pushover Analysis Results

Building	Yield Base Shear to Building Weight Ratio		Yield Roof Drift Ratio	
	X-Direction	Y-Direction	X-Direction	Y-Direction
B3	0.284	0.285	0.010	0.011
H3	0.376	0.378	0.008	0.008
B9	0.153	0.142	0.011	0.011
B20	0.096	0.078	0.006	0.007

Table 2-18 Base Shear Demand to Capacity Ratios

Building	Base Shear (*kip*)				
	Demand	Capacity		D/C Ratio	
	Code	X-Direction	Y-Direction	X-Direction	Y-Direction
B3	487	2079	2068	0.23	0.24
H3	1036	3057	3049	0.34	0.34
B9	841	3517	3327	0.24	0.25
B20	701	2735	2219	0.26	0.32

The D/C ratios for Buildings B3 and H3 are 0.24 and 0.34, respectively. This large over strength factor suggests that the design of these buildings was governed by drift limitations as opposed to strength. The design base shear for Building H3 is more than twice the design base shear of Building B3 that demonstrates that this study's hospital building is designed for more severe loads than this study's office buildings. The yield strength of Building H3 is greater than that of Building B3 but the yield drift has decreased from 1.0% to 0.8%. This demonstrates that this study's hospital building is designed to be stronger and generally less flexible.

Buildings B9 and B20 has D/C ratios of 0.25 and 0.32, respectively. Once again the drift limitations most likely governed the design of these structures. The yield drift of Building B9 is 1.1%, which is the largest of all the buildings. The post-yield stiffness of the Building B9 is noticeably less than either of the 3-story buildings. The yield drift of Building B20 is 0.6%, much less than the other buildings. This is due to a greater contribution of the P-delta forces acting on the columns. This contribution is also observed in the pushover curve that develops a negative slope beyond 5% roof drift (Figure 2-15). Building B20 is the only building with a noticeable difference in the pushover curve between the two directions. The difference is due to the geometry of building. In the x-direction there are 6 bays, all of which contain moment frames, whereas there are only 5 bays of moment frames in the y-direction. In addition to that, the gravity columns in the x-direction are spaced at twice the dimension of the y-direction, which provides a larger moment arm resisting the overturning moment of the building.

SECTION 3
GROUND MOTIONS AND INCREMENTAL DYNAMIC ANALYSIS PROCEDURE

3.1 Introduction

A database of nonlinear building response information was generated using the structural models discussed in Chapter 2 through the use of an Incremental Dynamic Analysis (IDA) procedure. IDA develops a relationship between the expected response of a given structure and the intensity of ground excitation by performing a series of nonlinear dynamic analyses in which the applied ground excitation is systematically scaled to various intensity levels. To avoid bias in the data, IDA is generally performed using a suite of ground motion records. This study has adopted a suite of 21 ground motion records selected from the PEER-NGA Database based on criteria establish by the ATC-63 project. In this chapter the IDA procedure, its associated terminology, and ground motion selection criteria, characteristics, and manipulations are presented.

3.2 Incremental Dynamic Analysis (IDA)

Incremental Dynamic Analysis (IDA) was adopted for this investigation to provide a methodology for systematically generating a comprehensive database of nonlinear building response information which includes a range of building responses from linear elastic responses up to unstable collapsed responses (Vamvatsikos and Cornell, 2002). The IDA methodology is conceptually similar to that of nonlinear static analysis except IDA uses ground motions of increasing intensity as opposed to increasing the levels of applied static force to generate a structural demand-capacity relationship. The procedure itself involves subjecting a structural model to a suite of seismic events each scaled to multiple levels of intensity, tracking the response, and producing a relationship between the obtained level of response and the applied intensity of ground motion. While the IDA methodology may be used to explore the characteristics of several response parameters, the majority of this study was focused on the floor acceleration response characteristics in yielding structures.

3.2.1 Terminology

The concept of IDA is simple, yet the importance of clearly defining all of the terms associated with the methodology cannot be overemphasized. To begin, the fundamental concept of IDA requires the definition of a particular ground motion record, $\boldsymbol{a_o}$, known as the "as-recorded" ground motion record which is typically selected from a database of recorded ground motions, such as PEER-NGA Database (PEER, 2006). In order to represent several levels of earthquake intensity, simple multiplicative scaling of the amplitudes of this record is introduced, $\boldsymbol{a_\lambda} = \lambda \cdot \boldsymbol{a_o}$.

Scale Factor (SF): The scale factor (SF) is the non-negative scalar that when multiplicatively applied to the "as-recorded" acceleration, $\boldsymbol{a_o}$, produces the target scaled acceleration record, $\boldsymbol{a_\lambda}$. As a result, a one-to-one mapping of the scaled acceleration record with the unscaled acceleration record is achieved. If the scale factor is equal to one, then the "as-recorded" acceleration record is obtained, however, for a scale factor greater than one, the acceleration record is said to be scaled up, and likewise for a scale factor less than one, the acceleration record is scaled down.

Scaling acceleration records is common in both research and in practice, yet concern often arises regarding the validity of the response of a structure to a scaled acceleration record. The concern is generally related to "weaker" records not being "representative" of "stronger" ones (Vamvatsikos and Cornell, 2002). Ultimately this reduces simply to a comparison of Probabilistic Seismic Demand Analysis (PSDA) and Incremental Dynamic Analysis (IDA). While, PSDA estimates the seismicity through a bin approach, which separates a large number of unscaled ground motions from a wide range of earthquakes into bins, IDA achieves a similar estimation through the incremental scaling of a select few motions. In fact, PSDA and IDA may be used interchangeably if care is taken in the selection of the motions and a sufficient number of motions are used for the IDA (Makie and Stojadinovic, 2002). However, due to the sensitivity of IDA to the selection of ground motions, there are cases when large dispersion and low confidence in the IDA curves will be present. In these cases it is generally agreed that PSDA is the better choice because of its more comprehensive representation of ground motion content. On the other hand, large magnitude seismic events are rare thus there are a limited number of high intensity ground motion records available. Therefore finding an unbiased set of high intensity records for use in the PSDA methodology is challenging. That being said, IDA was adopted for this study with the confidence that the motions selected provide a sufficient variety of ground motion content. The set of ground motions have been deemed appropriate for IDA by the ATC-63 project (FEMA, 2009) from which the set was developed.

Intensity Measure (IM): The intensity measure (IM) is a non-negative, monotonic, scalable measure of the intensity of the acceleration record. Several IMs have been suggested but the two most common are Peak Ground Acceleration (PGA) and the 5% damped spectral acceleration of the fundamental period of the structure ($Sa(T_1,5\%)$). These scalar values, in addition to being monotonic, are also proportional to the SF (Vamvatsikos, and Cornell, 2002). In this study, the PGA of the motions was used as the IM.

Damage Measure (DM): The damage measure (DM), or structural state variable, is a non-negative scalar value intended to track the response of the structure in progressive analyses. This value is obtained from the output of a particular nonlinear dynamic analysis. There are several appropriate DM values that may be used depending on the intent of the study, such as maximum interstory drift, maximum roof drift, peak floor acceleration, or peak base shear. Any one or more of these values that indicates an achieved level of response may be used as the DM (Vamvatsikos and Cornell, 2002). In this research, the maximum interstory drift of both directions was monitored through the analyses as the DM.

IDA Curve: IDA Curves depict the structural performance as defined by a particular damage measure, for example maximum interstory drift, as a function of an intensity measure, for example peak ground acceleration. The curve is most commonly plotted such that the independent variable, IM, is on the vertical axis and the dependent variable, DM, is on the horizontal axis. The curve is plotted in this manner because the IM is analogous with force and this form of plotting preserves the form of most stress-strain, or force-displacement curves (Vamvatsikos and Cornell, 2002). In this form, the IDA curve is reversed from most graphical relationships in which the independent variable is plotted along the horizontal axis therefore lines parallel to the vertical axis may intersect the curve in more than one point.

Multi-Record IDA: Due to record-to-record variability, IDA is most commonly performed for a suite of ground motions and produces a set of IDA curves that typically fit under a lognormal distribution. Considering the values of DM at a given level of IM, the mean and standard deviation of the set adequately defines the expected value and dispersion until the first IDA curve becomes unstable and the DM becomes infinite and so does the mean. If the median, 16% fractile, and 84% fractile of the DMs at a given level of IM are calculated, this problem is avoided and the median IDA curve becomes infinite when 50% of the curves are infinite. Assuming that the IDA curves are both continuous and monotonic, the *x*% fractile of the DM for a given IM is equivalent to the (100% - *x*%) fractile of the IM for a given DM. It has been documented that defining the median, 16% fractile, and 84% fractile curves in this manner fits well into the lognormal distribution (Vamvatsikos and Cornell, 2002).

3.2.2 Nonlinear Dynamic Analysis

As discussed in Chapter 2, the structural models used in this investigation are three-dimensional, and all three components of the ground motion were used to excite the structure. The ground motion major component (horizontal component with the larger PGA)was oriented in the x-direction (East-West), the minor component in the y-direction (North-South), and the vertical component in the z-direction (up-down). This orientation was consistent for all 21 events. The SF of a particular IM for an individual event was applied to all three components of the corresponding event.

Newmark integration was used to solve the nonlinear equations of motion (Chopra, 2007). The average integration method was assumed using a Newmark $\beta = 0.25$ and $\gamma = 0.5$. The structure's inherent damping was applied using Rayleigh damping (Chopra, 2007) of 5% assigned to a period of twice the fundamental period of the structure and 0.8 times the fundamental period of the structure to account for the elongation of period due to yielding of the structure.

3.2.3 Scaling Algorithm

Because of the variability of the input motions, an algorithm was developed in this study to scale the IM in such a way as to minimize the number of nonlinear response history analyses performed while maintaining a certain density of data points along the IDA curves. Various algorithms optimize the number of analyses, and Vamvatsikos and Cornell (2004) have developed one of the most efficient scaling algorithms, the hunt-and-fill method. This method consists of three phases. Its implementation in this study is summarized in Table 3-1 and depicted in Figure 3-1. The first is the initial climb phase in which the IM space is initialized with a very small initial IM level (in this study the initial IM, PGA, was set to 0.005g). There are two reasons for setting a small initial IM: (1) to produce an elastic structural response and (2) to prevent negative DM values when fitting a spline interpolation function on the data set. The next part of the initial climb is a geometrically increasing series of IM levels attempting to locate the IM level corresponding to structural instability. For the purpose of this study, structural instability was defined as the condition when any interstory drift ratio falls between 5% and 7%. Thus, in order to automate this iterative routine, a tool command language (tcl) script was developed and implemented into the OpenSees models (see Chapter 2). The script defines the initial climb phase by performing the initial IM step, setting the IM to $IM_{initial}$ = 0.005, as previously mentioned. Following the initial step, the IM step enters a “while” loop that increases the IM according to (3-1) until the associated DM of the previous step is greater than the maximum allowable DM, DM_{max} = 0.07.

$$IM_i = IM_{i-1} + n_{step} IM_{step} \tag{3-1}$$

where: n_{step} counts the iterations within the initial climb “while” loop and geometrically increases IM_{step}, IM_{step} is a constant increment that is increased by n_{step} resulting in a geometric step increment. For this study, the value of IM_{step} was set to 0.1g.

Once this condition ($DM \geq DM_{max}$) is satisfied the initial climb phase is complete and the algorithm transitions into the Hunt phase. One critical step in this transition is to define the infinite point, defined on the IDA curve (IM_{inf}, DM_{inf}) as the minimum IM that creates a DM > DM_{max}. A limit is then applied to DM_{inf} such that, $DM_{inf} < DM_{ult} = 0.15$. Limiting DM_{inf} by DM_{ult} bounds the slope of the line connecting the previously converged step with the infinite step, i.e. the secant slope, to a value that will allow for faster convergence to a point within the DM window.

Table 3-1 Theoretical IDA Algorithm Example

	Iteration	IM	DM	Counters	Commentary
Phase 1-Initial Climb	*Initial IM Step = Small*				
	1	0.005	0.0005		
	while DM < 0.07			*nStep*	<= Counts the number of steps to in the initial climb
	2	0.105	0.0010	1	
	3	0.305	0.0070	2	*IM(i) = IM(i-1) + nStep.IMstep*
	4	0.605	0.0120	3	IMstep = 0.1
	5	1.005	0.0250	4	nGap = nStep upon exiting the while loop
	6	1.505	0.0320	5	
	inf	2.105	0.1500	6	<= Locate the infinite point and exclude it from the iteration counter
Phase 2-Hunt	*while DM < 0.05*			*nHunt*	<= Counts the number of hunting iterations limit set to 5
	7	1.698	0.0450	1	$m = (IM_{inf} - IM(i-1))/(DM_{inf} - DM(i-1))$
	8	1.795	0.0550	2	$IM(i) = IM(i-1) + m(DM_{max} - DM(i-1)$
Phase 3-Fill	*for 1 to nGap = 6*			*nFill*	<= Counts the number of filling iterations and locates the current gap to fill
	9	0.055	0.0008	1	
	10	0.205	0.0050	2	
	11	0.455	0.0150	3	*IM(i) = [IM(nFill) + IM(nFill+1)]/2*
	12	0.805	0.0200	4	
	13	1.255	0.0380	5	
	14	1.602	0.0305	6	

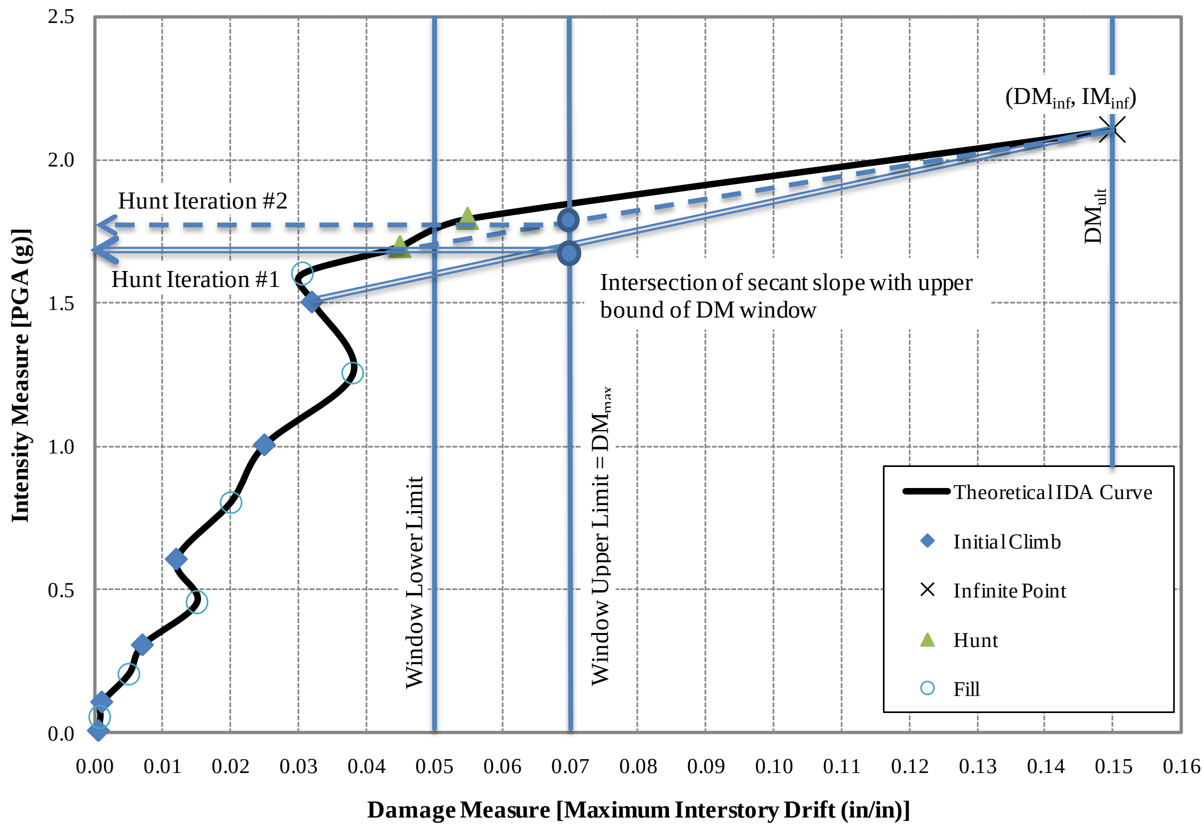

Figure 3-1 Theoretical IDA Curve using Hunt and Fill Algorithm

The Hunt phase iterates the IM level in an attempt to find a data point within the predetermined DM window. The DM window for this study is set between 5% drift and 7% drift. The Hunt phase consists of another while loop that iterates the IM level according to (3-3) until either a data point within the window is located or a maximum number of hunting iterations are performed. The number of hunting iterations was limited to five in this study.

$$IM_i = IM_{i-1} + m\left(DM_{\max} - DM_{i-1}\right) \tag{3-2}$$

where:

$$m = \frac{IM_{\inf} - IM_{i-1}}{DM_{\inf} - DM_{i-1}} \tag{3-3}$$

If the loop exits due to reaching a limit of hunting iterations, the IDA curve is assumed to have "flatlined" and the DM of the last iteration is set to the DM_{max} value before moving on to the final phase of the algorithm. This assumption is made in order to produce a better spline interpolation function of the “flatline.” However, if the Hunt loop exits by finding a data point within the window or if the Hunt phase is bypassed by identifying a data point within the window in the initial climb phase, the algorithm will transition into the third and final phase: the Fill phase.

The third phase, the Fill phase, is implemented through the use of a “for” loop. The loop iterates on the number of gaps to be filled in the initial climb. For each gap the next IM is set by referencing the IM values on either side of the IM gap being filled and generates an IM value as the average of these two IM values. The number of iterations in this phase is dependent upon the number of iterations required in the first phase: a counter in the initial climb “while” loop is used to define the number of iterations in the filling “for” loop.

Once all three phases of the algorithm are completed, the script generates a matrix of the IM and DM values for the current event and saves it to an output file. An example of the method can be seen in Table 3-1 and a graphical representation is shown in Figure 3-1. The initial climb phase is shown using diamond-shaped markers except for the “infinite” point which is marked by an “X.” The two iterations of the Hunt phase are shown graphically with secant lines, with the arrows indicating the next IM determined from the intersection of the secant line with the upper bound of the DM window. Finally, the Fill phase is shown with open-circle markers.

3.3 Ground Motion Set

The ATC-63 project developed a set of 22 “far-field” ground motions from recorded seismic events around the world (FEMA, 2009). These motions were collected for the purpose of performing Incremental Dynamic Analysis to develop the collapse margin ratio of a structure (FEMA, 2009). Though the focus of this investigation was not primarily in the study of the seismic capacity of buildings (the intended use of the data collected for the ATC-63 project), it was adopted for this investigation because the set of motions has been deemed appropriate for use with Incremental Dynamic Analysis.

3.3.1 Ground Motion Selection Criteria

The ground motion selection criteria followed by ATC-63 project (FEMA, 2009) was determined with the objective of assembling a set of motions that achieve the following: (1) the motions are compliant with the code-prescribed nonlinear dynamic analysis procedure, specifically Section 16.1.3.2 of ASCE 7-05 (ASCE,2005), (2) the motions are recorded from strong earthquakes, (3) there is a sufficient number of motions, and (4) the motions are independent of the site location and soil type. Due to the lack of available recorded data, the conclusion was drawn that it was not possible to assemble such a set of motions that would completely satisfy all of the required criteria. There are simply not enough records of sufficient strength to collapse current code compliant structures, and instead of synthesizing strong motion records, the ATC-63 committee adopted IDA, which allowed for the progressive scaling of a select few ground motion records. As a result, ATC-63 developed a set of recorded motions of sufficient variability to be used in IDA. The selection criteria developed by the ATC-63 project report (FEMA, 2009) are listed below and supported with a brief discussion of the intent of each rule.

- **Source Magnitude – M ≥ 6.5.** Large magnitude events produce strong, long duration ground motions that affect a large population of buildings.
- **Source Type – Strike-slip and Reverse (Thrust) Sources.** These types of sources are the most common of the western United States.
- **Site Conditions – Soft Rock and Stiff Soil Sites.** Soft rock (NEHRP Soil Class C) and stiff soil (NEHRP Soil Class D) were used so that soft soil effects would be negligible.
- **Site-Source Distance – Greater than 10 km.** The 10 km limit was selected for distinguishing far-field motions. The average of the Campbell (PEER, 2006) and Joyner-Boore (PEER,2006) distances was used to compare with the 10 km limit.
- **Number of Records per Event – Not more than "two" from any Event.** This criterion was set to eliminate event bias in the record set.
- **Strongest Ground Motion Records – Peak ground acceleration (PGA) greater than 0.2 *g* and peak ground velocity (PGV) greater than 15 cm/sec.** These limits were set to collect

records that produce structural damage yet retain enough records to provide sufficient record-to-record variability.

- **Strong Motion Instrument Capability – Valid frequency content greater than 0.25 Hz.** Allows for valid input for tall building structures with elastic periods of up to 4 seconds.
- **Strong Motion Instrument Location – Free field locations (or ground floors of small buildings).** This criterion is used to eliminate the effect of soil-structure interaction on the record.

The ATC-63 report collected motions from the PEER-NGA Database (PEER, 2006) because of its large number of ground motion records and its availability of fault-normal and fault parallel components of the ground motions. The availability of the vertical components of these ground motion records was essential for this study. All but one of the records in the ATC-63 "far field" set had a vertical component and as a result the set used in this study contains 21 motions as opposed to the 22 actually catalogued within the report. These 21 events (63 components) were used in the IDA procedure of this current investigation.

3.3.2 Event and Record Information

The set of ground motions comprised 21 events from 14 different earthquakes occurring between 1971 and 1999 is recorded in Table 3-2 which lists the name, year, and magnitude of the earthquake, as well as the name of the recording station. Six of these earthquakes occurred in the United States (California) while the remaining eight took place in five different countries around the world. Earthquake magnitudes range from M6.5 to M7.6, with an average magnitude of M7.0.

Table 3-2 Ground Motion Record List and Site Information

ID	Earthquake			Recording Station	Site Data		Source Type	Site-Source Distance (km)			
	Name	Year	Mag.	Name	NEHRP Class	V_{s30} (m/s)		Epicentral	Closest Plane	Campbell	Joyner Boone
1	Northridge	1994	6.7	Beverly Hills-Mul.	D	356	Thrust	13.3	17.2	17.2	9.4
2	Northridge	1994	6.7	Canyon Country-WLC	D	309	Thrust	26.5	12.4	12.4	11.4
3	Duzce, Turkey	1999	7.1	Bolu	D	326	Strike-Slip	41.3	12.0	12.4	12.0
4	Hector Mine	1999	7.1	Hector	C	685	Strike-Slip	26.5	11.7	12.0	10.4
5	Imperial Valley	1979	6.5	Delta	D	275	Strike-Slip	33.7	22.0	22.5	22.0
6	Imperial Valley	1979	6.5	El Centro Array #11	D	196	Strike-Slip	29.4	12.5	13.5	12.5
7	Kobe, Japan	1995	6.9	Nishi-Akashi	C	609	Strike-Slip	8.7	7.1	25.2	7.1
8	Kobe, Japan	1995	6.9	Shin-Osaka	D	256	Strike-Slip	46.0	19.2	28.5	19.1
9	Kocaeli, Turkey	1999	7.5	Duzce	D	276	Strike-Slip	98.2	15.4	15.4	13.6
10	Kocaeli, Turkey	1999	7.5	Arcelik	C	523	Strike-Slip	53.7	13.5	13.5	10.6
11	Landers	1992	7.3	Yermo Fire Station	D	354	Strike-Slip	86.0	23.6	23.8	23.6
12	Landers	1992	7.3	Coolwater	D	271	Strike-Slip	82.1	19.7	20.0	19.7
13	Loma Prieta	1989	6.9	Capitola	C	289	Strike-Slip	9.8	15.2	35.5	8.7
14	Loma Prieta	1989	6.9	Gilroy Array #3	D	350	Strike-Slip	31.4	12.8	12.8	12.2
15	Manjil	1990	7.4	Abbar	C	724	Strike-Slip	40.4	12.6	13.0	12.6
16	Superstition Hills	1987	6.5	El Centro Imp. Co.	D	192	Strike-Slip	35.8	18.2	18.5	18.2
17	Cape Mendocino	1992	7	Rio Dell Overpass	D	312	Thrust	22.7	14.3	14.3	7.9
18	Chi-Chi, Taiwan	1999	7.6	CHY101	D	259	Thrust	32.0	10.0	15.5	10.0
19	Chi-Chi, Taiwan	1999	7.6	TCU045	C	705	Thrust	77.5	26.0	26.8	26.0
20	San Fernando	1971	6.6	LA-Hollywood	D	316	Thrust	39.5	22.8	25.9	22.8
21	Friuli	1976	6.5	Tolmezzo	C	425	Thrust	20.2	15.8	15.8	15.0
-	**Minimum**	**1971**	**6.5**	-	-	**192**	-	**8.7**	**7.1**	**12.0**	**7.1**
-	**Maximum**	**1999**	**7.6**	-	-	**724**	-	**98.2**	**26.0**	**35.5**	**26.0**
-	**Average**	-	**7.0**	-	-	**381**	-	**40.7**	**15.9**	**18.8**	**14.5**

The site and source information of each event in the set is also summarized in Table 3-2. The site information includes the NEHRP soil site classification and the shear wave velocity as well as the site-source distance characteristics of the epicentral, the closest plane, Campbell, and Joyner-Boore distances (PEER, 2006). Each of the four distances provides a different estimation of the proximity of the recording station to the origin of the fault rupture. The source mechanism type is also included. Fifteen of the events are recorded in sites classified a Soil Class D (stiff soil) while six are classified as Soil Class C (soft rock). Fourteen of the events are products of strike-slip faults while seven are a result of thrust (or reverse) fault rupture. To be consistent with the selection criteria, the average of the Campbell and Joyner-Boore distances range from 11.1km to 26.4 km from the source with an average site-source distance of 16.7 km.

Table 3-3 lists critical event information from the PEER-NGA Database, including the record sequence number and the names of the major, minor, and vertical component record files. Additionally, the table provides the PGA, PGV, Arias intensity, the "as-recorded" duration, and the shortened duration. The values listed for PGA, PGV, and arias intensity (Arias, 1970) correspond to the maximum of all three components. The minimum, maximum, and average PGA of the set are 0.21 g, 0.82 g, 0.42 g, respectively. The minimum, maximum, and average PGV of the set are 19 cm/sec, 115 cm/sec, and 47 cm/sec, respectively. As shown in Figure 3-2, the distribution of PGAs within the set is fairly normal, as is the distribution of PGVs shown in Figure 3-3. The minimum, maximum, and average values of the arias intensity, a measure of the energy of the ground motion used to determine the duration of strong shaking (Bommer et al., 1999) within each record – of the set are 0.29 m/sec, 7.59 m/sec, and 2.38 m/sec, respectively. The "as-recorded" durations range from 20 sec to 100 sec with an average duration of 45 sec. The strong shaking portions of each event ranged from 7 sec to 64 sec with an average duration of 19 sec.

Because this investigation incorporated the vertical component of ground motion record, it was important to characterize the typical ratio of vertical excitation to horizontal excitation. The peak vertical acceleration (PGA_v) is compared with the peak horizontal acceleration (PGA_h) in Figure 3-4. The code establishes an upper bound for this relationship by approximating the PGA_v as 2/3 of the PGA_h. This approximation appears to be fairly appropriate for the 21 events selected in this investigation.

Table 3-3 PEER-NGA Record Information and Event Characteristics

ID	PEER-NGA Record Information				PGA	PGV	Arias Intensity	Recorded Duration	Shortened Duration
	Record Seq. No.	File Names							
		Major	Minor	Vertical	g	cm/sec	m/sec	sec	sec
1	953	NORTHR/MUL279	NORTHR/MUL009	NORTHR\MUL-UP	0.517	62.8	4.50	30.00	9.74
2	960	NORTHR/LOS270	NORTHR/LOS000	NORTHR\LOS-UP	0.482	44.9	1.98	20.00	9.35
3	1602	DUZCE/BOL090	DUZCE/BOL000	DUZCE\BOL-UP	0.822	62.1	3.72	55.90	13.81
4	1787	HECTOR/HEC090	HECTOR/HEC000	HECTOR\HECVER	0.337	41.7	1.87	45.31	14.12
5	169	IMPVALL/H-DLT352	IMPVALL/H-DLT262	IMPVALL\H-DLTDWN	0.351	33.0	3.29	99.92	63.90
6	174	IMPVALL/H-E11230	IMPVALL/H-E11140	IMPVALL\H-E11-UP	0.380	42.1	1.96	39.04	16.82
7	1111	KOBE/NIS000	KOBE/NIS090	KOBE\NIS-UP	0.509	37.3	3.35	40.96	12.21
8	1116	KOBE/SHI000	KOBE/SHI090	KOBE\SHI-UP	0.243	37.8	0.83	40.96	16.55
9	1158	KOCAELI/DZC270	KOCAELI/DZC180	KOCAELI\DZC-UP	0.358	58.9	1.33	27.19	14.48
10	1148	KOCAELI/ARC000	KOCAELI/ARC090	KOCAELI\ARCDWN	0.219	39.6	0.29	30.00	13.29
11	900	LANDERS/YER270	LANDERS/YER360	LANDERS\YER-UP	0.245	51.4	0.92	44.00	25.48
12	848	LANDERS/CLW-TR	LANDERS/CLW-LN	LANDERS\CLW-UP	0.417	42.3	2.17	27.97	17.34
13	752	LOMAP/CAP000	LOMAP/CAP090	LOMAP\CAP-UP	0.529	35.0	4.41	39.96	13.95
14	767	LOMAP/G03000	LOMAP/G03090	LOMAP\G03-UP	0.555	44.7	2.09	35.95	13.27
15	1633	MANJIL/ABBAR--L	MANJIL/ABBAR--T	MANJIL\ABBAR--V	0.515	52.1	7.59	53.52	33.46
16	721	SUPERST/B-ICC000	SUPERST/B-ICC090	SUPERST\B-ICC-UP	0.358	46.4	1.06	40.00	22.52
17	829	CAPEMEND/RIO360	CAPEMEND/RIO270	CAPEMEND\RIO-UP	0.549	43.8	2.49	36.00	18.88
18	1244	CHICHI/CHY101-N	CHICHI/CHY101-E	CHICHI\CHY101-V	0.440	115.0	2.90	90.00	30.41
19	1485	CHICHI/TCU045-N	CHICHI/TCU045-E	CHICHI\TCU045-V	0.512	39.1	1.37	90.00	11.77
20	68	SFERN/PEL090	SFERN/PEL180	SFERN\PEL-UP	0.210	18.9	0.65	28.00	12.29
21	125	FRIULI/A-TMZ000	FRIULI/A-TMZ270	FRIULI\A-TMZ-UP	0.351	30.8	1.20	36.35	6.62
-	-	-	-	**Minimum**	**0.210**	**18.9**	**0.29**	**20.00**	**6.62**
-	-	-	-	**Maximum**	**0.822**	**115.0**	**7.59**	**99.92**	**63.90**
-	-	-	-	**Average**	**0.424**	**46.6**	**2.38**	**45.29**	**18.58**

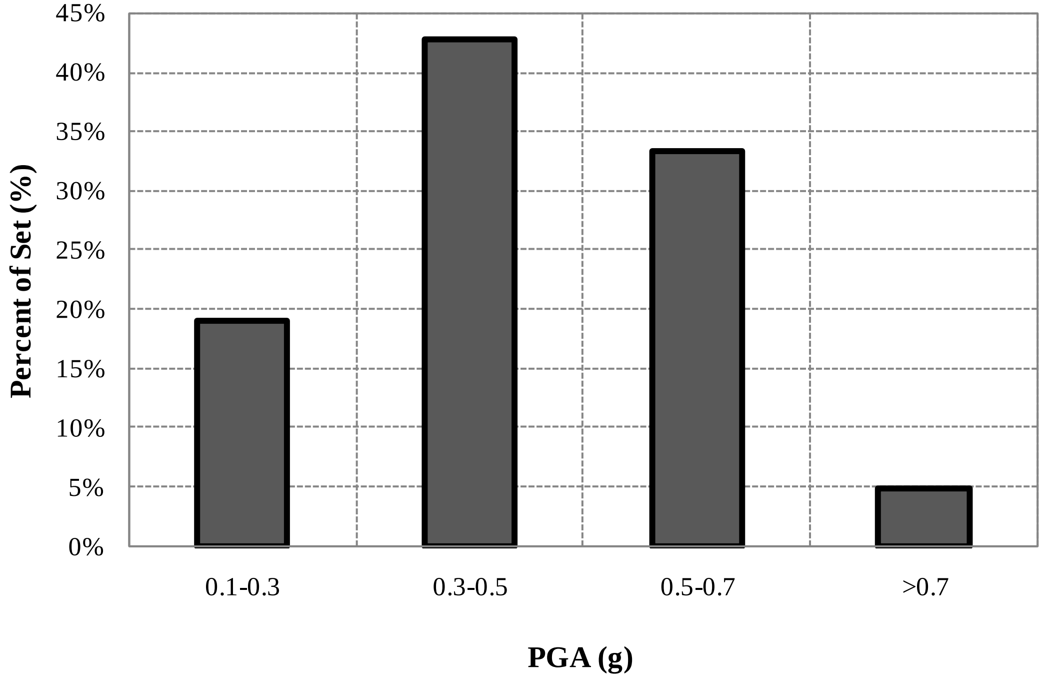

Figure 3-2 Ground Motion PGA Distribution

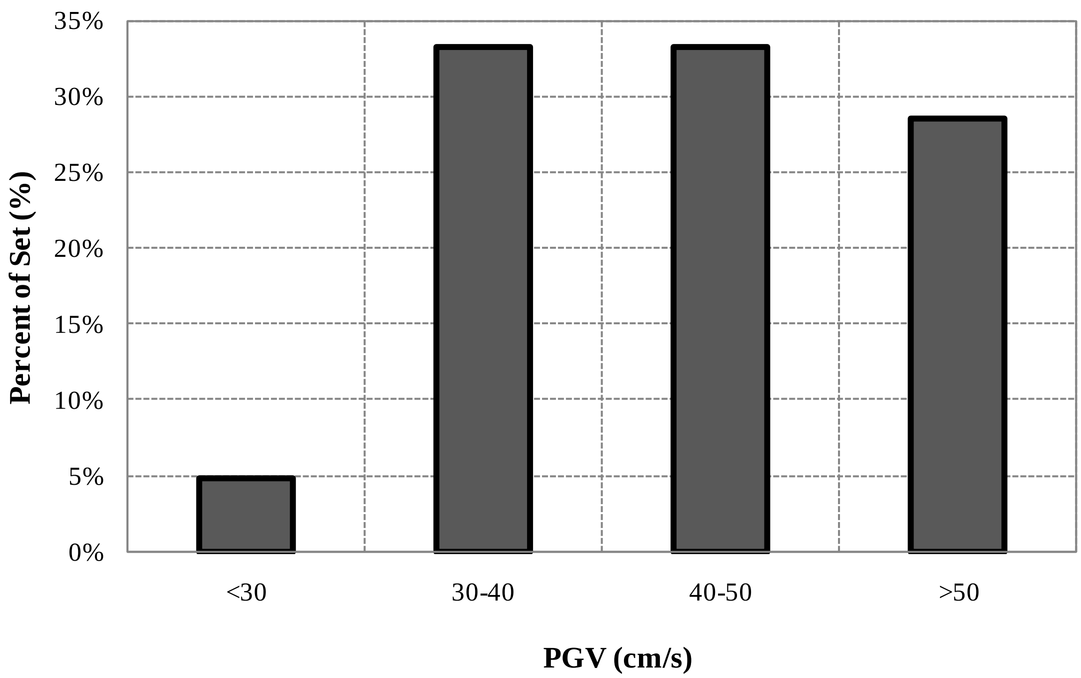

Figure 3-3 Ground Motion PGV Distribution

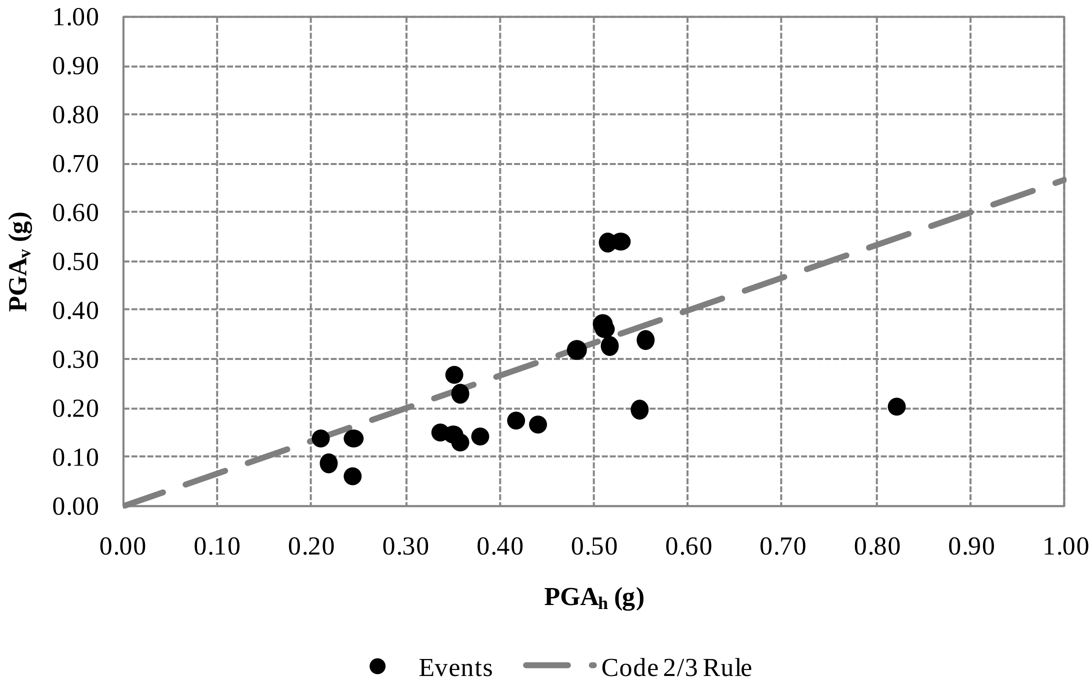

Figure 3-4 Comparison of Vertical PGA to Horizontal PGA

3.3.3 Acceleration Spectra

A MATLAB (Mathworks Inc, 2004) script was developed to derive the 5% damped elastic acceleration spectra for each of the motions. The elastic acceleration spectra of the "as-recorded" major, minor, and vertical components are presented in Figure 3-5. The elastic acceleration spectra of the shortened major, minor, and vertical components are presented in Figure 3-6. In comparing the "as-recorded" spectra to the shortened spectra, it was observed that cutting the acceleration records had a minimal effect on the acceleration spectra. The elastic acceleration spectra after normalizing the records based on their respective PGA are shown in Figure 3-7. The comparison of the mean acceleration spectra of the "as-recorded", shortened, and normalized records for each component is shown in Figure 3-8. The mean of the horizontal components is compared to the design spectra for the 1994 UBC and the 2006 IBC in Figure 3-9.

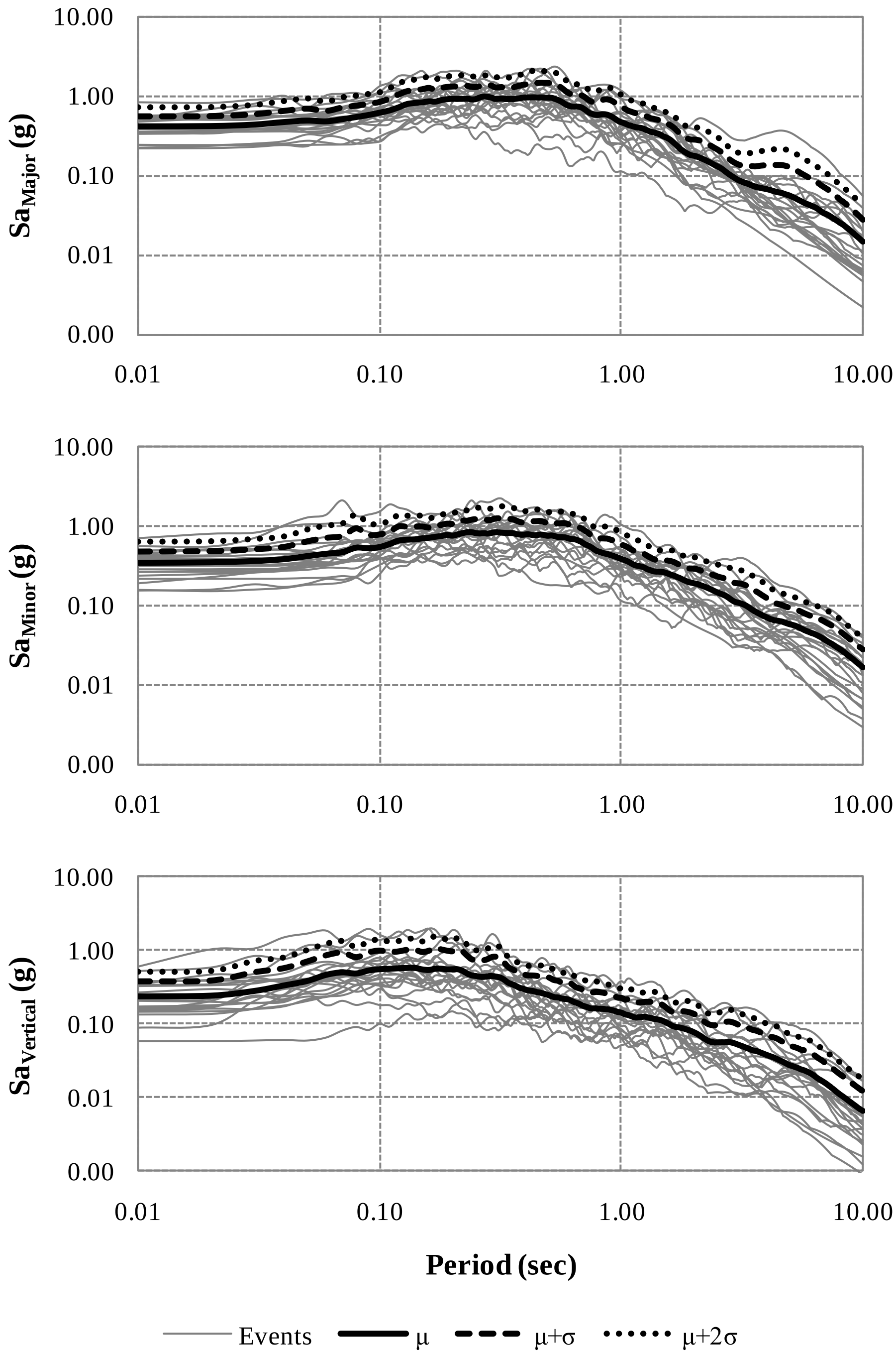

Figure 3-5 "As Recorded" Acceleration Spectra

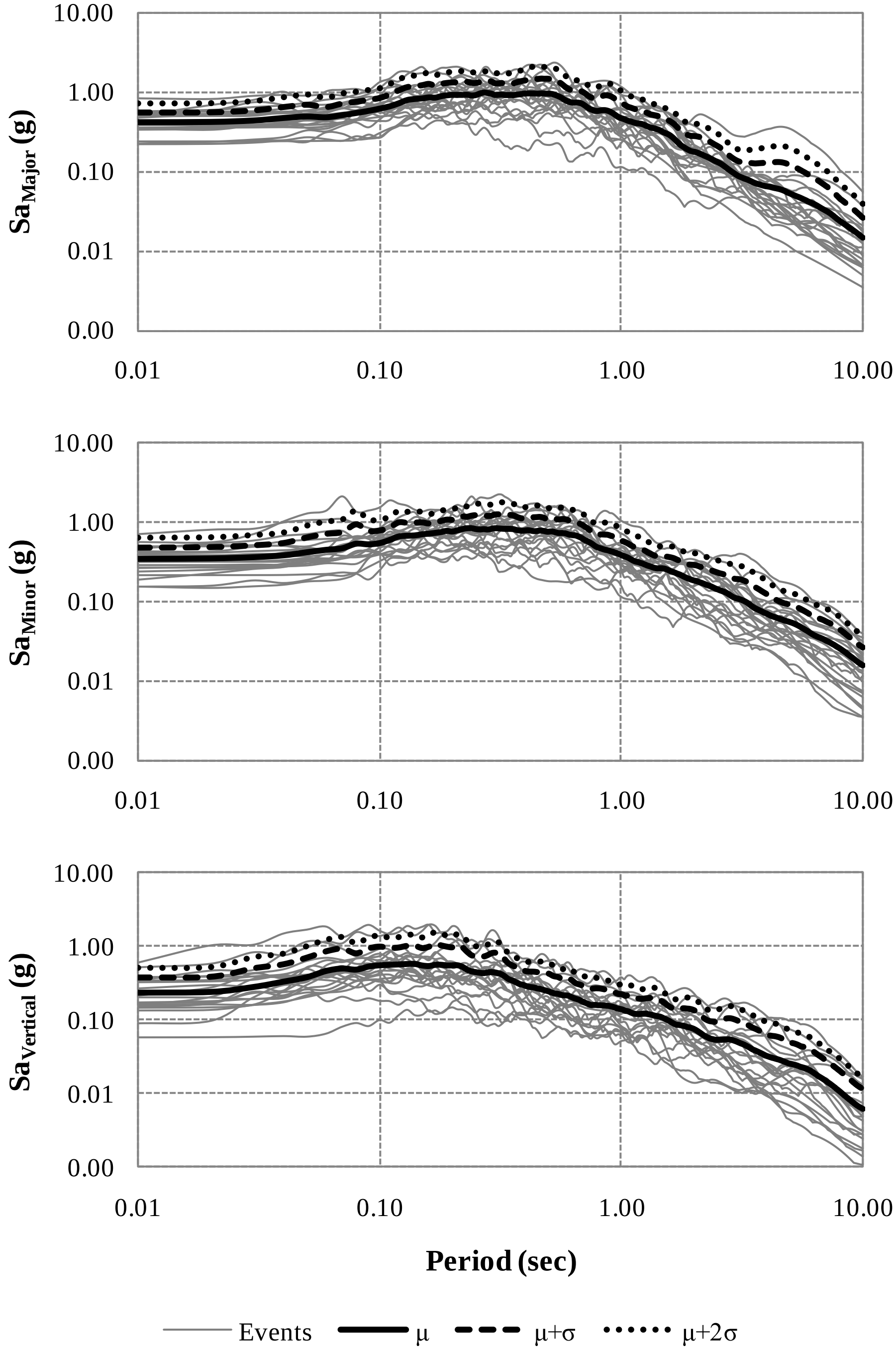

Figure 3-6 Shortened Acceleration Spectra

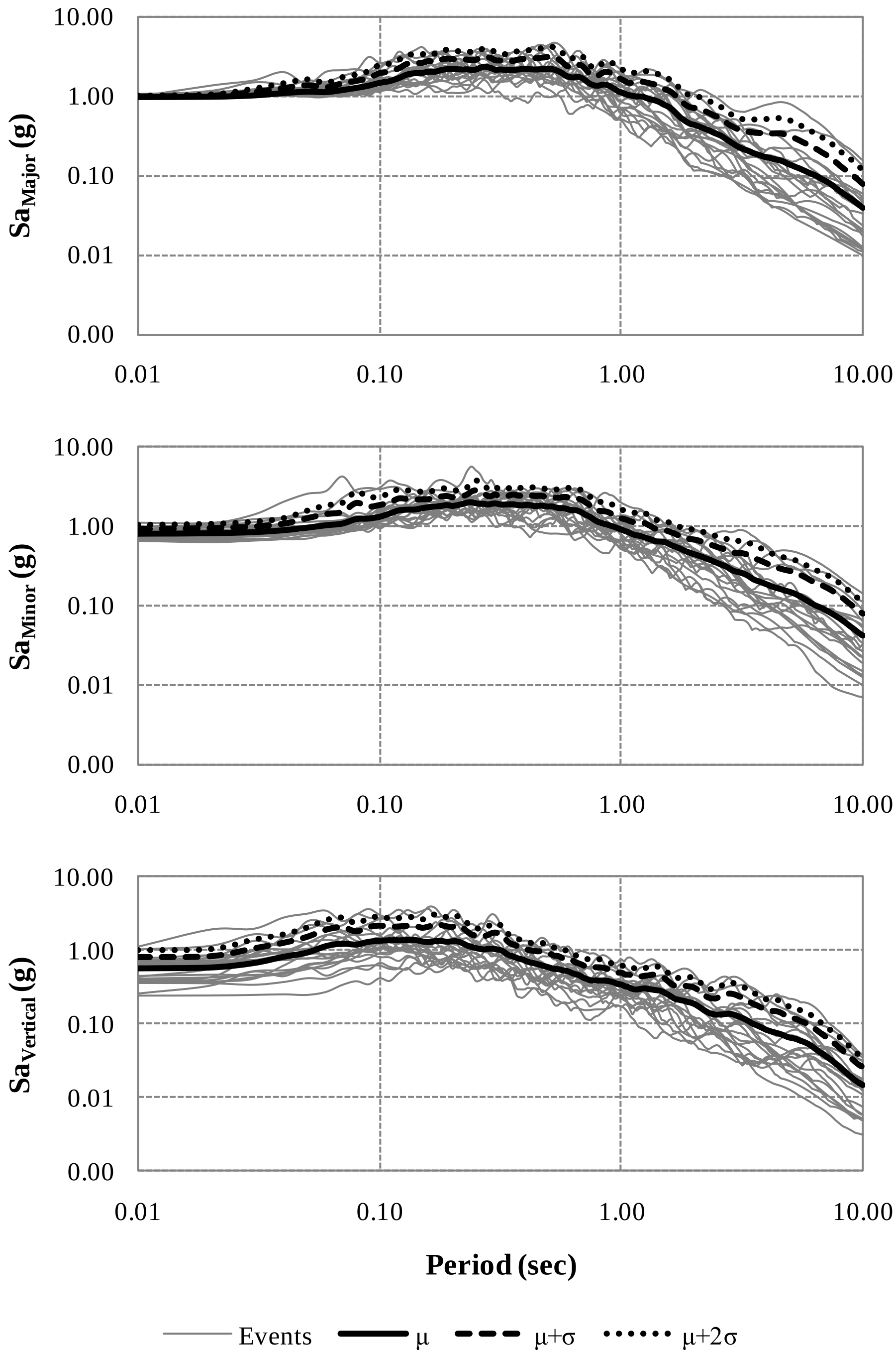

Figure 3-7 Normalized Acceleration Spectra

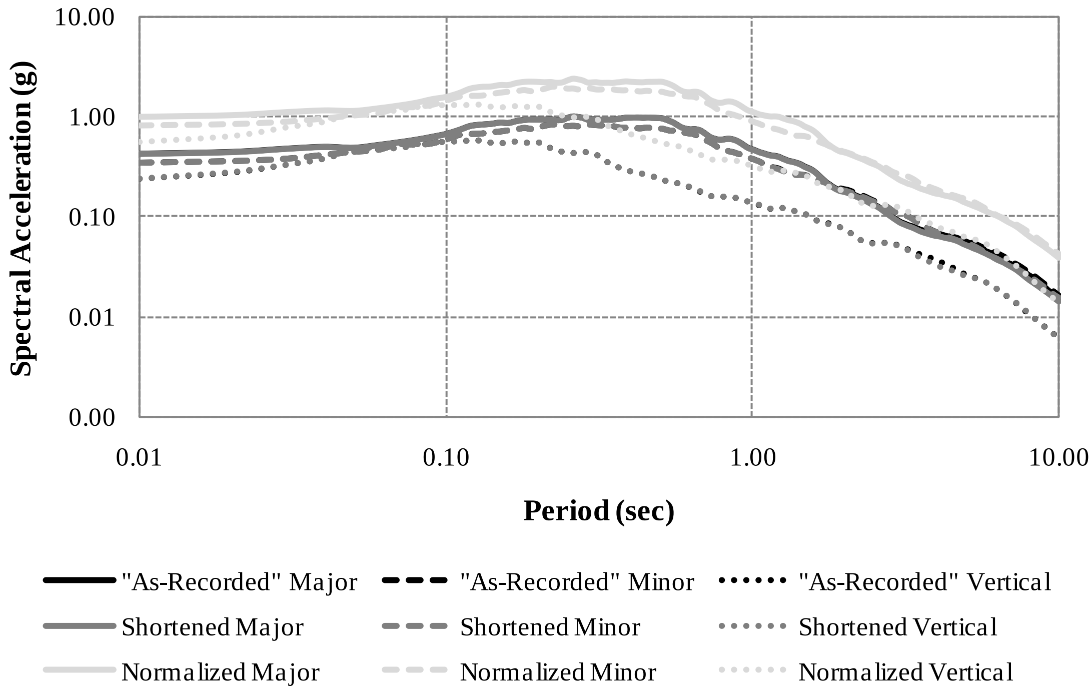

Figure 3-8 Effect of Acceleration Record Manipulations on Acceleration Spectra

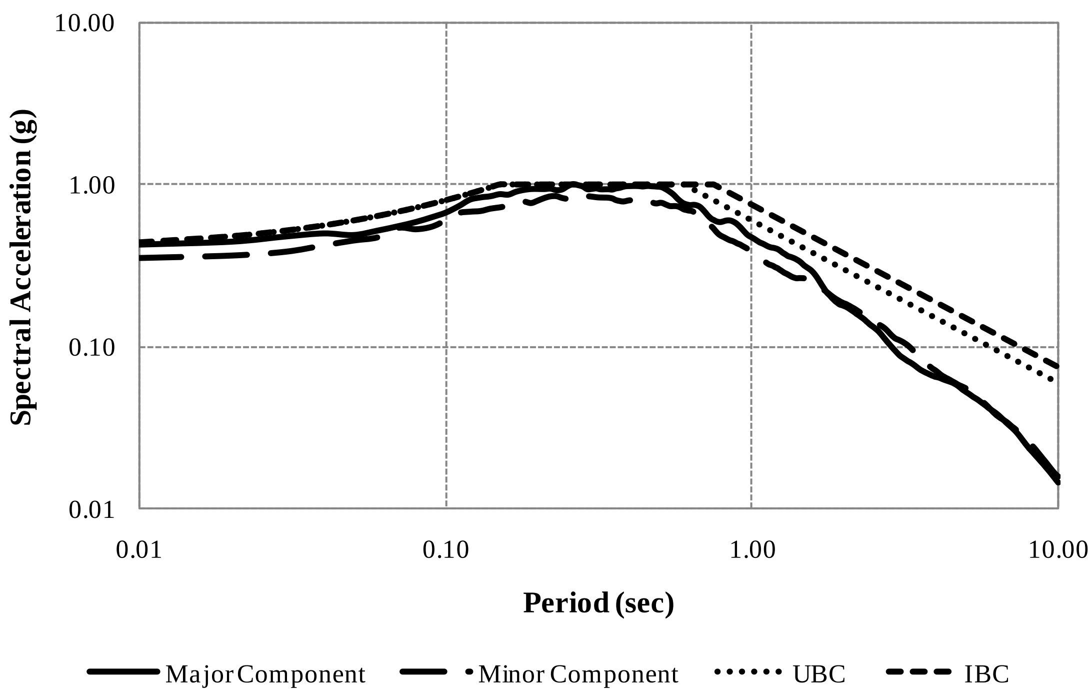

Figure 3-9 Comparison of Horizontal Spectra with Code Design Spectra

3.4 Summary

The Incremental Dynamic Analysis procedure was performed using a suite of 21 ground motions selected from the PEER-NGA Database based on the criteria established by the ATC-63 project. As a result of numerous nonlinear response history analyses a database of structural responses was generated. The upcoming chapters will present the critical information collected and observations recorded as well as generate conclusions and recommendations for the expected floor acceleration response of steel moment frame structures.

SECTION 4
INCREMENTAL DYNAMIC ANALYSIS RESULTS AND DRIFT DEMANDS ON NONSTRUCTURAL COMPONENTS

4.1 Introduction

After performing the IDA of all four structures for each of the 21 ground motion events, a database of results from a total of 1,233 nonlinear response history analyses was produced. From this database the response quantities essential to the evaluation of seismic demands on nonstructural components were extracted, organized, and post-processed. Raw response quantities such as floor displacements, and floor accelerations were extracted and used as the foundation for the derived quantities used in several IDA curves. These curves facilitate the derivation of several critical relationships presented throughout the remainder of this report. This chapter introduces the IDA results, defines the intensity measures and damage measures used to generate the IDA curves, and describes the procedure used to develop relationships between damage measures using by combining IDA curves. Also presented in this chapter is a discussion of the drift demands of nonstructural components mounted on these buildings.

4.2 Incremental Dynamic Analysis Results

The discussion of analysis results appropriately begins with the development of several IDA curves that relate an intensity measure (IM) of the ground excitation to a particular damage measure (DM) of the structure. As mentioned in Chapter 3 several choices of both IM and DM exist. This study presents only 5 sets of IDA curves directly, however each is of particular importance. Before presenting the curves, the selected IMs and DMs are first introduced.

4.2.1 Intensity Measures

Recall that the intensity measure (IM) is defined to quantify the intensity of the applied ground acceleration. Two different IMs, peak ground acceleration (PGA) and spectral acceleration ($SA(T_1,5\%)$), were selected for the purpose of demonstration in this chapter.

4.2.1.1 Peak Ground Acceleration (PGA)

The peak ground acceleration is frequently used as a measure of ground motion intensity. Although PGA is generally defined as the maximum ground acceleration in one of the two orthogonal horizontal components of ground motion, this study defines PGA as the maximum of the vector sum of the two horizontal acceleration components. The bidirectional nature of this quantity takes advantage of the three-dimensional models in order to provide a more accurate approximation of the true horizontal acceleration imparted to the structure.

4.2.1.2 Spectral Acceleration (SA(T_1,5%))

An alternative measure of the ground motion intensity was defined as the ordinate of the elastic 5% damped bidirectional acceleration spectrum at the elastic fundamental period of the structure. The generation of such a spectrum considers the 5% damped elastic response of a single-degree-of-freedom system with known period under each horizontal component of the excitation individually. The vector sum of the acceleration responses is computed for each time step and the maximum recorded as the spectral acceleration value for that particular period of structure. The spectral acceleration corresponding to the period of the structure provides an estimate of the peak horizontal acceleration response of an elastic structure with common periods in each orthogonal horizontal direction. As opposed to PGA, the SA(T_1,5%) accounts for both amplitude and frequency content of the ground motion.

4.2.2 Damage Measures

The damage measure (DM) is a measurement of the structural response to the applied ground acceleration. There are several suitable quantities that may be used as the DM depending on the intent and nature of the study. Typically when the building performance is the focus of study, DMs such as maximum interstory drift or maximum roof drift are used. However, for the assessment of seismic demands on nonstructural components a measure of the acceleration response of the structure is also necessary to quantify the level of acceleration, and thus inertial forces, applied to the nonstructural components. The three DMs listed below are used in the IDA curves presented in this chapter.

4.2.2.1 Maximum Peak Interstory Drift (θ_{max})

The interstory drift of a given story is defined as differential displacement between the adjacent floors defining the story divided by the story height. The vector sum of the interstory displacement in each of the horizontal directions was used to define the interstory drift for each story of the building. The maximum peak interstory drift (θ_{max}) is the maximum value of interstory drift of any story throughout the duration of the ground motion event. This measure defines the maximum bidirectional drift throughout the building and is critical for the design of drift-sensitive nonstructural components such as vertical pipe runs and partition walls.

4.2.2.2 Peak Roof Drift (θ_R)

The peak roof drift (θ_R) is calculated by dividing the roof displacement by the total building height. In order to achieve a bidirectional measure of the roof drift, the maximum vector sum of the two horizontal components of roof displacement defines the roof drift. Roof drift was considered as a primary damage measure because it offers a global measure of displacement demand that is readily converted to a measure of global ductility.

4.2.2.3 Global Drift Ductility (μ)

The global drift ductility was calculated using (4-1):

$$\mu = \frac{\theta_R}{\theta_{Ry}} \qquad (4\text{-}1)$$

Where, θ_R = maximum roof drift, and θ_{Ry} = yield roof drift that is defined as the minimum yield drift from the nonlinear pushover analyses in each orthogonal direction discussed in Chapter 2. The definition of ductility provides a quantitative measure of the extent of structural yielding, hence damage.

4.2.2.4 Peak Floor and Roof Acceleration (PFA, and $\mathrm{PFA_R}$)

The peak floor acceleration of any floor was defined as the maximum vector sum of the horizontal components of acceleration of the floor. For the purpose of plotting IDA curves, the roof level PFA was denoted by $\mathrm{PFA_R}$.

4.2.3 IDA Statistical Analysis

The selected IM-DM pairs were evaluated for each analysis. Continuous IDA Curves over the IM domain were generated by fitting the spline (Mathworks Inc., 2004) to the discrete data points for each event. Once the 21 IDA curves were generated, a statistical evaluation of the median and dispersion of the events was performed. This study follows the common assumption of a lognormal distribution (Medina and Krawinkler, 2003); (Vamvatsikos and Cornell, 2002). With this assumption, a comparison of two methods of evaluating the central value (median DM given and IM) and dispersion (standard deviation of the natural logarithm of the DMs given an IM) was carried out.

The first method is based on counted statistics, in which the 21 DM values for a given IM are arranged in an ascending list, then the average of the 3^{rd} and 4^{th} smallest DM defines the 16% fractile, the 11^{th} smallest DM defines the median, and the average of the 17^{th} and 18^{th} smallest DM defines the 84% fractile. Using this method, the dispersion was determined according to (4-2).

$$\sigma_{\ln x} = \ln(\frac{x_{84}}{x_{50}}) \tag{4-2}$$

Where, x_{84} is the 84% fractile DM for a given IM and x_{50} is the median DM for a given IM.

The second method is based on computed statistics. In this method the central value and dispersion are evaluated according to (4-3) and (4-4), respectively.

$$\bar{x} = e^{\overline{\ln x}} \tag{4-3}$$

$$\sigma_{\ln x} = \sqrt{\sum_{i=1}^{n} \frac{(\ln x_i - \overline{\ln x})^2}{n-1}} \tag{4-4}$$

Where, $\overline{\ln x}$ is the mean of the natural logarithm of the data. A comparison of the two methods is presented in Figure 4-1, which depicts the 16% fractile, median, and 84% fractile IDA curves for Building H3. Figure 4-2 compares the dispersion of the DM over the IM domain for both counted and computed statistics. From these comparisons it is noted that the two methods are initially similar but become increasingly dissimilar with increasing IM. This is due to the increasing number of dynamically unstable systems. The computed results are sensitive to these instabilities because the DM values of all 21 events are used in the calculation, therefore if several very large DM values are included the computed values are easily distorted. This is avoided with counted statistics because the values are determined based only on a select few of the DM values. For this reason counted statistics were used throughout this study.

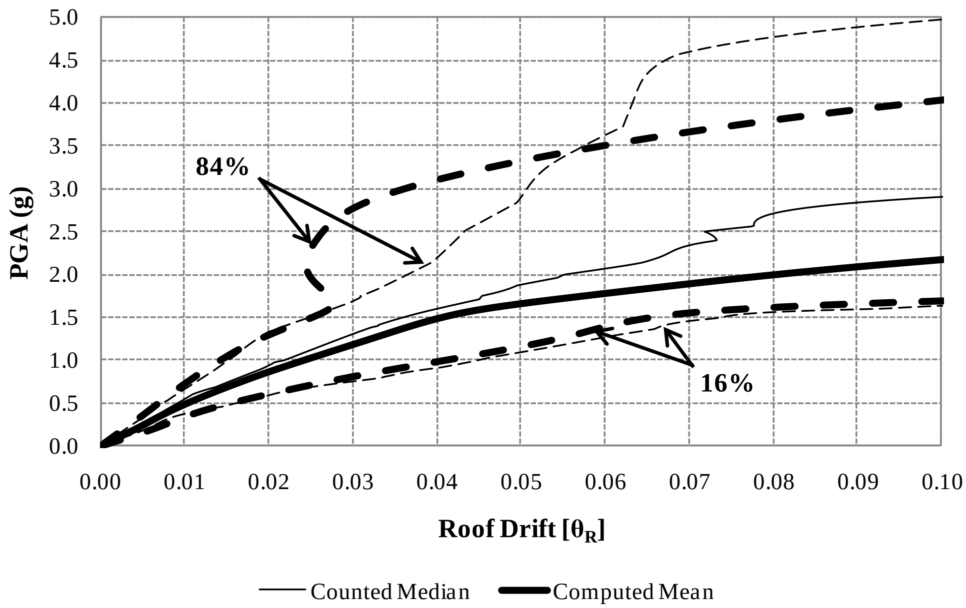

Figure 4-1 Comparison of Counted vs. Computed Statistics for IDA Results

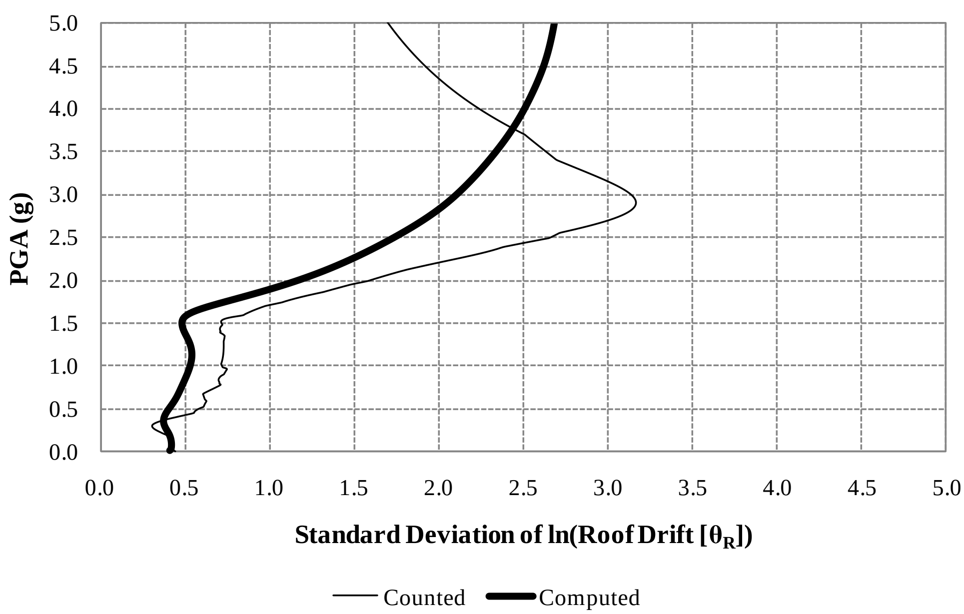

Figure 4-2 Comparison of Counted vs. Computed Dispersion in IDA Results

4.2.4 IDA Curves

The IDA curves presented in this section illustrate a number of demand-capacity relationships of each of the four buildings. These curves relate the ground motion intensity to the floor response, therefore providing a link between the demand on the structure and the demand on the nonstructural components.

4.2.4.1 PGA vs. θ_{max}

The first set of IDA curves plots the PGA against θ_{max}. These curves for each building are shown in Figure 4-3 through Figure 4-6 in which each individual event curve as well as the minimum, maximum, median, 16% fractile, and 84% fractile curves are depicted. A comparison of the median curves is shown in Figure 4-7 as well as a comparison of the dispersion in the data shown in Figure 4-8. These curves relate the intensity of the ground motion in terms of PGA to the level of interstory drift response, which provides a foundation for determining the level of earthquake which may cause various levels of damage due to interstory drift.

In comparing these figures it was noted that the level of drift at which the curves "flatline" is consistently between 8% and 9% interstory drift for all buildings. Because θ_{max} is closely related to instability in SMRF lateral load-resisting systems the consistent nature of the instability drift limit was expected. The small difference between 8% for the taller structures and 9% for the shorter structures is attributed to P-delta effects increasing the moment demands at smaller levels of drift for the taller, heavier structures.

The intensity of ground motion required to force global instability is greater for taller buildings. The taller buildings also have longer periods which results in decreased acceleration demands on the structure because of the smaller ratio of $SA(T_1)/PGA$, thus greater PGA is required to produce a high level of response.

While Building B3 and Building H3 have similar periods, Building H3 appears to require stronger ground motions to induce similar levels of response of Building B3. This is attributed to the difference in design strength between office and hospital structures.

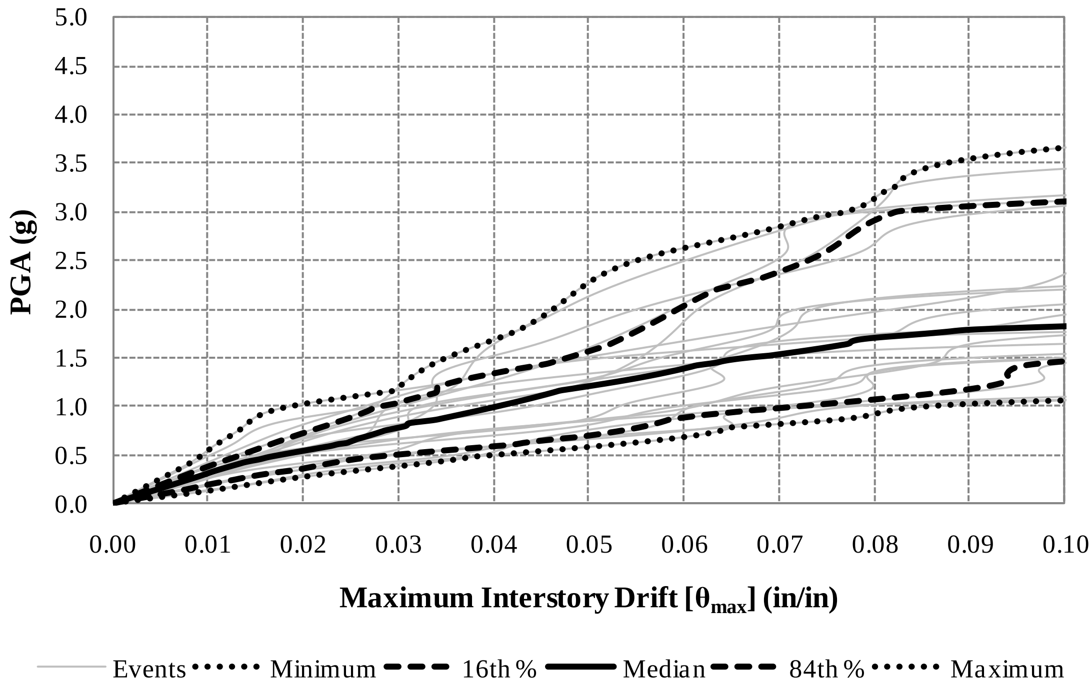

Figure 4-3 IDA PGA vs. θ_{max} [B3]

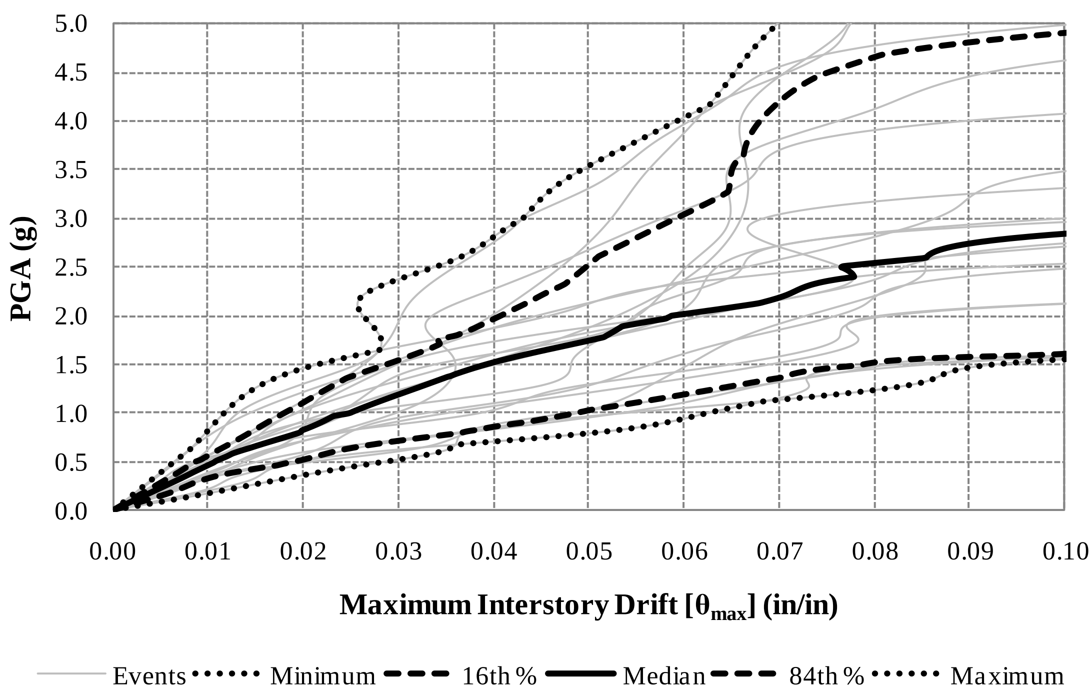

Figure 4-4 IDA PGA vs. θ_{max} [H3]

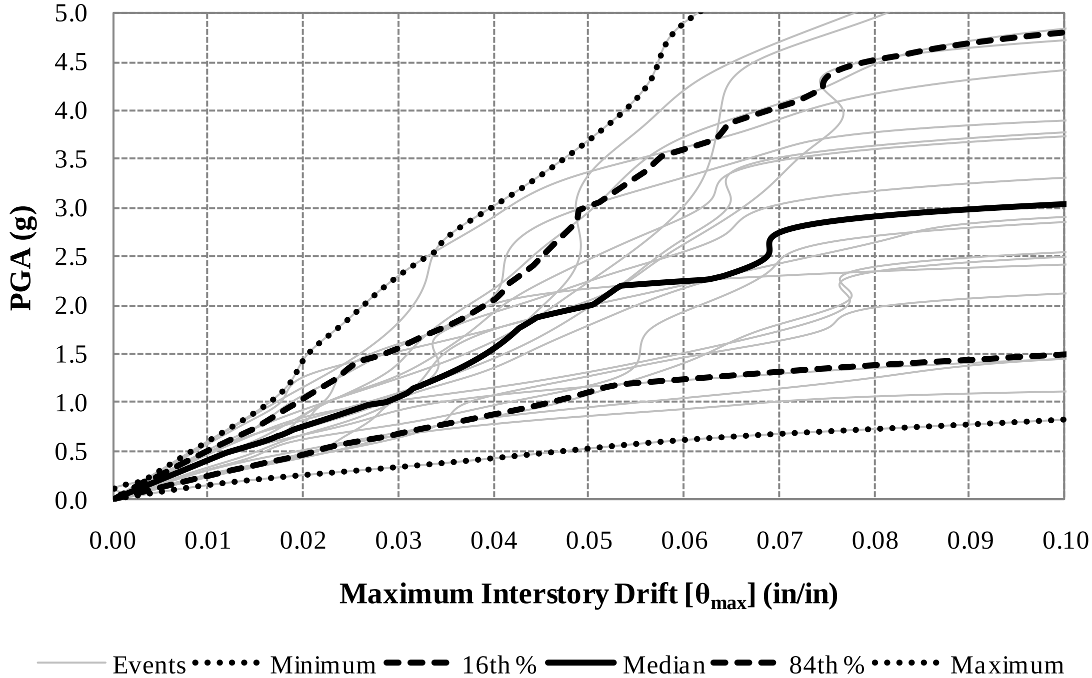

Figure 4-5 IDA PGA vs. θ_{max} [B9]

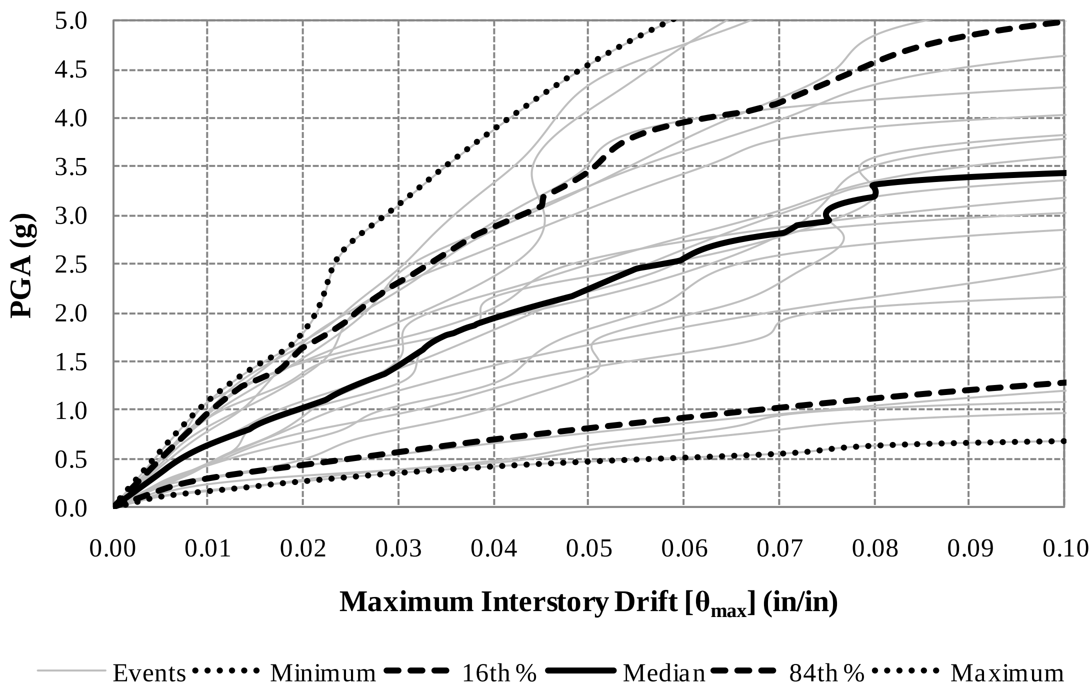

Figure 4-6 IDA PGA vs. θ_{max} [B20]

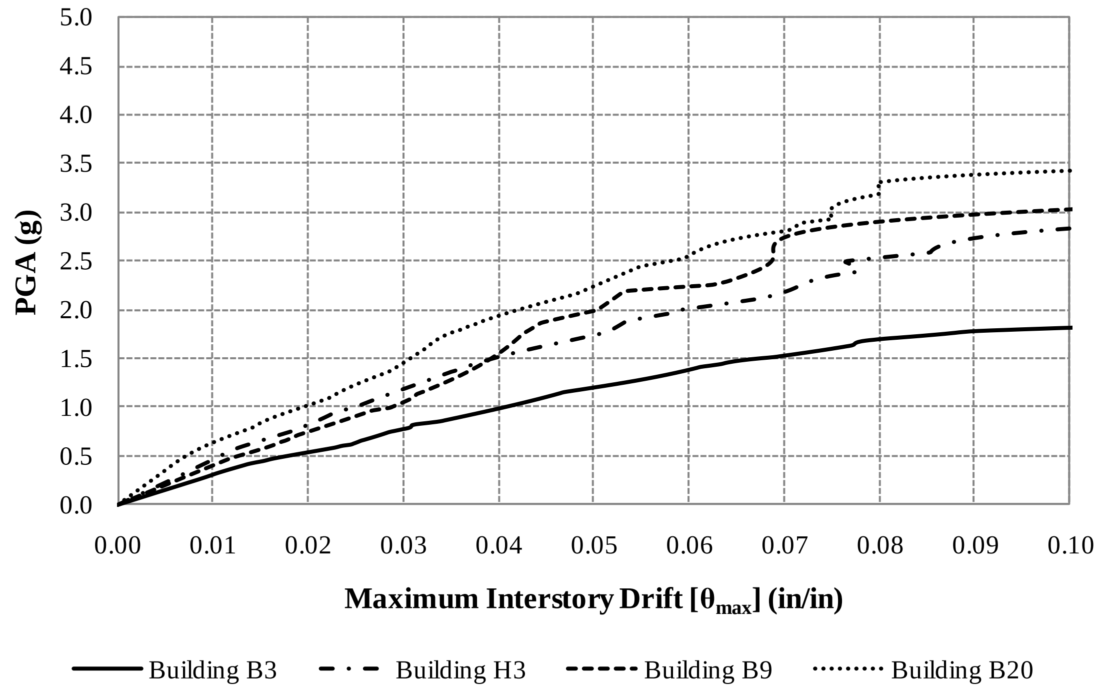

Figure 4-7 Median Comparison of IDA PGA vs. θ_{max}

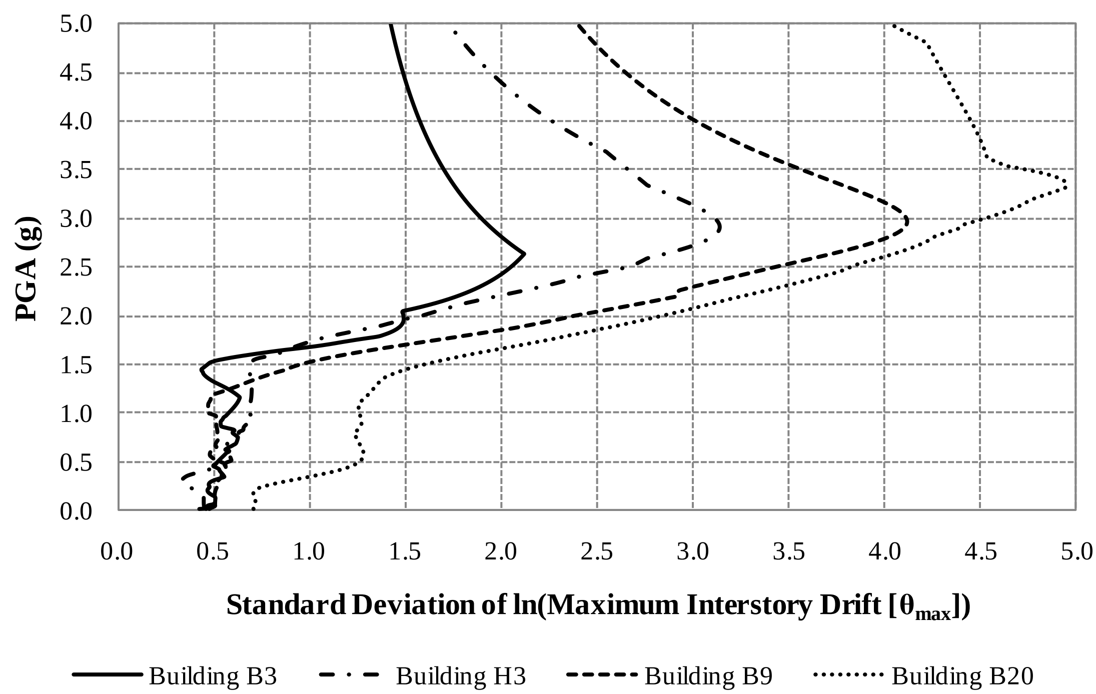

Figure 4-8 Dispersion Comparison of IDA PGA vs. θ_{max}

The dispersion in the maximum interstory drift is observed to remain fairly constant for PGAs up to 1.5 g and then it increases with increasing ground motion intensity. This sudden increase in dispersion of the DM is attributed to exceeding the IM at which the 84% fractile of the DM approaches infinity (16% of the events produce instability in the building). Coincidentally, this occurs at a PGA of approximately 1.5 g for each building. Once this point is exceeded, Building B9 and Building B20 experience a greater increase in the dispersion. The initial dispersion in the DM is consistent among buildings with the exception of Building B20 which is slightly greater than the other buildings. This is assumed to be due to the influence of the higher modes.

4.2.4.2 SA(T_1,5%) vs. θ_{max}

The next set of IDA curves plots SA(T_1,5%) versus θ_{max} in Figure 4-9 through Figure 4-12, which present each individual event curve along with the minimum, maximum, median, 16% fractile, and 84% fractile curves. A comparison of the median curves is presented in Figure 4-13; also a comparison of the dispersion is depicted in Figure 4-14. Switching the IM to SA(T_1,5%) relates the intensity of the ground motion to the elastic fundamental period of the structure and in doing so provides a representation of ground motion intensity that accounts for the resonant properties of the building.

Comparing this set of curves against the previous set provides evidence that the amount of dispersion in the elastic region of these curves is greatly reduced from the previous set. Because the elastic response of these structures is dominated by the first mode, using the spectral acceleration of the ground motion at the first modal period of the structure more accurately estimates the seismic demand imposed on the structure by the ground motion, thus reducing the dispersion in the demand-capacity curves.

It is also observed that the spectral acceleration required to produce large drifts in taller buildings is less than in shorter buildings. This observation is consistent with the design codes which require lower seismic design factors for long period structures.

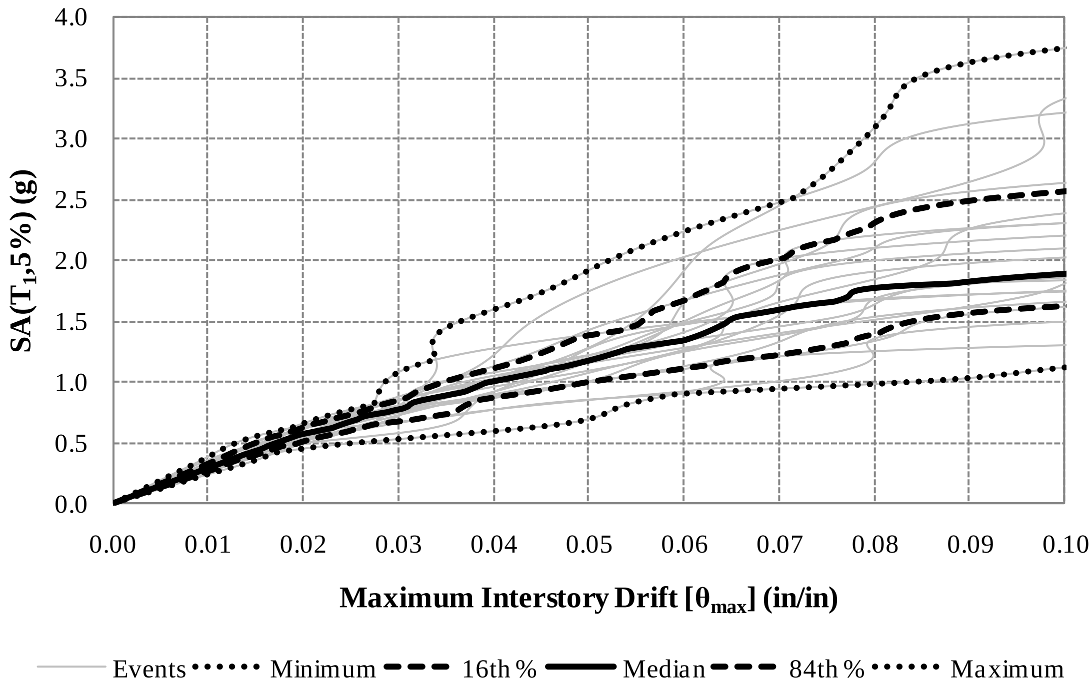

Figure 4-9 IDA SA(T_1,5%) vs. θ_{max} [B3]

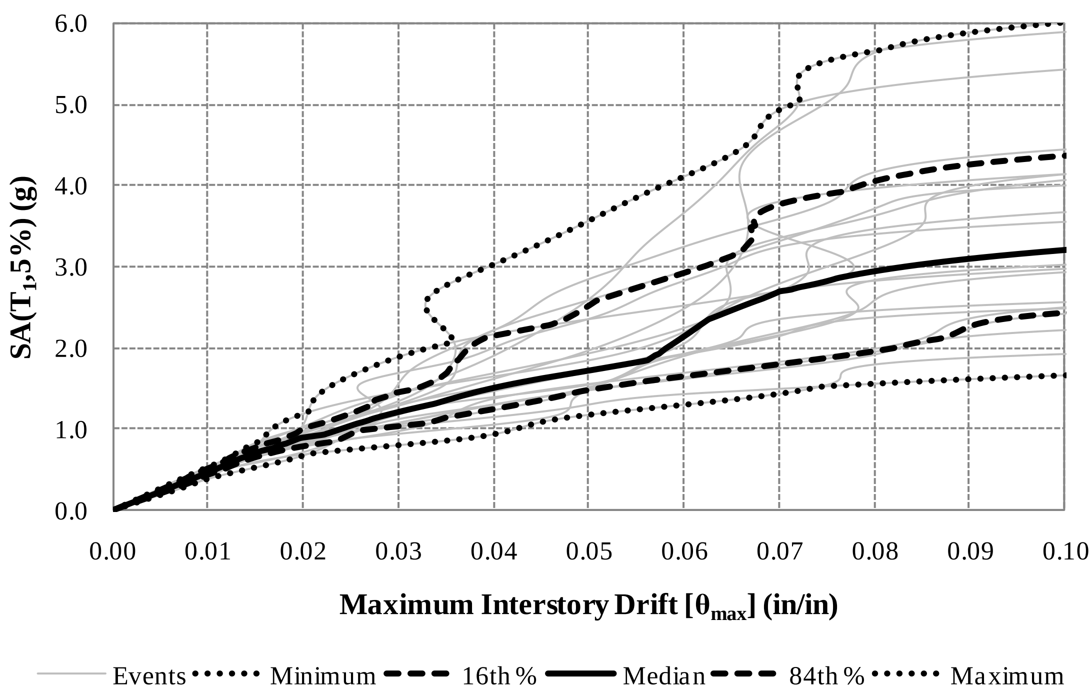

Figure 4-10 IDA SA(T_1,5%) vs. θ_{max} [H3]

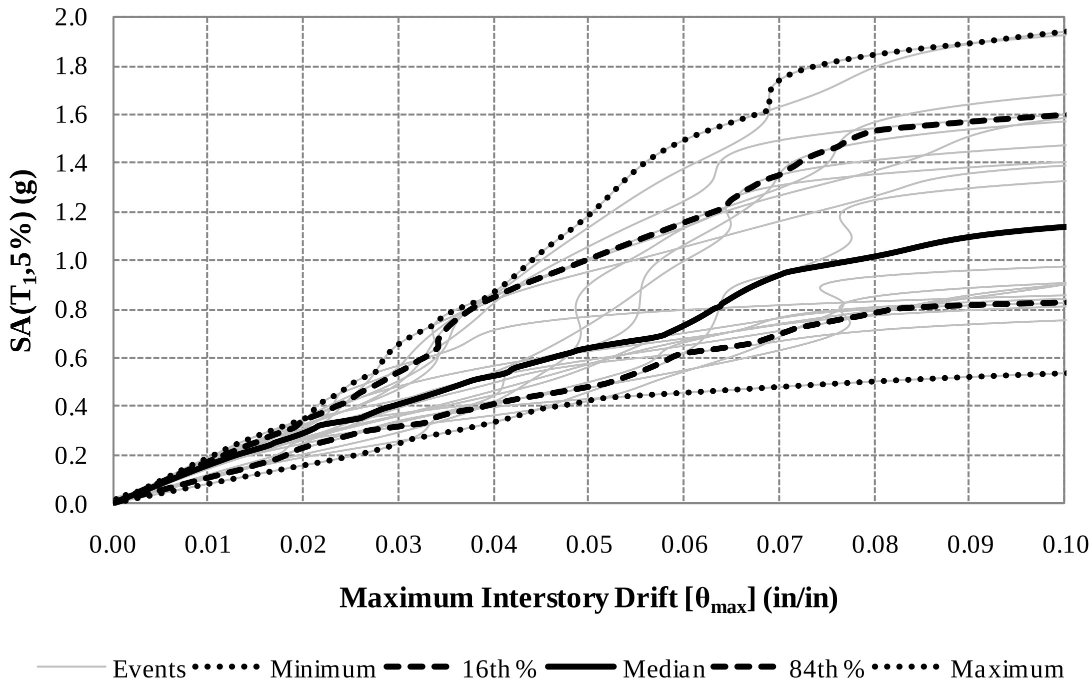

Figure 4-11 IDA SA(T_1,5%) vs. θ_{max} [B9]

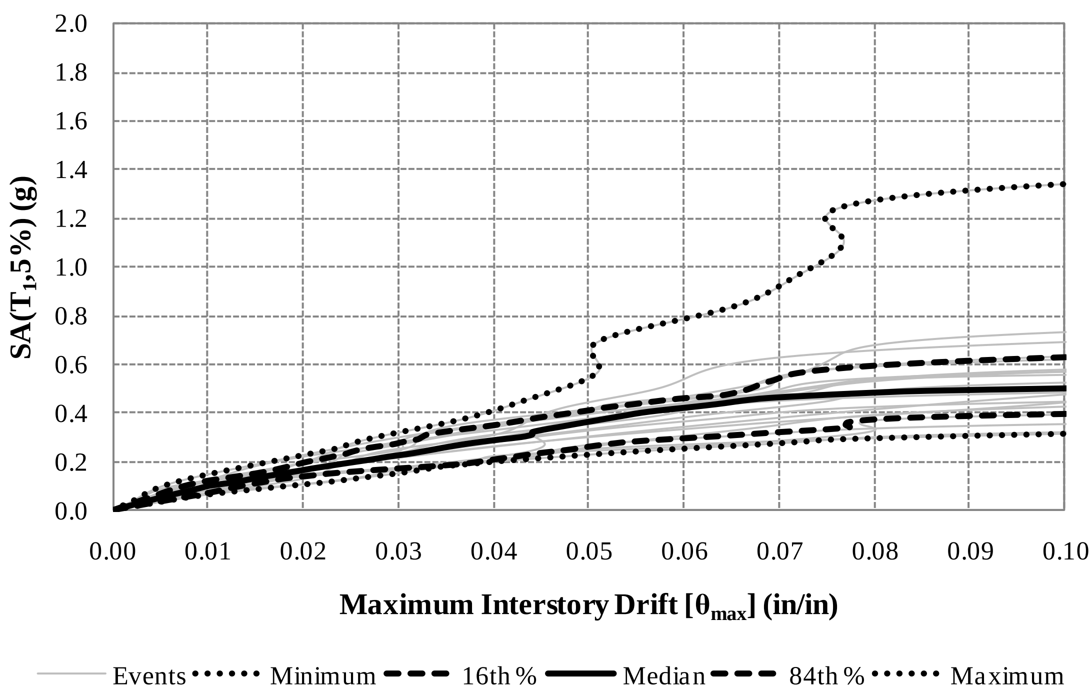

Figure 4-12 IDA SA(T_1,5%) vs. θ_{max} [B20]

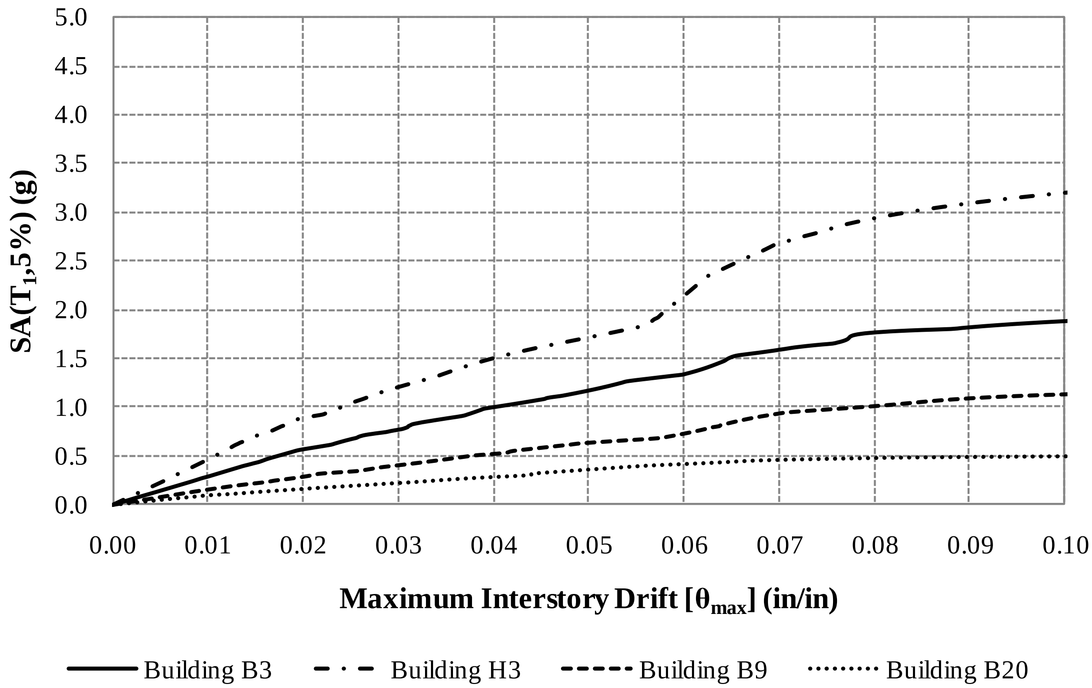

Figure 4-13 Median Comparison of IDA SA(T_1,5%) vs. θ_{max}

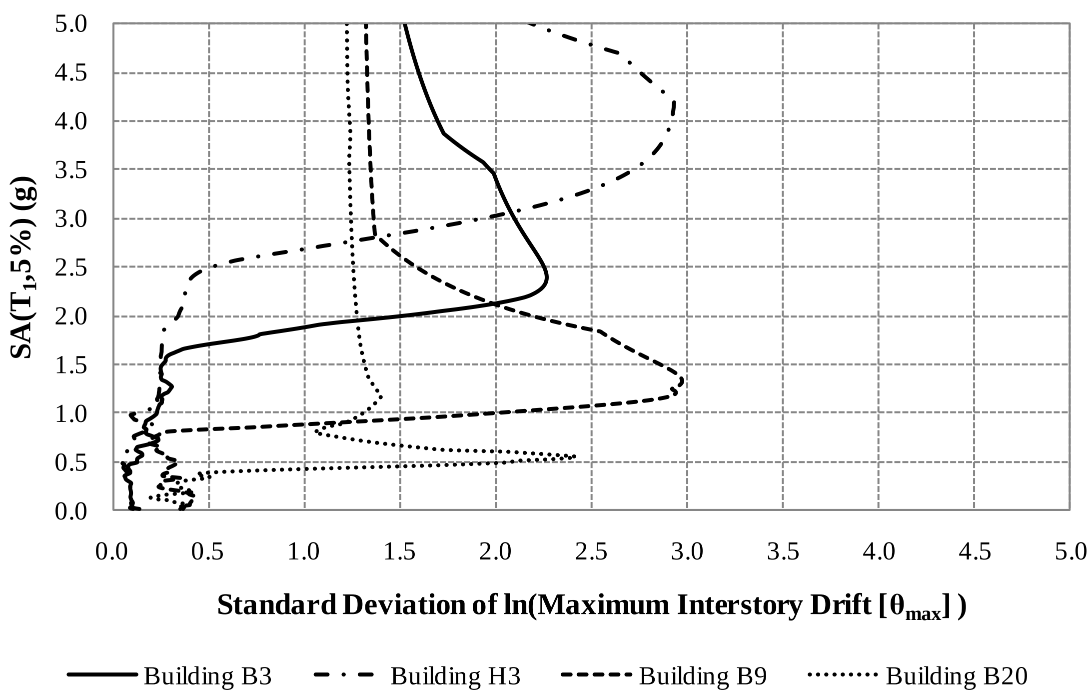

Figure 4-14 Dispersion Comparison of IDA SA(T_1,5%) vs. θ_{max}

Examining the comparison of the dispersion confirms the previous observation that the dispersion of DM values is reduced in the initial elastic region. The influence of the higher modes is more prevalent in this set however as both Building B9 and B20 show greater dispersion in the elastic region than the shorter buildings. While the trend observed in the previous set, that the dispersion in the DM suddenly increases after instability of 16% of the events, holds true for this set as well, the IM at which this occurs for each building is no longer similar. In this set it is possible to distinguish the stronger buildings from the weaker ones by observing the IM associated with the increased dispersion.

4.2.4.3 PGA vs. θ_R

The next set of IDA curves plots PGA versus θ_R in Figure 4-15 through Figure 4-18, which presents each individual event curve along with the minimum, maximum, median, 16% fractile, and 84% fractile curves. A comparison of the median curves is presented in Figure 4-19. In addition a comparison of the dispersion is presented in Figure 4-20. Changing the DM from θ_{max} to θ_R provides a global perspective of the level of drift as opposed to a local interstory perspective. In doing so a measure of average structural drift is developed, which leads to a measure of average structural ductility.

The examination of these curves in comparison with the first set of curves shows that the roof drift at which each structure becomes unstable is far less consistent among structures than interstory drift. It is commonly observed in mid- to high-rise SMRF systems that a majority of the lateral deformation occurs in the lower floors while the upper floors experience far less interstory drift. As a result, the drift profile in taller SMRFs is generally not uniform throughout the height. This explains why the roof drift at which Building B20 becomes unstable is significantly less than Building B3. Section 4.3.3 discusses in further detail this observation as it compares the drift profiles of the four buildings. The dispersion in the roof drifts for a given PGA follows similar trends to the dispersion in the maximum interstory drifts.

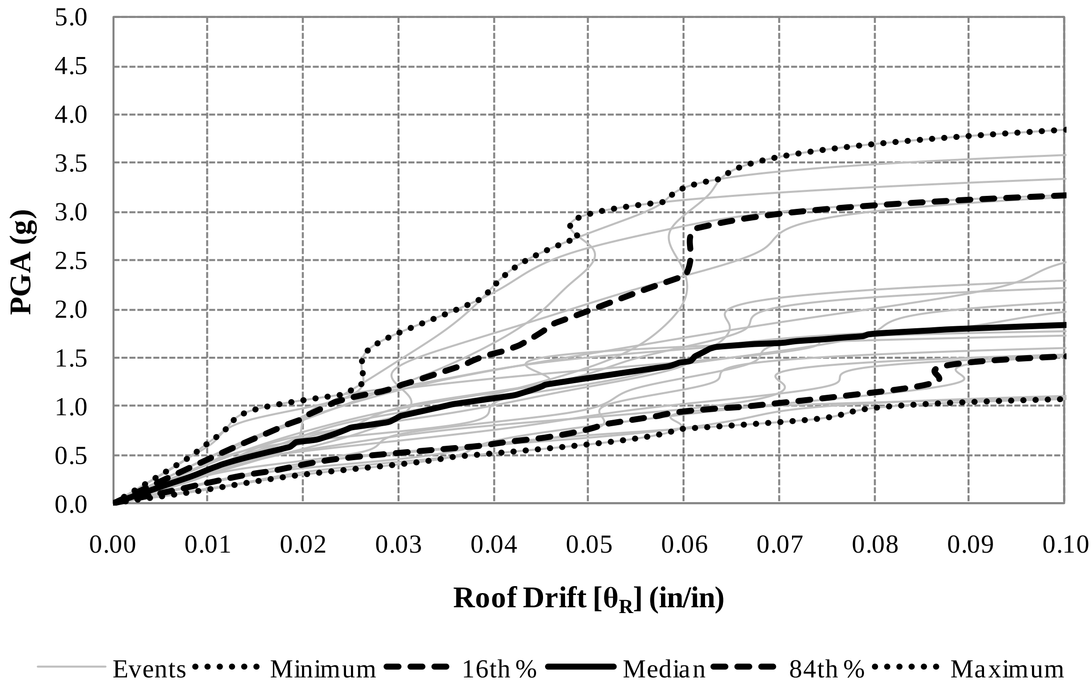

Figure 4-15 IDA PGA vs. θ_R [B3]

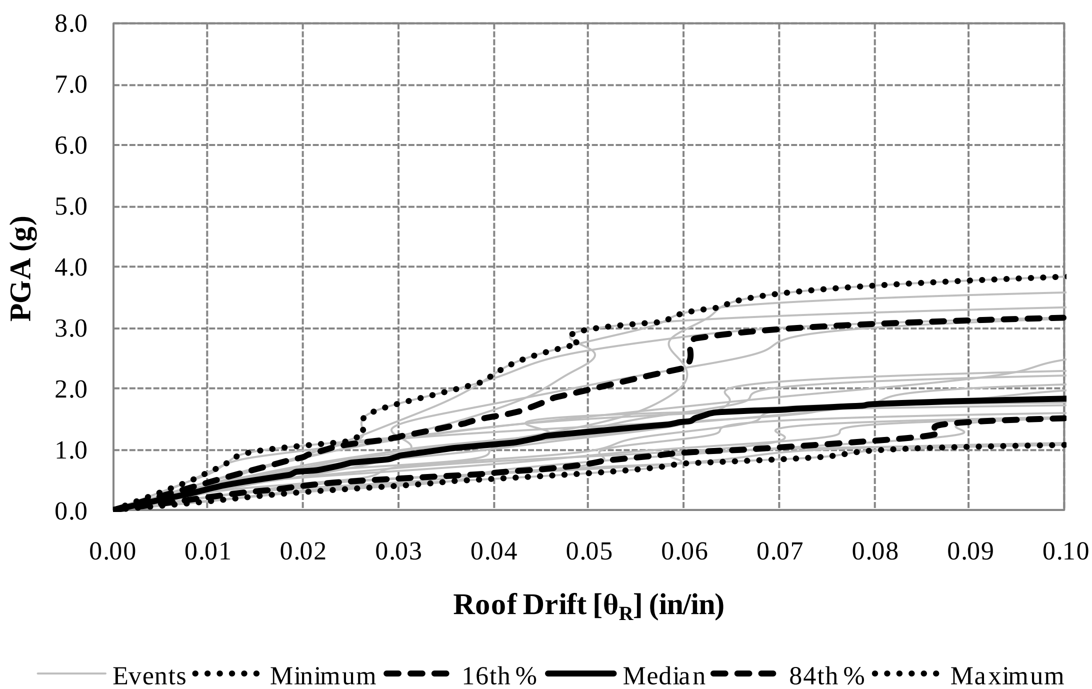

Figure 4-16 IDA PGA vs. θ_R [H3]

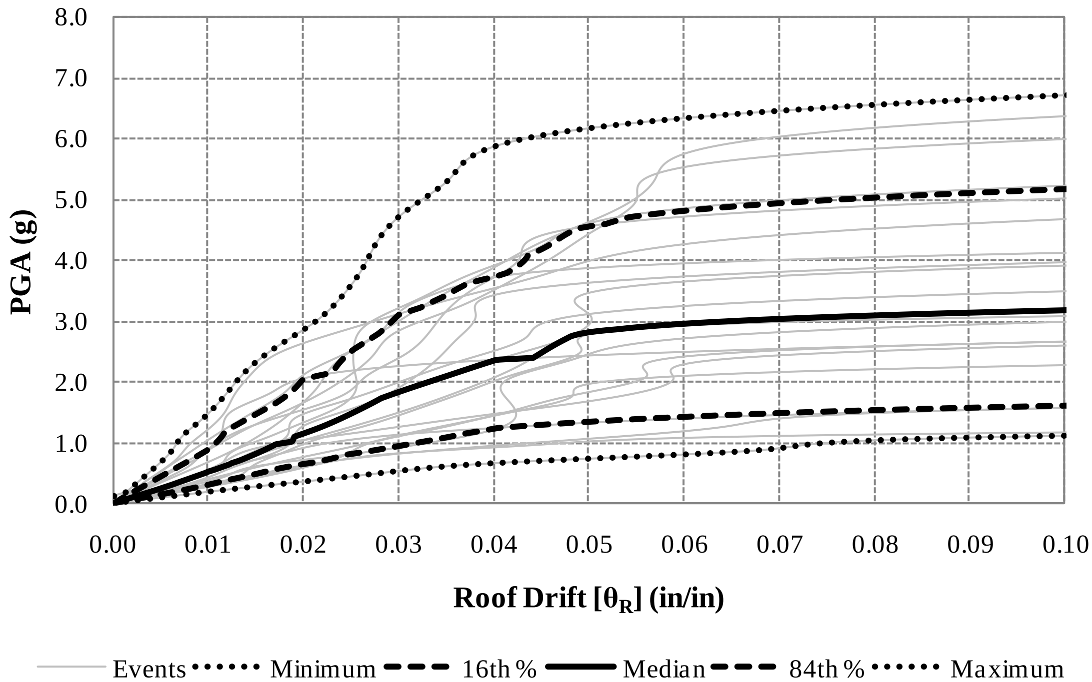

Figure 4-17 PGA vs. θ_R [B9]

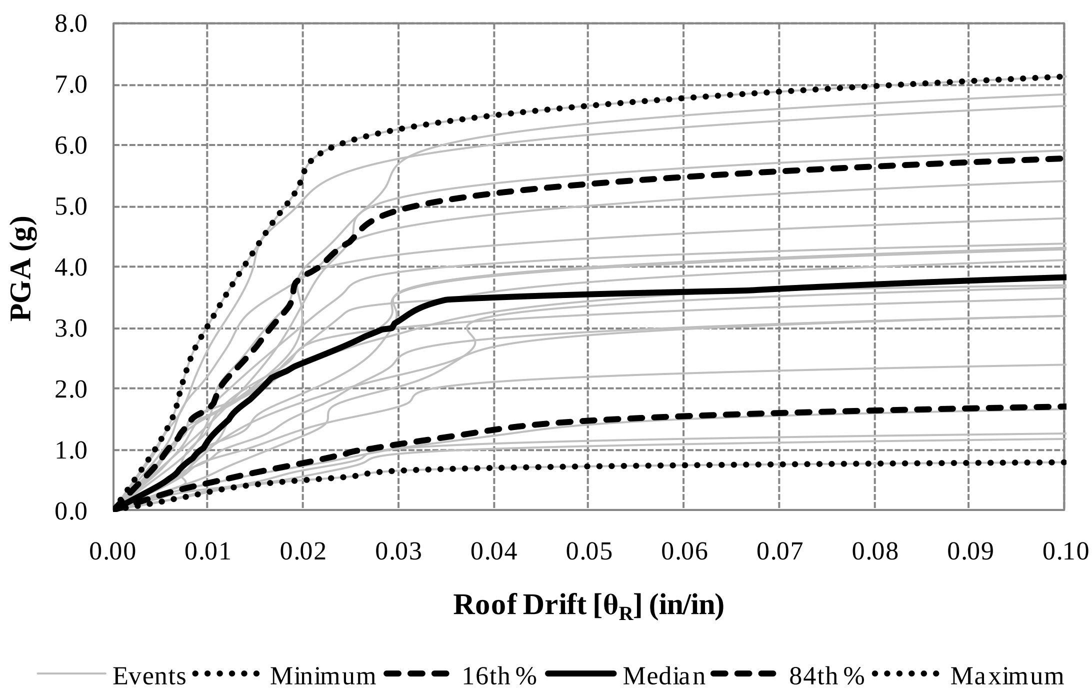

Figure 4-18 IDA PGA vs. θ_R [B20]

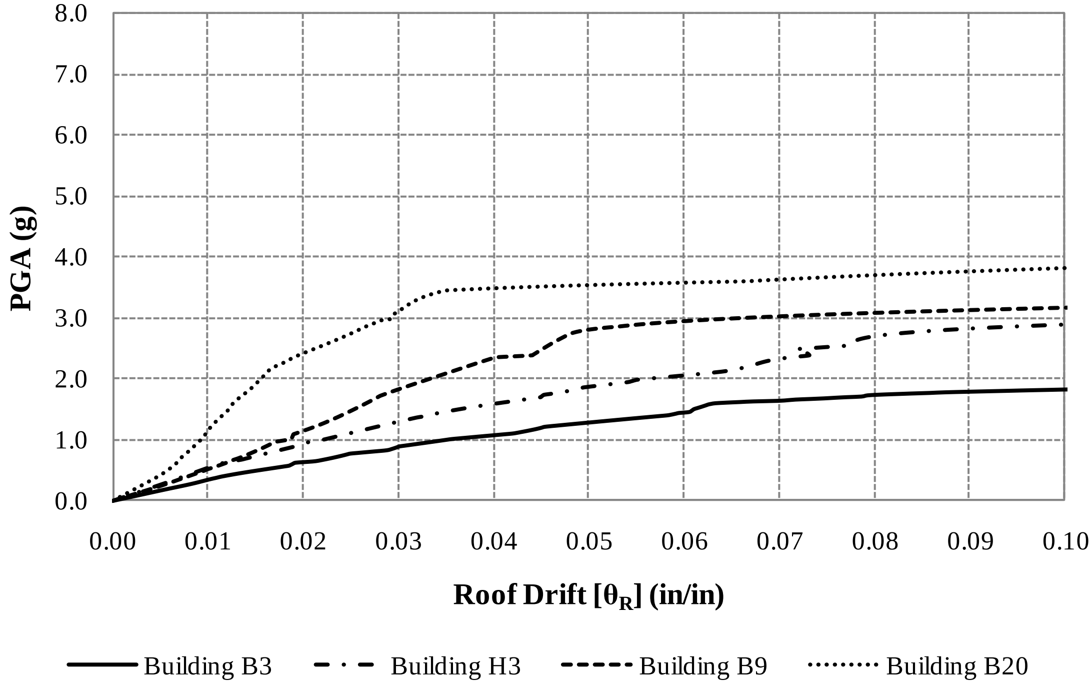

Figure 4-19 Median Comparison of IDA PGA vs. θ_R

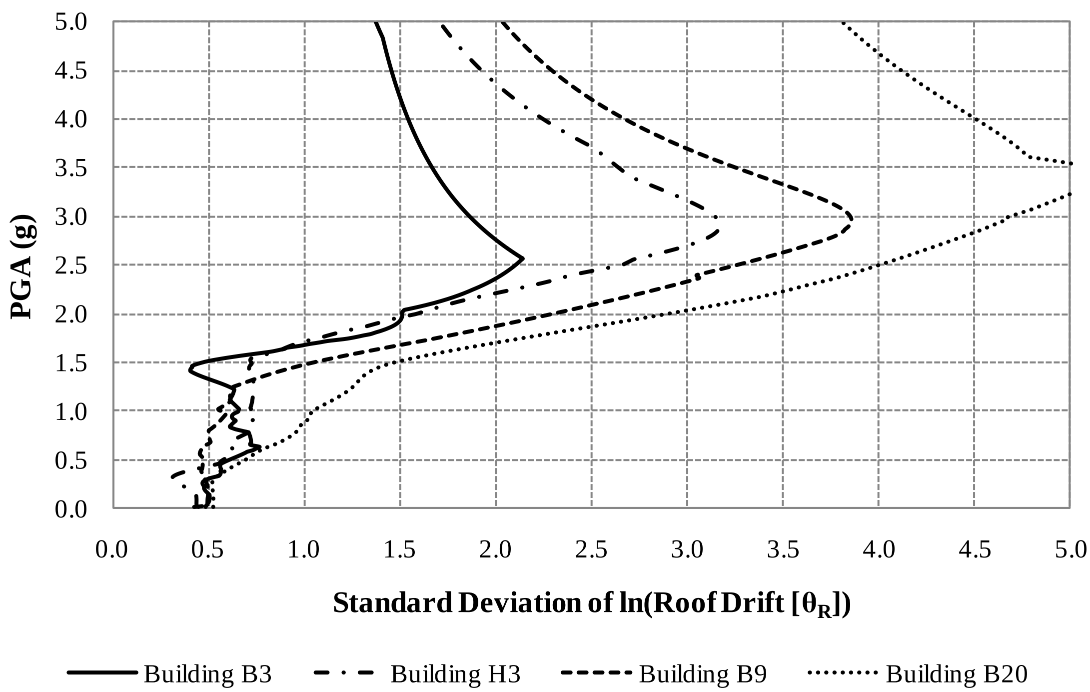

Figure 4-20 Dispersion Comparison of IDA PGA vs. θ_R

4.2.4.4 SA(T_1,5%) vs. θ_R

The last set of IDA curves using a drift measure as the DM plots SA(T_1,5%) versus θ_R in Figure 4-21 through Figure 4-24, in which each individual event curve is shown along with the minimum, maximum, median, 16% fractile, and 84% fractile curves. A comparison of the median curves is presented in Figure 4-25 while the dispersion is compared in Figure 4-26. This IM-DM pair defines a set of curves with coordinates similar to the nonlinear static pushover curves of Chapter 2. As such, the median IDA curves are compared the pushover curves in Figure 4-27.

From this set of IDA curves it is noted that the dispersion of the IDA curves is reduced using SA(T_1,5%) as opposed to PGA, which confirms the previously drawn conclusion. Also, the IDA curves have greater capacity than the pushover curves. This observation is common to IDA as presented in (Vamvatsikos and Cornell, 2002) and holds true for this study as well. Lastly, the initial slopes of the IDA and pushover curves are equal. The initial elastic period of the structure determines the slope of these lines and the fact that they are comparable verifies the similarity of the coordinate system in which the curves are plotted.

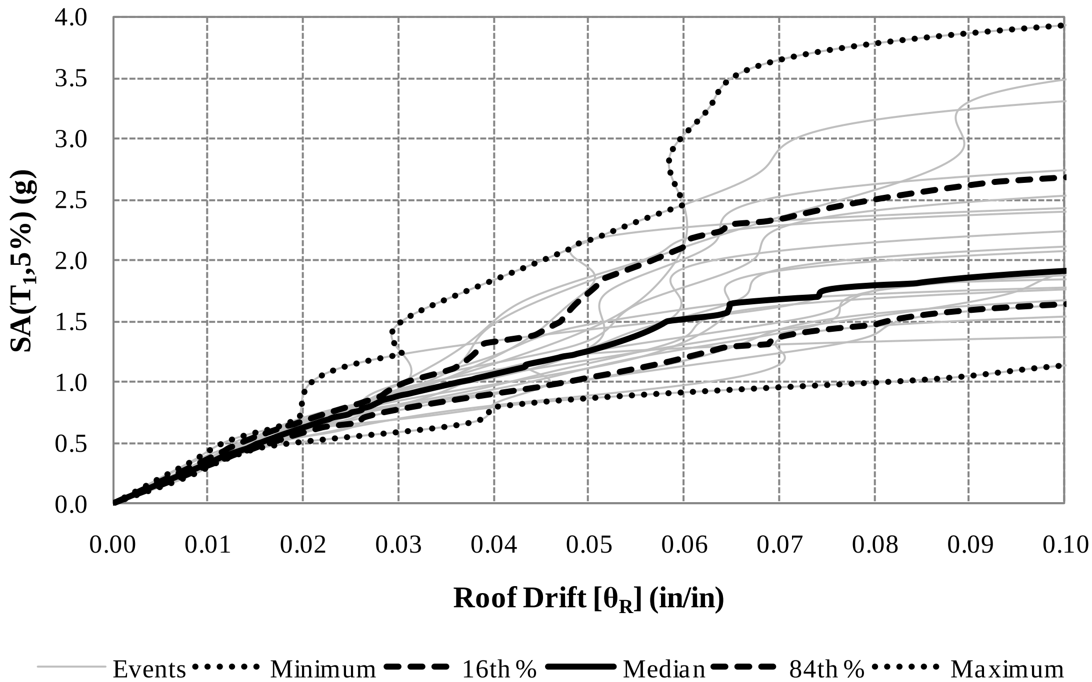

Figure 4-21 IDA SA(T_1,5%) vs. θ_R [B3]

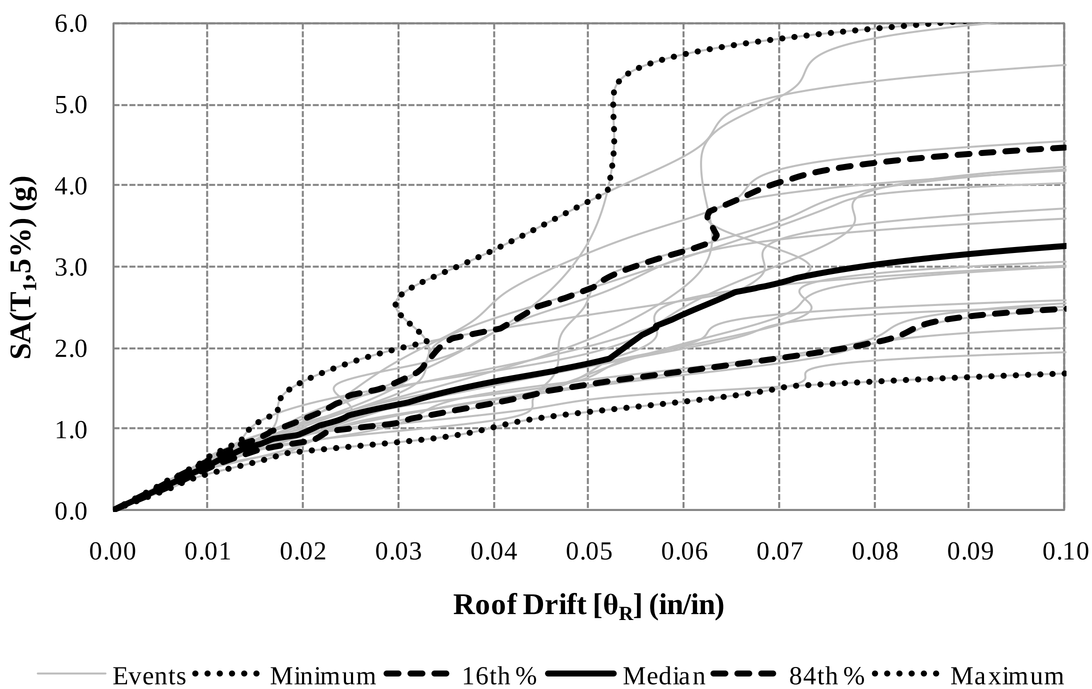

Figure 4-22 IDA SA(T_1,5%) vs. θ_R [H3]

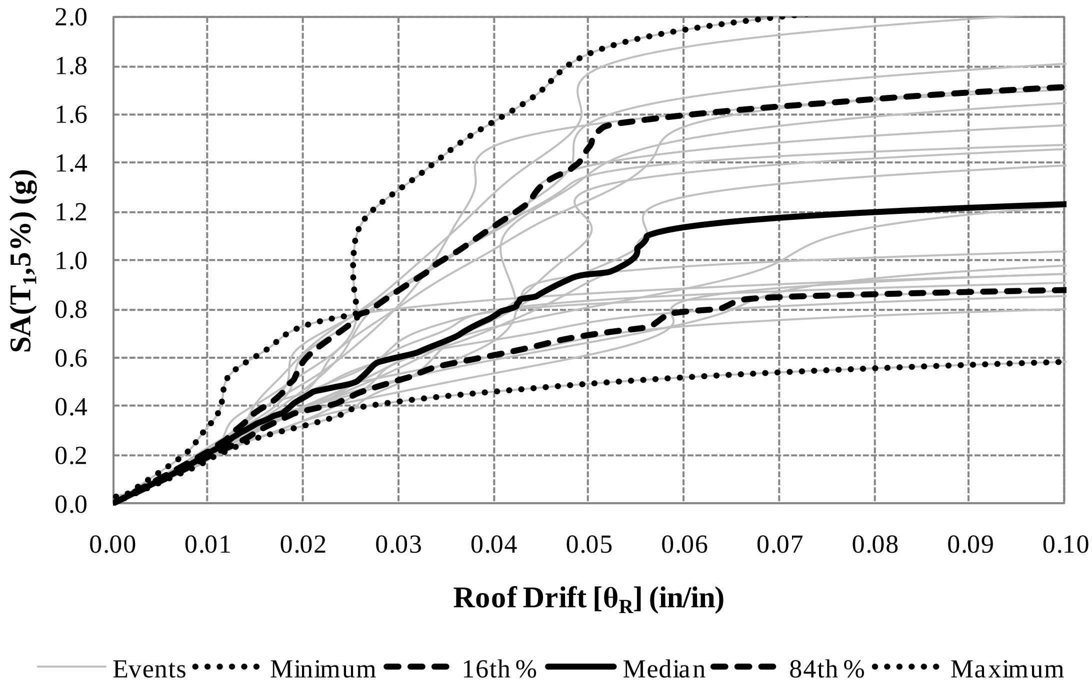

Figure 4-23 IDA SA(T_1,5%) vs. θ_R [B9]

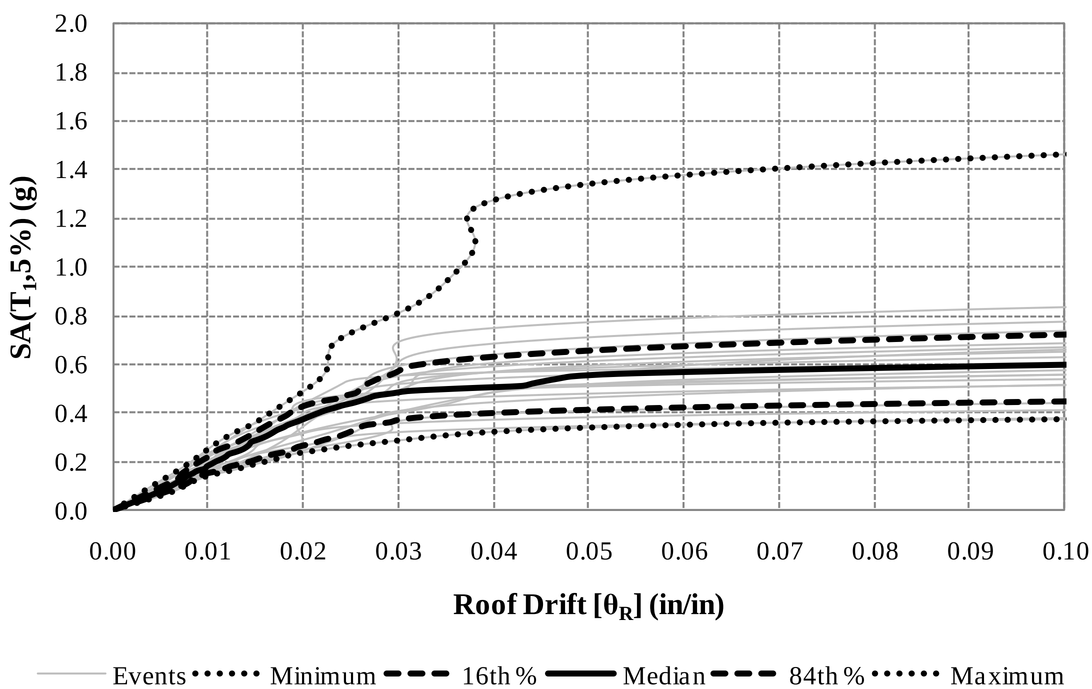

Figure 4-24 IDA SA(T_1,5%) vs. θ_R [B20]

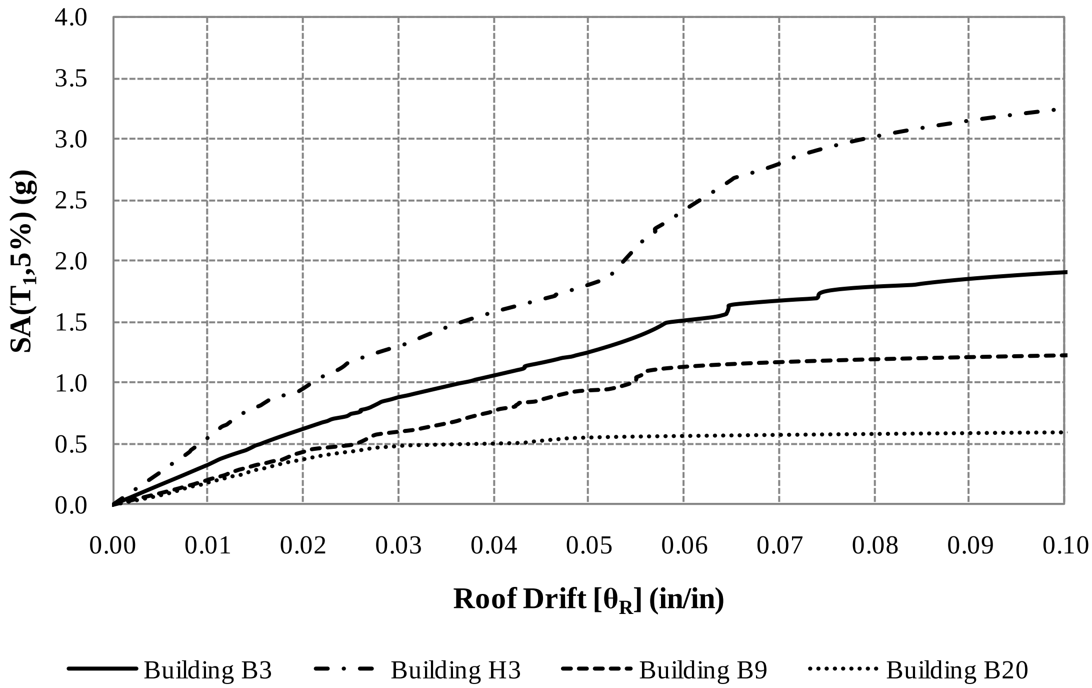

Figure 4-25 Median Comparison of IDA SA(T_1,5%) vs. θ_R

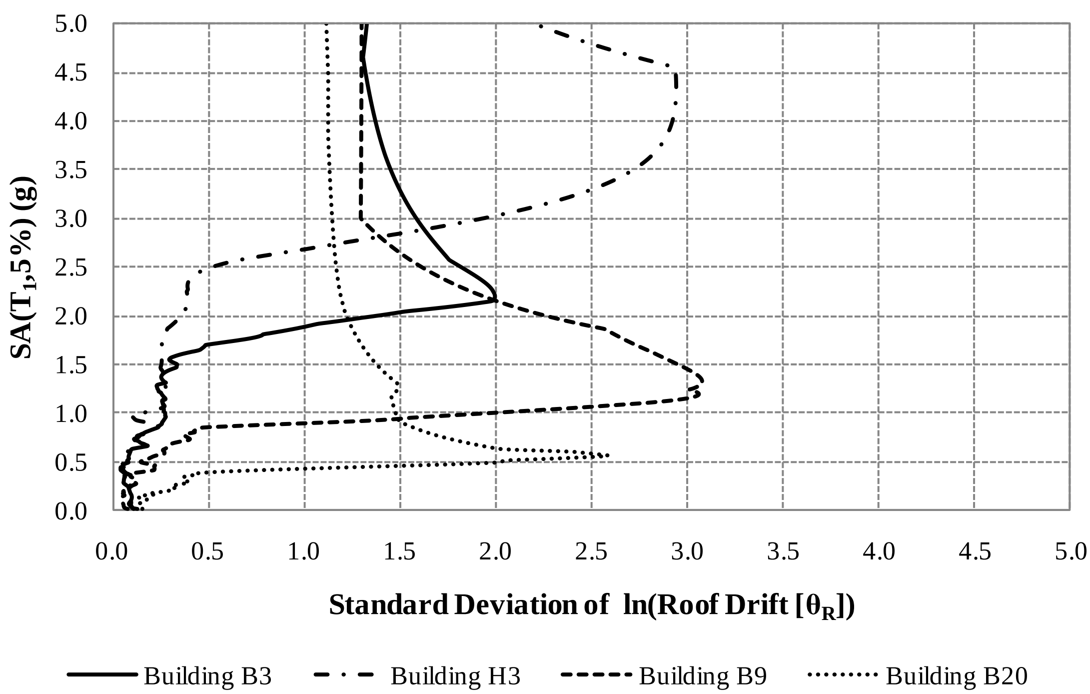

Figure 4-26 Dispersion Comparison of IDA SA(T_1,5%) vs. θ_R

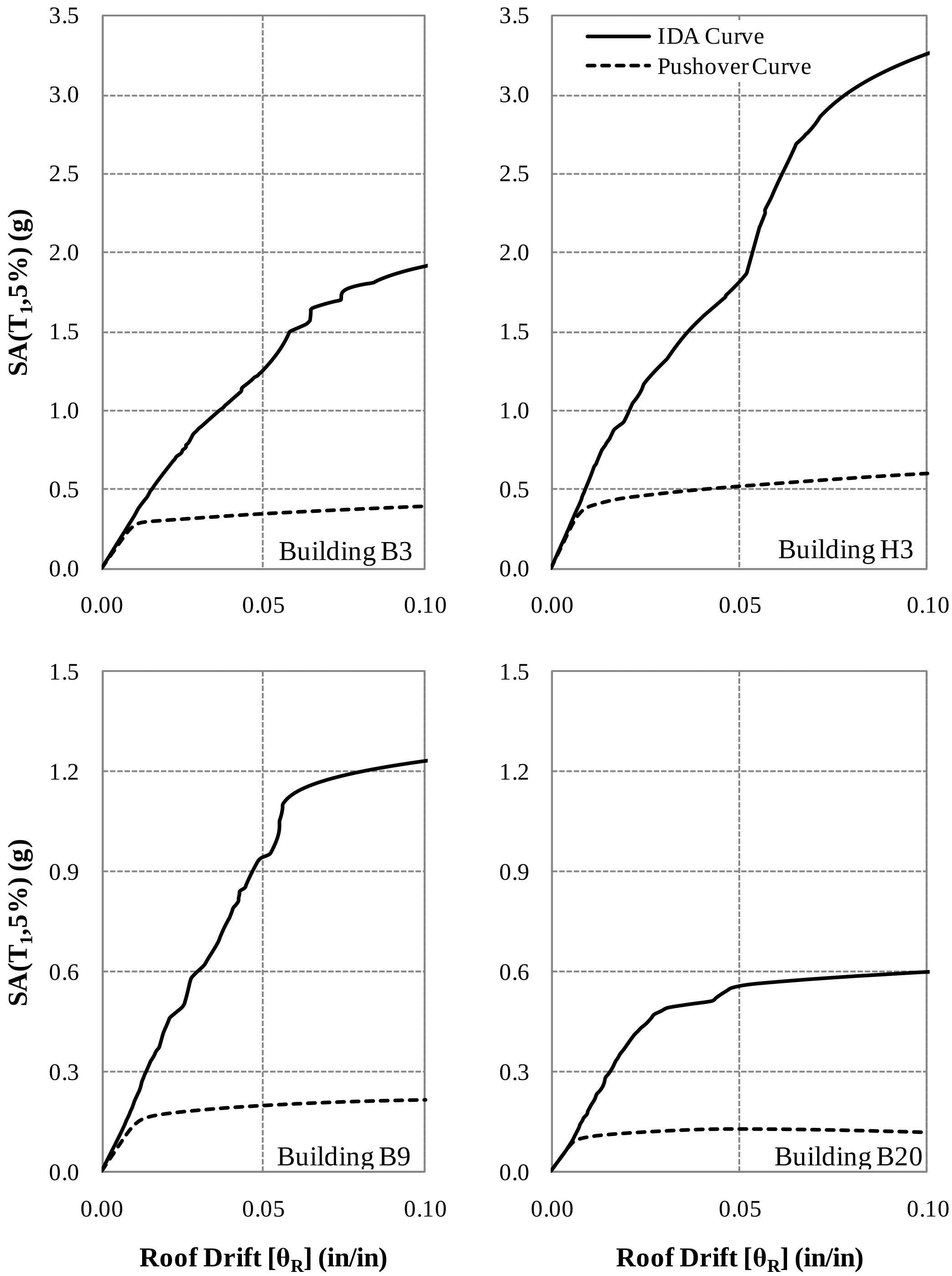

Figure 4-27 Comparison of IDA and Pushover Curves

4.2.4.5 PGA vs. PFA_R

The final set of IDA curves presented in this study plots PGA against PFA_R in Figure 4-28 through Figure 4-31, which depict each individual event curve in addition to the minimum, maximum, median, 16% fractile, and 84% fractile curves. The median curves and dispersion are compared in Figure 4-32 and Figure 4-33, respectively.

The first obvious observation when looking at these curves is that the shape of the curve is very different from those which use a measure of response displacement as the DM. This IM-DM pair produces curves which converge to infinite slope as opposed to a slope equal to zero. Similar to the previous curves, there is an initial linear region of the curve which occurs prior to the structure yielding. It was noted that the initial slope of the PGA-PFA_R curves varies among buildings. In addition, it was observed that the maximum roof acceleration achieved by the stronger buildings exceeds that of the weaker buildings.

4.2.5 Combination of IDA Curves for Assessment of Engineering Demand Parameters

Many of the relationships derived in the remainder of this report are based on the combination of IDA curves in order to correlate two damage measures. This is completed using the following process. First, two sets of IDA curves are generated; the first set uses one of the objective DM, the second set uses the other objective DM, and each uses the same IM. The next step takes advantage of the fact that the IDA curves are generated as functions of the IM by recognizing that data points of the first set correspond to data points of the second set through similar values of the IM. As a result, new data pairs are formed by collecting the DMs of corresponding IMs and plotting the relationship between DMs of the two IDA sets. This procedure is mapped in Figure 4-34.

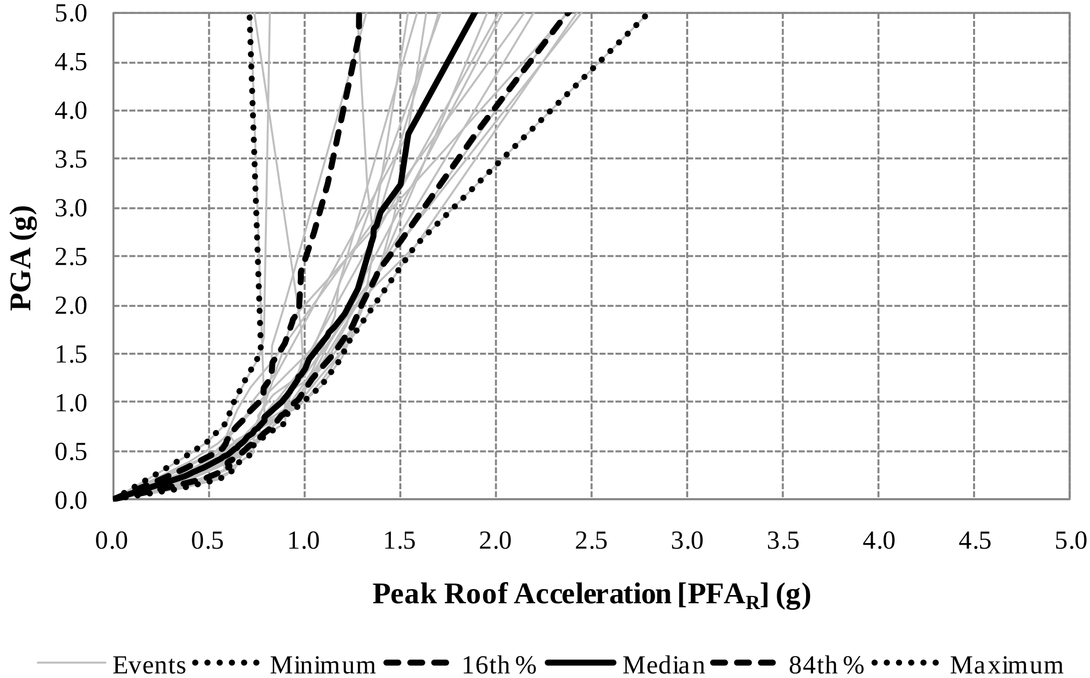

Figure 4-28 IDA PGA vs. PFA_R [B3]

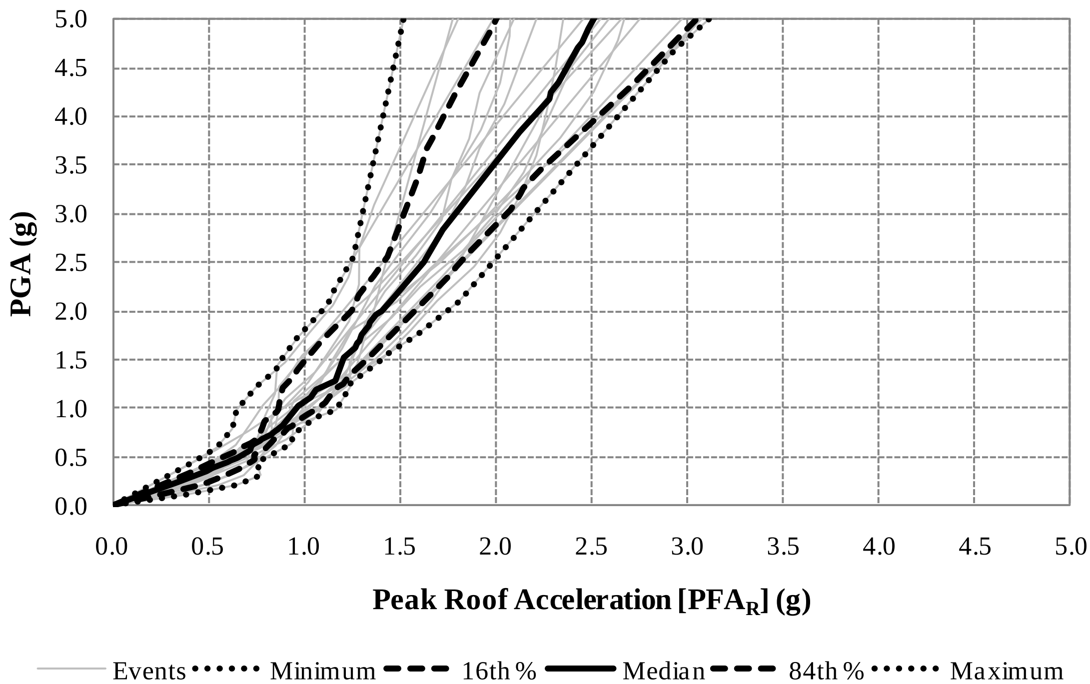

Figure 4-29 IDA PGA vs. PFA_R [H3]

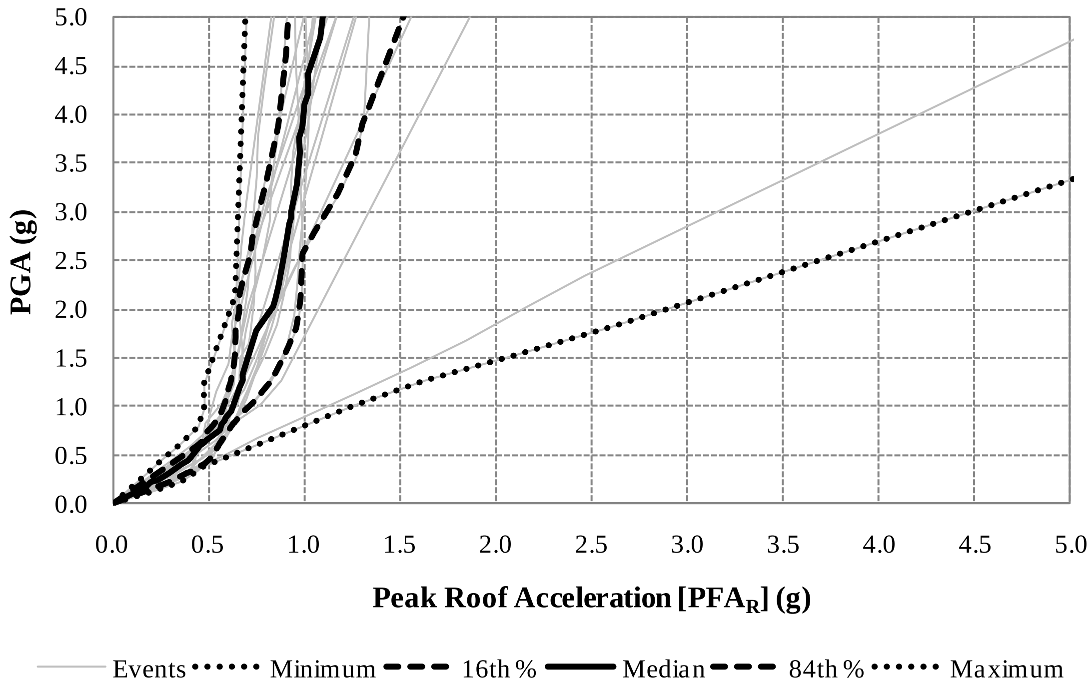

Figure 4-30 IDA PGA vs. PFA_R [B9]

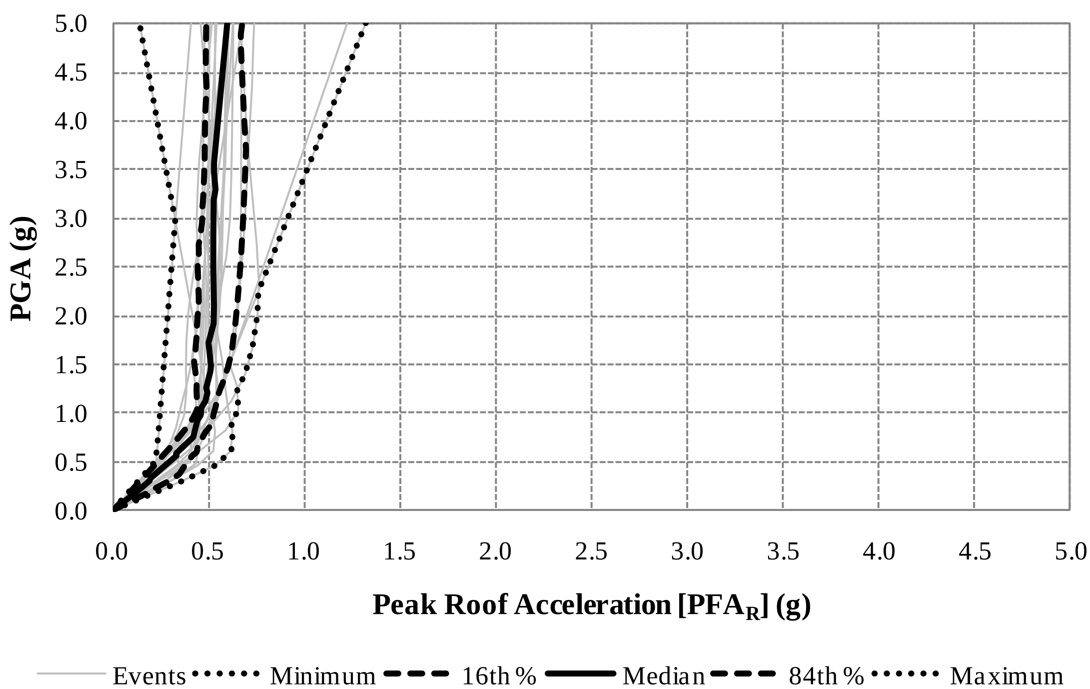

Figure 4-31 IDA PGA vs. PFA_R [B20]

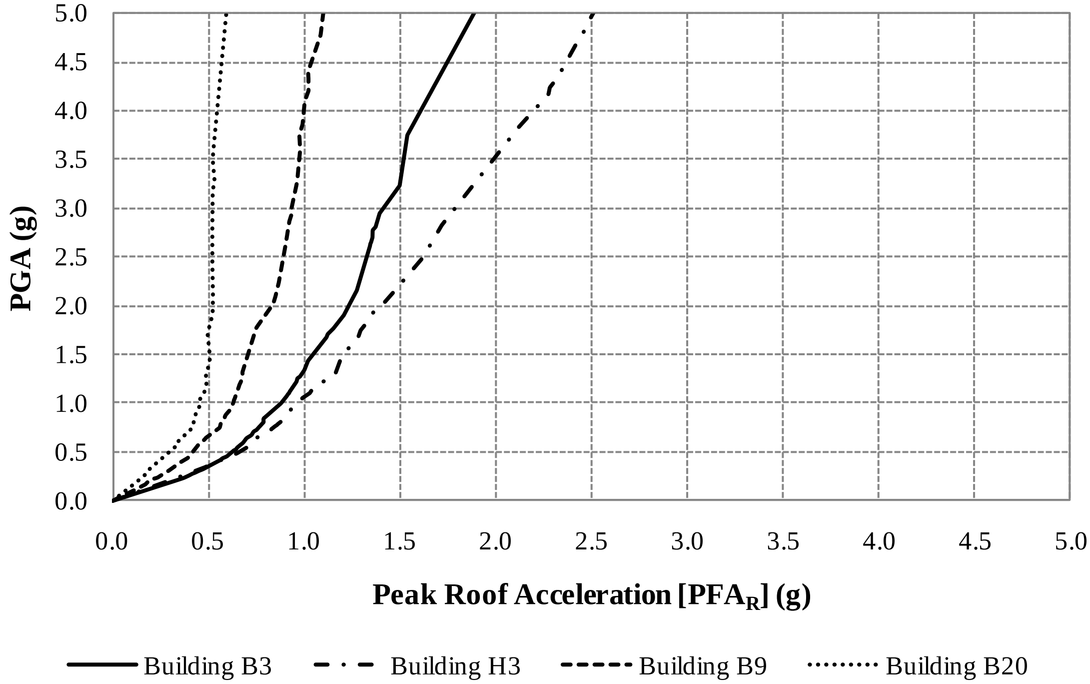

Figure 4-32 Median Comparison of IDA PGA vs. PFA_R

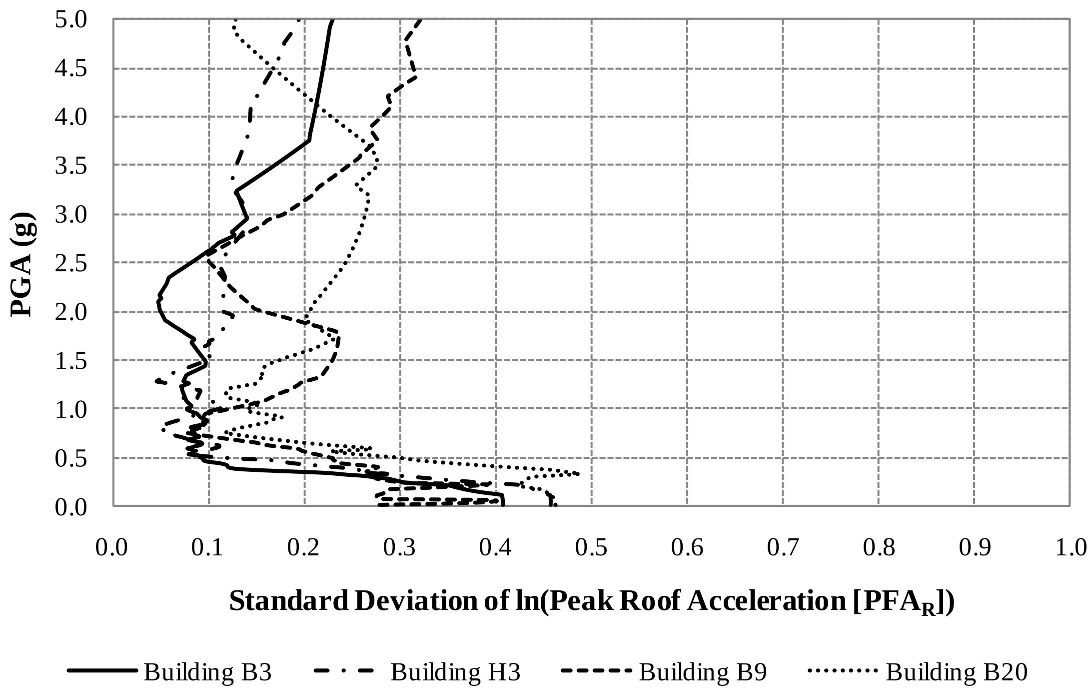

Figure 4-33 Dispersion Comparison of IDA PGA vs. PFA_R

Another part of the data processing worth noting is the development of constant ductility curves. This procedure is highlighted in the flow chart shown in Figure 4-35. The procedure takes the data from specific nonlinear analyses (runs) and fits a spline curve creating the IDA curve for each event. Then in a similar manner to Figure 4-34 interpolates and intensity that corresponding to a given ductility level. This intensity of motion most probably was not specifically run through a nonlinear analysis, however it is assumed to produce a ductility of the specified level through interpolation. With this interpolated intensity the corresponding objective response parameter is determined from its IDA curve. This procedure makes the assumption that in developing the IDA curves the runs are at small enough intervals to introduce relatively small error from interpolation. This assumption is more appropriate at low levels of intensity when the buildings respond elastically, and more error is introduced as the nonlinearity is present.

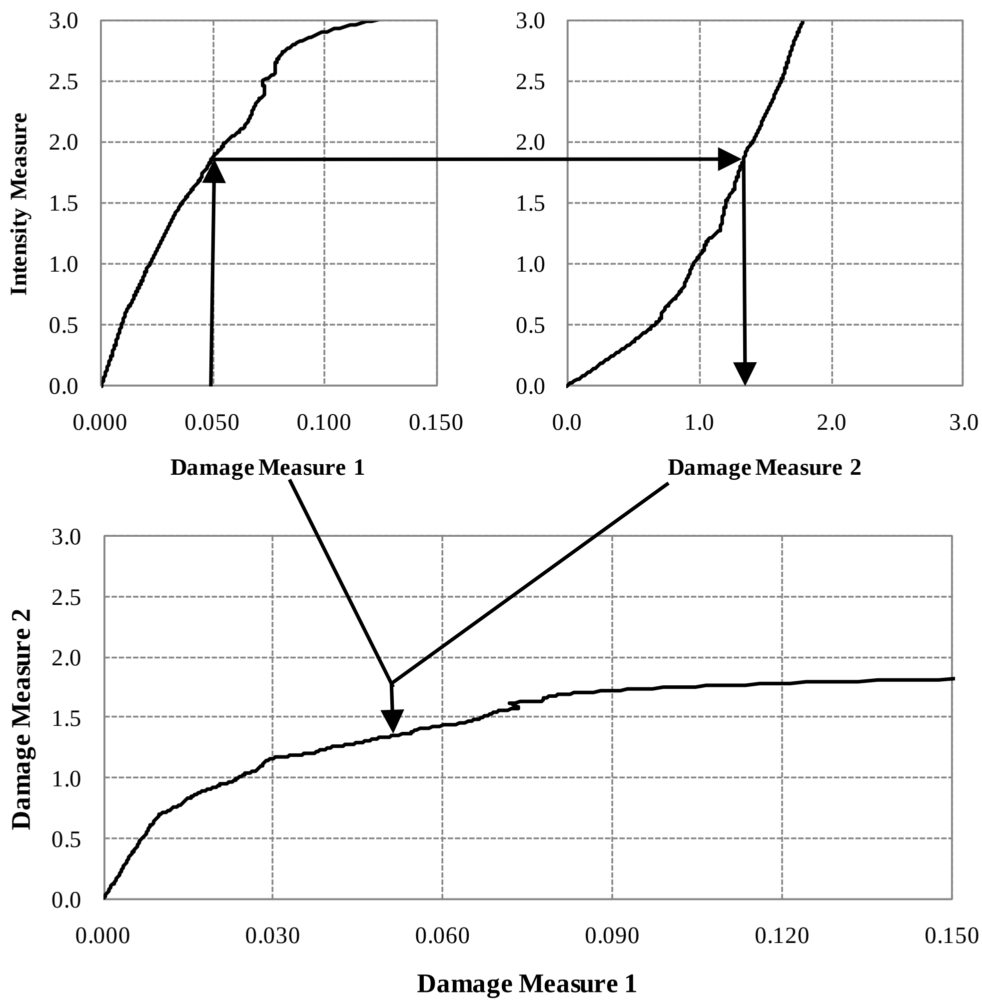

Figure 4-34 Combination of two IDA Curves

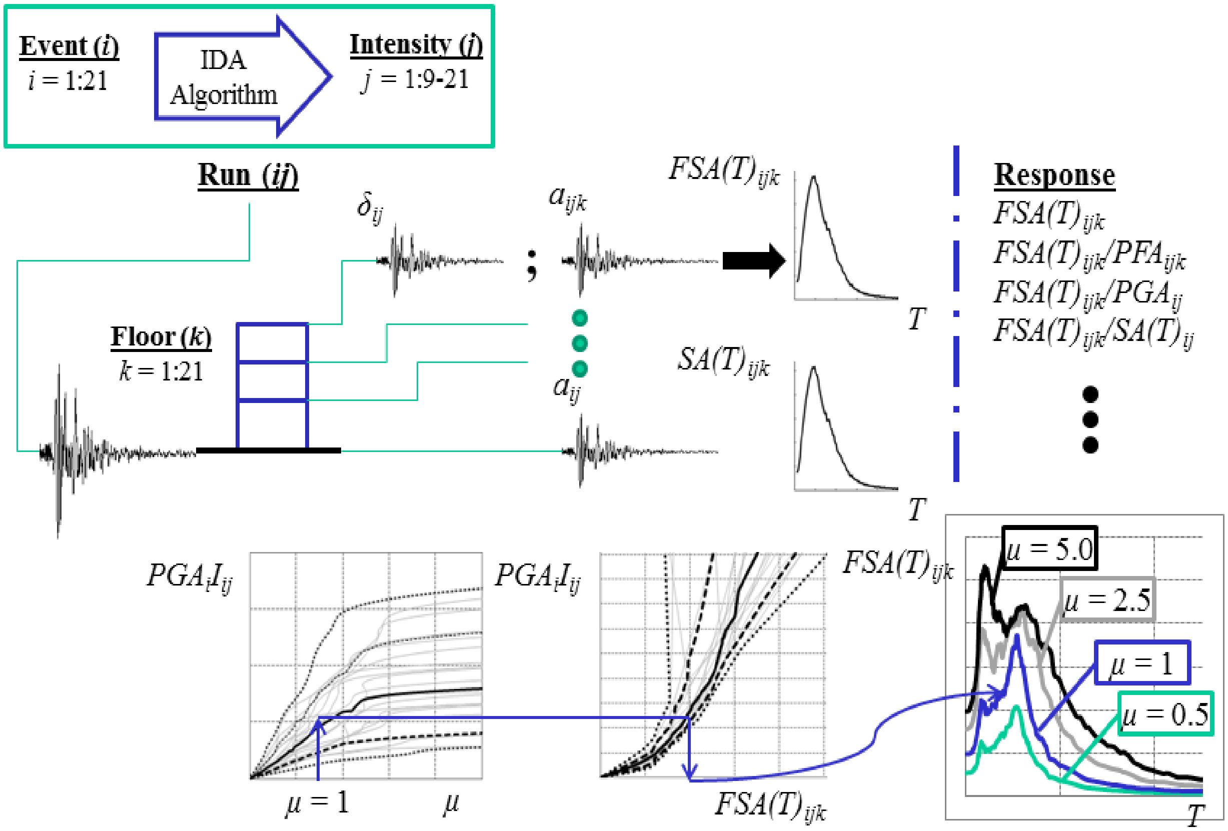

Figure 4-35 Development of Constant Ductility Curves

4.3 Drift Demands on Nonstructural Components

Several nonstructural components such as partition walls, vertical pipe runs, exterior cladding, and many others are sensitive to damage induced by large drifts experienced in the supporting structure during a significant seismic event. Therefore understanding the drift response of the supporting structure is critical to the seismic performance assessment of both the structural and nonstructural systems. The following sections identify and discuss factors which influence the drift demands on nonstructural components, present the IDA results used to assess the demands on the drift-sensitive nonstructural components, and evaluate the current code provisions for drift demands on nonstructural components.

4.3.1 Factors Influencing the Drift Demands on Nonstructural Components

Assessing the seismic demands on drift-sensitive nonstructural components is essentially the same as evaluating the drift response of the supporting structure. If the lateral stiffness of the nonstructural components is assumed to be negligible compared to the lateral stiffness of the structure, then it is acceptable to neglect the nonstructural components from the computational model. In which case, the drift demands on the nonstructural components correspond directly to the drift response of the structure. Therefore, the factors that influence the drift demands on nonstructural components are the same parameters that define variations in the drift response of the structure. Such parameters include, mode shapes, modal participation factors, type of structure, level of ductility, and distribution of ductility throughout the height of the structure.

The influence of the modal properties on drift response is well known. The overall displacement response of the structure is defined by the mode shapes and participation factors; such is the basis for the modal response analysis procedures in the current code (ASCE, 2010). While these properties are well known for elastic response of the structure, they are constantly changing once the structure begins to yield. The type of structure also has a significant influence on the drift response not only because of its effect on the mode shapes but also the way in which the yielding within the structure is distributed. The level of ductility experienced by the supporting structure is directly related to the drift response of the structure because ductility is commonly defined by the drift response.

It is not within the scope of this work to quantify the level of influence each of these factors has on the drift response of the supporting structure. This study simply provides basic drift response results from the IDA in order to establish trends in the demands imposed on drift-sensitive components mounted on SMRFs.

4.3.2 Assessment of Current Code Provisions

In the ASCE 7-10 (ASCE, 2010), the relative displacement of nonstructural components with two connection points on the same structure shall be defined by the difference between the deflections of the two connection points. These deflections maybe calculated using elastic analysis but must include the deflection amplification factor, C_d, per section 12.8.6 of ASCE 7-10 (ASCE, 2010). However, the relative displacement of the nonstructural system is not required to be considered greater than the difference in elevation of the connection points times the allowable drift angle. The allowable drift angle is a function of the occupancy category and type of structural system and ranges between 0.007 and 0.025.

These recommendations assume that the relative displacement demands on the nonstructural components within a structure are equal to the drift response of the supporting structure. The design demands of drift-sensitive nonstructural components are particularly dependent on the ability to accurately predict the drift response of the supporting structure.

4.3.3 Results and Discussion

While much of the pertinent drift response information was established in the discussion of IDA curves in Section 4.2.4, some additional relationships comparing the selected DMs are also relevant. The maximum interstory drift throughout the height of the structure is critical to the assessment of the nonstructural component demands because it represents the largest drift demand imposed in the building. In many cases this maximum drift demand is imposed to only one story of the building (soft story) while the other stories may experience significantly less interstory drifts. For the purpose of designing nonstructural components, it is critical to understand the variation in drift demands throughout the height of the structure so the more stringent design requirements may be used where needed in the building.

4.3.3.1 Ratio of Average Interstory Drift throughout the Height to Roof Drift

The average interstory drift throughout the height of the structure defines an average drift demand on nonstructural components throughout the height of the structure. For buildings with uniform drift profiles, the average interstory drift throughout the height of the structure is equal to the interstory drift of each and every story of the building and also corresponds to the roof drift. However, due to the influence of mode shapes, modal participation, and yielding within the structure, buildings rarely perform in this manner. By normalizing the average interstory drift throughout the height by the roof drift, a ratio quantifying the building's deviation from uniform drift is defined as θ_{avg}/θ_R. If the drift profile of the building is uniform this ratio is equal to 1.0.

Figure 4-36 compares the median ratio as a function of PGA for each building. From this figure it is apparent that the ratio remains relatively constant as the intensity increases. Also the ratio is approximately 1.0 for the shorter buildings (B3 and H3) and tends to increase as the period of the building is increased. Based on the definition of the ratio, it was expected that the shorter buildings with nearly linear first mode shapes, high first mode participation factors, and short periods would maintain ratios close to 1.0. In review of the taller buildings however, it is noted that the ratio increases as the period of the structure increases. Also that as the intensity is increased the ratio of the taller buildings also increases slightly as opposed to remaining constant like the shorter buildings. This is due to the increased influence of the higher modes as the building begins to yield. These observations confirm the previous conclusions of the influence of higher modes on the drift response of the respective buildings and offer a different representation of the drift responses generated in this study.

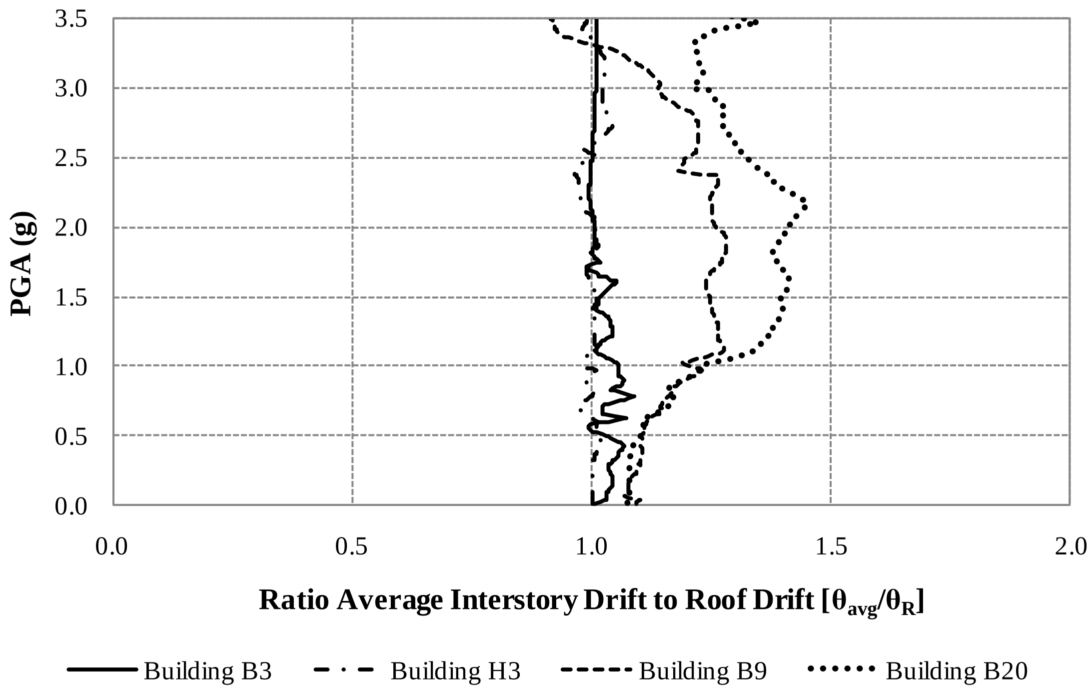

Figure 4-36 Median Ratio of Average Interstory Drift to Roof Drift

4.3.3.2 Ratio of Maximum Interstory Drift throughout the Height to Roof Drift

A similar ratio is defined by normalizing the maximum interstory drift throughout the height by the roof drift as θ_{max}/θ_R. This ratio quantifies the lack of uniformity in the drift profile by defining the ratio between the observed maximum interstory drift throughout the height against the idealized uniform drift.

The median ratios for each building are plotted against PGA in Figure 4-37. Once again it is observed that the shorter buildings maintain a constant ratio as the intensity is increased while the taller buildings show significant increases in the ratio as the building begins to yield. This increase represents the migration of the maximum interstory drift from the top of the building to the bottom of the building as the intensity and level of yielding is increased. This is more apparent in the following section which discusses the drift profiles of the buildings. With this migration the maximum interstory drift throughout the height accumulate in the lower stories. This does not occur in the shorter buildings because the yielding is more evenly distributed throughout the height of the structure.

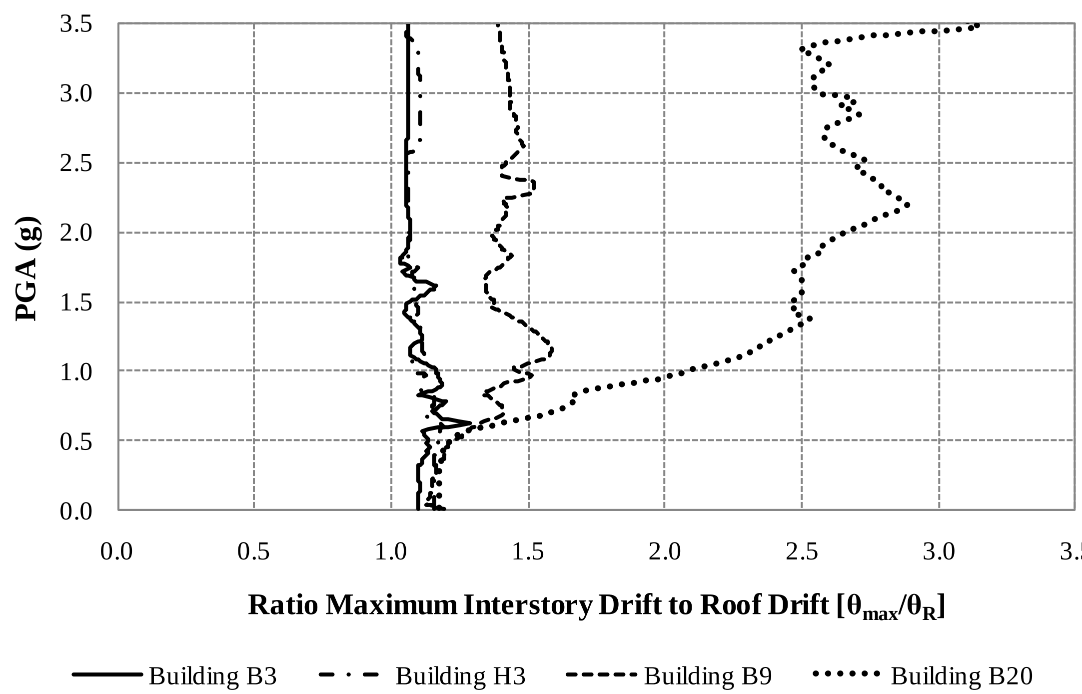

Figure 4-37 Median Ratio of Maximum Interstory Drift to Roof Drift

4.3.3.3 Drift Profiles

The drift profiles depict the stories that experience the most interstory drift demands. For taller moment frame structures the distribution of interstory drift throughout the height of the structure changes significantly as the building begins to yield. Figure 4-38 through Figure 4-41 show the median drift profiles for each building at four levels of ductility. It is noted that the elastic drift profiles for all of the buildings are uniform. This is due to the linear nature of the first mode shapes of each of the buildings. In the elastic state particularly for the shorter buildings which have high first mode participation and linear first mode shape, the drift profiles are expected to be uniform. As the level of yielding in the buildings is increased the drift profiles are drastically changed, especially for the taller buildings. In Building B20, the lower stories experience significantly more drift than the upper stories which shows that a majority of the yielding in the building is occurring in these lower floors.

4.4 Summary

This chapter has presented and discussed some of the results of the IDA study, described the dispersion in the results, demonstrated the way in which further results were processed, and discussed the drift demands on nonstructural components in the four buildings of this investigation. The IDA results are shown to provide a foundation for the discussion of demands on nonstructural components within moment frame structures. The upcoming chapters build upon this foundation to assess the acceleration demands on nonstructural components.

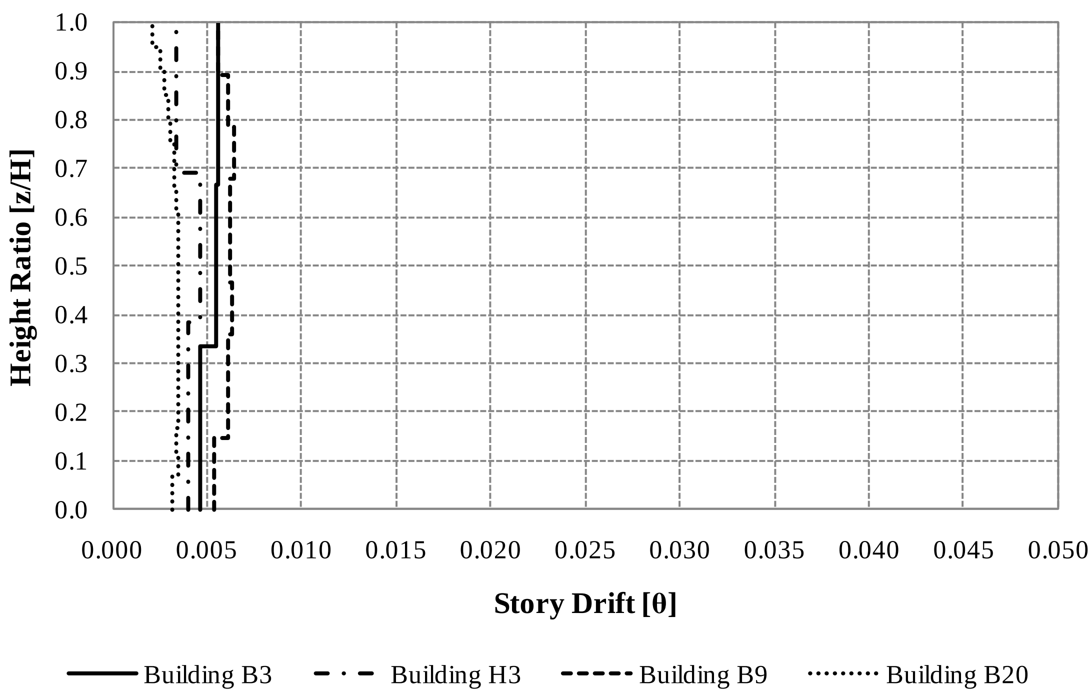

Figure 4-38 Drift Profile Comparison [Elastic]

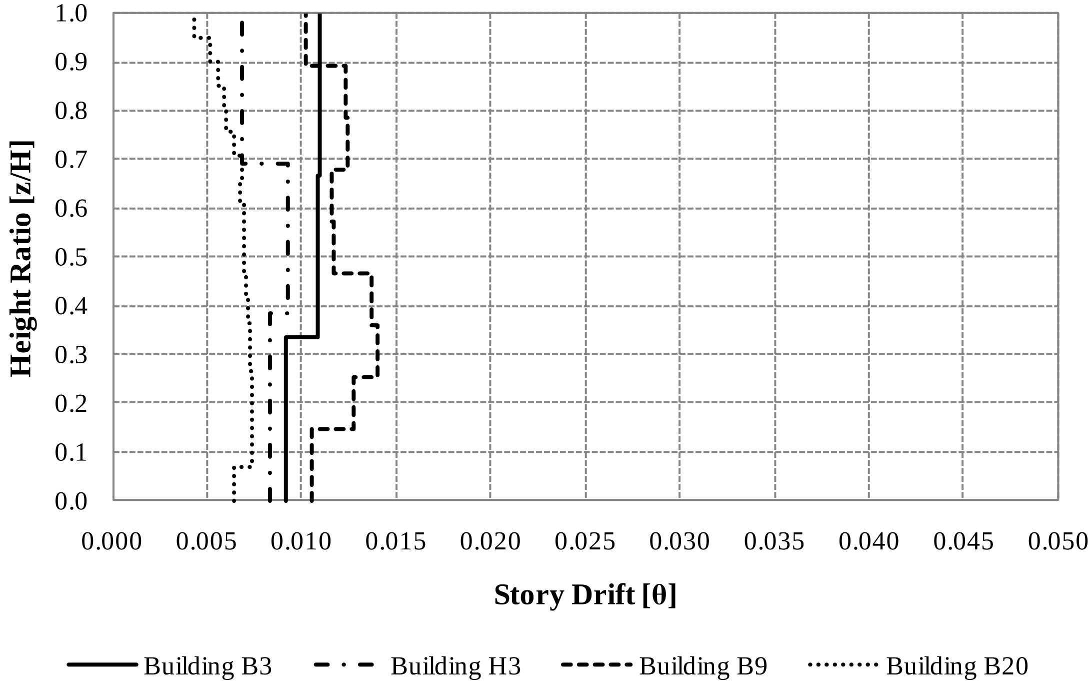

Figure 4-39 Drift Profile Comparison [μ = 1.0]

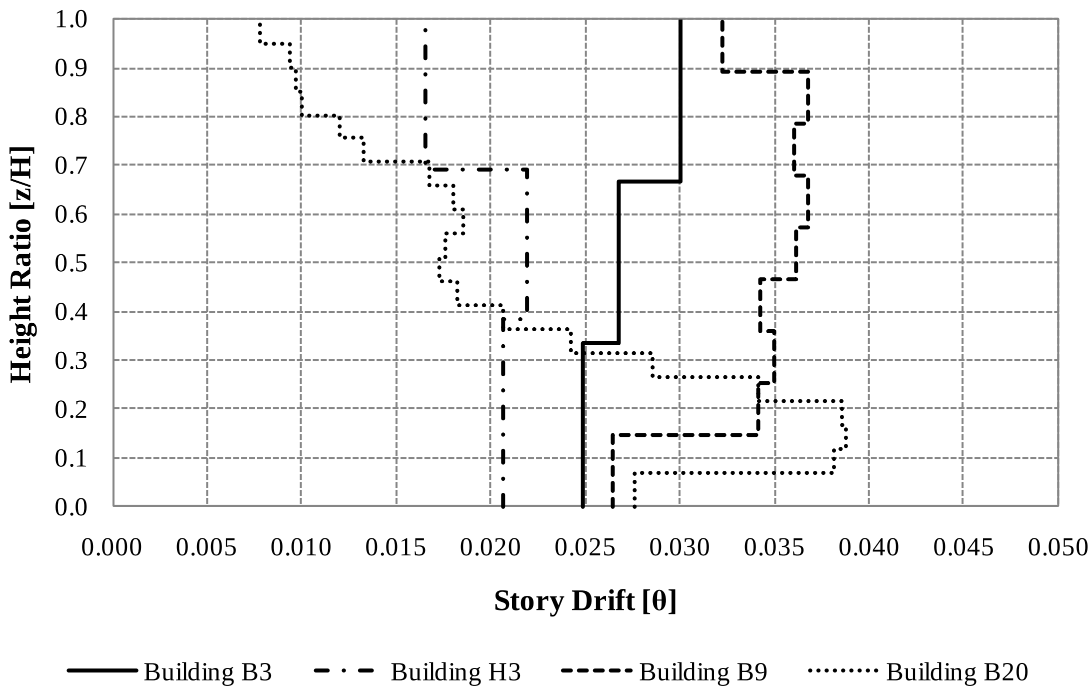

Figure 4-40 Drift Profile Comparison [μ = 2.5]

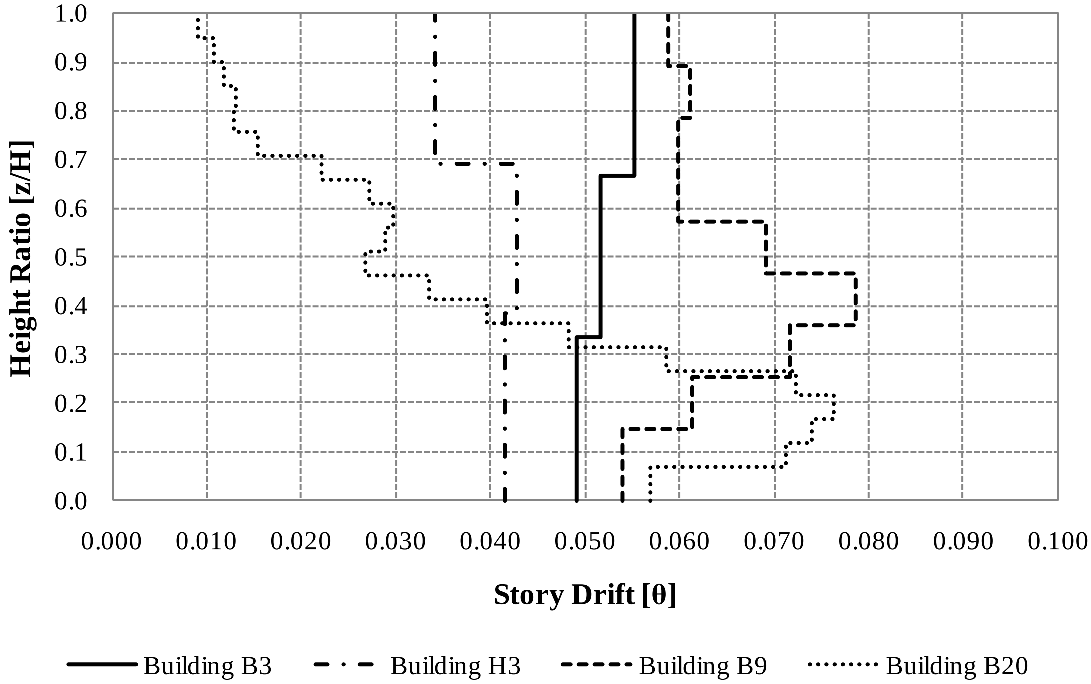

Figure 4-41 Drift Profile Comparison [μ =5.0]

SECTION 5
HORIZONTAL ACCELERATION DEMANDS ON NONSTRUCTURAL COMPONENTS

5.1 Introduction

Nonstructural components can be categorized into two classes of sensitivity, namely acceleration-sensitive and drift-sensitive (FEMA, 1997b). Nonstructural components such as piping systems, ceiling systems, ventilation ducts, machinery, bookcases, and many other nonstructural components as well as building contents are examples of acceleration-sensitive components. Improving the understanding of the acceleration and force demands on these nonstructural components has been the objective of several recent studies. These studies aimed to formulate the expected lateral acceleration demands on both rigid and flexible nonstructural components throughout the building. Most of these studies are conducted by performing several linear and nonlinear analyses of idealized models such as the continuum model suggested by Taghavi and Miranda (2006), or the single bay two dimensional frames used by Medina et al. (2006) subject to a suite of unidirectional ground motions. As a result of these studies factors including dynamic interaction between the nonstructural components and the supporting structure, nonstructural damping ratios, type of lateral load-resisting structural system, reduction of stiffness in the lateral load-resisting system through the height of the building, nonlinear behavior of the supporting structure, and location along the height of the supporting structure have been shown to influence the seismic response characteristics of nonstructural components within the building.

In the present study, three-dimensional models of a total of four building structures have been subjected to all three components of a series of ground motions. Various response quantities have been monitored. More specifically, floor acceleration and interstory drift responses have been recorded to investigate seismic demand characteristics imposed on nonstructural components that may be located throughout the structures. It is noted that the Incremental Dynamic Analysis approach has been adopted to facilitate the evaluation of response characteristic due to varying levels of ground motion intensities. In addition to presenting the results of the IDA study, this chapter reviews the current code provisions, recommendations from previous studies, as well as proposes suggestions for simple adjustments to the current code provisions used in the calculation of horizontal acceleration demands on nonstructural components.

5.2 Factors Influencing the Horizontal Acceleration of Nonstructural Components

5.2.1 Dynamic Interaction between the Structure and Nonstructural Components

Due to the large variety of nonstructural components with varying mass, stiffness, installation and attachment details, etc., generally it is difficult to accurately and efficiently model the interaction between the nonstructural components and their supporting structure. Coupled modeling techniques, which consider the structural and nonstructural systems in the same model, create problems for conventional methods of analysis due to the large discrepancies in various values of mass, stiffness, and damping throughout the model (Villaverde, - 2004). As a result, various alternative methods of analysis have been developed to simplify the process of design of nonstructural components.

One of the first simplified methods of analysis and still widely accepted is known as the floor response spectrum method. In this method, the response of the supporting structure is uncoupled from that of the nonstructural component. This is achieved by generating the floor level time history response of the supporting structure; subsequently floor response spectra are generated. This two-step process has been proven accurate for nonstructural components whose masses are much smaller than the masses of their supporting structures and natural frequencies are not too close to those of the supporting structure (Villaverde, R., 2004).

However, by uncoupling the analysis of the nonstructural component from the structure, the floor response spectrum method may provide overly conservative estimates of the response of nonstructural components whose ratio of nonstructural mass to structural mass are too large or whose natural frequencies resonate with those of the structure (Villaverde, R., 2004). There have been several studies which have developed appropriate limits of the nonstructural component mass ratio for use with the floor response spectrum method. Sing and Ang (1974) determined that for mass ratios up to 0.10, analysis of an uncoupled system is acceptable for the estimation of the acceleration response of the supporting structure itself; however, mass ratios should not exceed 0.01 when approximating the response of the nonstructural components. The US Nuclear

Regulatory Commission (USNRC, 1978) suggests that most nonstructural components are light compared to the mass of the supporting structure and that the use of uncoupled models is acceptable in these cases. Nevertheless, there are nonstructural systems whose stiffness, mass and resulting frequency range induce significant dynamic interaction between the nonstructural component and the supporting structure. In these cases it is required to use a coupled model to account for these effects (USNRC, 1978). The American Society of Civil Engineers' (ASCE) standard for the seismic design of nuclear facilities (ASCE, 1987) requires the use of a coupled model when the nonstructural component is mounted to a relatively flexible wall or floor system for which the interaction effects are significant. The dynamic interaction need not be considered for nonstructural components whose mass is less than 1% of that of the structure supporting it. An additional relationship is defined between the mass and frequency ratios of the nonstructural component to the supporting structure that may be used to determine whether or not an uncoupled model is acceptable. In this relationship, as the mass ratio increases and the frequency ratio approaches 1.0 (a condition in which the nonstructural component is in tune with a dominant dynamic mode of the supporting structure) the need to consider the effects of dynamic interaction between the two systems increases (ASCE, 1987).

While many others, such as Igusa and Der Kiureghian (1985) and Chen and Soong (1988), have shown that ignoring the effects of dynamic interaction may lead to significant errors in the calculated response of nonstructural components, the floor response method is still a commonly accepted method.

This study utilizes the floor response spectrum method to determine the acceleration response of elastic nonstructural components on inelastic supporting structures. While some level of conservatism is introduced in these results, in light of the previous discussion, the results are acceptable for most nonstructural components lighter that 1% of the weight of the supporting structure. Thus, the results obtained in this study are applicable to light nonstructural components.

5.2.2 Damping Ratio of Nonstructural Components

Damping has a major effect on the response of both the nonstructural component as well as the supporting structure. Overestimation of the critical damping ratio could result in an unconservative estimation of the acceleration response of the floors and nonstructural components. Therefore, proper selection of the damping ratio of both the nonstructural component as well as the supporting structure is critical.

Current building codes (ICC, 2006) suggest that 5% of the critical damping be assigned to the supporting structure. As for the damping assigned to the nonstructural components, there is some debate as to what is appropriate. Villaverde (2004) suggests that the damping ratios of nonstructural components are much less than the supporting structure and consistently uses examples of damping ratios in the order of 0.5% of the critical damping. Other studies, such as Miranda and Taghavi (2006) and Medina et al. (2006), use 5% damping for both the nonstructural component and supporting structure. Biggs and Roesset (1970) provide 2% and 5% damping for the nonstructural components and supporting structure, respectively.

Villaverde (2004) has pointed out that when dynamic interaction is significant, because the damping of the nonstructural component is much lower than the damping of the supporting structure, the damping in the overall system is not uniform. As a result, the response of the nonstructural components is governed by a system without classical modes, and thus non-classical damping is present in the system. If this is not accounted for it has been shown that the results may show significant error, especially when the frequency of the nonstructural component is in tune with one of the dominant frequencies of the supporting structure. Igusa and Der Kiureghian (1985) claim that if the vibration modes of the nonstructural component and its supporting structure are not in resonance the system is classically damped.

As explained in Chapter 3, Rayleigh damping was applied to the structures such that a 5% damping ratio was in 0.8 and 2.0 times the fundamental period of the building. To quantitatively explore the effect of the nonstructural component damping, floor acceleration spectra were developed assuming critical damping ratios of 0.5%, 2.0%, 5.0%, and 10.0%.

5.2.3 Structural System of Supporting Structure

The structural system of the supporting structure influences the floor level acceleration response, which in turn influences the acceleration response of the nonstructural components mounted on the floors of the structure. The influence of the structural system on the acceleration response comes from the variation of mode shapes and modal participation factors between building systems. As an example, moment-resisting frame structures deform similar to a shear beam whereas braced frames deform similar to flexural beams. As a result, there are significant differences in the mode shapes and modal participation factors of these two systems.

Taghavi and Miranda (2006) demonstrate the effect of the lateral load-resisting system through the use of a continuum model in which the relative amount of shear to flexural deformation in the structure is controlled by a single parameter. Changing this parameter facilitates the representation of systems ranging from moment-resisting frames to braced frames or shear wall buildings. In their study it is shown that there is significant difference in mode shapes and modal participation for buildings of equal period with different structural systems. This difference directly influences the acceleration response of the floors.

Taghavi and Miranda (2006) also investigated the effect of reducing the stiffness through the height of the structure. Their results show that the reduction of lateral stiffness along the height of the building has little influence on the modal characteristics of braced frame or shear wall buildings and slightly greater, yet still insignificant effect on moment-resisting frame buildings.

Medina et al. (2006) analytically studied stiff moment-resisting frame buildings with periods designed to be equal to 0.1 times the number of stories and uniform lateral stiffness distribution over the height of the structures. The acceleration response of these structures followed similar trends to those presented by Taghavi and Miranda (2006).

5.2.4 Nonlinear Behavior of Supporting Structure

The acceleration response of the nonstructural components of a building is influenced by nonlinear behavior of the supporting structure. Including the effects of inelastic response of the supporting structure has been a topic of recent studies (Lin and Mahin, 1985); (Villaverde, R., 1987); (Rodriguez et al., 2002); (Taghavi and Miranda, 2006); (Medina et al., 2006). All of which agree that the peak floor accelerations are reduced when accounting for nonlinearity in the supporting structure. Rodriguez et al. (2002) and Medina et al. (2006) similarly introduced nonlinearity into the investigated structures through increasing the scale factor of the applied ground motions. Rodriguez et al. (2002) made use of three concrete shear wall buildings to investigate the influence of structural nonlinearity while considering two different hysteretic rules. Their research indicates that the peak floor acceleration amplification factor (PFA/PGA) of the roof level remains constant for low ground motion scale factors, signifying the elastic response of the structure. This constant region is followed by a significant decrease in peak acceleration amplification factor with increased scale factor. Conclusions of their work suggest that the maximum peak acceleration amplifications of the roof occurs when the building is behaving elastically, that these amplifications are greater for shorter structures, and that the increased levels of ductility have less effect on the reduction of these amplifications for taller buildings (Rodriguez et al., 2002). Similar results were concluded in the studies by Medina et al. (2006) for regular moment-resisting frame structures.

Rodriguez et al. (2002) proposed a simplified method for estimating floor acceleration amplification profiles assuming that the effect of yielding primarily effects the acceleration responses associated with the first mode of vibration of the structure. Discussed in more detail later in the chapter, an alternative simplified method is proposed in the present study.

Counting on the effect of nonlinearity in the response of nonstructural component seems to be counter intuitive to the objective of protecting the nonstructural components. However, there may be instances in which some level of yielding under severe ground motions would not impair the functionality of the nonstructural component. In such cases counting on the ability of the nonstructural component to deform in a ductile manner would be beneficial to an economical design. For this reason, more research is needed in the field to generate reliable response modification factors for nonstructural components. Villaverde (1997) also suggests that more research is needed to quantify the proper modification factors to account for the nonlinear response of nonstructural components and their mounting systems. The research presented in this report, treats the nonstructural component as a linear elastic single degree of freedom system, and thus does not account for nonlinearity of the nonstructural component or its connections.

5.3 Current Code Approach

For design purposes, Chapter 13 of ASCE 7-10 (ASCE, 2010) includes the seismic design requirements for nonstructural components, which is used for general purpose assessment of the seismic demands of the nonstructural components within a building. For qualification testing, the

AC 156 (ICC, 2006) document provides the shake table testing requirements of nonstructural components and systems. Each of these documents are based on a similar understanding of nonstructural components, consequently many of the demand equations are common.

During a seismic event the ground acceleration is amplified at each floor of the building by the modal participation factors and mode shapes of structure (Chopra, 2007). The following formulation derives the acceleration amplification relationship which is used in the current code. The absolute floor acceleration response of a structure is the summation of the relative response acceleration and the ground acceleration of the structure as shown in (5-1).

$$\ddot{u}_t = \ddot{u} + \ddot{u}_g \tag{5-1}$$

Using a modal analysis formulation the relative acceleration response can be expressed by (5-2).

$$\ddot{u}(t) = \Gamma \phi \ddot{D}(t) \tag{5-2}$$

In which, $\ddot{u}(t)$ is the relative acceleration, n is the number of modes, Γ is the modal participation factor, ϕ is the mode shape, and $\ddot{D}(t)$ is the modal response obtained from solving (5-3).

$$\ddot{D}(t) + 2\xi\omega\dot{D}(t) + \omega^2 D(t) = -\ddot{u}_g(t) \tag{5-3}$$

The combination of (5-1) and (5-2) in the frequency domain results in (5-4).

$$\ddot{u}_t(\omega) = \ddot{u}_g(\omega) + \Gamma \phi \ddot{D}(\omega) \tag{5-4}$$

To facilitate the discussion of floor acceleration amplification the modal acceleration response is assumed to be the product of an amplification factor, α, and the ground acceleration, $\ddot{u}_g(\omega)$, as shown in (5-5).

$$\ddot{D}(\omega) = \alpha \cdot \ddot{u}_g(\omega) \tag{5-5}$$

By substituting (5-5) into (5-4), the absolute acceleration response is expressed in (5-6).

$$\ddot{u}_t(\omega) = \ddot{u}_g(\omega) + \alpha\Gamma\phi\ddot{u}_g(\omega) = (1 + \alpha\Gamma\phi) \cdot \ddot{u}_g(\omega) \tag{5-6}$$

The term $(1+\alpha\Gamma\phi)$ is the amplitude of the acceleration amplification which is currently taken as $(1+2\,{}^{z}\!/\!{}_{H})$ for all frequencies. This version of acceleration amplification term was formulated in the 1997 NEHRP Provisions (FEMA, 1997b) based on the examination of building floor response acceleration records during strong ground motions with peak ground accelerations greater than 0.1 g. The "z/H" term approximates the mode shape, ϕ, of the building as a straight line, and the "2" is an empirical estimation of the product of the acceleration amplification factor, α, and the modal participation factor Γ.

5.3.1 ASCE 7-10 Provisions

Chapter 13 of the ASCE 7-10 establishes minimum design criteria for nonstructural components that are permanently attached to structures. The seismic force demands on nonstructural components are determined in accordance with Section 13.3.1 of ASCE 7-10. In which, the horizontal seismic design force, F_p, may be determined in accordance with (5-7) or (5-8).

$$F_p = \frac{0.4a_p S_{DS} W_p}{\left(\frac{R_p}{I_p}\right)}\left(1+2\frac{z}{H}\right) \tag{5-7}$$

In which,

F_p = seismic design force
S_{DS} = short period spectral acceleration
a_p = component amplification factor that varies from 1.0 to 2.5
I_p = component importance factor that varies from 1.0 to 1.5
W_p = component operating weight
R_p = component response modification factor that varies from 1.0 to 12
z = height in the structure of point of attachment of component
H = average height of the structure

With this equation the code provides an equation for which the nonstructural component may be designed without any knowledge of the supporting structure. This type of equation is convenient for manufacturers of widely used nonstructural systems as it allows for the design of a common component which may be implemented in many types of buildings in a known geographic area with assumed seismicity, S_{DS}. With this in mind, this type of code approximation should provide a conservative estimate of the seismic force demand on nonstructural components.

Alternatively, if the designer of the nonstructural components has access to a model of the supporting structure, modal analysis may be used to develop the seismic force demands on the nonstructural components in accordance with (5-8).

$$F_p = \frac{a_i a_p W_p}{\left(\frac{R_p}{I_p}\right)} A_x \tag{5-8}$$

Where a_i is the acceleration at the i^{th} level obtained from the modal analysis and where A_x is the torsional amplification factor determined by Eq. 12.8-14 (ASCE 7-10). This equation offers a refined approximation of the seismic demands on nonstructural components over the equation presented in (5-7) at the cost of performing a modal analysis of the supporting structure. While this may be beneficial for special cases in which the capacity of connection details of the nonstructural components may be greatly reduced with an improved estimate of the design forces, this method does not lend itself to generalized use as it requires a model of the building capable of performing modal analysis. Designers of nonstructural components rarely have such models readily available.

Independent of which of the previous equations are employed F_p may not be taken as less than:

$$F_p = 0.3 S_{SD} I_p W_p \tag{5-9}$$

Nor is F_p required to be taken as greater than:

$$F_p = 1.6 S_{DS} I_p W_p \tag{5-10}$$

The upper bound established by (5-10) limits the design acceleration of the nonstructural component to four times the peak ground acceleration. Upon further inspection of the combination of (5-7) and (5-10) it can be concluded that for flexible components (a_p = 2.5) located in the upper six-tenths of the structure (z/h > 0.3), the design force is governed by the upper bound (5-10). For this reason it is common for manufacturers of nonstructural anchorage systems to simply design based on the upper limit provided by (5-10).

The estimate of the seismic force provided by (5-7) may be decomposed in the following manner. The peak ground acceleration of the design ground motion including site-soil effects is approximated as $0.4S_{DS}$. The component amplification factor, a_p, represents the component acceleration or floor spectral acceleration normalized by the peak floor acceleration. The amplification up the height of the building is accounted for through the linear expression $(1+2\, z/H)$, which represents the peak floor acceleration normalized by the peak ground acceleration. With these terms now defined the design equation is represented once more in terms used throughout this chapter in (5-11).

$$FSA = 0.75PGA \le PGA\left(\frac{FSA}{PFA}\right)\left(\frac{PFA}{PGA}\right) \le 4.0PGA \qquad (5\text{-}11)$$

Where, FSA is the floor spectral acceleration which represents the acceleration of the nonstructural component, PFA is the peak floor acceleration which represents the acceleration of rigid nonstructural components, and PGA is the peak ground acceleration which is approximated as 40% of the short period design ground spectral acceleration, S_{DS}. Using this representation of the code design equation, each of the three terms is discussed in relation to the results of this study.

5.3.2 AC 156 Provisions

The purpose of AC 156 is to establish the minimum requirements for the seismic qualification shake table testing of nonstructural components. The provisions within AC 156 relate to the seismic design of nonstructural components as established by the 1997 Uniform Building Code as well as the 2006 International Building Code. The criteria presented in AC 156 are applicable to nonstructural components with fundamental frequencies greater than 1.3 Hz (ICC, 2006).

The AC 156 document specifies a required response spectrum which is derived from the code design equations of the 1997 UBC or the 2006 IBC. The normalized required response spectrum is presented in Figure 5-1. The values of A_{FLX} and A_{RIG} are defined in (5-12) and (5-130) below.

$$A_{FLX} = S_{DS}\left(1 + 2\frac{z}{H}\right) \tag{5-12}$$

$$A_{RIG} = 0.4S_{DS}\left(1 + 2\frac{z}{H}\right) \tag{5-13}$$

In which the variables are the same as the ASCE 7-10 design equation presented in (5-7). The value of A_{FLX} is limited to a maximum of 1.6 times the S_{DS}.

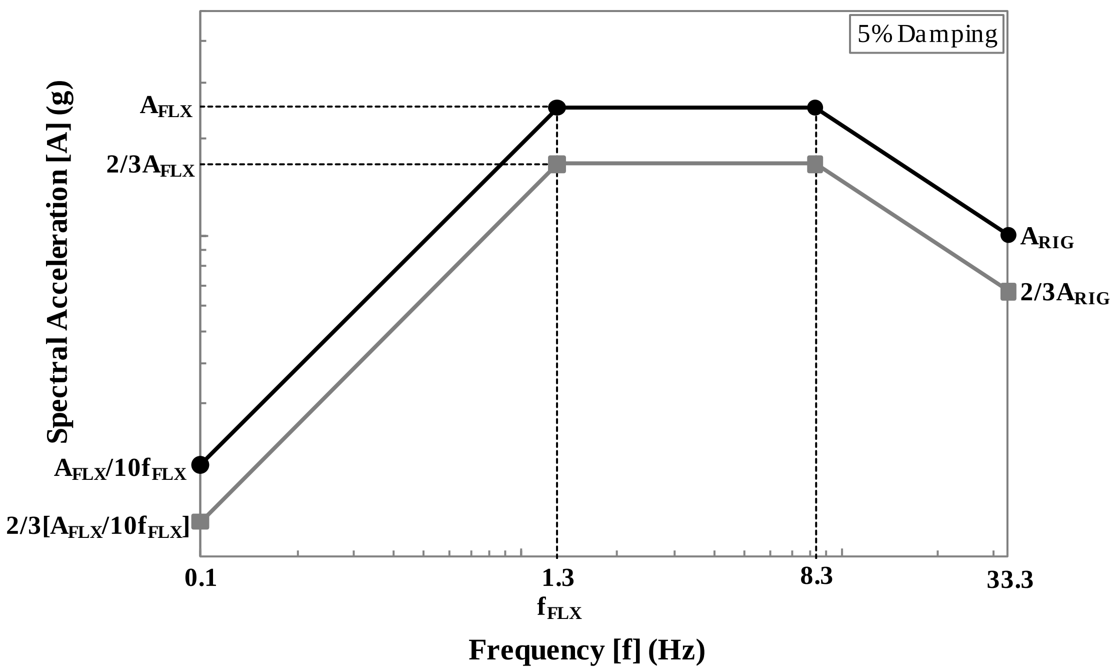

Figure 5-1 Required Response Spectrum Normalized for Nonstructural Components (AC 156)

5.4 Results and Discussion

Making use of the incremental dynamic analysis results presented in Chapter 4, the effect of several parameters on the acceleration demands on nonstructural components was investigated. The parameters explored include structural period, nonstructural component to structural period ratio, structural yielding, nonstructural component damping ratio, and relative mounting height of the nonstructural component within the height of the structure. Most of the recent studies have used simplified two dimensional models subjected to a unidirectional ground excitation. Taking advantage of the full three-dimensional models developed in this project, an assessment of the acceleration response of nonstructural components was performed. Using orthogonal horizontal floor acceleration responses, bidirectional floor acceleration spectra were generated and the effects of the above mentioned parameters on the horizontal acceleration response of nonstructural components are investigated in the following sections. The results are then compared to the current code provisions if applicable. The comparisons are discussed and conclusions are drawn which lead to recommendations for changing the current code provisions.

5.4.1 Normalization of Nonstructural Component Accelerations

One of the objectives of the present study is to demonstrate the influence of structural yielding on the floor acceleration response. To show this effect, Figure 5-2 through Figure 5-5 illustrate the median peak floor acceleration profiles for different levels of ductility of each building. In addition, Figure 5-6 through Figure 5-9 depict the median floor acceleration response spectra of each floor of Building B3 for different levels of ductility. In these figures ductility is defined according to the Section 4.2.2.3. Due to the effect of structural yielding, identifying trends in the data is difficult as the level of yielding in the building is dependent upon the intensity of the ground motion. Thus, quantification of the floor acceleration response of yielding structures was simplified by normalizing the floor acceleration by the peak ground acceleration.

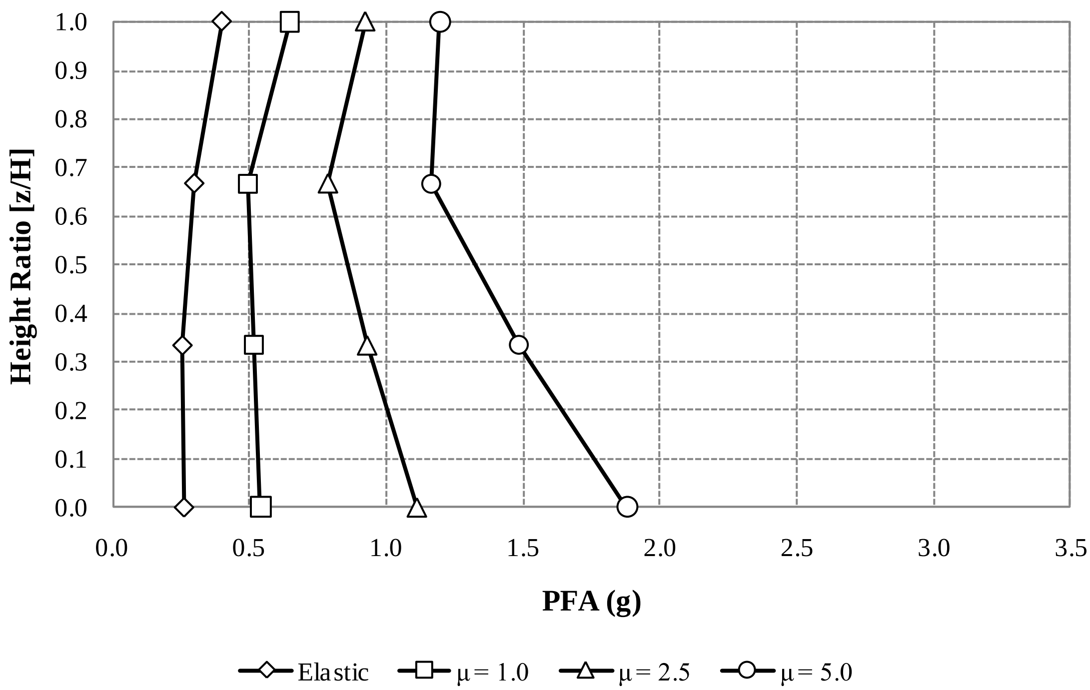

Figure 5-2 Median Peak Floor Acceleration [B3]

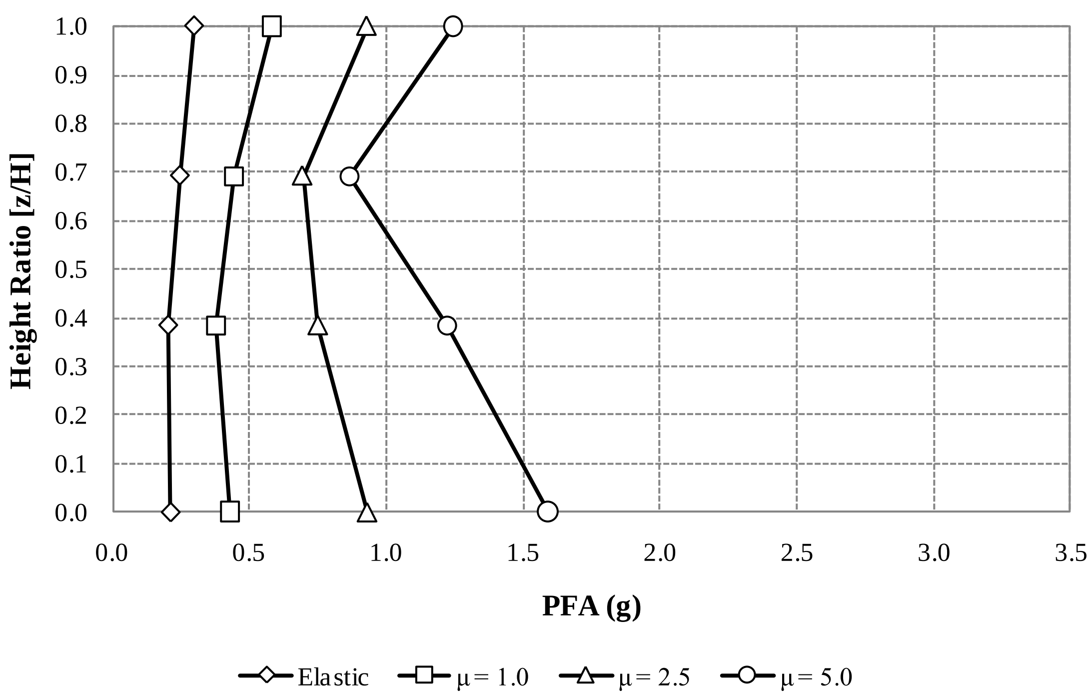

Figure 5-3 Median Peak Floor Acceleration [H3]

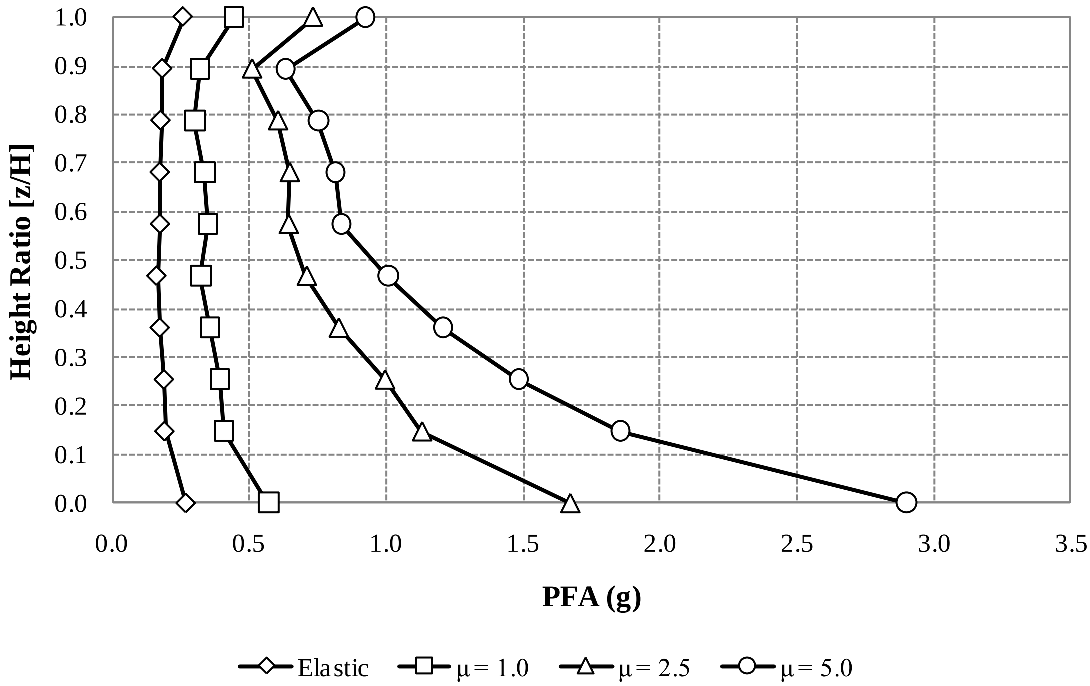

Figure 5-4 Median Peak Floor Acceleration [B9]

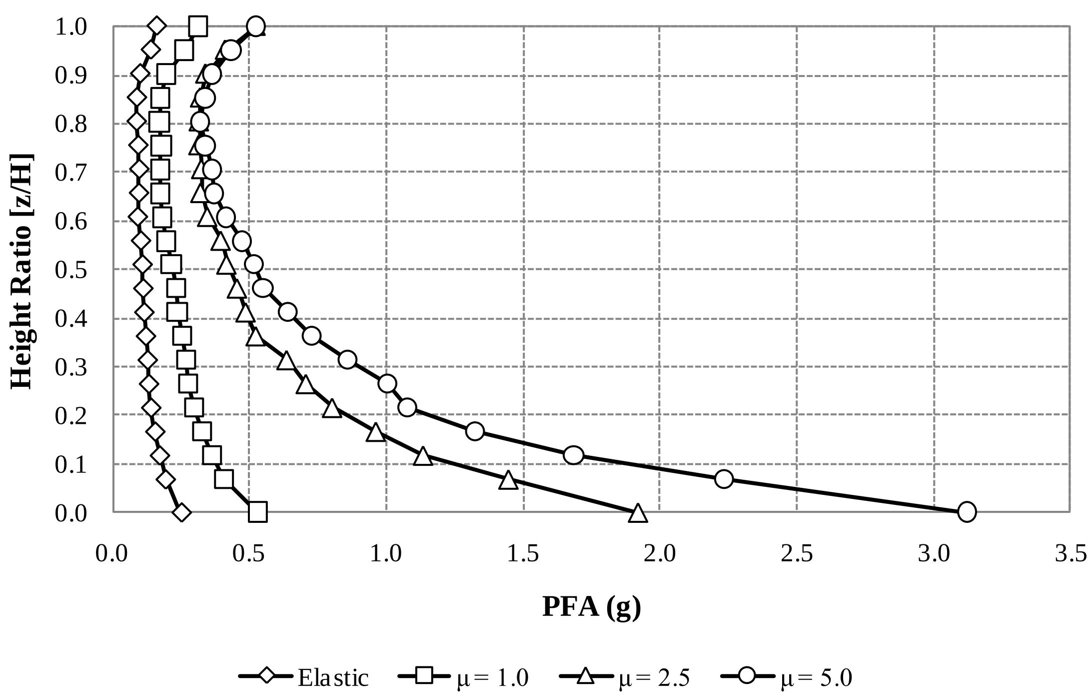

Figure 5-5 Median Peak Floor Acceleration [B20]

When examining the acceleration response of nonstructural components, there are two categories of components to consider, rigid components and flexible components. Rigid components have very short natural periods of vibration (less than 0.06 seconds (ICC, 2006)) thus have a comparable total acceleration response to that of the floor, while the acceleration response of flexible components which have longer natural periods (i.e. greater than 0.06 seconds (ICC, 2006)) may be amplified. For this reason, the peak floor acceleration (PFA) was used to describe the response of rigid nonstructural components while the floor spectral acceleration (FSA) was used to describe the response of flexible ones. For rigid nonstructural components, the peak floor acceleration, PFA, was normalized by the peak ground acceleration, PGA. The PFA/PGA ratio is referred to as the peak acceleration amplification factor in this study. This parameter is a measure of the dynamic amplification of the ground motion by the structure.

For flexible nonstructural components, the floor spectral acceleration, FSA, was normalized in three different ways. The first was normalization with the PGA. The FSA/PGA ratio is the total acceleration amplification since it accounts for the amplification provided by both the supporting structure and the nonstructural component. The component acceleration amplification factor was defined as the ratio of the floor spectral acceleration, FSA, to the peak floor acceleration, PFA. The FSA/PFA ratio is defined in Section 13.3.1 of ASCE 7-10 as a_p (ASCE, 2010). Alternatively, the spectral acceleration response of flexible components was normalized by the ground acceleration spectrum, FSA/SA. This parameter is referred to as the spectral acceleration amplification factor. This parameter is essentially a spectral domain function relating the floor response spectrum to the ground response spectrum. This was used to propose an envelope function that can be used to estimate the floor response spectrum for a given design acceleration (ground) response spectrum.

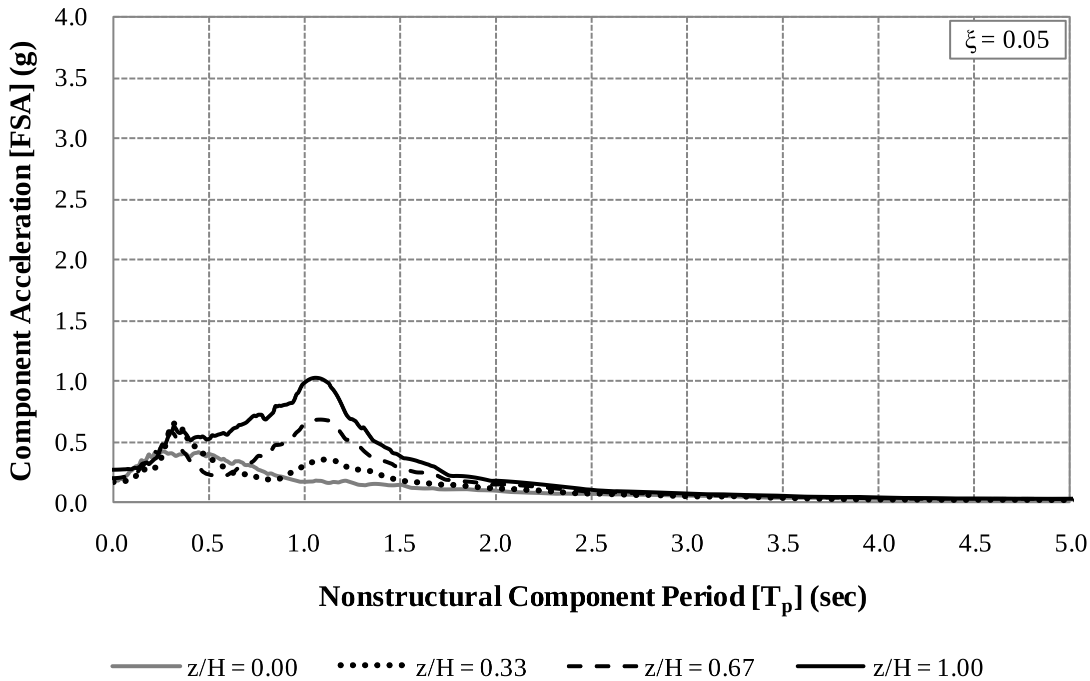

Figure 5-6 Median Floor Acceleration Spectra (Elastic) [B3]

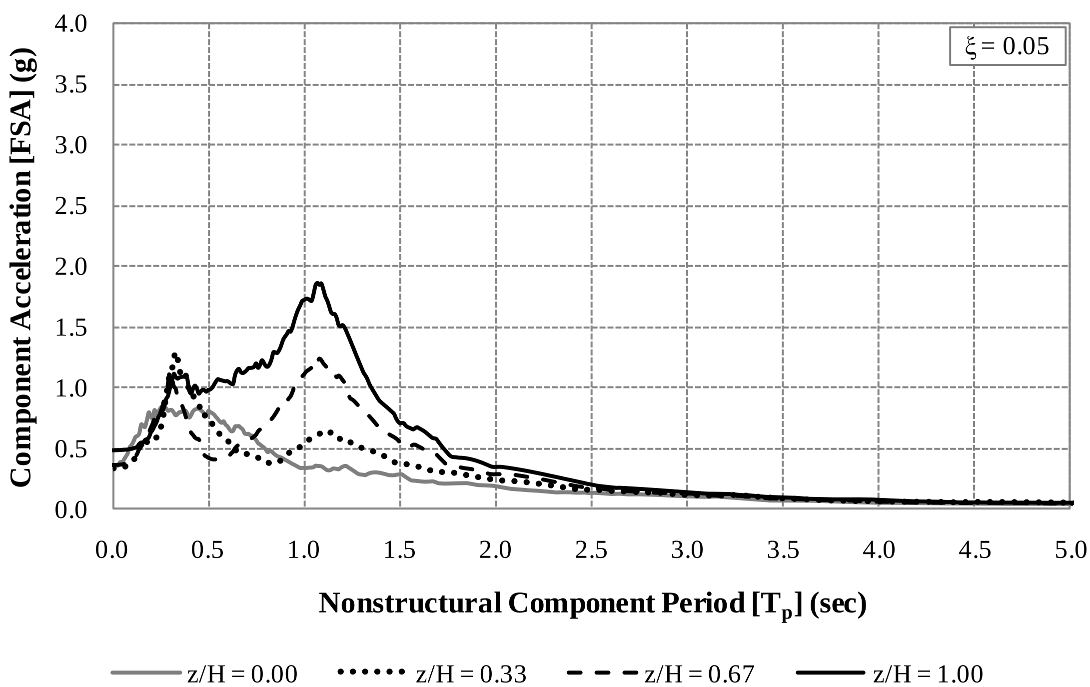

Figure 5-7 Median Floor Acceleration Spectra (μ = 1.0) [B3]

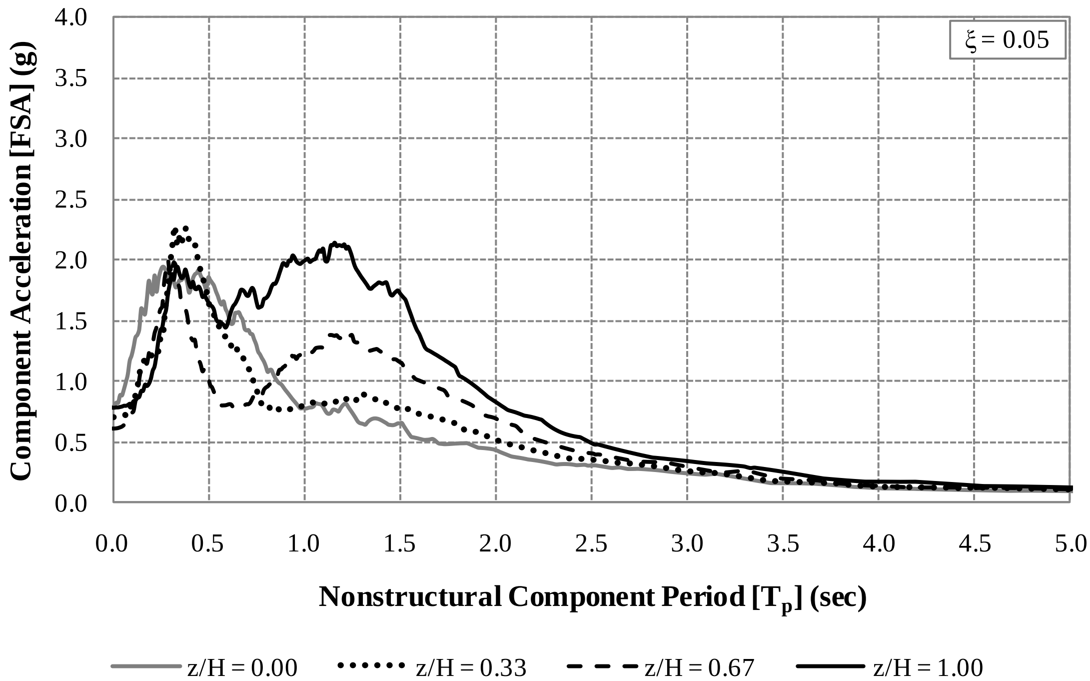

Figure 5-8 Median Floor Acceleration Spectra (μ = 2.5) [B3]

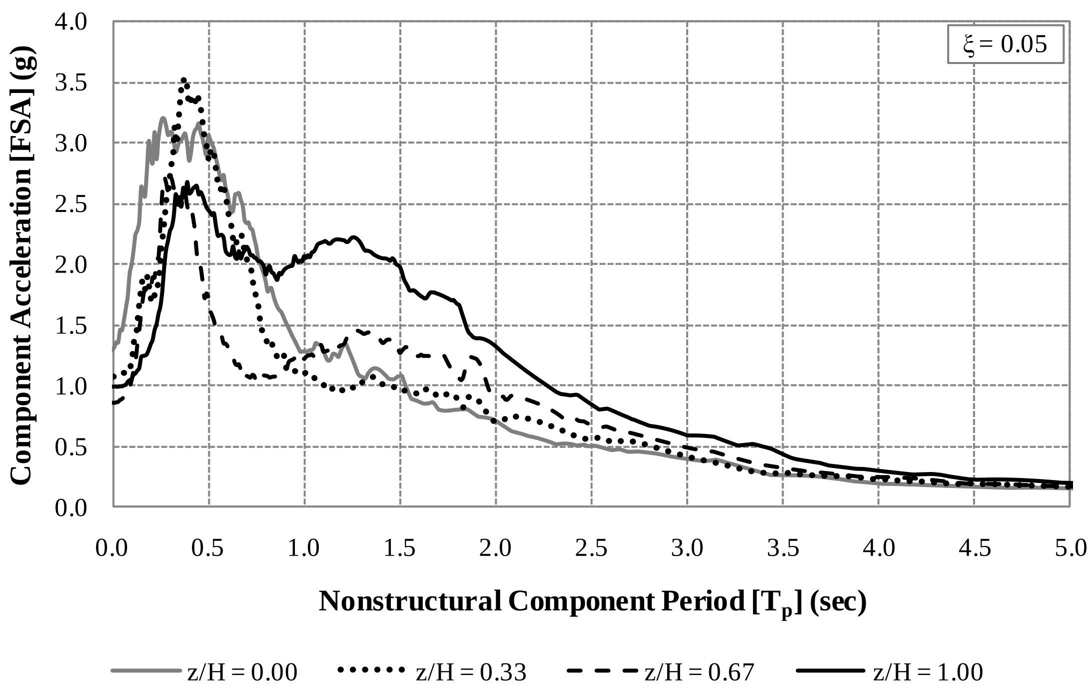

Figure 5-9 Median Floor Acceleration Spectra (μ = 5.0) [B3]

5.4.2 Effect of Period of Supporting Structure

Several previous studies have concluded that the modal periods of the supporting structure influence the response of the nonstructural components. Studies performed by Medina and Krawinkler (2003), Taghavi and Miranda (2006), and Medina et al. (2006) have shown that the PFA/PGA ratio is reduced as the period of the supporting structure is increased.

In addition, Medina et al. (2006) showed that component acceleration spectra peak near the modal frequencies of the supporting structure. They concluded that the period ratio is a critical parameter. Similar findings were concluded by Miranda and Taghavi (2009).

5.4.2.1 Rigid Nonstructural Components

The peak floor acceleration amplification factor (PFA/PGA) provided a representative parameter to assess the acceleration demands on rigid nonstructural components. The peak floor acceleration amplification factor is presented as a function of structural period in Figure 5-10. The median and 84% fractile PFA/PGA ratios of each building are plotted against their respective elastic structural periods. The figure depicts the relationship at floor level with z/H ratios of approximately 0.33, 0.67, and 1.0. It is apparent that the peak acceleration amplification of each floor decreases as the period of the supporting structure increases.

The peak acceleration amplification factor of the roof is nearly inversely proportional to the period of the building. This trend parallels the trend found in ground acceleration spectra. It is commonly accepted that the spectral acceleration in the long period range is inversely proportional to the period of the structure. With this assumed (5-14) was fit to the data in Figure 5-10.

$$\frac{PFA}{PGA} = 1 + \frac{T_{\max} - T}{T}\frac{z}{H} \tag{5-14}$$

In which T is the period of the supporting structure, T_{max} is the maximum structural period for which the peak acceleration of the roof is at least equal to the peak ground acceleration and is taken as 2.5, z is the mounting elevation of the nonstructural component, and H is the total height of the building. This proposed equation is discussed further in Section 5.6.1.

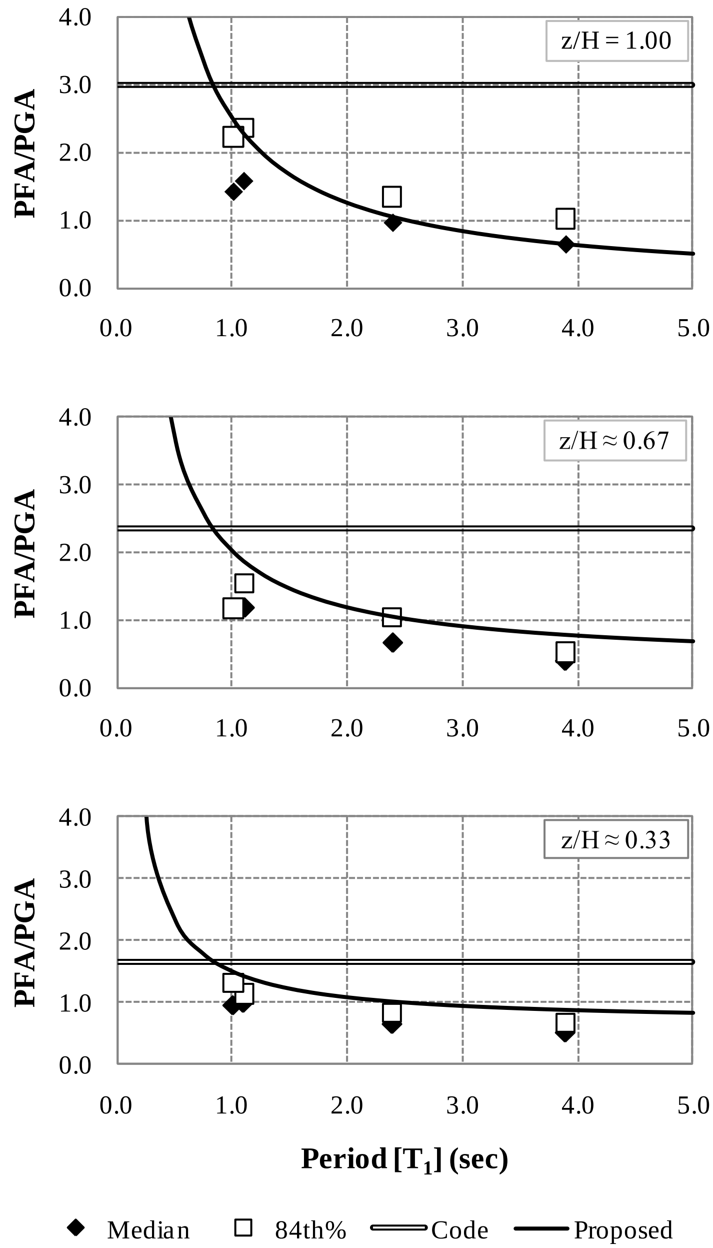

Figure 5-10 Influence of Structural Period on Peak Floor Acceleration Amplification

5.4.2.2 Flexible Nonstructural Components

In order to show the influence of the dynamic characteristics of the supporting structure on the acceleration response of flexible nonstructural components, the normalized total floor acceleration spectra (FSA/PGA) of each building responding elastically are presented in Figure 5-11 through Figure 5-14. The first two modal periods of the supporting structure are highlighted in these figures. Two important observations were made. First, the peaks in the total acceleration amplification spectra coincide with the modal periods of the supporting structure. The slight deviation of the peak from the modal periods of the supporting structure is attributed to the effect of the bidirectional nature of the total acceleration amplification spectra as explained in Section 4.2.1.2 and variation in modal frequencies in each orthogonal direction, which is particularly significant in Building B20. However, if this effect is neglected, normalizing the nonstructural component period by the fundamental period of the supporting structure eliminates the dependency of the spectra on the structural period and comparison among buildings is made possible. Second, the total acceleration amplification at the fundamental period of the supporting structure is reduced as the period of the structure increases.

5.4.3 Effect of Nonlinear Behavior of Supporting Structure

The effects of nonlinear behavior of the supporting structure have been examined in numerous prior studies (Lin and Mahin, 1985); (Villaverde, 1987); (Rodriguez et al., 2002); (Taghavi and Miranda, 2006); (Medina et al., 2006). All of the studies have shown that the peak floor acceleration amplification factors are reduced as the level of nonlinearity (yielding or ductility) is increased.

Similar trends are observed in the floor response spectra presented in Miranda and Taghavi (2009) and Medina et al. (2006), in which roof mounted nonstructural components in tune with the fundamental period of the structure experience a considerable reduction in peak acceleration as the level of yielding in the building is increased. While nonstructural components tuned to lower modes of vibration are not affected or conversely affected by the increased level of ductility in the supporting structure. This supports the assessment of Rodriguez et al. (2002) that the effect of yielding within the supporting structure is primarily concentrated in the acceleration response of the first mode of vibration of the supporting structure.

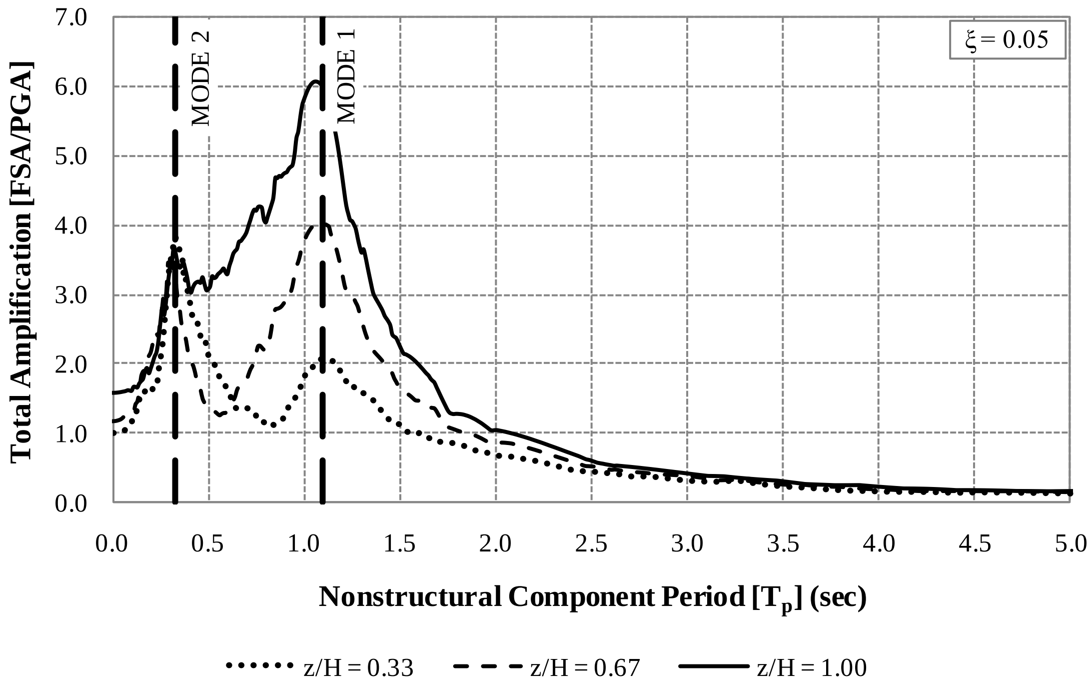

Figure 5-11 Influence of Modal Periods on Total Floor Acceleration Spectra [B3]

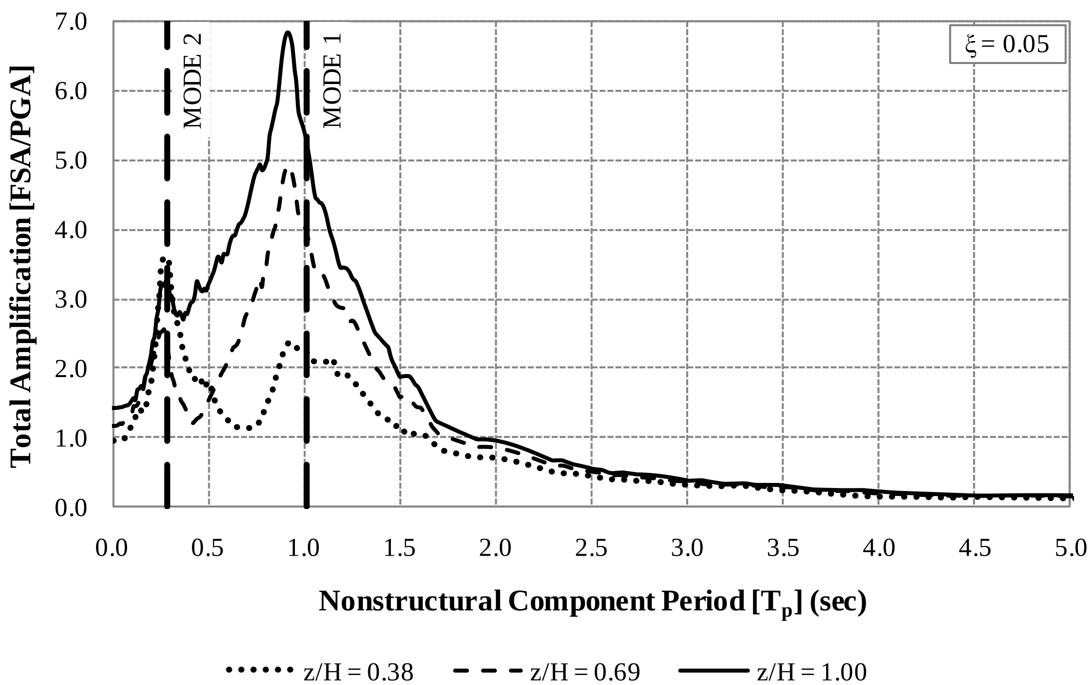

Figure 5-12 Influence of Modal Periods on Total Floor Acceleration Spectra [H3]

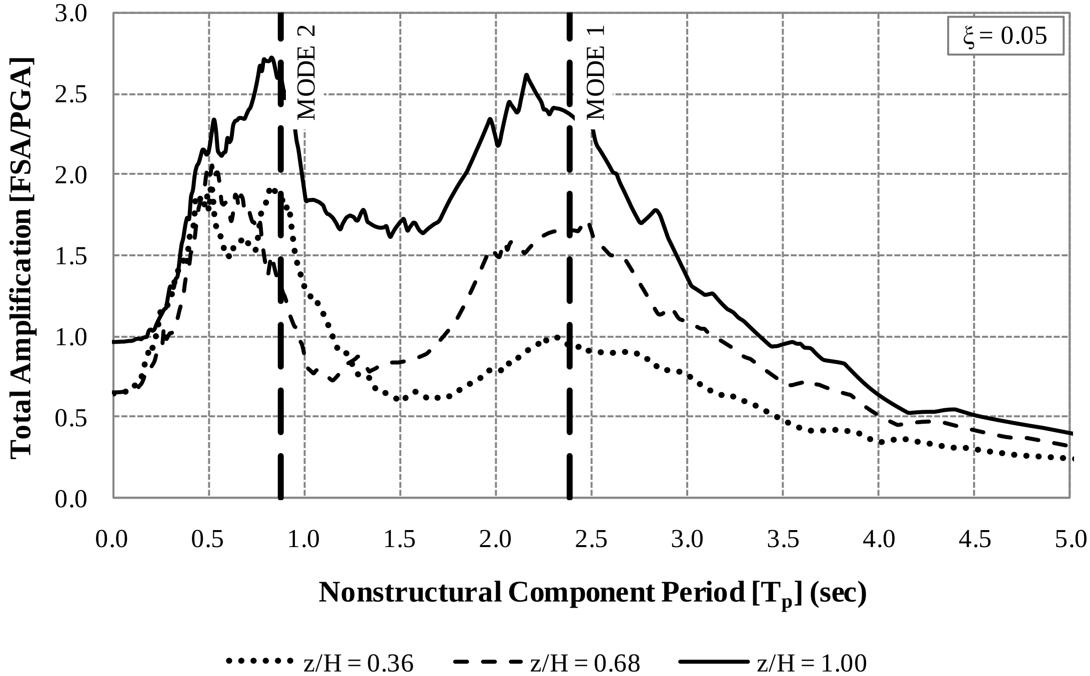

Figure 5-13 Influence of Modal Periods on Total Floor Acceleration Spectra [B9]

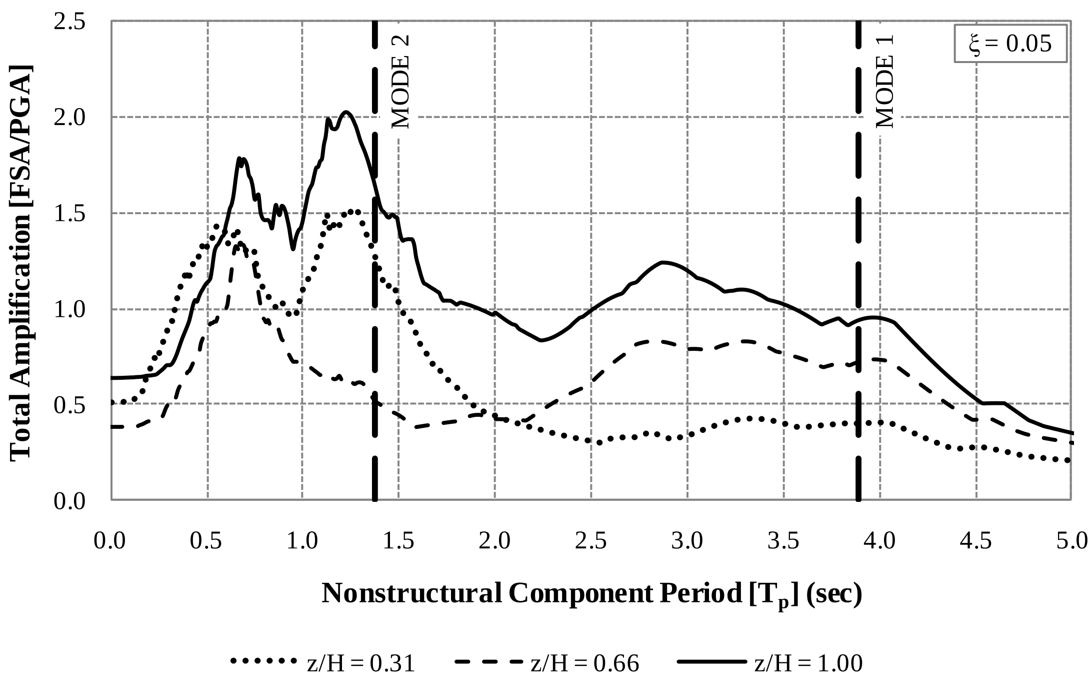

Figure 5-14 Influence of Modal Period on Total Floor Acceleration Spectra [B20]

5.4.3.1 Rigid Nonstructural Components

The correlation between peak acceleration amplification factor and global drift ductility (Section 4.2.2.3) is presented in the series of plots shown in Figure 5-15 through Figure 5-18. These figures show the peak acceleration amplification factor against roof drift as well as various levels of global drift ductility. The plots depict an initial region of constant peak acceleration amplification factor followed by a region of decreasing peak acceleration amplification factor with increasing ductility.

As the building yields two things happen that can explain the reduction in peak acceleration amplification with increased ductility. First, the lateral stiffness of the building is reduced causing an increase in the natural period of vibration. This in turn decreases the floor acceleration amplification. Second, yielding dissipates energy and introduces damping to the building. Increased damping also reduces the acceleration response thus decreasing the PFA/PGA ratio. Accounting for the elongated period of the building due to yielding is commonly achieved by introducing the effective period.

The concept of effective period approximates the period of a nonlinear system after it exceeds its yield point. Consider the force-displacement curve of the system shown in Figure 5-19. The ductility can be defined as:

$$\mu = \frac{D_{\max}}{D_y} \tag{5-15}$$

in which, D_{max} = maximum deformation related to the ductility levels in the system, D_y = yield deformation. If the system undergoes a maximum ductility, μ, the effective period of an equivalent system can be determined as shown in Figure 5-19.

$$T_{eff} = T\sqrt{\frac{\mu}{1+\alpha(\mu-1)}} \tag{5-16}$$

where α = post yield to initial stiffness ratio, which may be assumed to be equal to zero for an elastic-perfectly-plastic system.

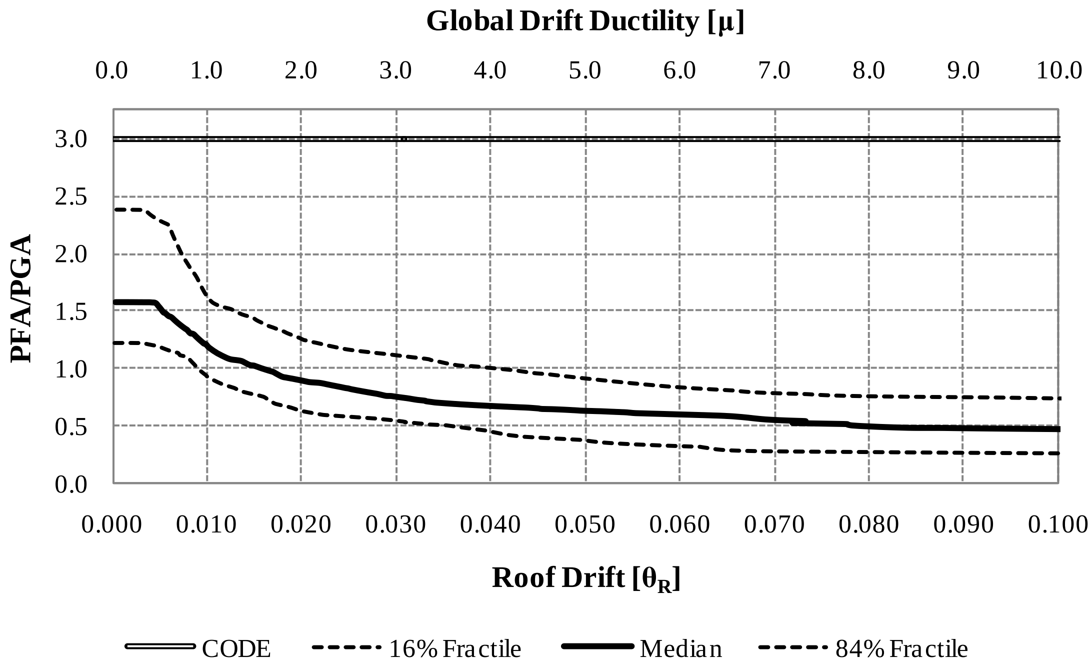

Figure 5-15 Influence of Ductility on Roof Acceleration Amplification [B3]

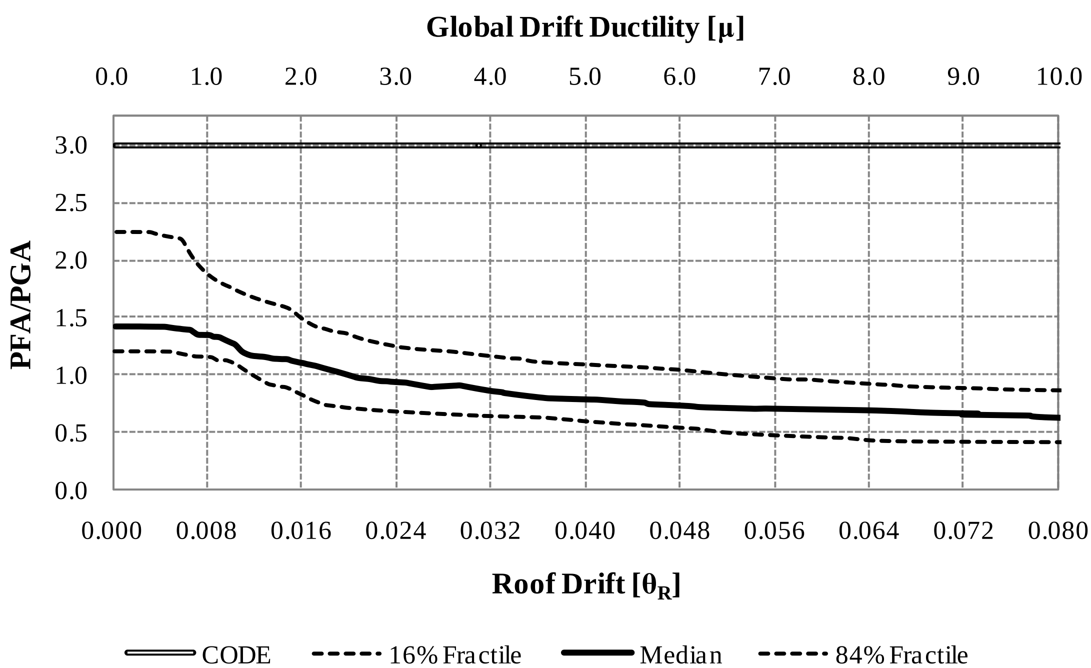

Figure 5-16 Influence of Ductility on Roof Acceleration Amplification [H3]

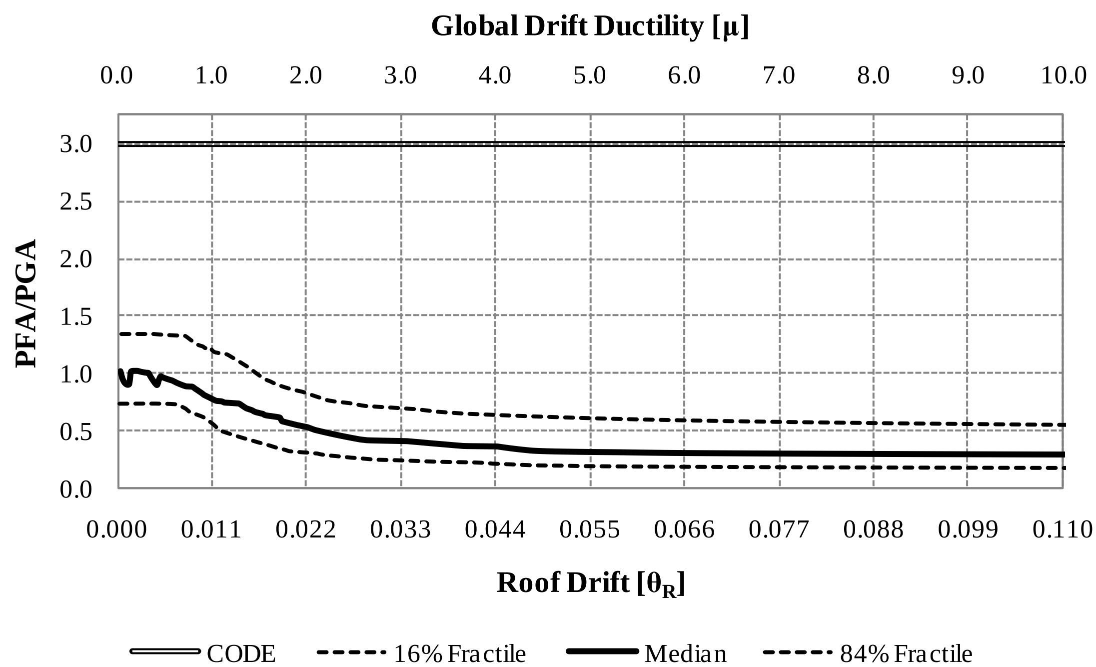

Figure 5-17 Influence of Ductility on Roof Acceleration Amplification [B9]

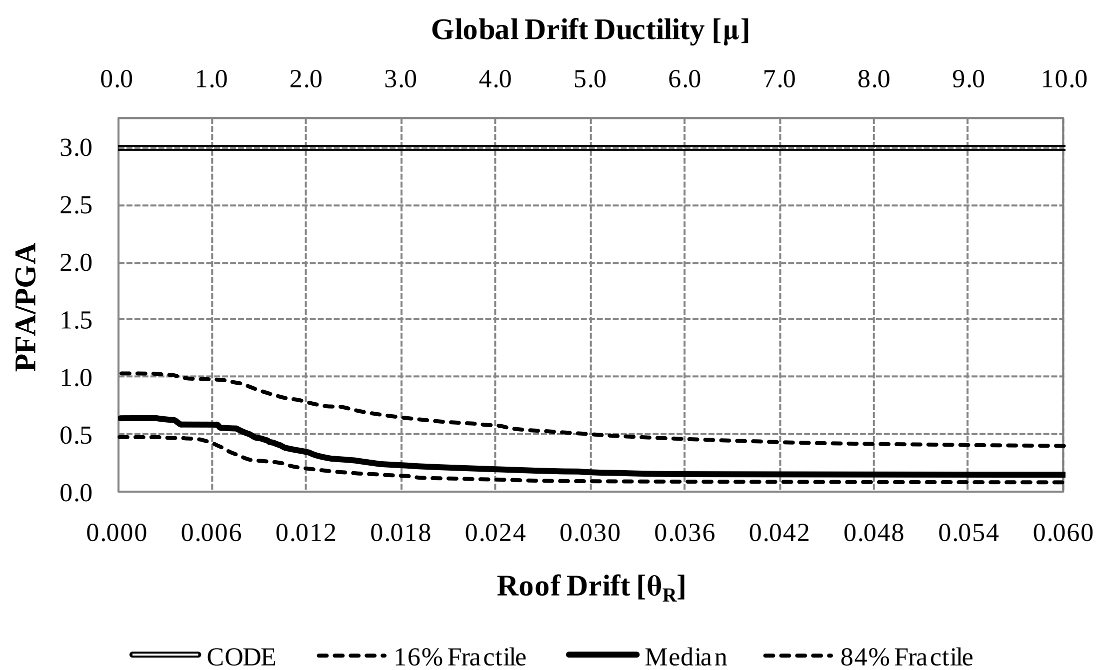

Figure 5-18 Influence of Ductility on Roof Acceleration Amplification [B20]

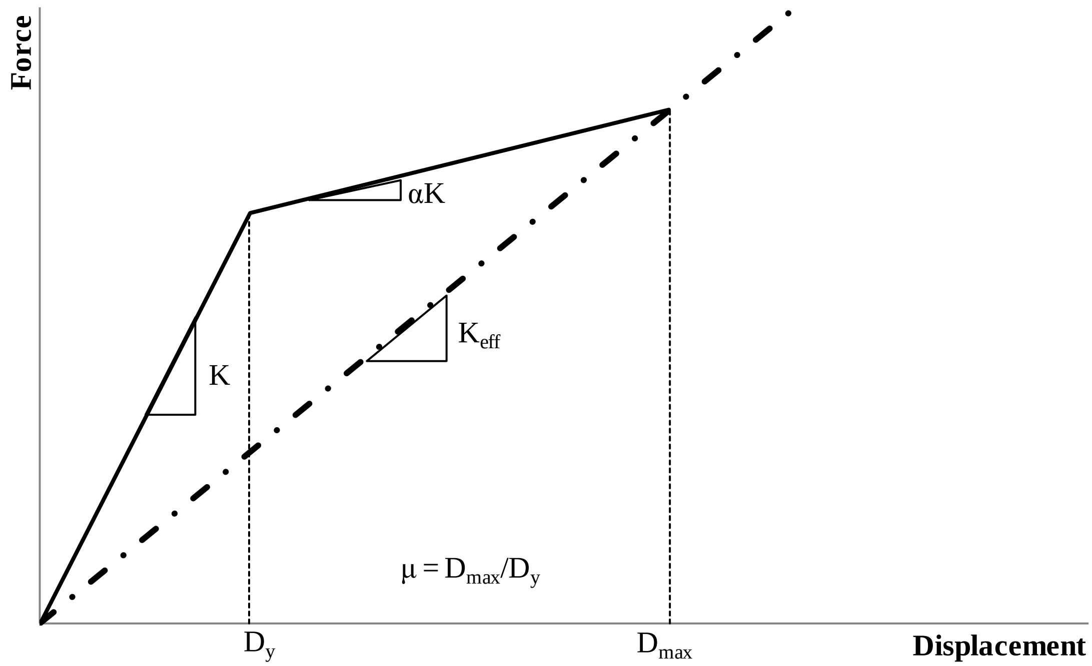

Figure 5-19 Effective Stiffness of a System with Post Yield Hardening

By relating the amount of ductility in the system to the period of the system it is possible to estimate the change in the peak acceleration amplification factor using a single term, the effective period.

5.4.3.2 Flexible Nonstructural Components

Increased levels of ductility also affect the response of flexible nonstructural components tuned to the modal frequencies of the supporting structure. This is evident in the total acceleration amplification as well as the component acceleration amplification. Figure 5-20 through Figure 5-23 show the median component amplification factors at the roof level of each building for various levels of ductility as a function of the ratio of nonstructural period to fundamental period of the supporting structure (T_p/T_1). In examining these curves a number of trends are evident.

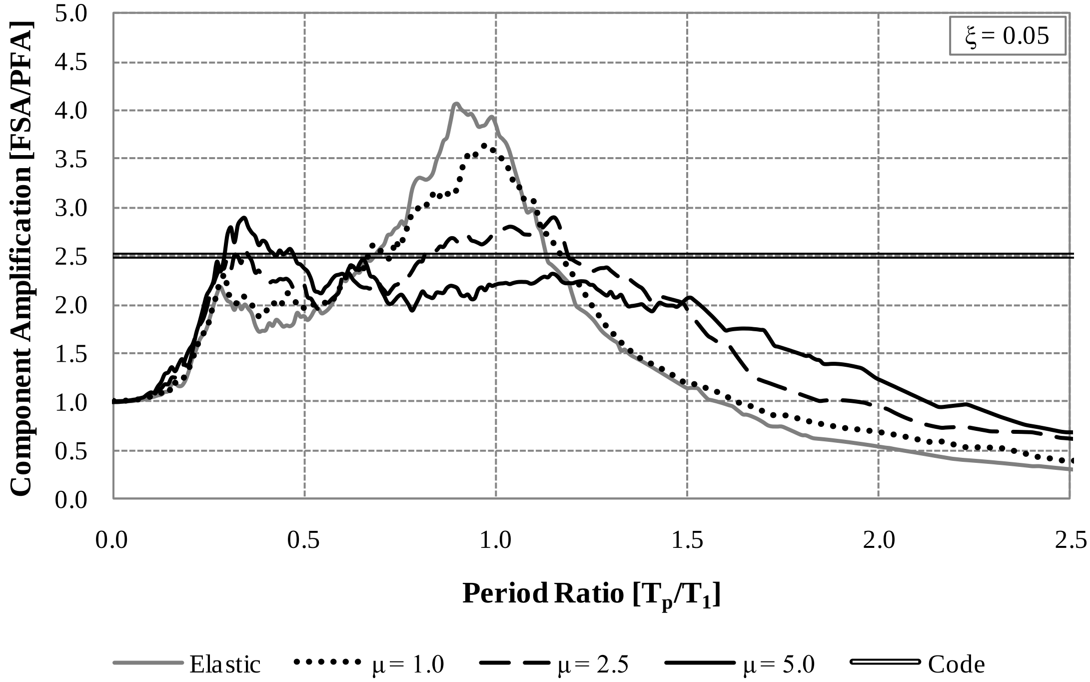

Figure 5-20 Influence of Ductility on Roof Component Amplification [B3]

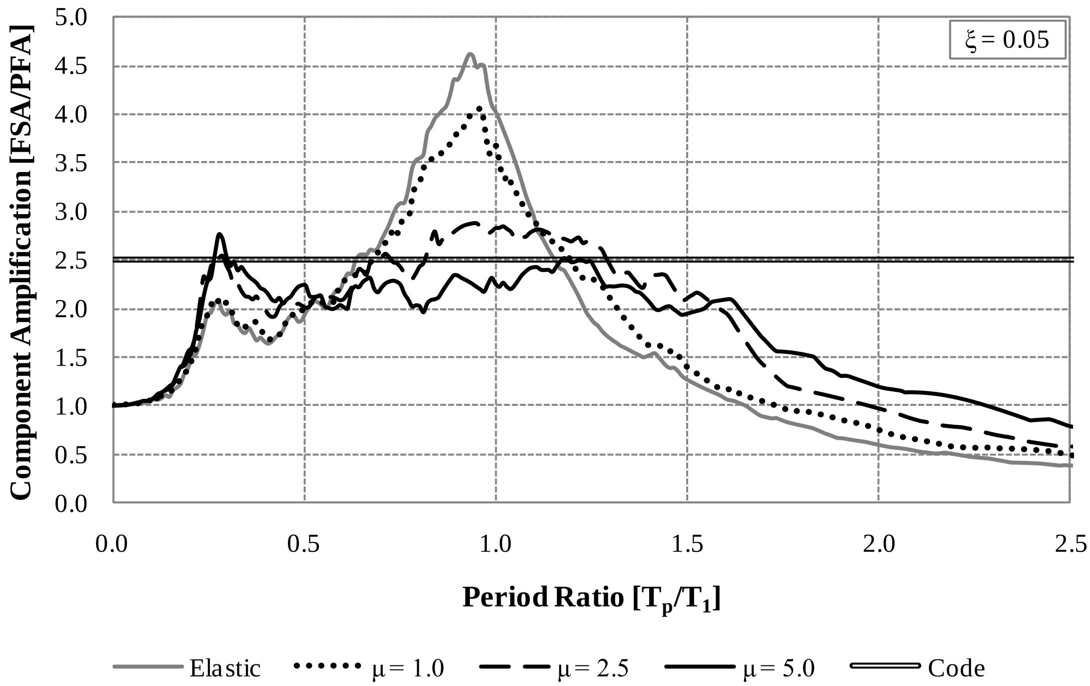

Figure 5-21 Influence of Ductility on Roof Component Amplification [H3]

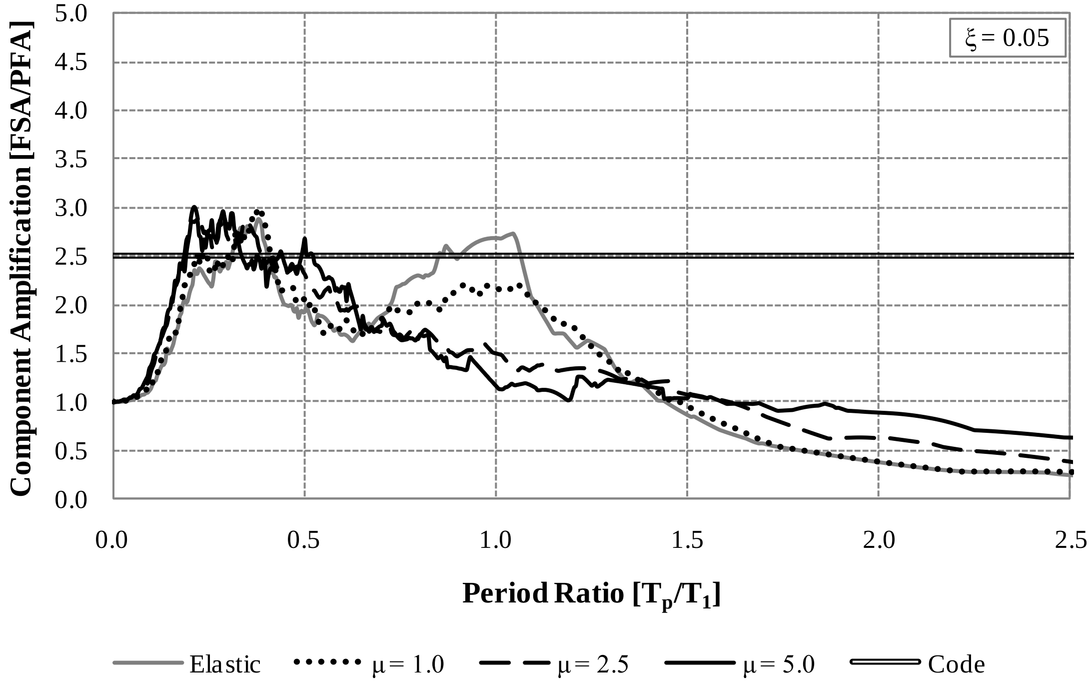

Figure 5-22 Influence of Ductility on Roof Component Amplification [B9]

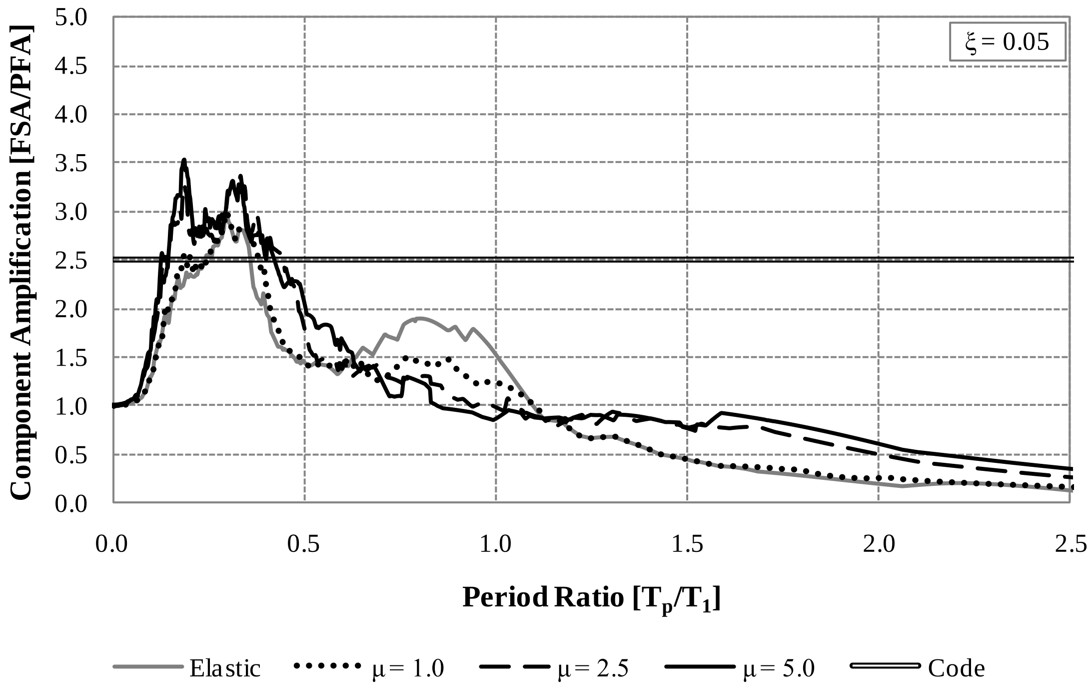

Figure 5-23 Influence of Ductility on Roof Component Amplification [B20]

The component amplification of nonstructural components tuned with the fundamental period of the supporting structure ($T_p/T_1 = 1$) is considerably diminished as the level of ductility in the supporting structure is increased. This however does not occur for nonstructural components tuned with the higher modes of the supporting structure. In fact, generally the component acceleration amplification factor is increased with increasing ductility for nonstructural components tuned with the higher modes of the supporting structure. This supports the conclusion (Rodriguez et al., 2002) that yielding in the supporting structure predominately affects the acceleration response contribution of the fundamental mode of vibration.

The peak associated with the fundamental mode of the supporting structure decreases in amplitude and also shifts to a higher period ratio. This shift is due to yielding of the supporting structure, which elongates its period. A wider range of large period ratios are affected as the level of ductility increases.

5.4.4 Effect of Relative Height of Mounting Location

Medina et al. (2006) observed that the maximum component accelerations generally occur at the roof level. Furthermore, the acceleration amplification associated with the fundamental mode of the supporting structure decrease with decreasing floor level more rapidly than those tuned to the higher modes. These observations provide evidence that the spectral accelerations as well as the peak floor accelerations are influenced by the mode shapes of the structure. Similar findings are shown in the studies by Taghavi and Miranda (2006).

The following results highlight the variations in the peak acceleration amplifications and the component acceleration amplifications throughout the height of the structure. Each of these relationships is used to develop recommendations for improvements to the current code later in the chapter.

5.4.4.1 Rigid Nonstructural Components

The peak floor acceleration amplification profiles are presented in Figure 5-24, which plots the elastic median and 84% fractile profiles of each building along with the current code-recommended profile. In addition, the influence of structural ductility on the peak acceleration amplification profiles is examined in Figure 5-25, which for each building presents the median peak acceleration amplification profiles for various levels of structural ductility.

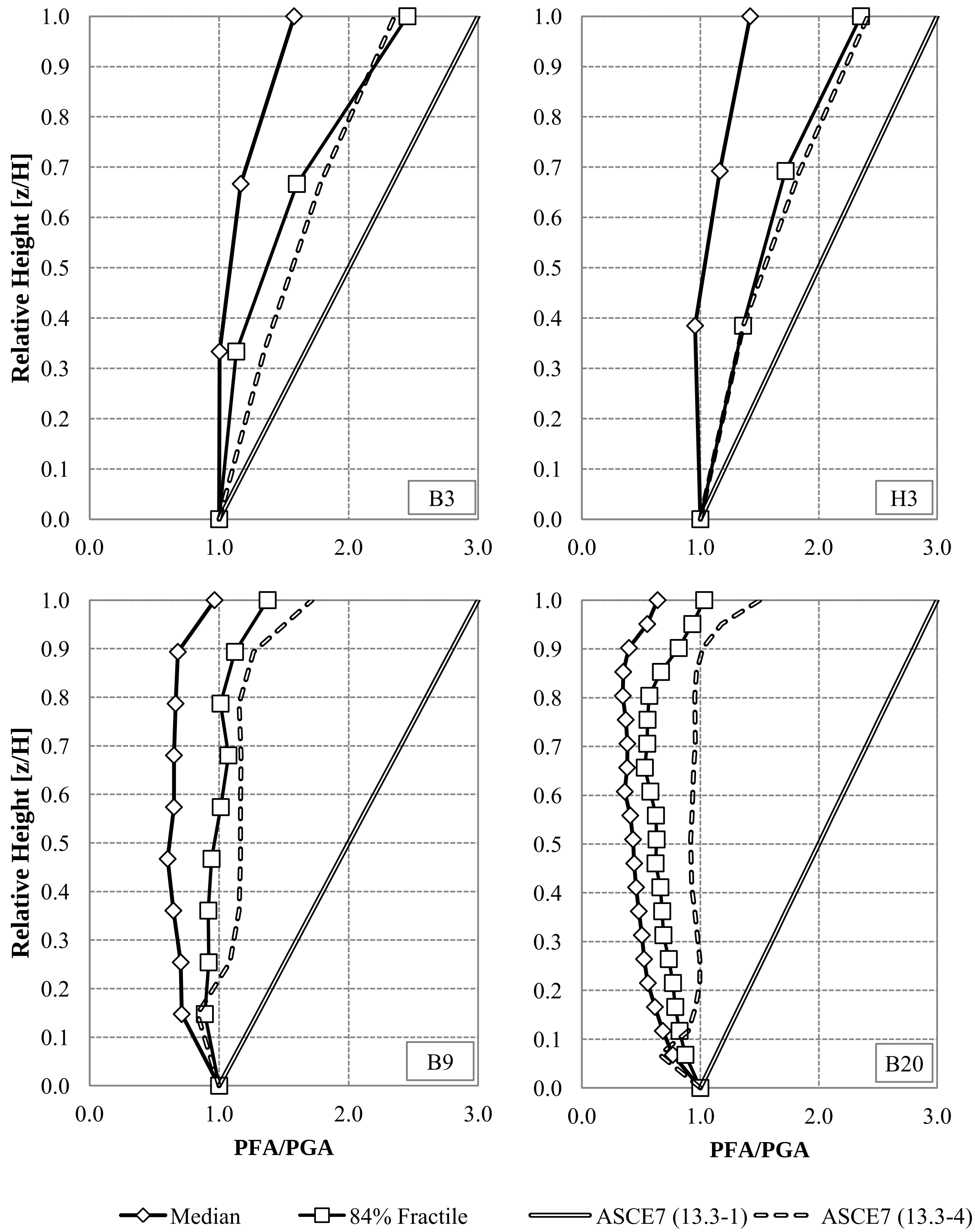

Figure 5-24 Effect of Relative Height on Peak Acceleration Amplification [B3, H3, B9, B20]

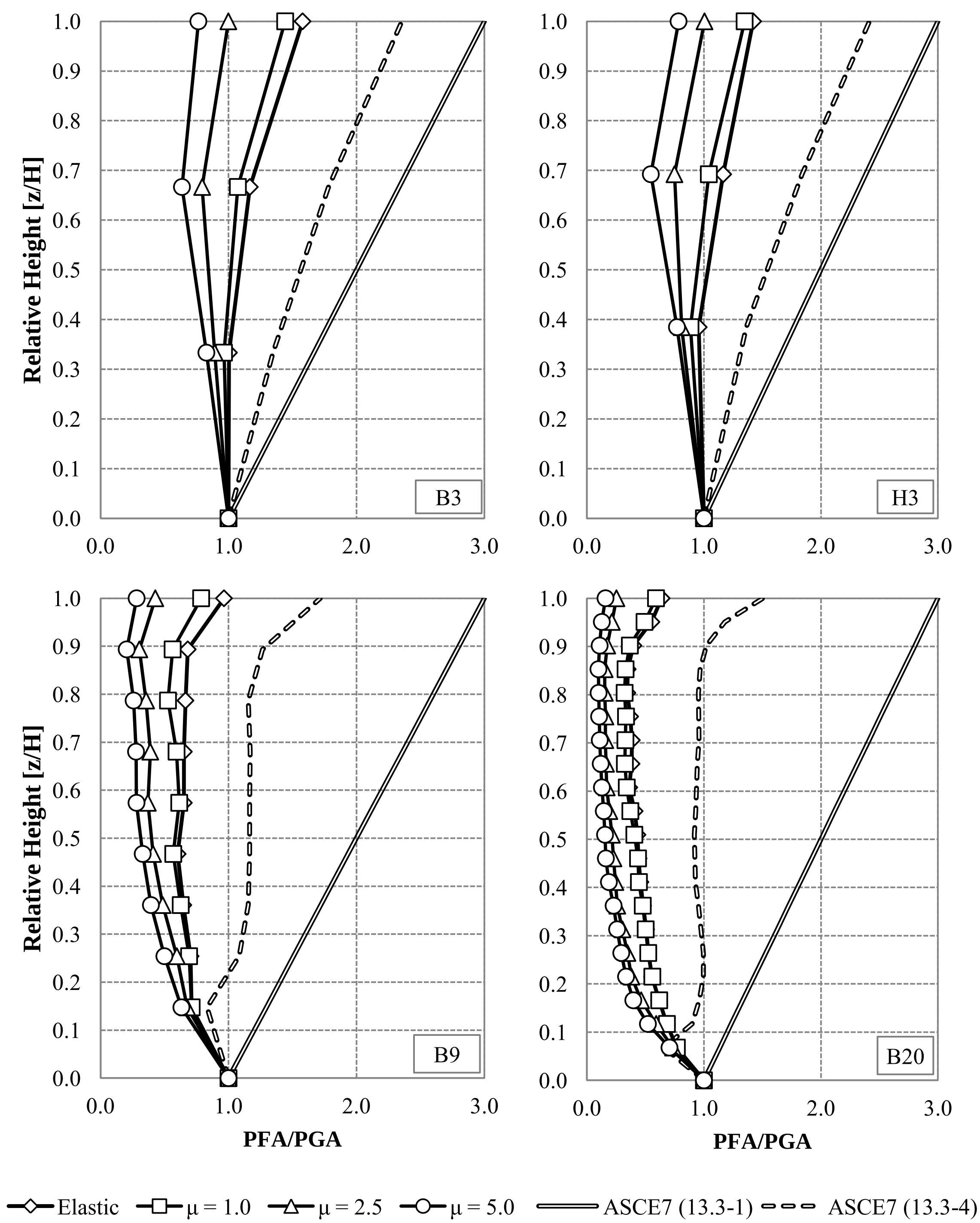

Figure 5-25 Influence of Ductility on Peak Acceleration Amplification [B3, H3, B9, B20]

It is noted that the influence of structural period is consistent throughout the relative height of the supporting structure. Also, as the level of ductility increases the peak acceleration amplification factor is decreased consistently throughout the height of the supporting structure. In addition, the peak acceleration amplification profiles of each of the buildings appear similar to the fundamental mode shapes of the supporting structures. This is expected as the fundamental mode of vibration is known to dominate the sway response moment-resisting frame buildings. An increasing influence of the higher modes of vibration, as seen in the sudden increase in the profile near the roof level, is evident in the profiles of the taller structures which have a larger participation factor for higher frequency modes.

5.4.4.2 Flexible Nonstructural Components

In the research presented by Miranda and Taghavi (2009), the period of the structure is shown to influence not only the peak floor response of the structure but the floor response spectra as well. Their paper introduces a unique profile view of the component acceleration amplification factor of components tuned with the periods of the supporting structure. Using this representation they are able to conclude that the component acceleration amplification factor is (1) not constant throughout the height of the structure, (2) depends on the fundamental period of the supporting structure, and (3) that the shape of the profile is dependent on which modal frequency the nonstructural component is in tune with.

In a similar nature, Figure 5-26 and Figure 5-27 show the elastic median component acceleration amplification profiles for nonstructural components tuned to the fundamental period and second mode period of the supporting structure, respectively. Again similar shapes to those presenting by Miranda and Taghavi (2009) are found, but the amplitudes presented in this study are smaller. Similar conclusions are made however and these are an integral part of the assessment of the current code.

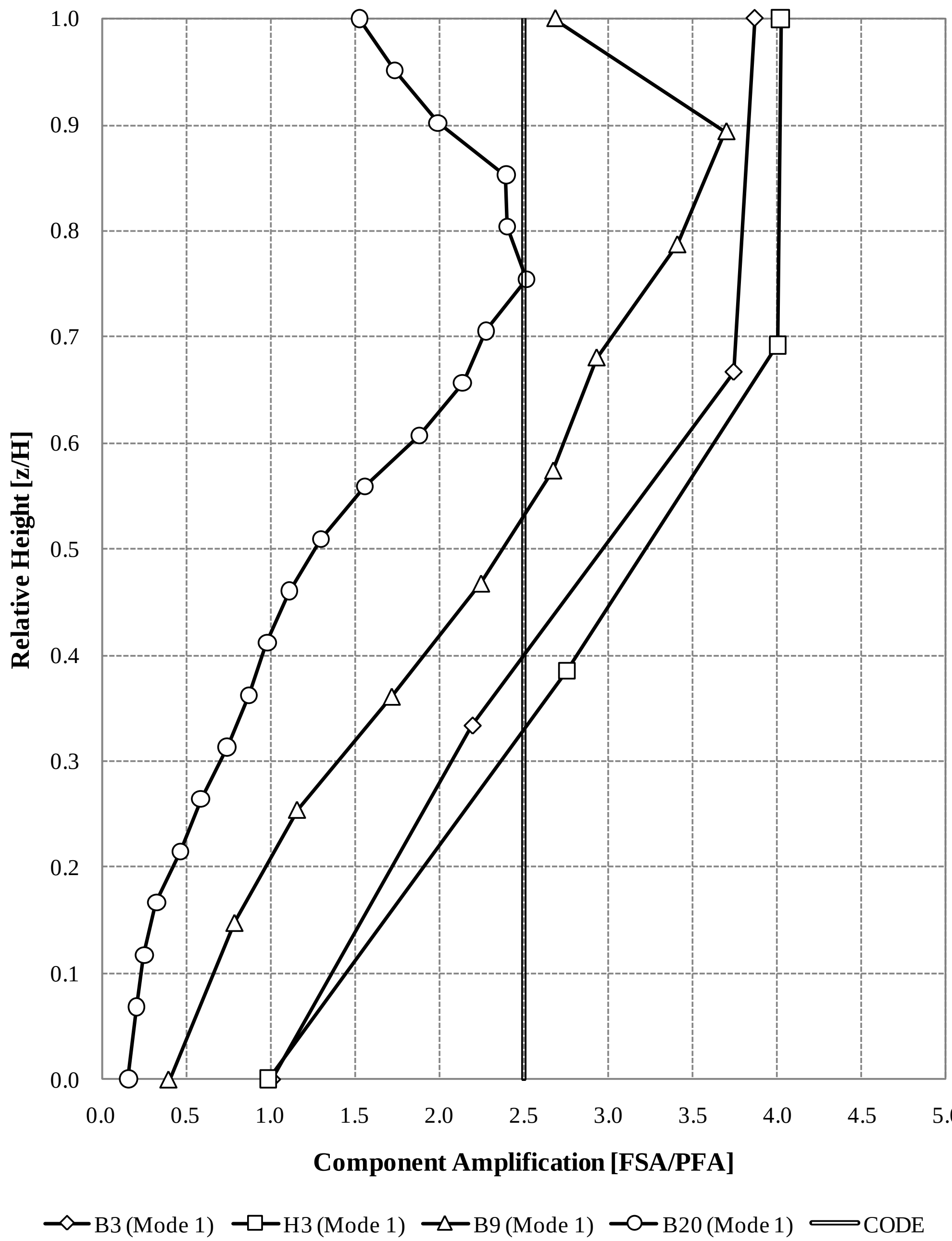

Figure 5-26 Influence of Relative Height on Component Amplification of Nonstructural Components Tuned to the Fundamental Period of the Building

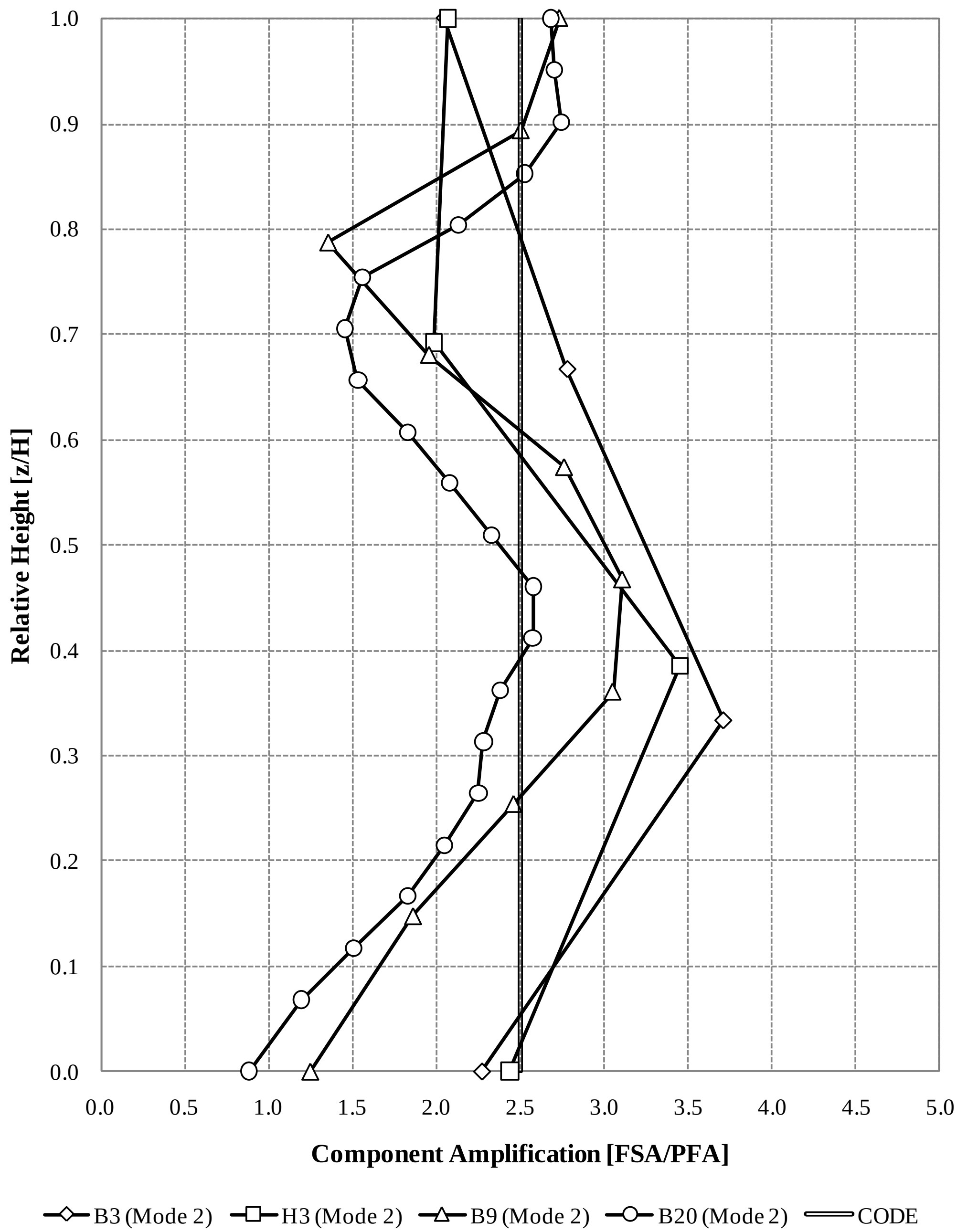

Figure 5-27 Influence of Relative Height on the Component Amplification of Nonstructural Components Tuned to the Second Modal Period of the Building

The influence of ductility in the supporting structure on the component acceleration amplification profiles is demonstrated in Figure 5-28 and Figure 5-29, which plot the profiles for nonstructural component tuned to the fundamental period and second mode period of the supporting structure, respectively, for various levels of ductility. Clearly, the nonlinearity of the structural response predominately affects the fundamental mode is validated. It can be seen that there is significant change in the profiles of nonstructural components tuned with the fundamental period of the structure while the influence on the profiles of those tuned with the second modal frequency is considerably less noticeable.

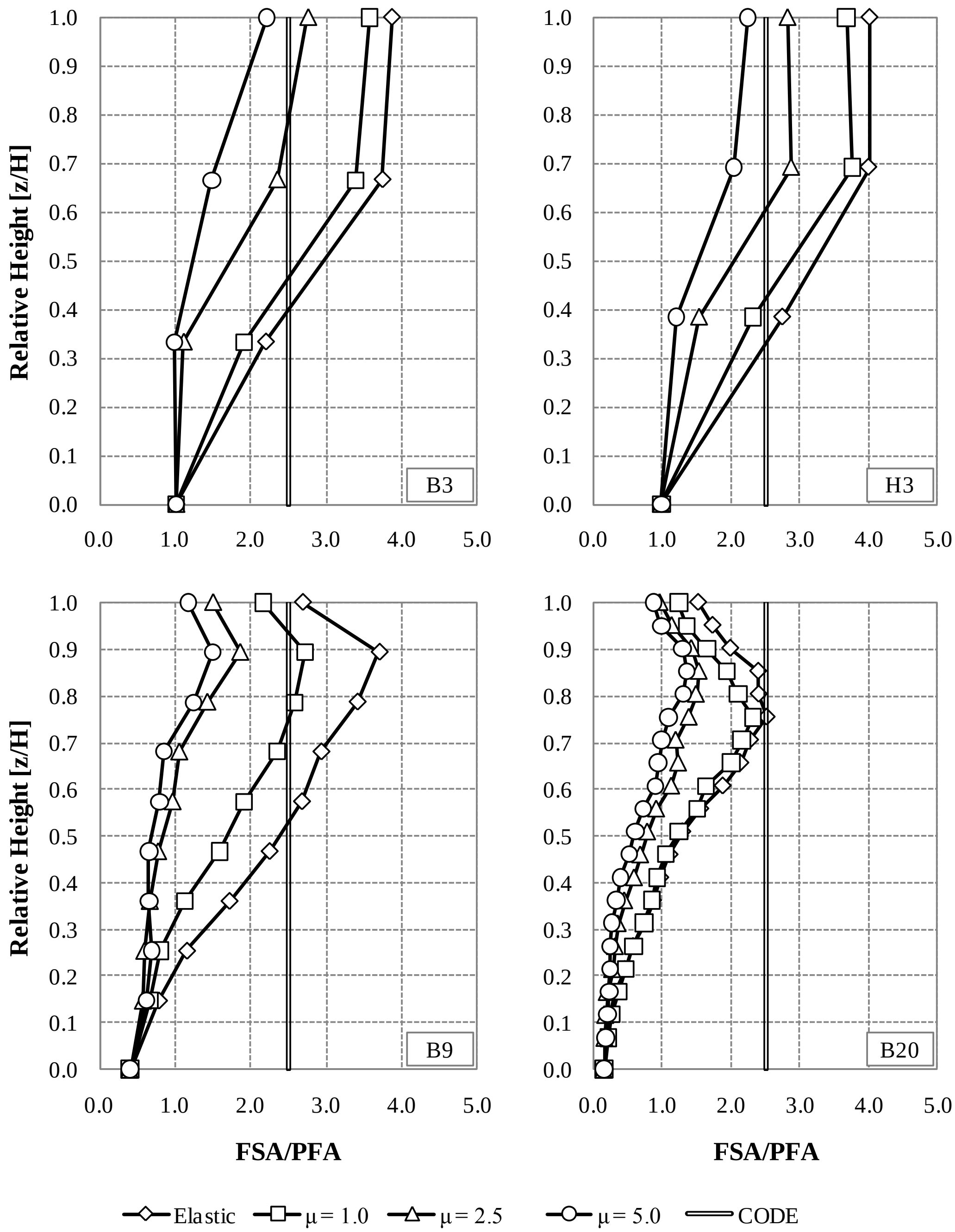

Figure 5-28 Influence of Ductility on the Component Amplification Profiles of Nonstructural Component Tuned to the Fundamental Period of the Building

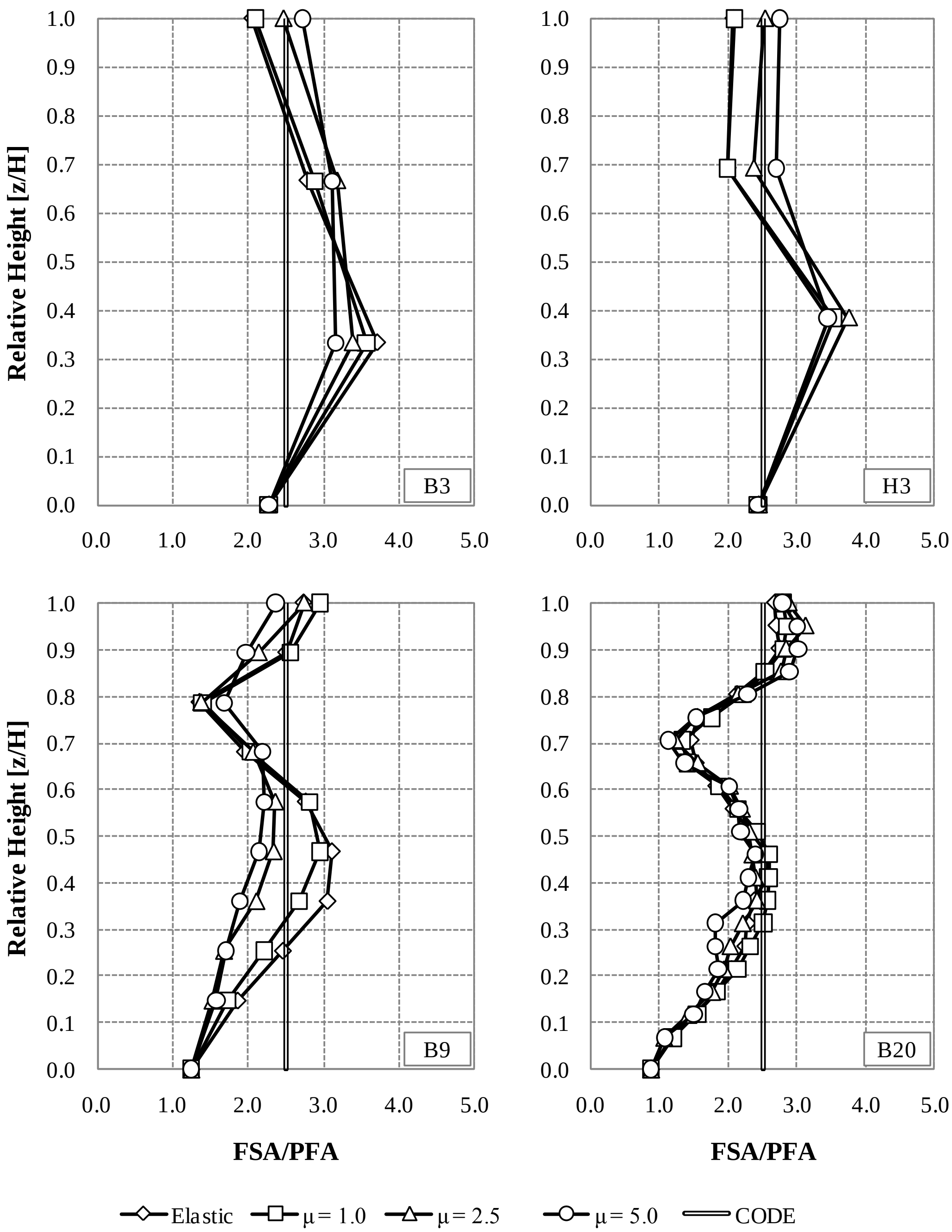

Figure 5-29 Influence of Ductility on the Component Amplification Profiles of Nonstructural Components Tuned to the Second Modal Period of the Building

5.4.5 Effect of Damping Ratio of Nonstructural Component

5.4.5.1 Rigid Nonstructural Components

The influence of damping on rigid nonstructural components is negligible, therefore the effect of damping ratio on the response of rigid nonstructural components is not considered in this study.

5.4.5.2 Flexible Nonstructural Components

The response of flexible nonstructural components is significantly influenced by their damping ratio. As mentioned before, often the damping ratios of nonstructural components are very small, sometimes in the order of 0.5% to 2.0%. However, there have been several estimates for the proper assumption of nonstructural component damping, which was discussed in detail in Section 5.2.2.

The influence of the nonstructural component damping ratio is studied by plotting the median roof total acceleration amplification spectra of Building B3 under elastic response as well as under moderate inelastic response ($\mu = 2.5$) for various nonstructural component damping ratios in Figure 5-30 and Figure 5-31, respectively. Figure 5-32 and Figure 5-33 illustrate the same curves normalized by total acceleration amplification of a 5% damped nonstructural component. The difference is fairly constant when not in resonance with the modal frequencies of the supporting structure, however the difference is slightly increased when the components are tuned with the supporting structure. Similar results were obtained for the other floors and structures.

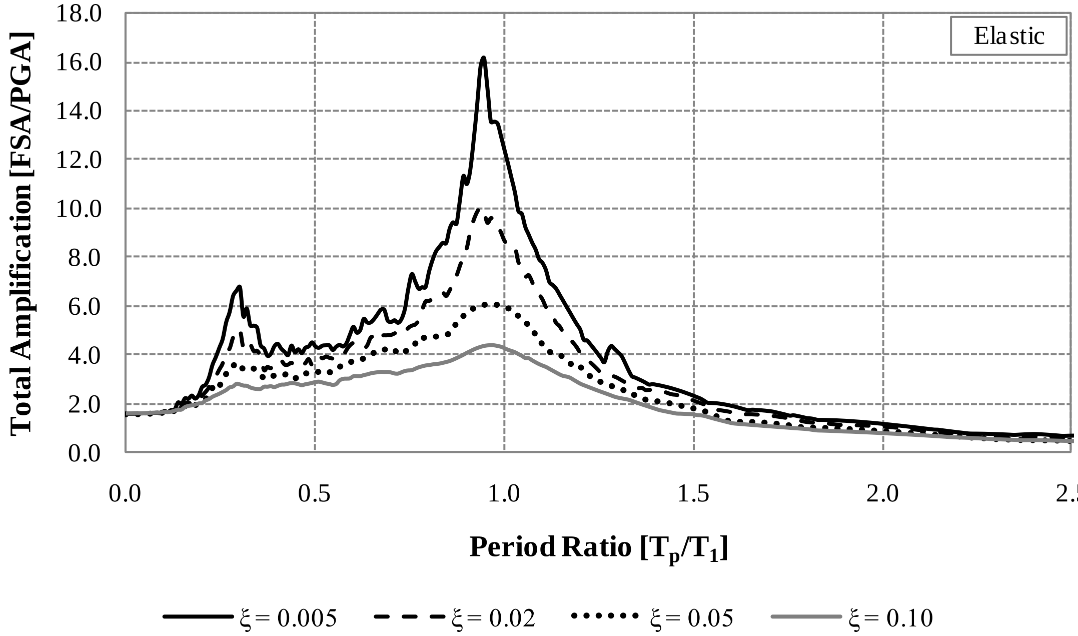

Figure 5-30 Influence of Nonstructural Damping Ratio on Elastic Total Floor Acceleration Spectra [B3]

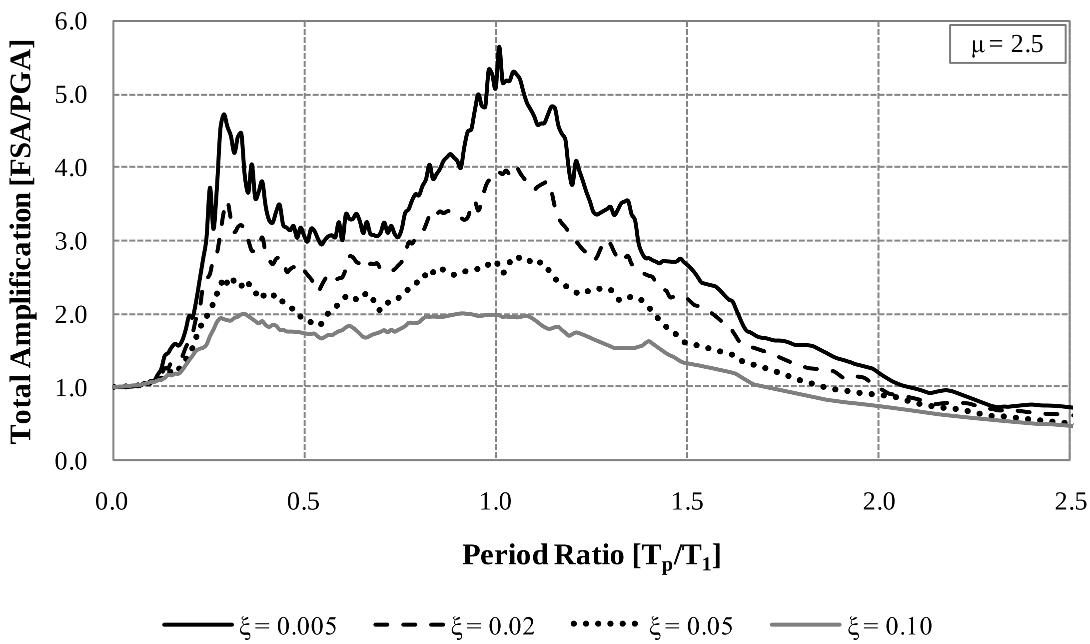

Figure 5-31 Influence of Nonstructural Component Damping Ratio on Moderately Ductile Total Floor Acceleration Spectra [B3]

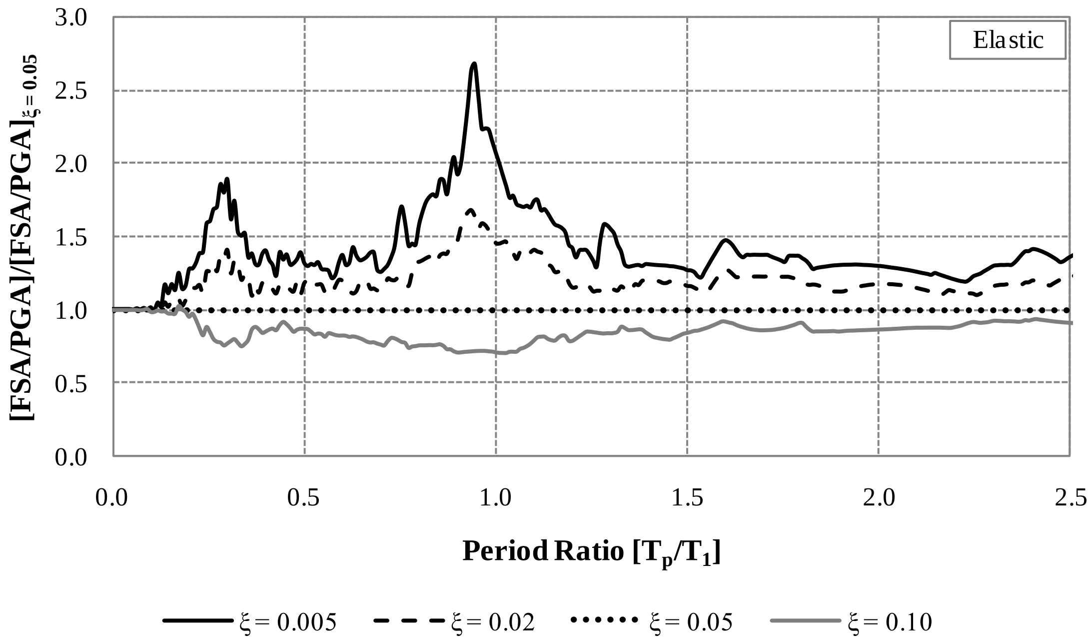

Figure 5-32 Relative Difference between Nonstructural Component Damping Ratios for Elastic Response [B3]

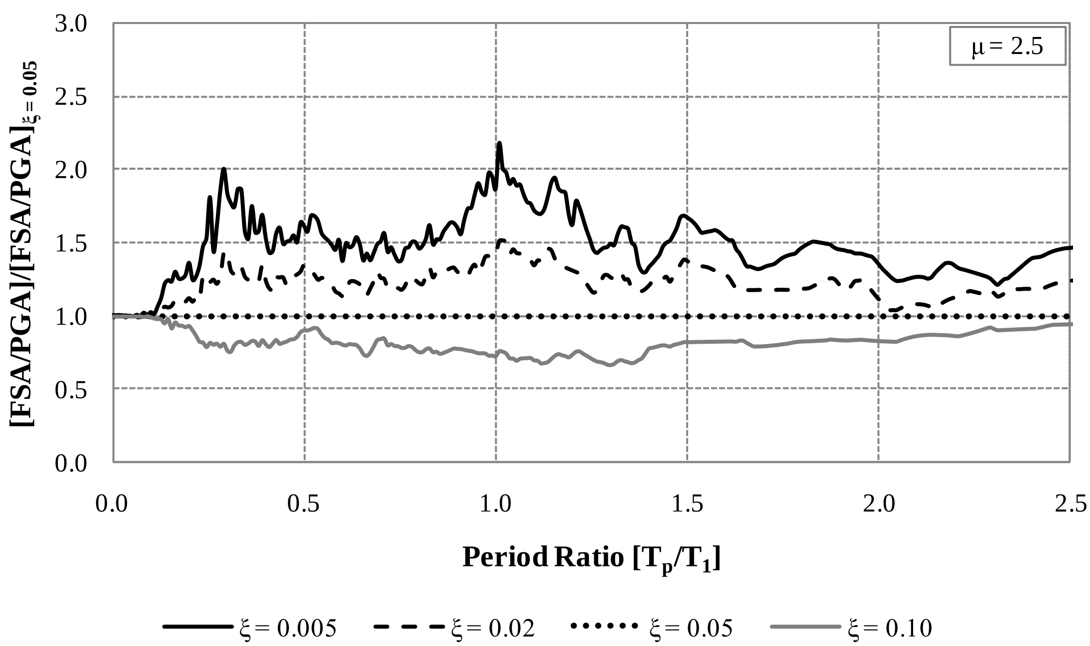

Figure 5-33 Relative Difference between Nonstructural Component Damping Ratios for Moderately Inelastic Response [B3]

5.5 Assessment of Current Code

A review of the ASCE 7-10 (ASCE, 2010) nonstructural design provisions as well as the nonstructural seismic qualification provisions outlined in the AC 156 (ICC, 2006) is presented in this section. The provisions as they are applicable to both rigid and flexible nonstructural components are examined.

It is understood that code provisions are intended to provide a reasonable estimate of the seismic demands anticipated during the design earthquake event. Throughout this document the terms “conservative” and “unconservative” are used to describe the estimation provided by the code and proposed equations relative to the analysis results. Assuming the analysis results are representative of typical flexible ductile steel moment frame buildings, the simplified equation is deemed to be “conservative” if the demand obtained by the equation is greater than observed in the analysis and “unconservative” if the demand obtained by the equation is less than observed in the analysis.

5.5.1 Peak Ground Acceleration (PGA)

The current code approximates the peak ground acceleration as 40 percent of the short period spectral acceleration. Comparing the ground motions used in this study with the recommended design spectrum of both the 1994 UBC (ICBO, 1994) as well as the 2006 IBC (ICC, 2006), the normalized code spectra fall within the median and 84% fractile spectra of the applied suite of motions, as shown in Figure 5-34. Consequently, the ground motion set used in this study provides similar characteristics to the design spectra, and thus the code-approximated peak ground acceleration is appropriate based on the set of motions used.

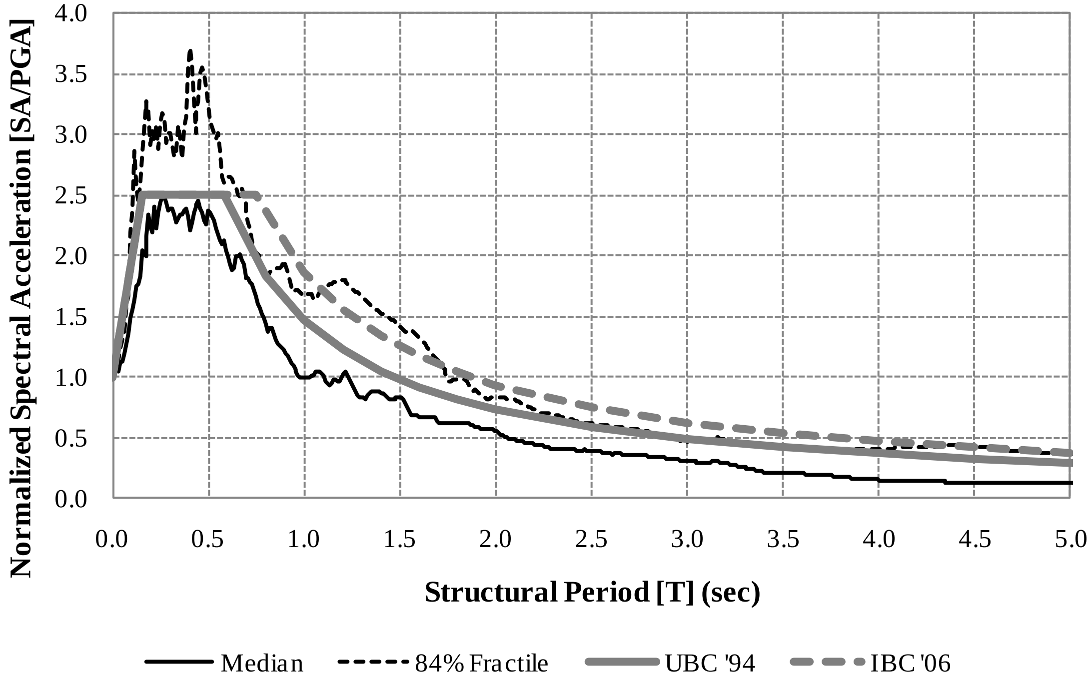

Figure 5-34 Normalized Ground Acceleration Spectra

5.5.2 Component Acceleration Amplification Factor (FSA/PFA)

Currently the ASCE 7-10 requires a component acceleration amplification factor, a_p, of 2.5 for flexible nonstructural components. This coincides with the accepted acceleration amplification of a single-degree-of-freedom system on the ground. The design acceleration spectrum required in the current seismic codes defines a short period acceleration of 2.5 times the peak ground acceleration. This amplification comes from the dynamic characteristic of the soil in relation to those of the system. For nonstructural components mounted within a building, however, a component acceleration amplification factor of 2.5 has been shown to be insufficient.

The results of this study along with several others have shown the inability of a constant approximation to capture the true nature of the component acceleration amplification factor. In many cases where the nonstructural component period is dissimilar to the period of the supporting structure, the code is conservative; however, as the period of the nonstructural component approaches the modal periods of the structure, the code becomes unconservative. In addition to its relationship with the period of the supporting structure, the component acceleration amplification factor has a great deal of dependency on the nonstructural component's location along the height of the structure as a result of the influence of mode shapes. One of the most extreme cases occurs for nonstructural components mounted approximately 70% up the height of the supporting structure. If these nonstructural components are tuned to the fundamental period of the supporting structure, the median component acceleration amplification factor may be as large as 4.0, while at the same location nonstructural components tuned to the second mode period of the supporting structure may experience no component amplification at all (a_p = 1.0). Thus there is clearly a dependency on the combination of location within the structure, the period ratio of the nonstructural component, and the mode shapes of the building.

5.5.3 Peak Acceleration Amplification Factor (PFA/PGA)

Along with the deficiencies in the component acceleration amplification factor, there are also short comings in the current calculation of the peak acceleration amplification factor. Currently the code defines a linear relationship throughout the height of the structure, assumes the peak floor acceleration of the base coincides with the peak ground acceleration of the motion, and the peak acceleration response at the roof is equal to three times the peak ground acceleration. This is independent of the period of the structure and any inelasticity expected in the structure, each of which have been shown to influence the peak acceleration amplification factor. Though the linear distribution of peak acceleration amplification throughout the height of the structure does not fit the best with the actual distribution, as noted by the results shown in Figure 5-24, for the results of this study a linear relationship can provide a fairly good approximation of the distribution. This is based on the observation that the true distribution of the peak acceleration amplification comes from a complex combination of the mode shapes, and modal contributions to the overall response which may not be easily obtained by simple design-oriented models. The results presented in Taghavi and Miranda (2006), more so than herein, indicate that a linear distribution of the peak floor acceleration amplification may not be representative of the actual response of buildings.

Overall, the approach of the current code equation is conservative, but the definitions of the component acceleration amplification and peak acceleration amplification lack the complexity to appropriately approximate the acceleration demands imposed on acceleration-sensitive nonstructural components.

The required response spectrum for a nonstructural component on the roof of each building is compared with the results from this investigation in Figure 5-35 through Figure 5-38. These plots compare the median elastic response roof acceleration spectra with the required response spectra based on an S_{DS} value taken as the median spectral acceleration of the ground at a period of 0.2 seconds for elastically responding buildings. From these plots it is clear that the code response spectrum is unconservative in some cases while over conservative in others. However, it was noticed that the observed unconservatism is due to the limit on the value of A_{FLX}. It has been shown that the peak accelerations of nonstructural components on certain floors may exceed 6 to 7 times the peak ground acceleration (note Figure 5-11 through Figure 5-14 showing the total acceleration amplification) when tuned to the fundamental period of the supporting structure. Therefore limiting the required response spectrum to 4 times the estimate of the peak ground acceleration is unconservative. In addition, because the required response spectrum is based on the current seismic design equation in the ASCE 7-10 there is no correlation between the type of supporting structure, the period of the supporting structure, or the amount of ductility experienced by the supporting structure. As previously emphasized each of these has a significant influence on the acceleration response of the nonstructural components and therefore should be accounted for in the derivation of the require response spectrum.

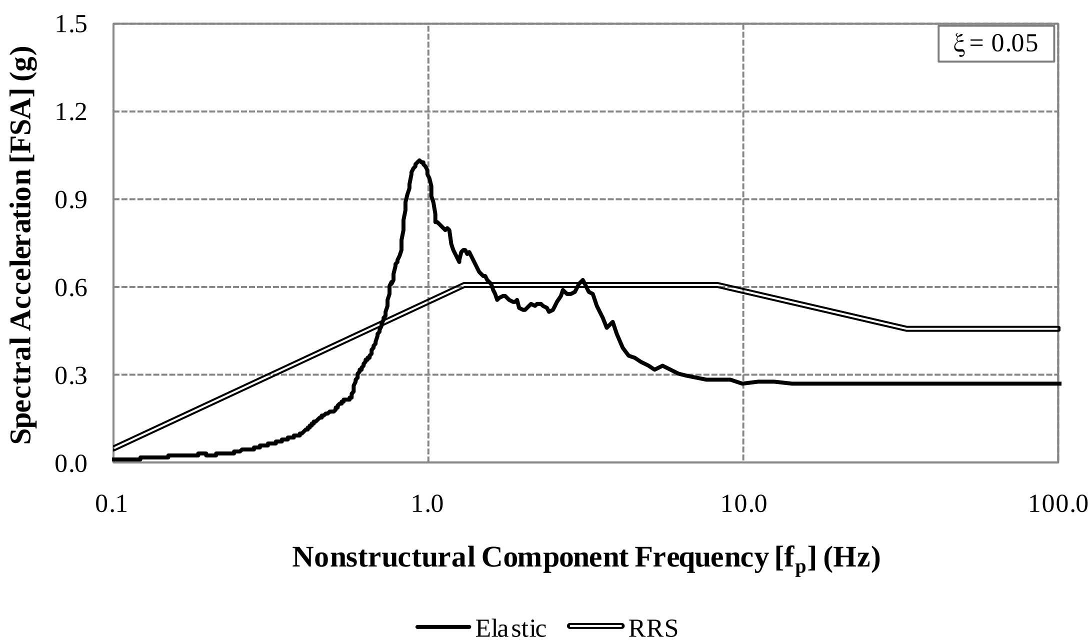

Figure 5-35 AC 156-Required Response Spectrum vs. Elastic Response [B3]

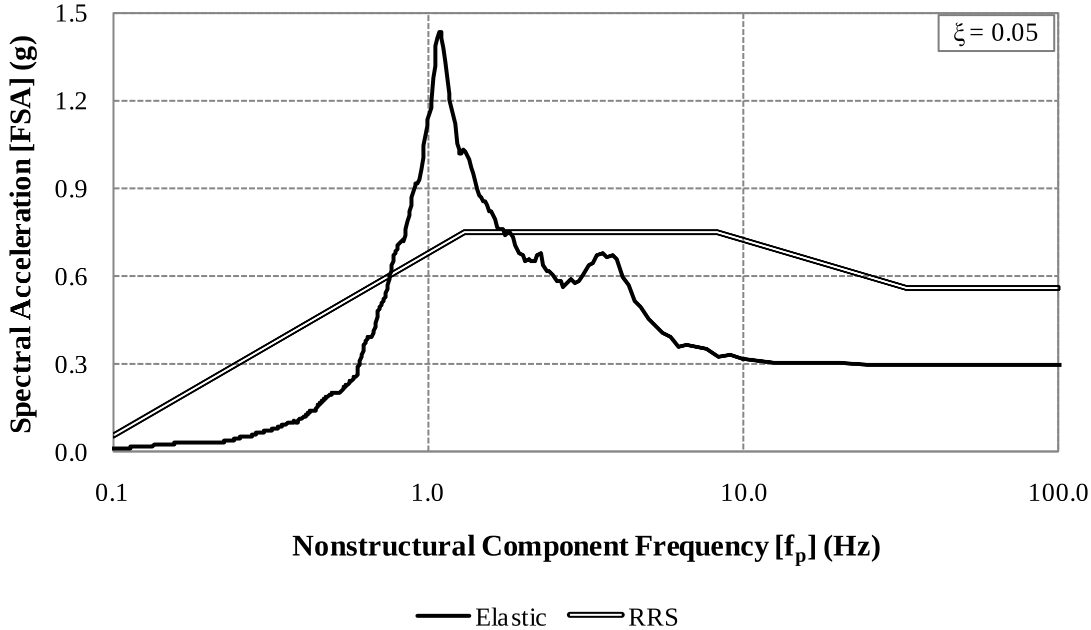

Figure 5-36 AC 156-Required Response Spectrum vs. Elastic Response [H3]

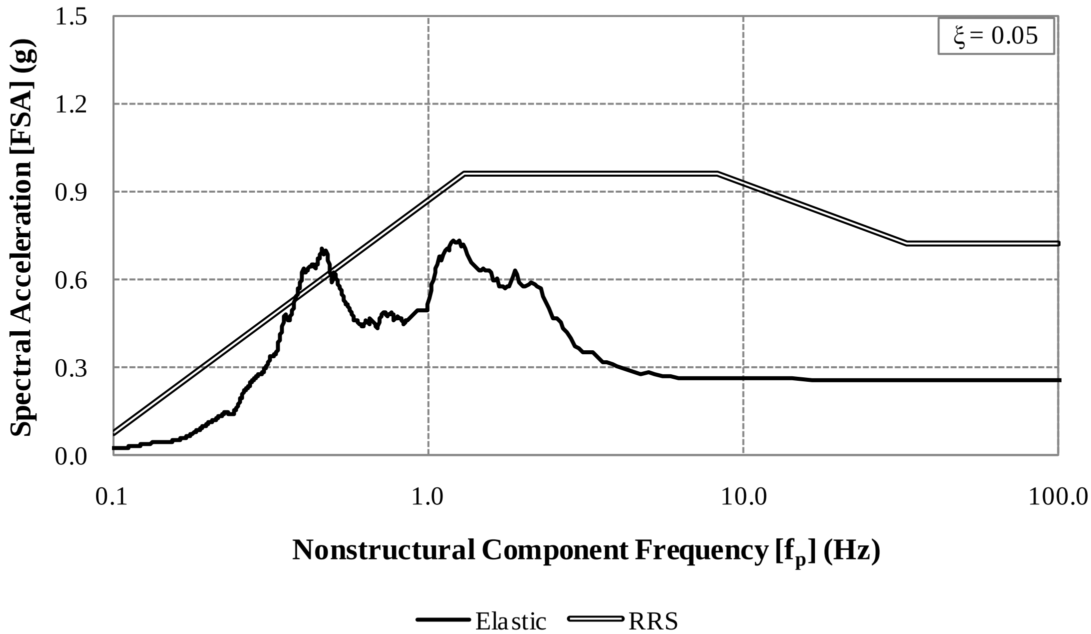

Figure 5-37 AC 156-Required Response Spectrum vs. Elastic Response [B9]

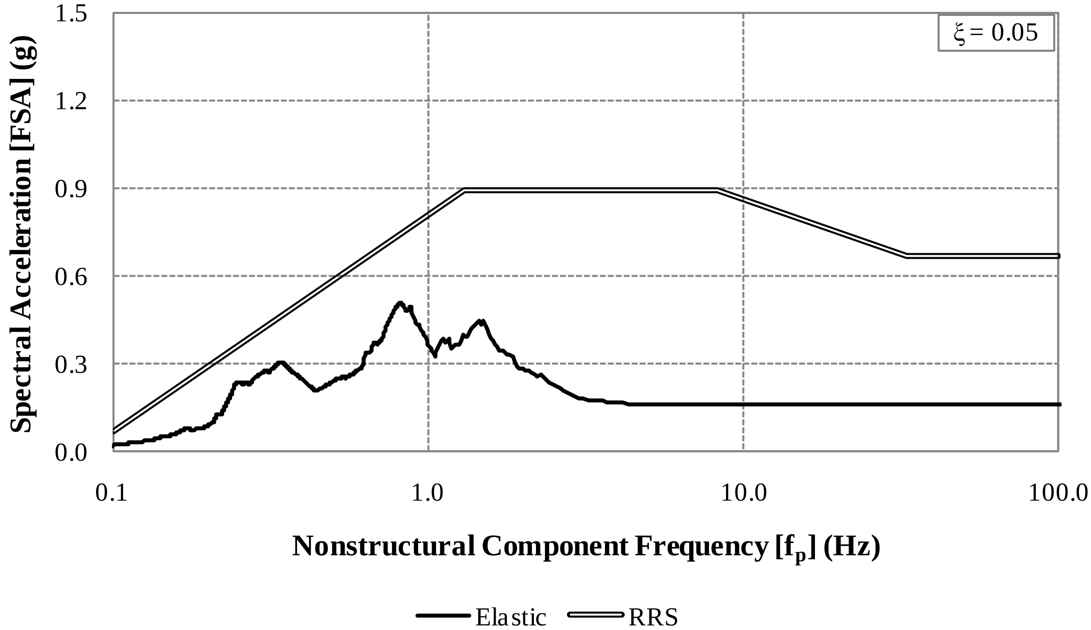

Figure 5-38 AC 156-Required Response Spectrum vs. Elastic Response [B20]

5.5.4 Effectiveness of Code Equation

Though each of the parts of the code equation presented in (5-7) has deficiencies, the sum of the parts may still provide an acceptable approximation. It has been shown that the equation has a tendency to overestimate the PFA/PGA ratio while underestimating the component amplification, a_p. An overall assessment of the complete equation can be obtained from Figure 5-39 through Figure 5-42, which plot the median and 84% fractile elastic roof component acceleration vs. the component period for each of the four buildings. These figures compare the results from this study against the ASCE 7-10 Eq. 13.1-1 and Eq. 13.1-2. It is observed that on average Eq. 13.1-1 provides an acceptable approximation of the peak component acceleration. However, the limiting Eq. 13.1-2 undermines this approximation by unconservatively capping the component acceleration to four times the peak ground acceleration. Secondary evidence of this observation is shown in the results shown by the total amplification presented in Section 5.4.1, in which it is noted that the median total amplification may be as great as 6.0 or 7.0 for elastic structural response. With these observations it is clear that there is room for improvement to the upper bound on the component acceleration.

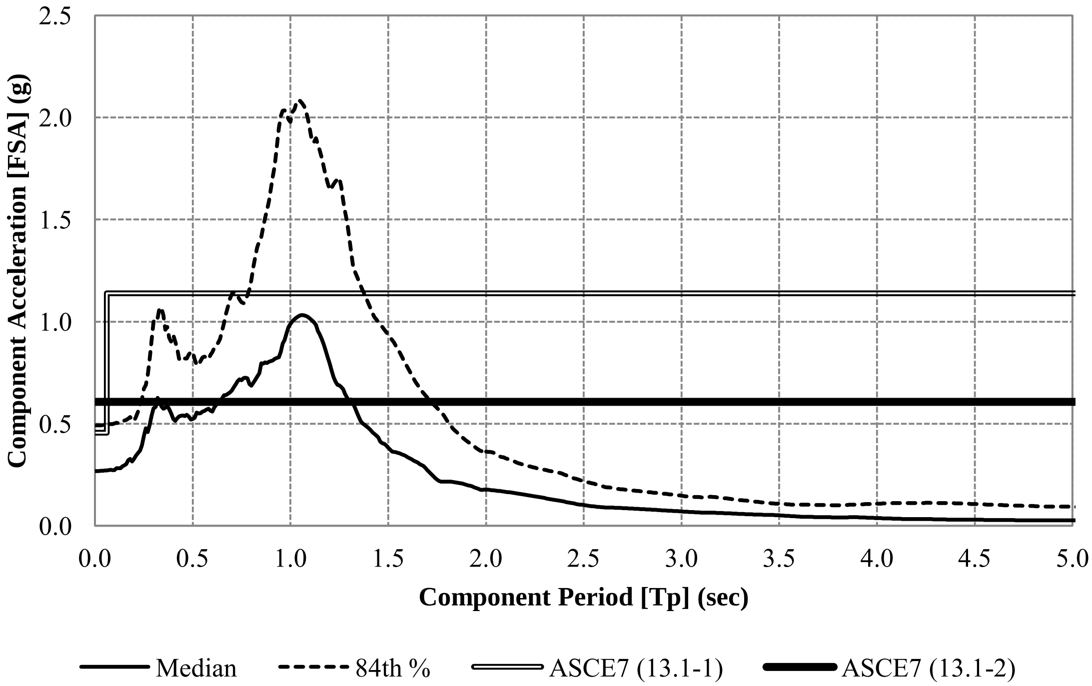

Figure 5-39 Roof Component Acceleration vs. Component Period [B3]

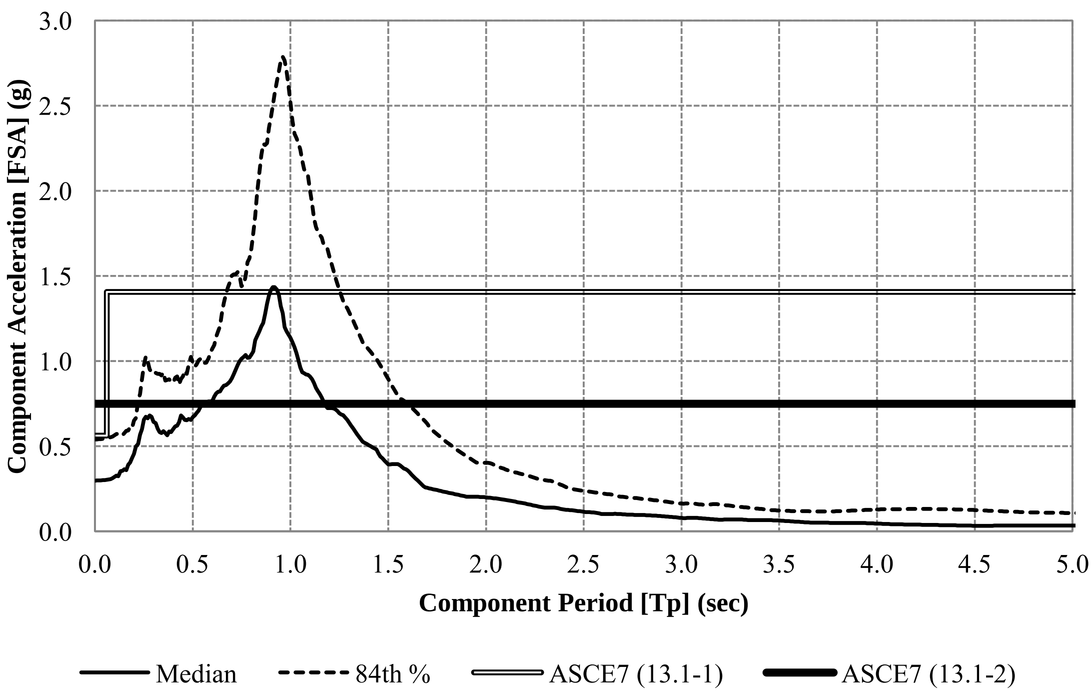

Figure 5-40 Roof Component Acceleration vs. Component Period [H3]

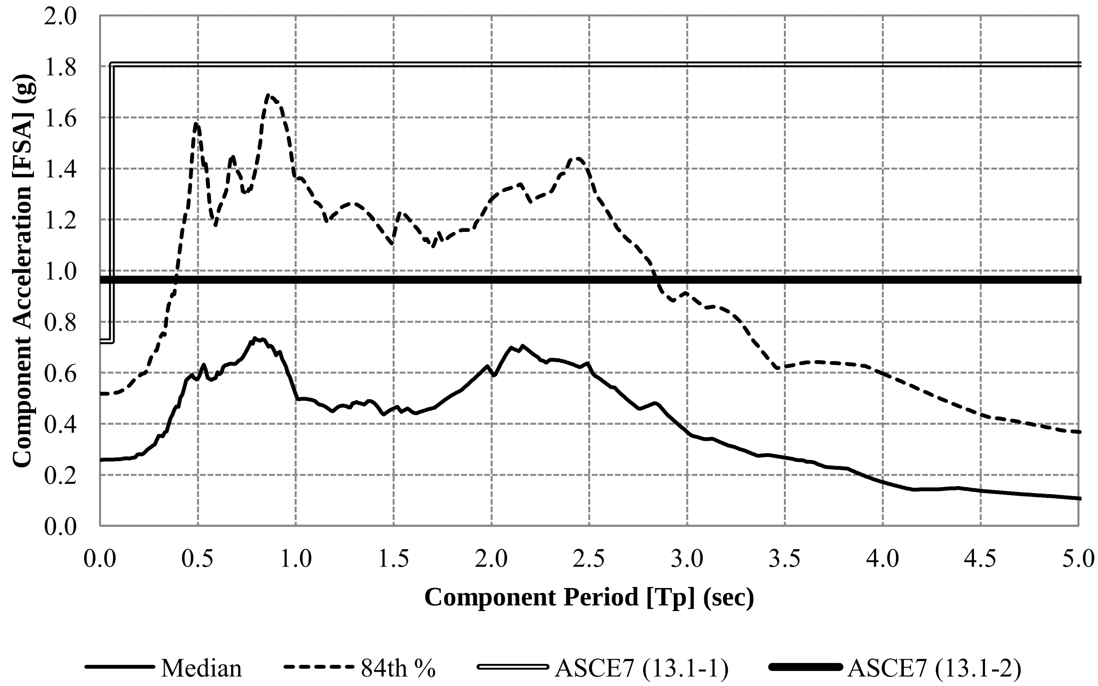

Figure 5-41 Roof Component Acceleration vs. Component Period [B9]

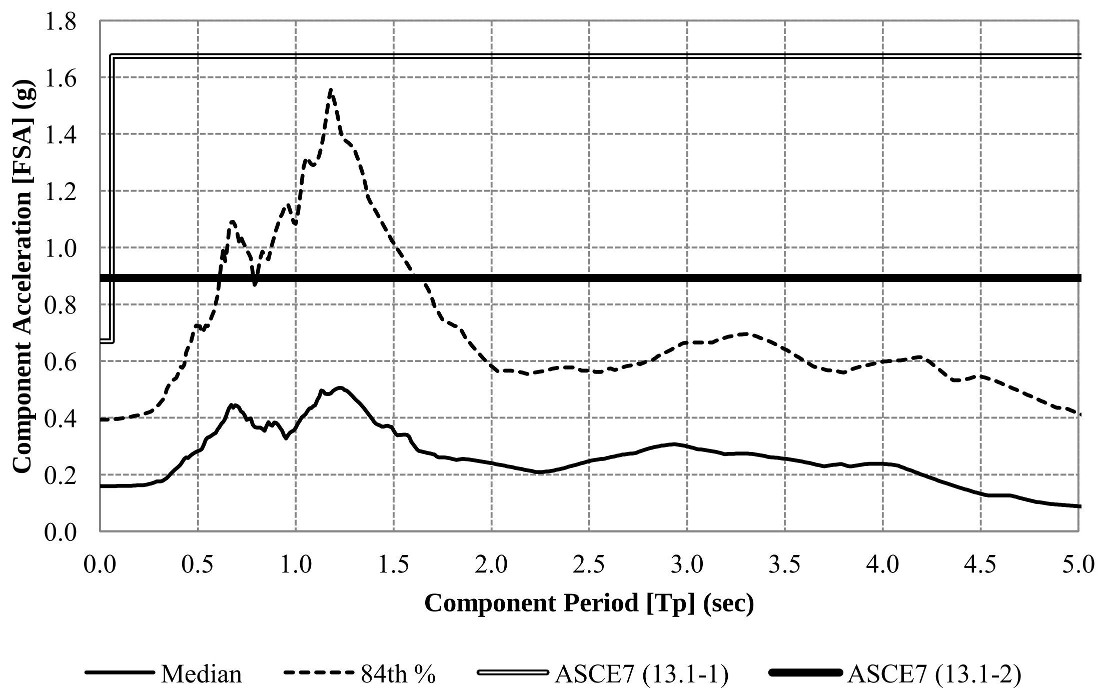

Figure 5-42 Roof Component Acceleration vs. Component Period [B20]

5.6 Recommendations for Code Improvement

In light of the shortcomings in the current code design equations, this study has developed several recommendations for their improvement. The first attempts to improve the current ASCE 7-10 design equation are presented in (5-7). The recommended improvement is then applied to the AC 156-required response spectrum. The second recommendation offers a different and more direct approach to estimating the acceleration demands on nonstructural components throughout the building. This recommendation proposes a spectral amplification function which is applied to the design ground response spectrum to establish a floor acceleration response spectrum which can be used to design nonstructural components depending on their natural frequencies.

5.6.1 Proposed Modification to ASCE 7-10 Equation

One of the primary inadequacies in the current design equation is that the fundamental period of the supporting structure is not accounted for. The current linear expression of the peak acceleration amplification factor is extracted from (5-7) and presented in (5-17).

$$\frac{PFA}{PGA} = 1 + 2\frac{z}{H} \tag{5-17}$$

It has been shown in Section 5.4.2 that for long period structures (T ≥ 1.0 seconds) the peak floor acceleration amplifications under elastic response are roughly inversely proportional to the period of the structure. Introducing this observation into the current linear approximation of the peak acceleration amplification profile leads to (5-18).

$$\frac{PFA}{PGA} = 1 + \frac{T_{\max} - T}{T}\frac{z}{H} \tag{5-18}$$

In which T is the period of the supporting structure, T_{max} is the maximum structural period for which the peak acceleration of the roof is at least equal to the peak ground acceleration, z is the mounting elevation of the nonstructural component, and H is the average height of the building.

Based on the present study T_{max} can be taken as 2.5 seconds. This value of T_{max} was used to plot the proposed acceleration amplification profiles against the current code, median and 84% fractile profiles for each building in Figure 5-43. This figure demonstrates that the proposed profile is still conservative for most floor elevations but reduces the over-conservatism of the current code for the long period structures.

In order to incorporate the influence of the level of ductility experienced in the supporting structure, the effective period is introduced into the proposed expression for peak amplification factor (5-18). By replacing the period of the structure with the effective period of the structure obtained using (5-16), the equation for peak acceleration amplification factor is expressed in (5-19).

$$\frac{PFA}{PGA} = 1 + \frac{T_{\max} - T\sqrt{\mu}}{T\sqrt{\mu}} \frac{z}{H} \tag{5-19}$$

In which μ, the global drift ductility defined in Chapter 4, estimates the level of yielding experienced in the structure. The proposed profiles using (5-19) are compared with the median and 84% fractile results as well as the current code profiles in figure 5-44 for buildings that experienced moderate levels of ductility. These profiles also show considerable improvement over the current code approximations while providing a conservative profile with respect to the analytical results.

In review of the two proposed improvements to the expression of peak acceleration amplification, the second option which includes the influence of structural ductility appears to offer the more comprehensive while still conservative estimate for the acceleration amplification profile. The relationship between drift ductility, μ, and the response modification factor, R, is well understood. Thus this equation could be rearranged in terms of the response modification factor of the structure to generate an expression that includes the nonlinearity in the response of the structure, which in turn is well-defined in terms already used in the design of the structure, namely period and response modification factor. While this seems ideal there is one small uncertainty, which is that the response modification factor is used to reduce the design forces in the structure to account for nonlinearity experienced by the structure during the design earthquake. Therefore, under the design level earthquake the amount of yielding is fairly accurately predicted and (5-19) is achieved. However, if a less intense earthquake occurs, which is more likely, the level of yielding is overestimated by considering the full response modification factor. This creates an uncertain amount of unconservatism in the estimate of the peak acceleration amplification profile, which in many cases will probably not lead to an unconservative estimate of the nonstructural component. Although the estimated peak acceleration amplification is underestimated, so too is the intensity of the ground motion, thus they counteract one another. The uncertainty related to the intensity of the ground motion and corresponding level of yielding experienced in the structure do not allow for a confident estimation of the peak floor accelerations using (5-19) or any modification in terms of response modification factor for design purposes. As an assessment tool when the level of ductility experienced by the structure is well known then (5-19) may be used with reasonable certainty. Contrary to (5-19), (5-18) will not underestimate the acceleration amplification profile depending of the intensity of the ground motion, thus it may be used reliably in design. Therefore it is the recommendation of this study that the code design equation be changed to (5-20) in order to improve the estimation of seismic force demands on nonstructural components throughout the building.

$$F_p = \frac{0.4 a_p S_{DS} W_p}{\left(\dfrac{R_p}{I_p}\right)}\left(1 + \frac{T_{\max} - T}{T}\frac{z}{H}\right) \tag{5-20}$$

In this equation the T_{max} shall be 2.5 subject to further investigation using a more comprehensive suite of buildings with different framing systems.

In addressing the over-conservatism in the peak acceleration amplification expression, the estimation of the seismic force demands using the proposed equation may be unconservative in some cases in which the component amplification factor is underestimated. Using the current value a_p equal to 2.5 has been shown (see Section 5.4.4) to be unconservative for many floors when the period of the nonstructural component is in tune with a modal frequency of the supporting structure. Thus, a procedure for improved estimation of the component amplification factor is proposed which is dependent on the relative height of the nonstructural component within the supporting structure as well as the period ratio between the nonstructural component and the supporting structure. This function should suggest increasing values of a_p as the period ratio approaches 0.3 and 1.0, which represent the locations in which the nonstructural component is in tune with the second and first modes of the structure, respectively. In addition the values of

a_p should vary with height in a pattern that mimics the absolute value of the nearest resonant mode shape. Due to the complexity of such a relationship it is recommended that the value of a_p simply be increased to better envelope the maximum value of nonstructural component amplification factors observed in this and previous studies (Taghavi and Miranda, 2006); (Medina et al., 2006).

Changing the ASCE 7-10 design equation can also be extended to the AC 156-required response spectrum. The difference between the required response spectrum and the observed results from the analytical models is reduced in the high frequency range, however it increases the unconservatism in the resonant frequency ranges. These observations are evident in Figure 5-45 through Figure 5-48, which compare the median results from the analytical investigation to the modified required response spectrum based on the improved design equation (5-18). However, the scope of the AC 156 document is to provide minimum requirements for nonstructural components with fundamental frequencies of at least 1.3 Hz. In this range, the required response spectrum still envelopes the median analytical results. While this study does not include any structures that have fundamental frequencies greater than 1.3 Hz, several buildings exist in which resonance with the first mode of vibration of the structure would be included in the scope of the AC 156-required response spectrum. In these cases it is estimated that with or without the implementation of the recommended improvement to the design equation that the required response spectrum would not accurately predict the amplitude or shape of the true floor response spectrum. It has been shown throughout this chapter that the floor response spectrum is significantly influenced by the fundamental period of the supporting structure. Consequently, it should be included in the derivation of the required response spectrum. If the nonstructural component is being designed without the knowledge of the supporting structure then a range of resonant frequencies should be assumed and the amplitude of the required response spectrum should be increased over this range of frequencies.

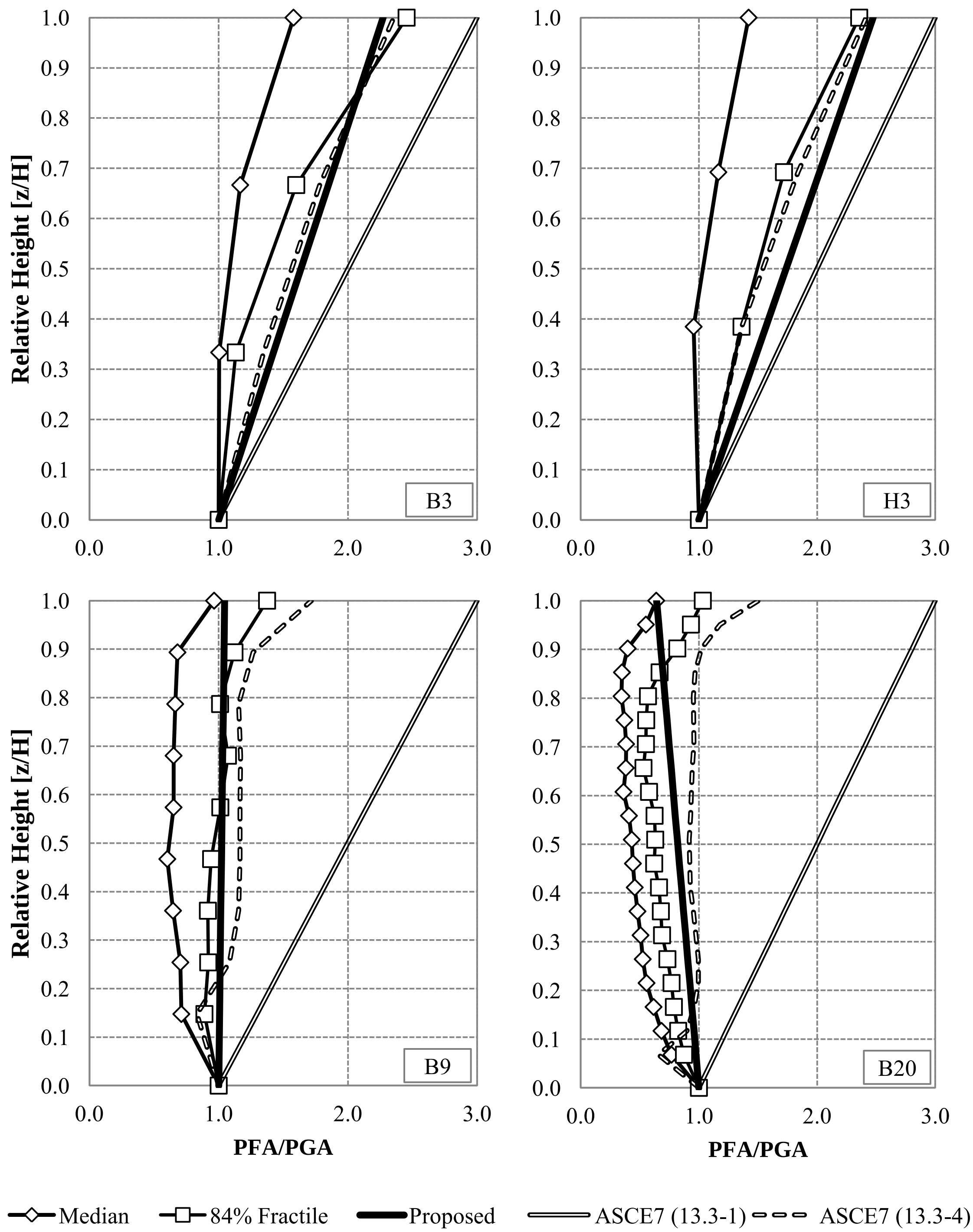

Figure 5-43 Improved Simplified Peak Acceleration Amplification Profile for Elastic Response

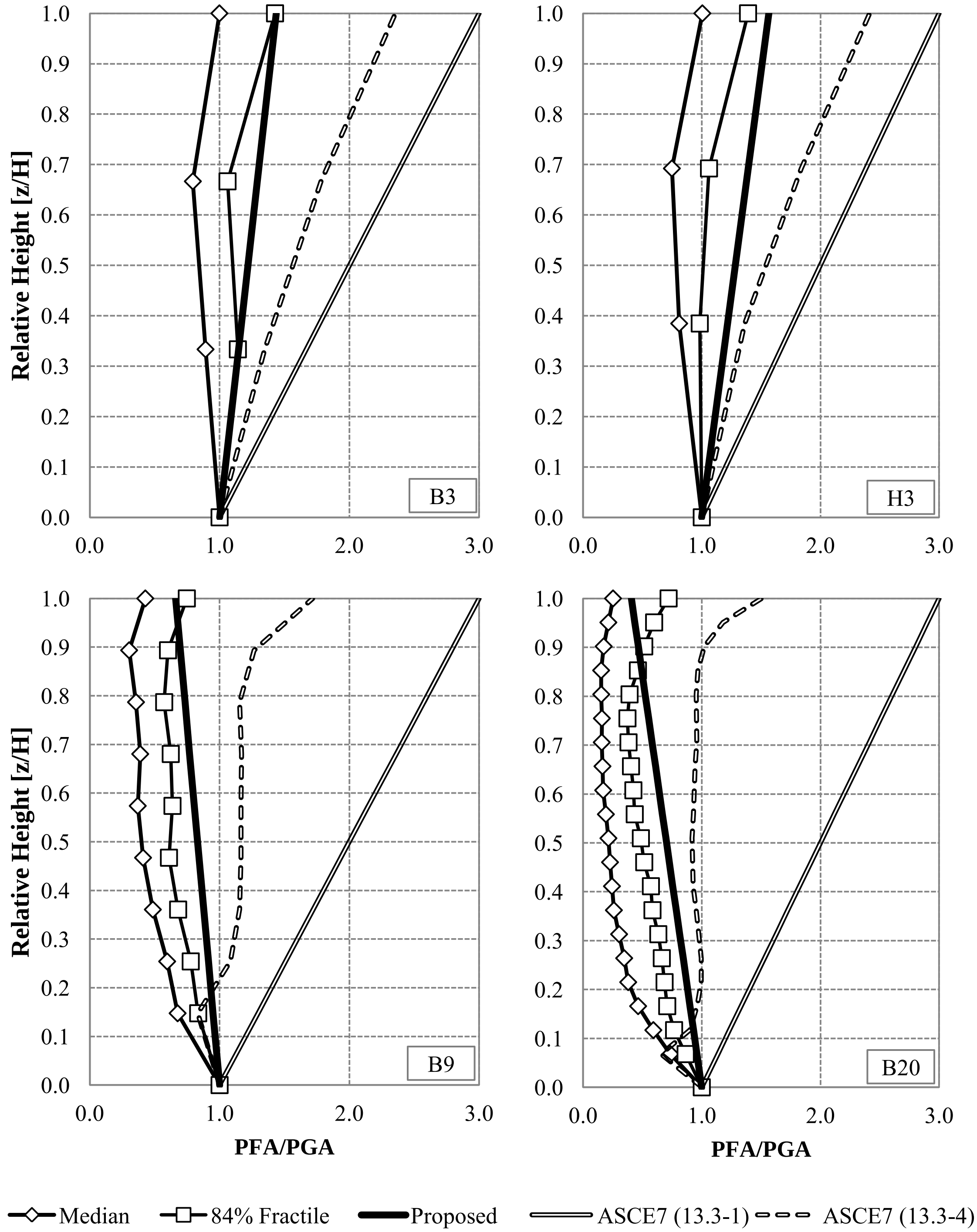

Figure 5-44 Improved Simplified Peak Acceleration Amplification Profile for Moderately Inelastic Response (μ = 2.5)

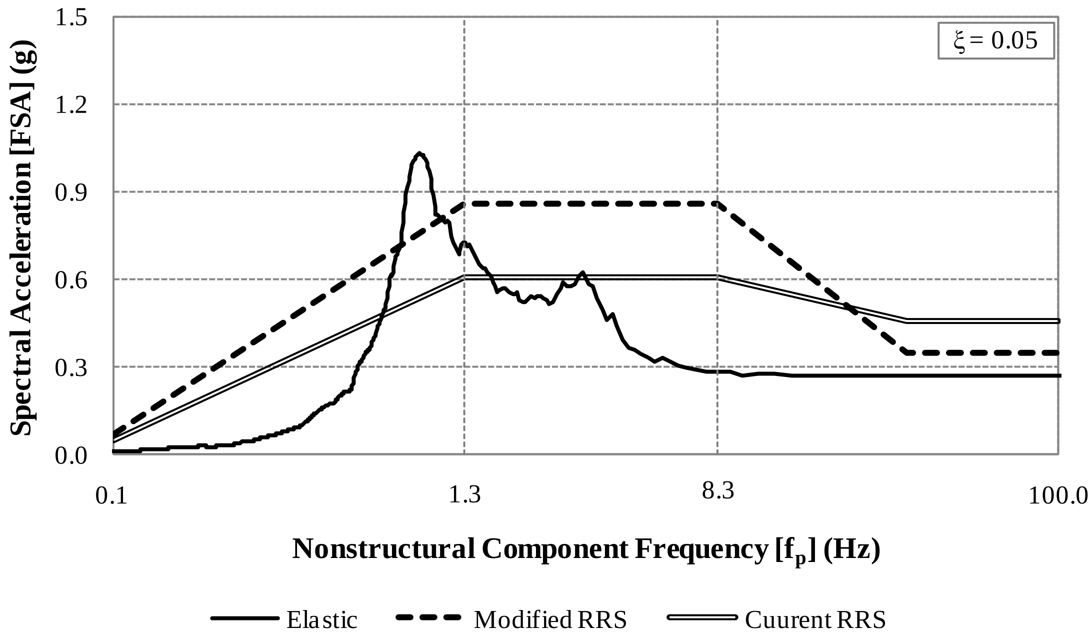

Figure 5-45 Influence of Recommendation on AC 156-Required Response Spectrum against Elastic Response [B3]

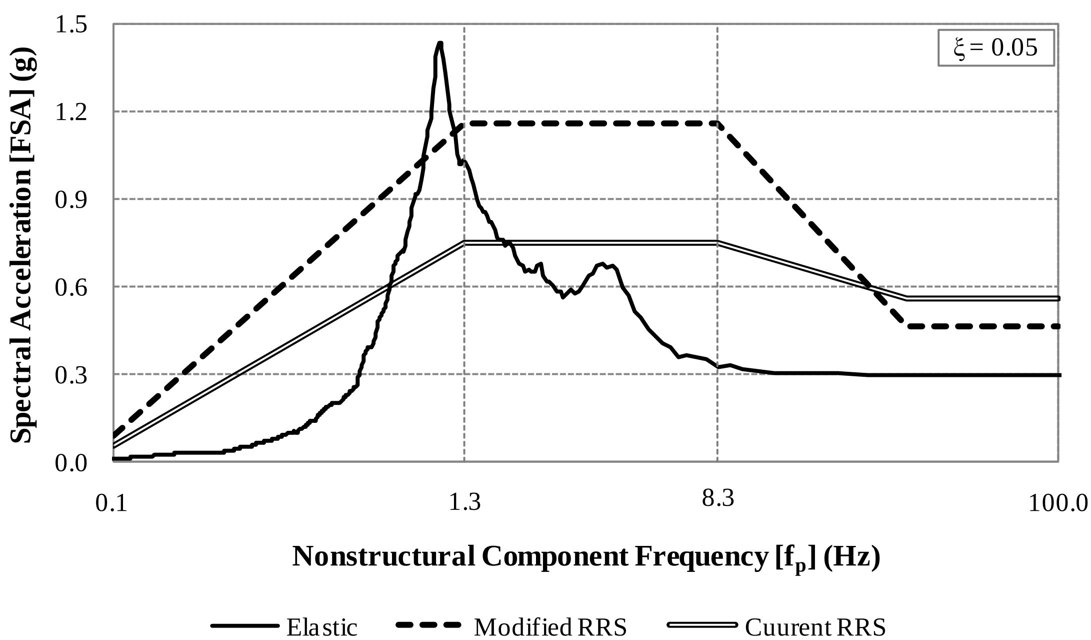

Figure 5-46 Influence of Recommendation on AC 156-Required Response Spectrum against Elastic Response [H3]

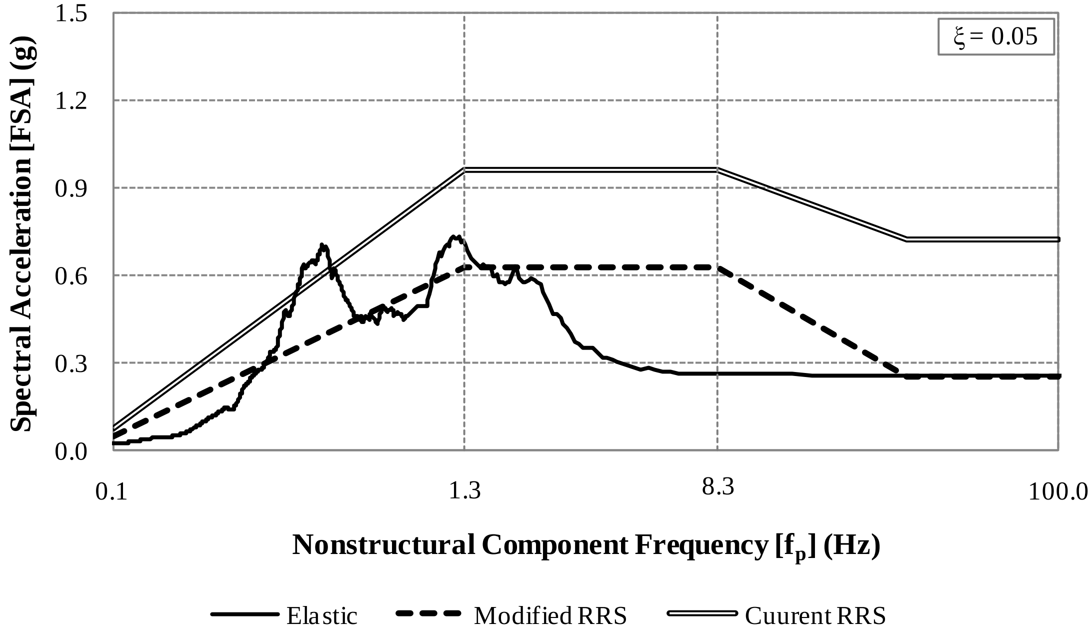

Figure 5-47 Influence of Recommendation on AC 156-Required Response Spectrum against Elastic Response [B9]

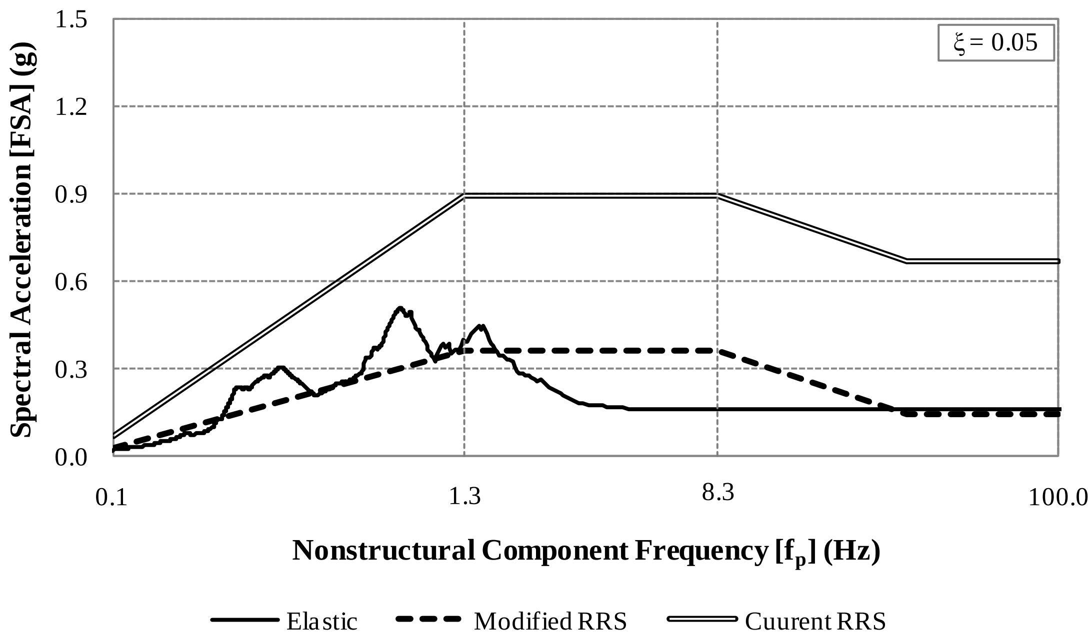

Figure 5-48 Influence of Recommendation on AC 156-Required Response Spectrum against Elastic Response [B20]

5.6.2 Proposed Design Acceleration Response Spectrum

This section explores an alternative approach for developing design accelerations for nonstructural components. In this approach, the results from this investigation were used to develop a multi-linear envelope spectral amplification function which amplifies the ground acceleration response spectrum used to design the building to achieve a nonstructural component design response spectrum. The resulting spectrum allows for a similar design procedure to that used to design the building itself.

To begin, the median elastic floor spectra are normalized by the ground acceleration response spectra for each building and presented in Figure 5-49 through Figure 5-52. It is shown that the spectral amplification also depends on several of the parameters identified previously (i.e. period ratio, relative height, and structural period). With these parameters in mind a simple multi-linear enveloping function was derived. The derivation of the proposed spectral acceleration function follows the logic presented below.

The dependency of the spectral amplification on the ratio of nonstructural period to structural period is obvious in examining the figures. A normalized horizontal axis provides a dependent variable for the spectral amplification that eliminates the influence of the period of supporting structure from the location of the peaks of the function. Once the horizontal axis was normalized the general shape of the function could be identified fairly simply. There appeared to be three consistently located peaks in the spectral amplification function, at period ratios of 0.0, 0.3, and 1.0.

The first peak at a period ratio equal to 0.0 was noted to be the peak floor acceleration divided by the peak ground acceleration. The development of this relationship was explored in detail in the previous sections. Thus, using the recommendation for the peak floor amplification this point could be defined as a function of the relative height of the floor and the period of the structure. This relationship was previously defined in (5-18).

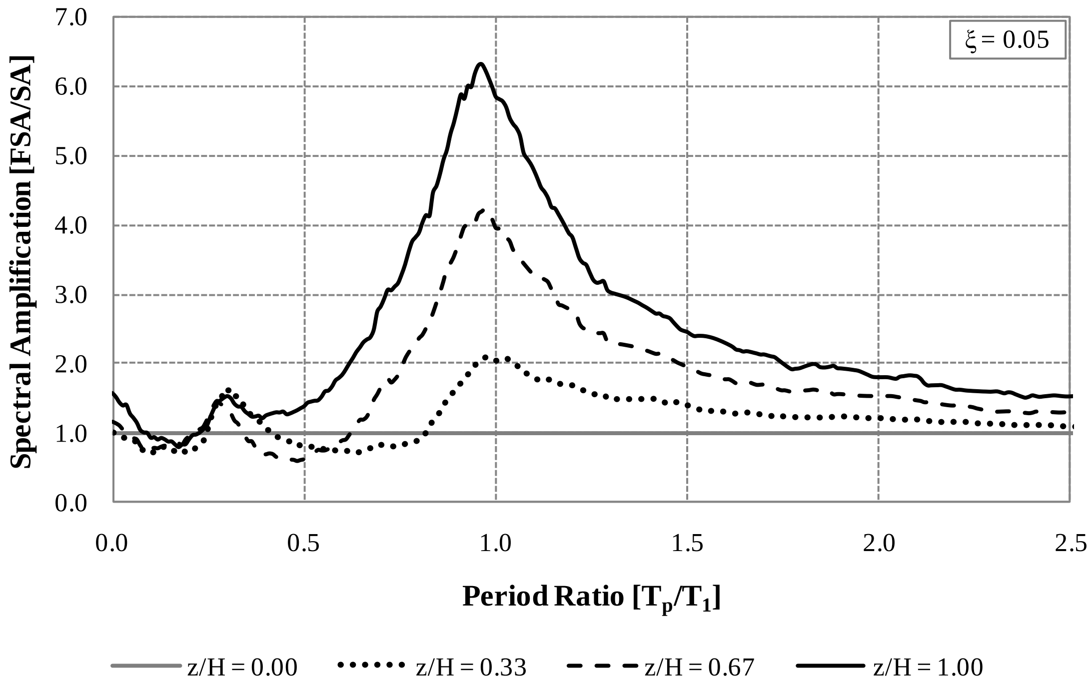

Figure 5-49 Influence of Relative Height on Spectral Amplification (Elastic) [B3]

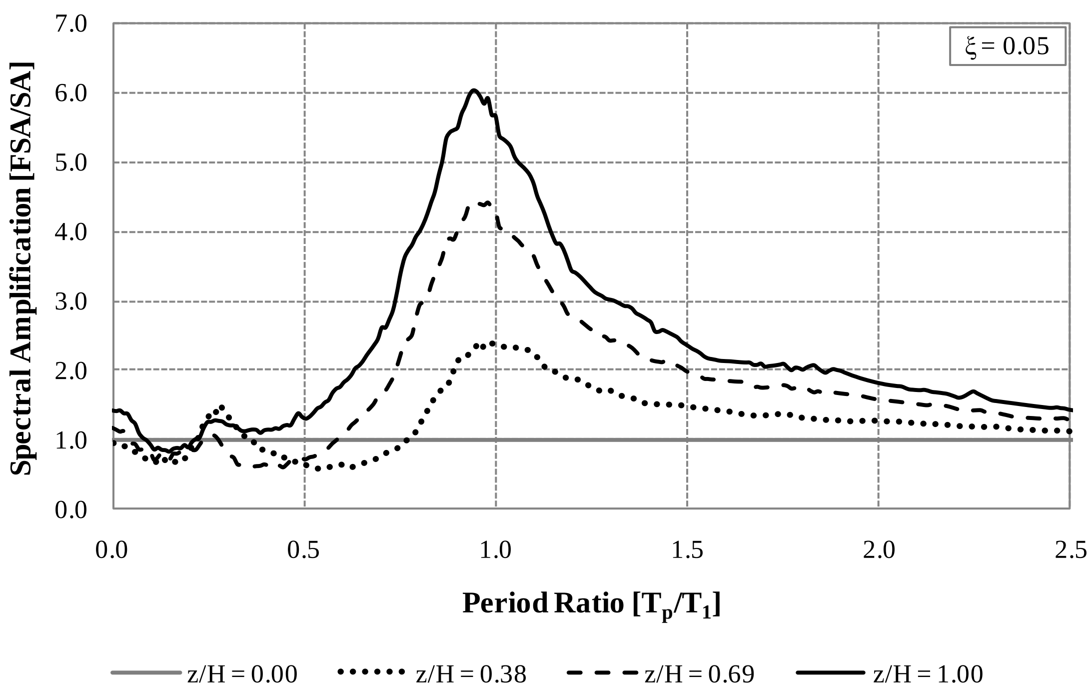

Figure 5-50 Influence of Relative Height on Spectral Amplification (Elastic) [H3]

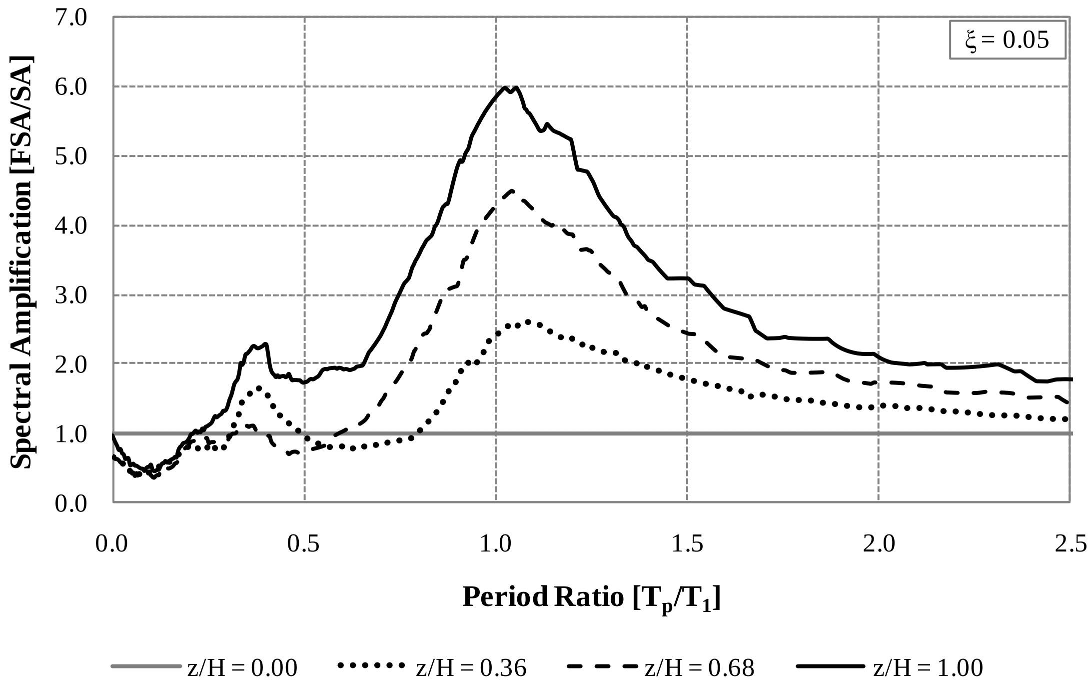

Figure 5-51 Influence of Relative Height on Spectral Amplification (Elastic) [B9]

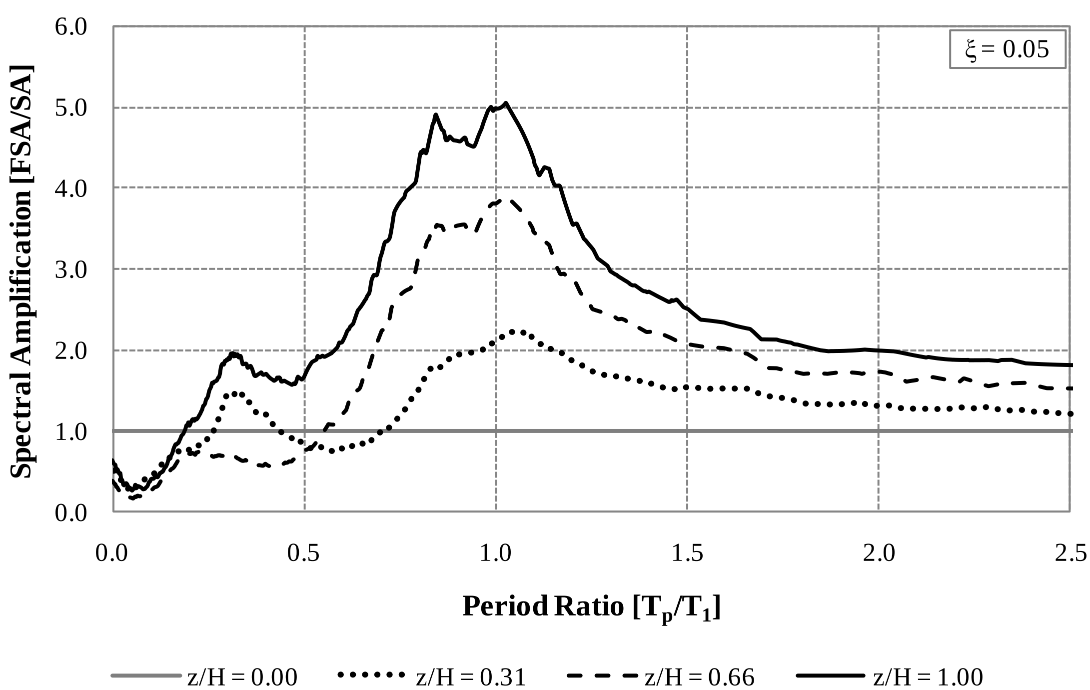

Figure 5-52 Influence of Relative Height on Spectral Amplification (Elastic) [B20]

The peak associated with the amplification of the higher modes of the structure presents itself near a period ratio of 0.3 fairly consistently from building to building. This peak is also dependent on the relative height. However the variation throughout the height of the structure is closely related to the mode shape that the nonstructural component is in resonance with. As the periods of the higher modes are relatively close to one another, the variation in the spectral amplification with respect to relative height is forced to transition within a very short period range and therefore interaction between the higher modes is prevalent. As a result, in order to simplify the spectral amplification function a conservative limit independent of the relative height was assigned. This peak was also observed to be greater in the higher-period structures in which more participation of the higher modes in expected. Consequently, a limit on the period ratio was used to determine the amplitude of the spectral amplification function for the higher-mode peak. It was found appropriate to require a spectral amplification of 2.0 for buildings in which 0.3 times the fundamental period was less than 0.4 seconds and 3.0 for all buildings in which the 0.3 times the fundamental period is greater than 0.4 seconds. Both the limit and the conservative amplitude were selected based on enveloping the peaks of the 84% fractile spectral amplification of each building in this investigation.

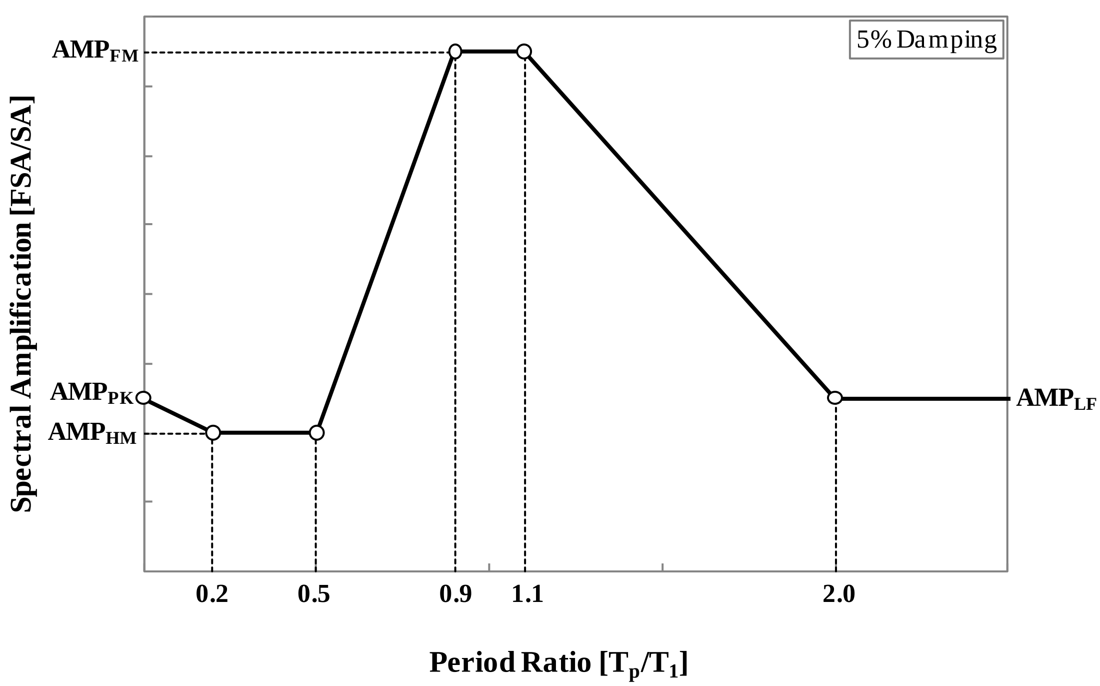

Figure 5-53 Proposed Normalized Spectral Amplification Function

The peak associated with the resonance between the nonstructural component and the fundamental mode of the building is clearly dependent on the relative height within the structure. However, the amplitude seemed to be independent of the period of the structure. Therefore, the determination of the amplitude was defined as a simple function of the relative height, and because the fundamental mode shape is approximately linear so too is the function defining the peak due to resonance with the fundamental mode.

Using the 84% fractile results as a guide, the following normalized spectral amplification function was developed. Figure 5-53 presents the normalized spectral amplification function vs. the nonstructural component period (T_p) normalized by the fundamental period of the supporting structure (T_1) to which (5-21) through (5-24) shall be applied.

$$AMP_{PK} = 1 + \frac{T_{\max} - T}{T}\frac{z}{H} \tag{5-21}$$

$$\begin{aligned} &\text{If } 0.3T < 0.4 \text{ sec}, \ AMP_{HM} = 2.0 \\ &\text{If } 0.3T > 0.4 \text{ sec}, \ AMP_{HM} = 3.0 \end{aligned} \tag{5-22}$$

$$AMP_{FM} = 1 + 6.5\frac{z}{H} \tag{5-23}$$

$$AMP_{LF} = 2.5\sqrt{\frac{z}{H}} \tag{5-24}$$

The proposed function is plotted against the 84%fractile results of Building B3 and Building B20 in Figure 5-54 and Figure 5-55, respectively. These figures demonstrate the conservative nature of the proposed amplification function for all regions of the spectrum.

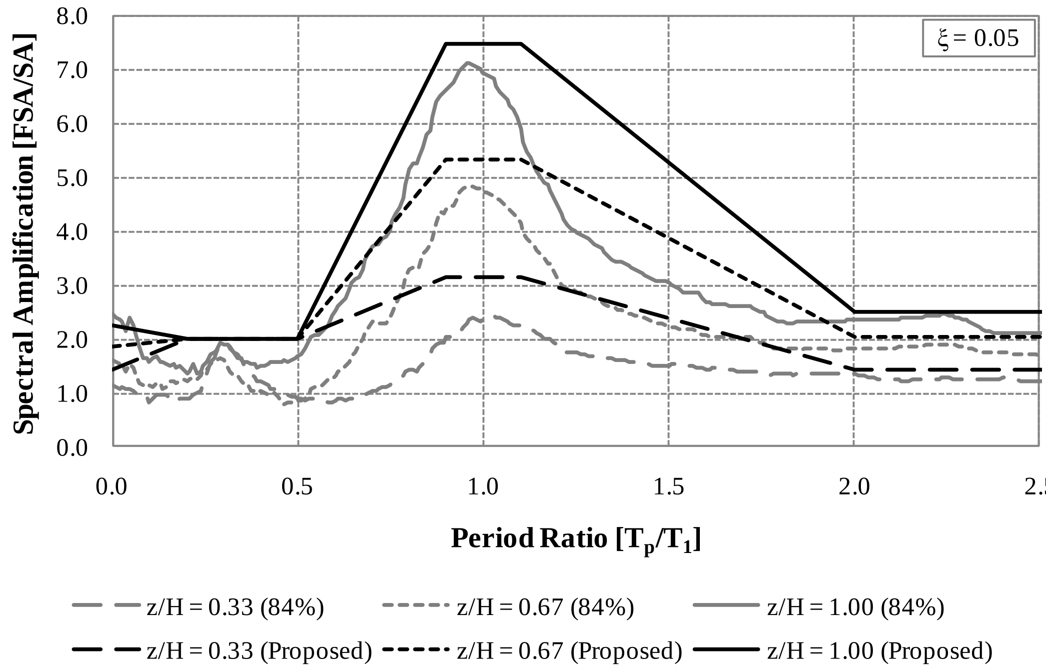

Figure 5-54 Proposed Spectral Amplification Function with 84% Fractile Results [B3]

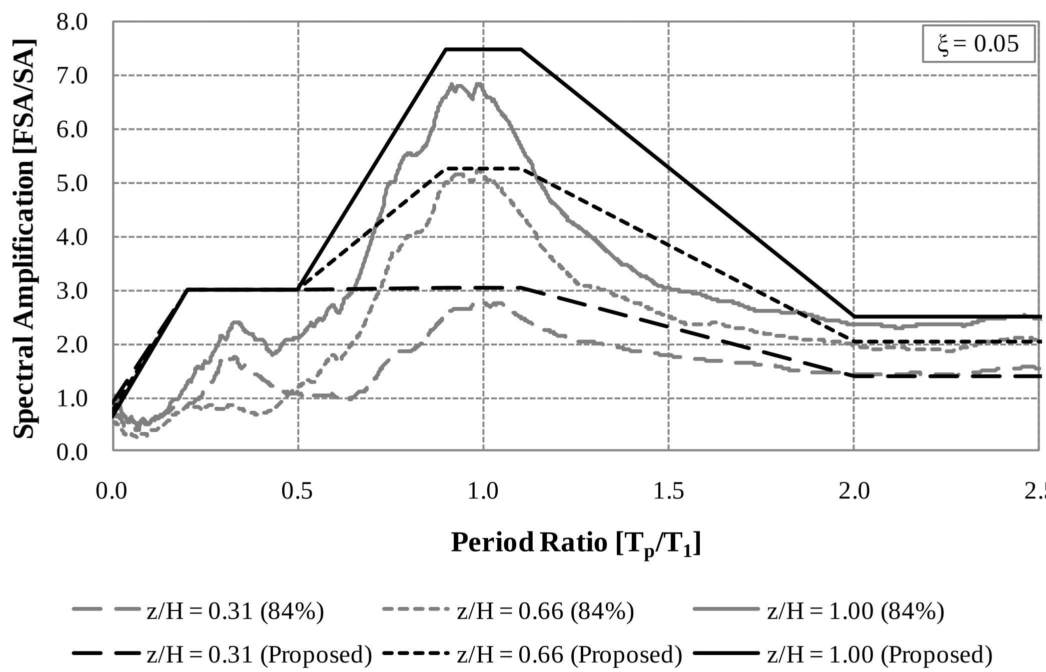

Figure 5-55 Proposed Spectral Amplification Function with 84% Fractile Results [B20]

A significant change in the amplification function occurs when the supporting structure exhibits nonlinear response to the earthquake event. This is exemplified in Figure 5-56, which plots the median spectral amplification for Building H3 at various levels of ductility. It is observed that while the spectral amplification remains nearly constant in the higher mode range there is a considerable decrease in the spectral amplification in the fundamental mode range. This again shows the impact of concentrated ductility effects in the fundamental mode response of the supporting structure. These observations were not included into the proposed spectral amplification function for the same reasons that the effect of ductility was not recommended in the modification to the design peak floor acceleration amplification function. The uncertainty in predicting the level of ductility due to the response of any given earthquake event is too great to risk underestimating the amplification effects. As a result, the spectral amplification function was developed assuming elastic response characteristics of the supporting structure, which facilitates a conservative estimate of the spectral amplification for all frequencies of nonstructural components.

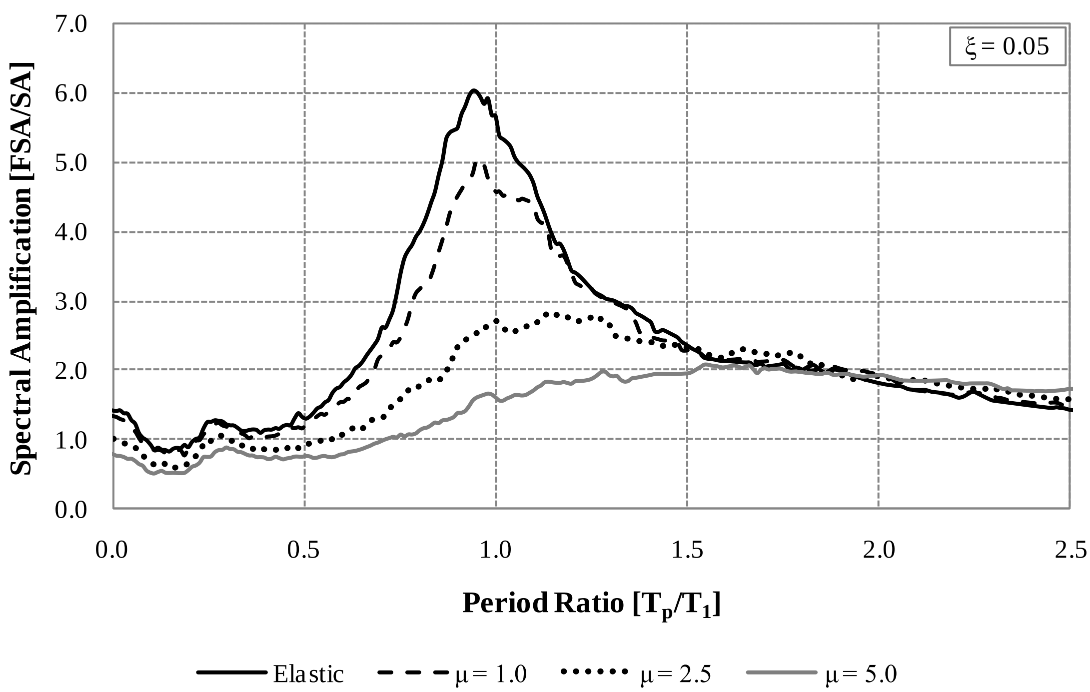

Figure 5-56 Influence of Ductility on Spectral Acceleration Amplification [H3]

5.7 Floor Acceleration Spectra Comparison

The previous sections have dissected the current code provisions and found inconsistencies between the code equations and the analytical results. For example, the ASCE 7-10 estimation of PFA was found to be significantly greater than the results while the component amplification, a_p, is underestimated for nonstructural components in tune with the supporting structure. Though it is important that these portions of the code equations be as accurate and as reasonable as possible, it is the sum of these parts that ultimately defines the demands on nonstructural components. This section presents two examples comparing the floor acceleration spectra generated by each of the discussed methods.

5.7.1 Building H3 Example

If Building H3 is located where it will perform nearly elastically (μ =1.0), the design spectrum is developed with site parameters S_{DS} = 1.0 g and S_{D1} = 0.5 g, as shown in Figure 5-57. This figure demonstrates that the median ground motion is comparable to the design earthquake (DE) spectrum while the 84th percentile ground motion is comparable to the maximum considered earthquake (MCE) spectrum. Considering this situation the unbounded ASCE 7 and AC 156 equations (5-7) and proposed spectral amplification function (SAMP) are compared with the median and 84th percentile results from the IDA study for each floor of the building in Figure 5-58. Meanwhile, similar plots are shown in Figure 5-59 when the upper bound of 1.6S_{DS} is considered. Lastly, Figure 5-60 includes the proposed modifications to the peak floor acceleration amplification in the ASCE 7 and AC 156 equations (5-20).

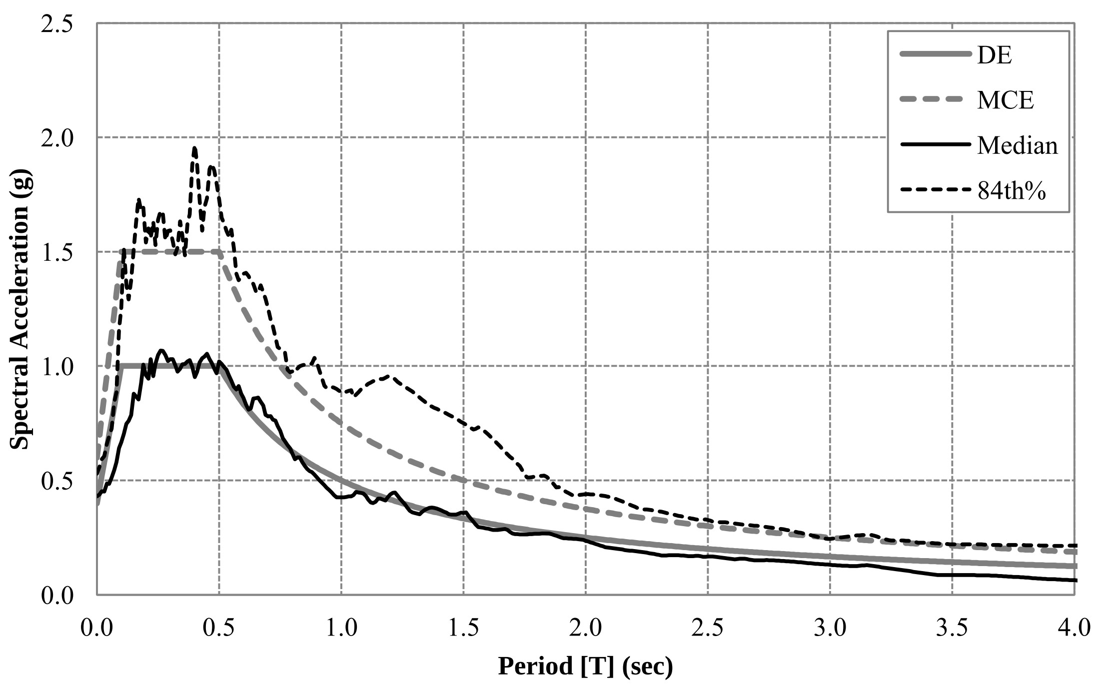

Figure 5-57: Design Spectrum for Essentially Elastic Response of Building H3

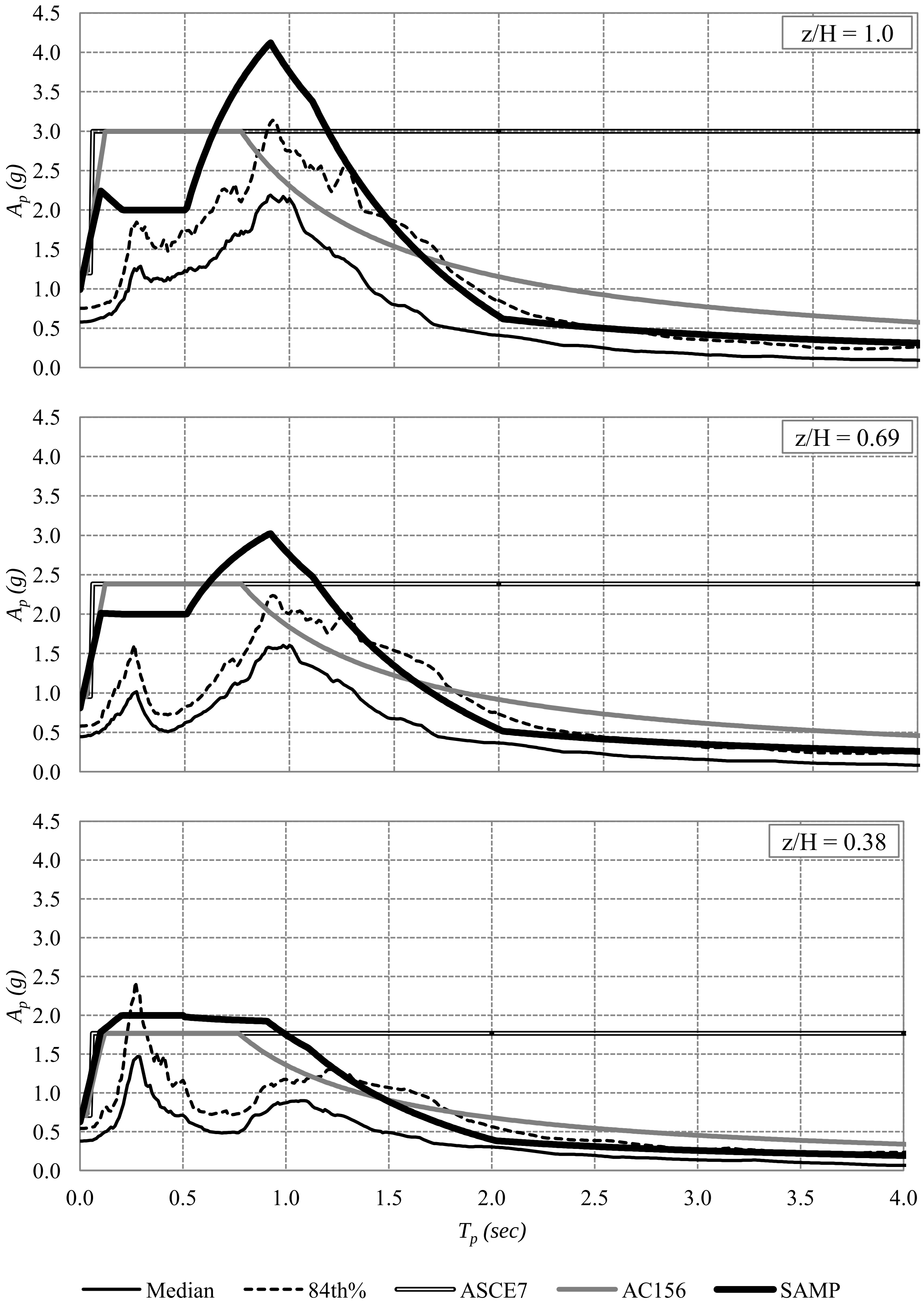

Figure 5-58: Comparison of Unbounded Floor Acceleration Spectra [H3]

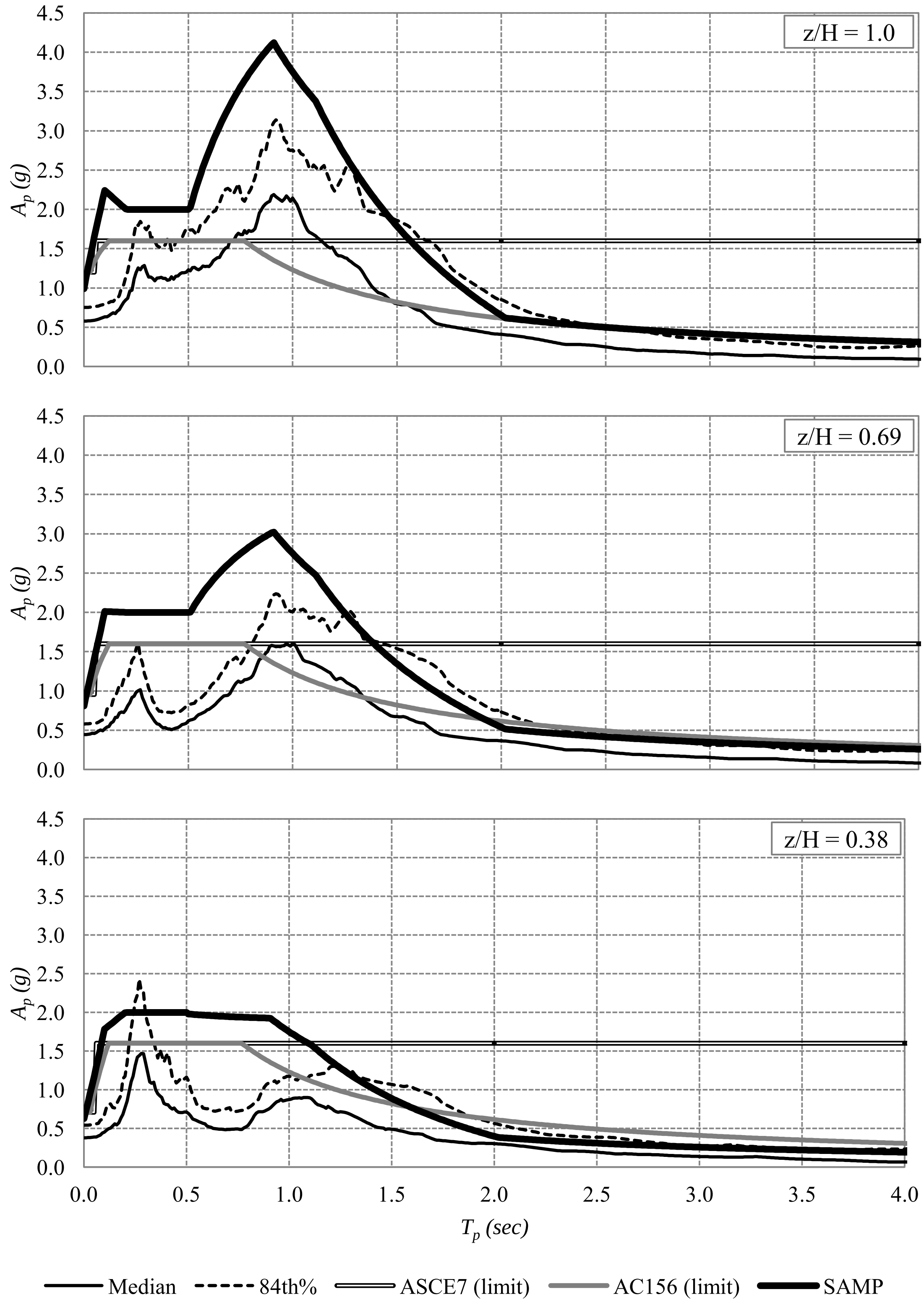

Figure 5-59: Comparison of Bounded Floor Acceleration Spectra [H3]

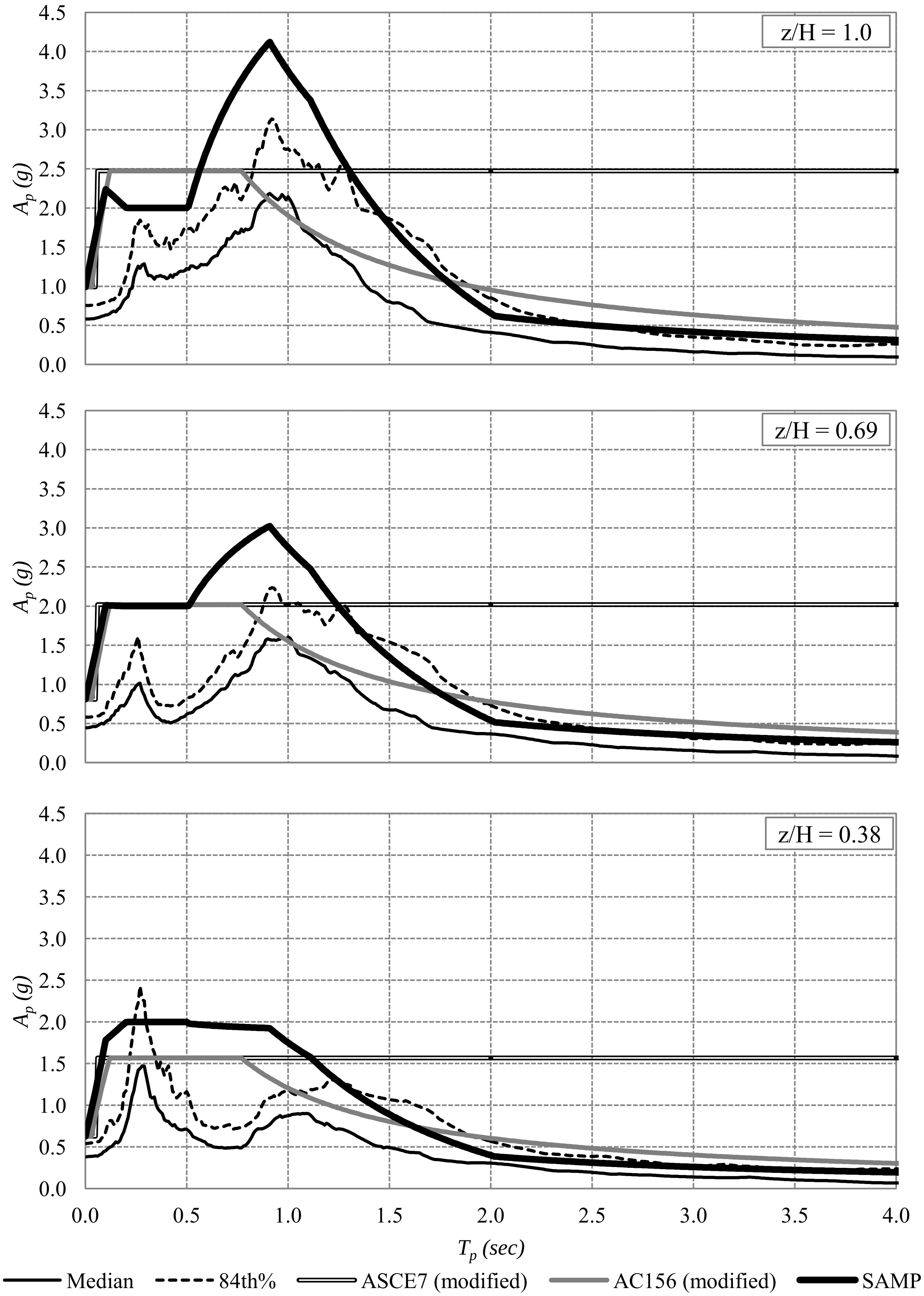

Figure 5-60: Comparison of Modified Floor Acceleration Spectra [H3]

From this example a number of observations are made. The component acceleration estimated by the ASCE 7 equation neglects the upper bound envelopes the median and essentially captures the peak 84th percentile demands. The AC 156 spectrum envelopes the median demands but underestimates the 84th percentile demands for longer nonstructural component periods. However, when the upper limit of $1.6S_{DS}$ is included the resulting spectra underestimate both the median and 84th percentile spectra for a wide range of nonstructural periods. This is particularly evident in the upper two floors of the building where the upper bound provides a greater reduction in the estimated component acceleration demand. With the current limit of $1.6S_{DS}$, all flexible components (a_p = 2.5) mounted in the top 70% of the structure are estimated to have the same acceleration demands. This upper bound overwrites the linear variation provided by the primary code estimate and is shown in this example to underestimate the achieved nonstructural component accelerations. Incorporating the proposed modification to the current code estimate (5-20) generates floor acceleration spectra that envelope the median demands while more closely estimating the acceleration of short period nonstructural components compared to the current provisions. These modifications do however require the knowledge of the structural period, which is not always available during the design of nonstructural component. Lastly, the proposed spectral amplification method generates floor acceleration spectra that more closely mimic the shape of the achieved floor acceleration spectra. The spectral amplification method is shown to envelope the 84th percentile demands over the majority of nonstructural component periods. While the currently proposed equations, (5-21) through (5-24), produce a spectra that may be slightly over-conservative, with additional research and refinement this method may be able to provide much improved estimates of floor acceleration spectra.

5.7.2 Building B9 Example

An example similar to the previous one is examined by considering Building B9 to be situated on a site where it responds elastically. The site parameters S_{DS} = 0.625 g and S_{D1} = 0.3125 g generate the ground spectra shown in Figure 5-61. This example demonstrates how the proposed spectral amplification method adjusts the shape of the estimated floor response spectra based on the period of the building. Also Figure 5-62 through Figure 5-64 show that the current ASCE 7 provisions including the $1.6S_{DS}$ limit may, in this case, provide a more reasonable estimate of the component acceleration than neglecting this limit. Particularly interesting is the AC 156 spectra, which include the upper bound equation. These spectra clearly underestimate the achieved floor acceleration spectra for longer period nonstructural components.

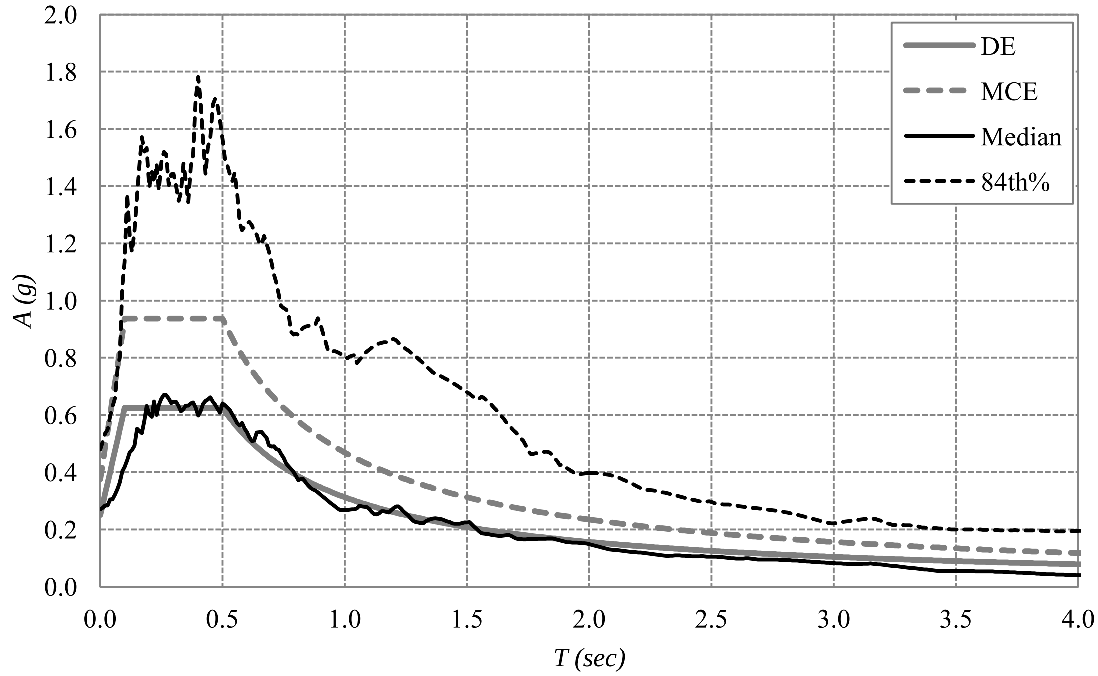

Figure 5-61: Design Spectrum for Elastic Response of Building B9

5.7.3 Example Summary

These two examples have demonstrated that the current code estimates of the floor acceleration spectra generally overestimate the median response of short period nonstructural components in flexible steel moment frame buildings (T > 1.0 sec). The upper limit of $1.6S_{DS}$ may significantly undermine the primary code provision and in doing so generate unconservative estimates of nonstructural component accelerations in some cases. The proposed modifications to the primary code equation may provide improved estimates of the component acceleration demands when the structural period is known. Lastly, the proposed spectral amplification method can improve the shape of the estimated floor spectra yet more research is needed to fine tune the equations for multiple types of buildings.

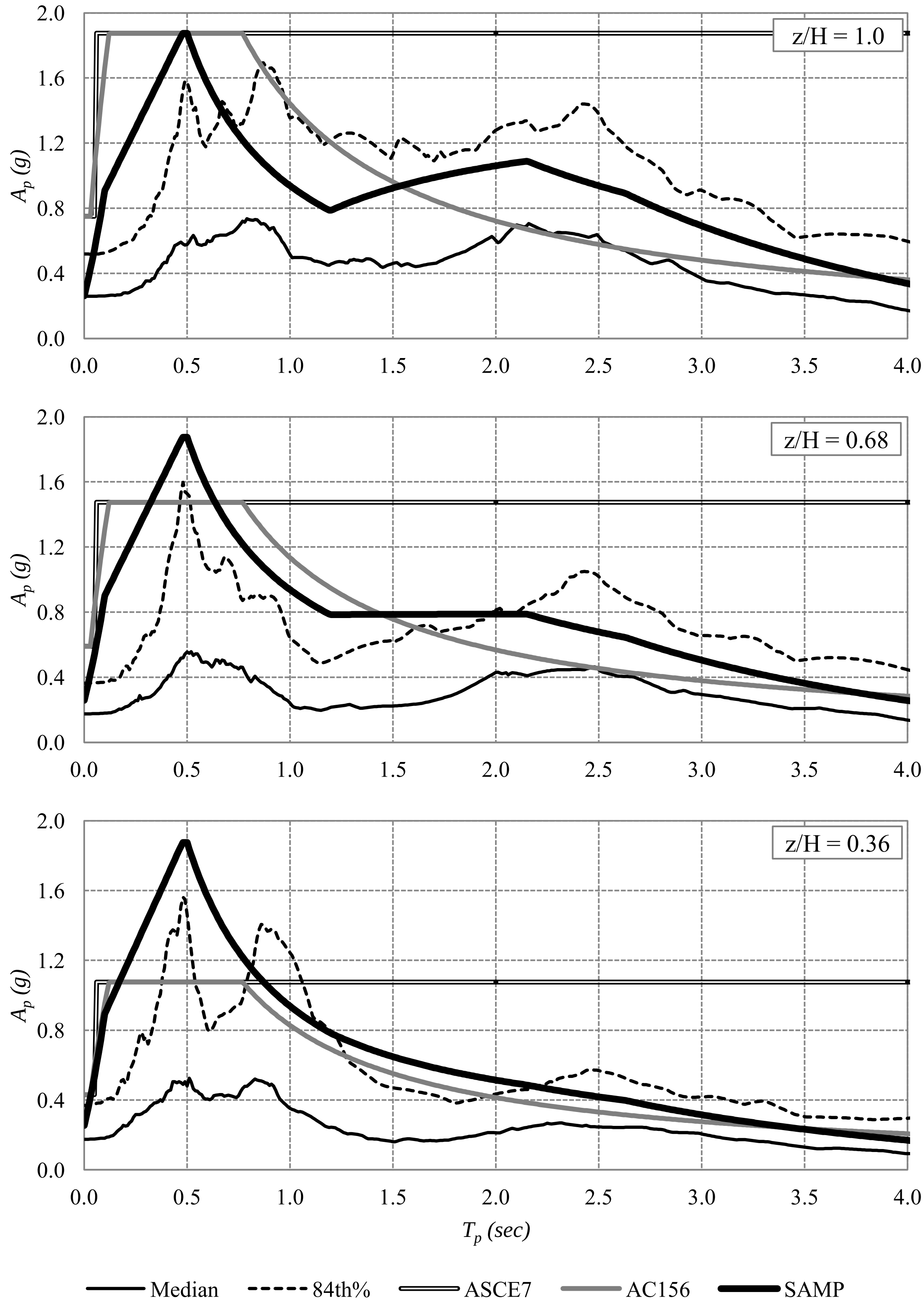

Figure 5-62: Comparison of Unbounded Floor Acceleration Spectra [B9]

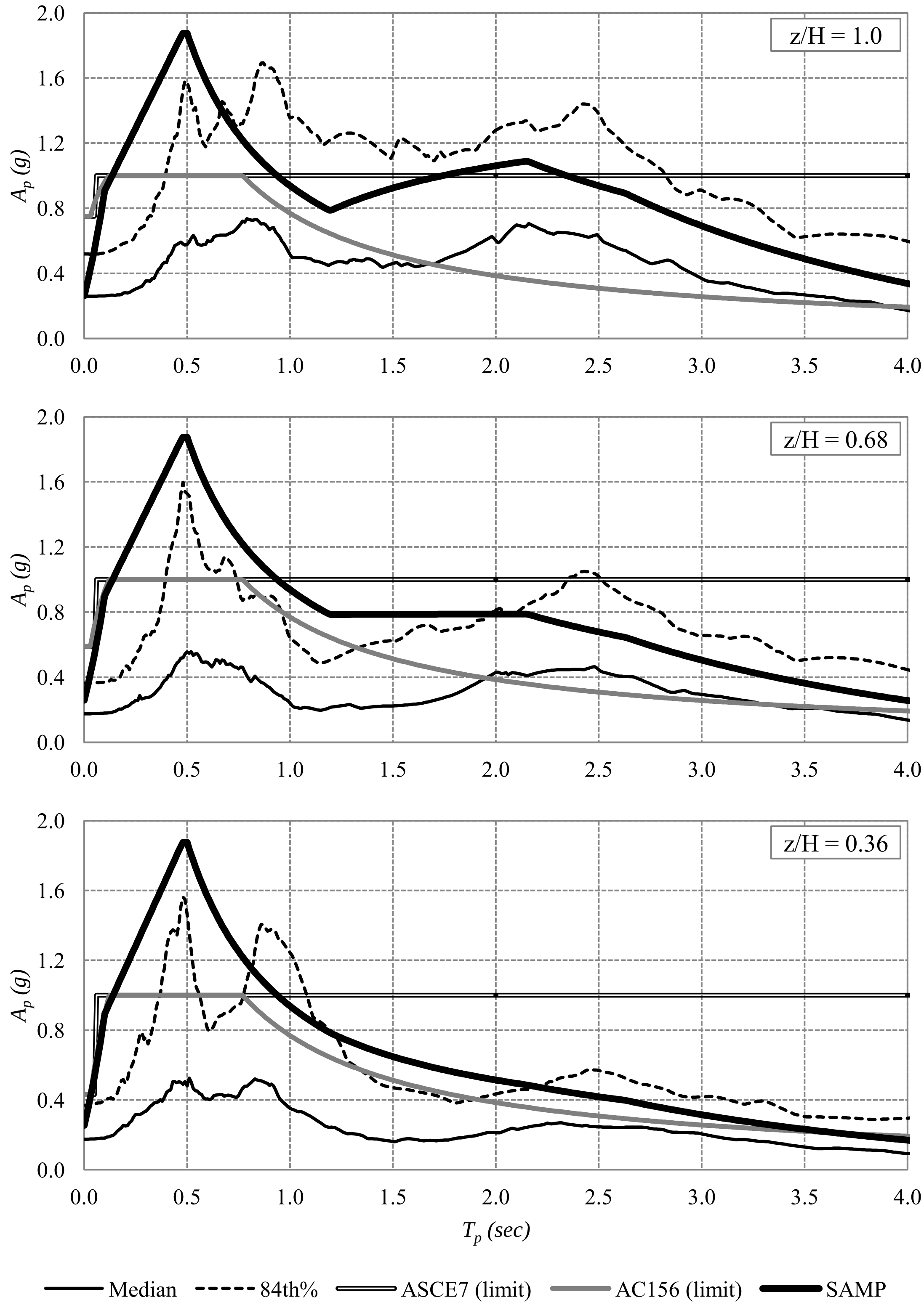

Figure 5-63: Comparison of Bounded Floor Acceleration Spectra [B9]

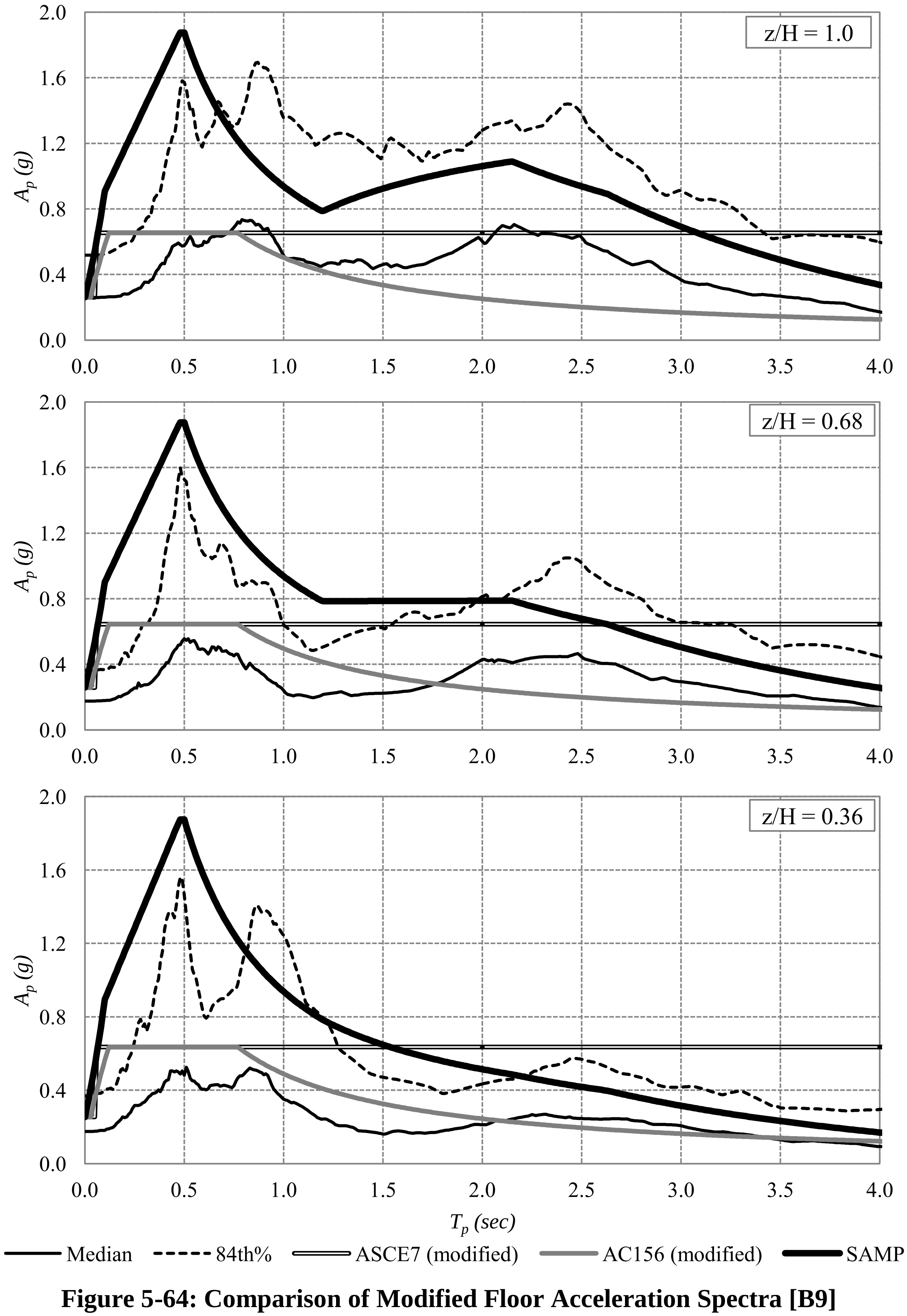

Figure 5-64: Comparison of Modified Floor Acceleration Spectra [B9]

5.8 Verification of Analytical Results with Field Data

5.8.1 1994 Northridge Reconnaissance Report

On January 17, 1994 a magnitude 6.7 earthquake shook the area surrounding Northridge, California. After the event several hundred strong ground motion and building response accelerograms were retrieved from recording stations throughout the greater Los Angeles area. Of these hundreds of records, a collection of building response records was accumulated in the report published by John A. Martin and Associates, Inc. Of the 20 buildings presented in this report, 17 experienced peak base accelerations greater than 0.25g, two were downtown skyscrapers, and one was base isolated (Naeim, 1997). The records assembled in this reconnaissance report were used in this study to verify the findings and recommendations presented in the previous sections.

5.8.1.1 Definition of Similar Buildings

As the findings of this study are predicated on the acceleration response of steel moment frame structures it only makes sense to verify the results based on the response of moment frame buildings. Therefore, the following buildings were selected for comparison.

Building NR1: The Burbank, 6-story commercial building is a steel moment frame building designed in 1976 and constructed in 1977. The gravity load-carrying system consists of 3" concrete slab over metal deck supported by steel frames. The lateral load resisting moment frames are located at the perimeter of the building. The peak horizontal unidirectional acceleration recorded at the base was 0.36g in the east-west direction. The maximum roof drift ratio recorded was 0.39%, and no structural damage was observed. The FFT analysis indicated a fundamental period of vibration of 1.28 sec for each of the orthogonal directions.

Building NR2: The Los Angeles 5-story warehouse is a reinforced concrete building constructed in 1970. The exterior ductile concrete frames provide resistance against lateral loads. The peak base acceleration recorded was 0.25g in the north-south direction. The maximum roof drift ratio recorded was 0.2%, and no damage was reported. The FFT analysis indicated N-S and E-W fundamental periods of 1.46 and 1.37 seconds, respectively.

Building NR3: The Los Angeles 54-story office building was designed in 1988 and constructed in 1988-1990. The gravity load-carrying system consists of 2.5” concrete slabs on 2” metal deck supported by steel frames. The lateral load-resisting system consists of perimeter tubular steel moment frames which step twice in elevation. The peak base acceleration recorded was 0.14g in the north-south direction. The maximum roof drift ratio recorded was 0.08%, and no damage was experience in the structural system. The FFT analysis determined the N-S and E-W fundamental periods to be 6.0 and 4.8 seconds, however significant higher mode participation was evident and the periods of the predominant modes were closer to 2.0 and 1.8 seconds, respectively.

Building NR4: The Los Angeles 7-story UCLA math and science building was constructed as an addition to an existing structure separated by seismic expansion gaps. The building consists of 2.5” concrete slabs on metal deck supported by steel frames to carry the gravity loads in the upper part of the building (from the third floor up). This part of the building has a lateral load resisting system consisting of steel moment frames while the bottom two stories consist of concrete shear wall systems. The peak base acceleration recorded was 0.29g. There was evidence of slight structural damage in the form of residual drift. Though the maximum global roof drift ratio was only 0.47% a majority of this was concentrated in the steel moment frame. The FFT analysis identifies the N-S and E-W fundamental periods as 0.66 and 1.02 seconds, respectively. For the purpose of comparison in this study the shear wall systems of the first two stories is assumed to provide sufficient stiffness and strength to neglect the effect of these floors and consider the third floor as the base excitation of the 5-story steel moment frame structure above.

Building NR5: The Sherman Oaks 13-story commercial building was designed in 1964. The vertical load carrying system is made up of 4.5” thick one-way concrete slabs supported on concrete beams, girders, and columns. The lateral load-resisting system consists of moment-resisting reinforced concrete frames above the basement. The peak ground acceleration recorded was 0.46g. The maximum roof drift ratio recorded was 0.67%, only light structural damage was observed in the form of small cracks in the beams, slabs, girders and walls. The N-S and E-W fundamental periods from the FFT analysis were 2.6 and 2.9 second, respectively.

Building NR6: The Van Nuys 7-story hotel was designed in 1965 and constructed in 1966. The gravity load-carrying system consists of 8” and 10” concrete slabs supported on concrete columns and perimeter spandrel beams. The lateral load resistance is provided by interior column-slab frames and perimeter column-spandrel beam frames. The peak ground acceleration recorded was 0.45g. The maximum roof drift ratio recorded was 1.17%, which produced heavy structural damage including a shear failure of an exterior column at the fourth floor. The FFT analysis showed that the N-S period elongated from 1.4 to 2.2 seconds and the E-W period elongated from 1.3 to 1.8 seconds.

5.8.1.2 Comparison of Peak Acceleration Amplification

A comparison of the peak acceleration amplification profiles observed in these buildings with the current code as well as the proposed improvements is presented in Figure 5-65. It is noted that the current code is extremely conservative compared to the observed response of the these six moment frame structures while the proposed improvement which accounts for the period of the structure reduces the conservatism considerably yet remains greater than the observed data in all but one case. In this case the period of the structure is so long that the earthquake did not excite the fundamental mode, as a result, the shape of the amplification profile is different from the other structures. This indicates that there must be some upper limit of structural period for which the proposed equation is applicable. As this study has only analytically examined four buildings with periods ranging from 1 second to 4 seconds, the upper limit of the proposed equation's effectiveness should be 4 seconds. That being established, the proposed design equation appears to show significant improvement over the current equation for both the analyzed buildings as well as the field instrumented buildings.

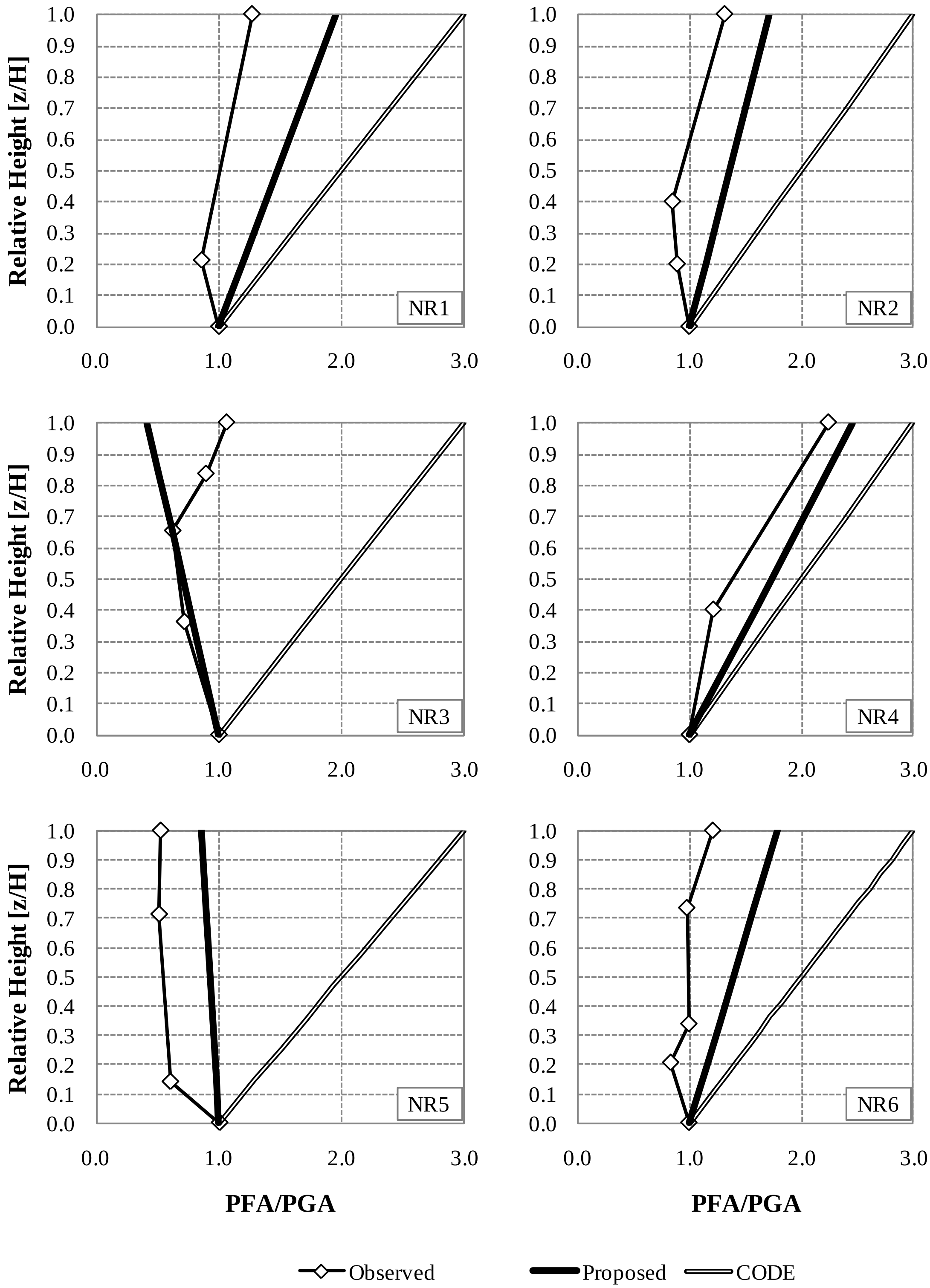

Figure 5-65 Comparison of Proposed Design Equation against Northridge Observations

5.8.1.3 Comparison of Spectral Acceleration Amplification

A comparison of the proposed spectral acceleration amplification function against the observed spectral accelerations of six buildings during the Northridge earthquake is presented in figure 5-66. Contrary to the proposed improvement of the peak acceleration amplification, the proposed spectral acceleration function has poor agreement with the observed data. There are a few reasons for these differences. Buildings NR1 and NR2 follow similar trends to the analytical study, however the peak spectral amplification when the nonstructural component is in resonance with the fundamental mode is observed to be approximately 1.5 times the value predicted by the proposed function. It is possible that both of these buildings show extreme cases that are outside the one standard deviation of the mean for which the proposed equations were developed. Building NR3 has a very long natural period well outside the bounds of the analytical study. The large participation of the higher modes of this structure is identified in the large peak in the short period ratio range. There is inherent error associated in the acceleration readings near the fundamental period due to the dependable frequency range of the instrument used to record the acceleration records. Buildings NR4 and NR5 are unique in that they each have rather different periods of vibration in each of the two orthogonal horizontal directions. As a result, their amplified period range in wider than the buildings whose periods are similar in each direction. This is represented in the observed peak outside the predicted envelope. Lastly, Building NR6 showed signs of inelastic behavior and thus the peak spectral amplification is vague and significantly less than expected.

While the direct comparison of the spectral amplification observed in these buildings does not show optimal correlation with the proposed function, when combined with the code idealized ground spectrum that best fits that of the observed ground acceleration, the proposed method generates a reasonable prediction of the floor acceleration spectra, shown in Figure 5-67. This validates the spectral amplification methodology as a legitimate procedure for generating floor acceleration spectra, however additional research is needed to fine-tune the proposed equations for a wider range of building types.

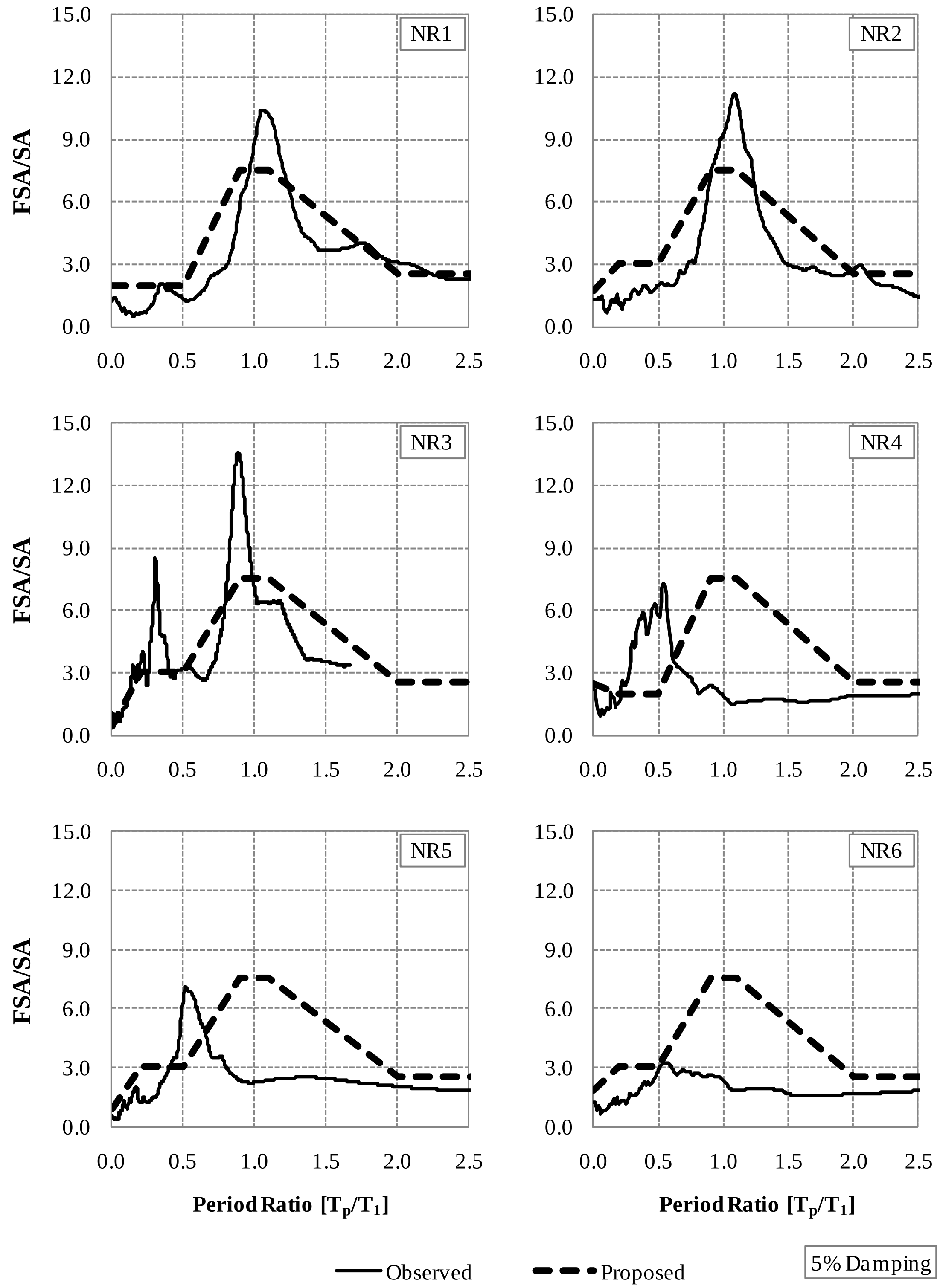

Figure 5-66 Comparison of Proposed Spectral Amplification Function against Northridge Observations

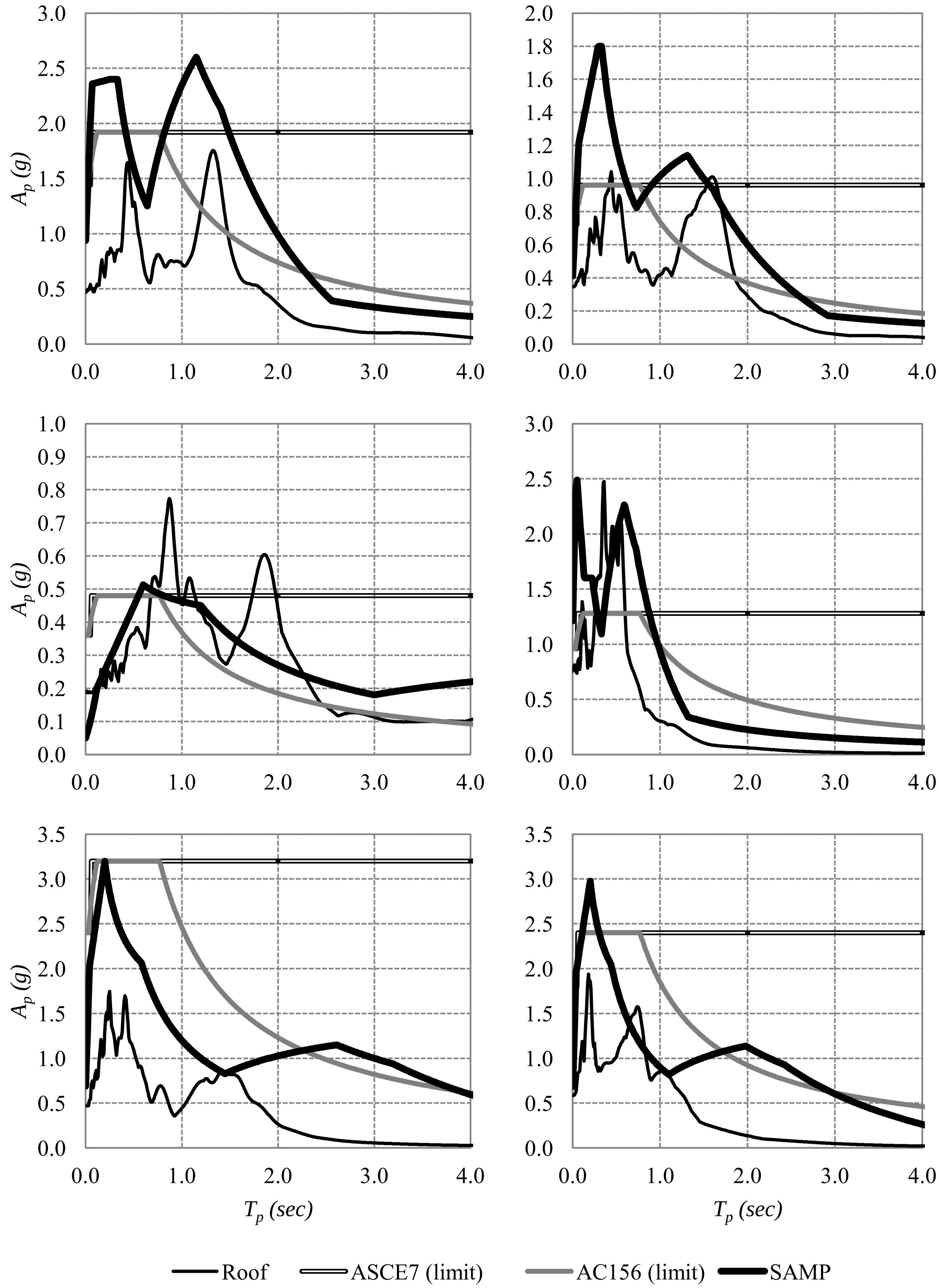

Figure 5-67: Comparison of Proposed Spectral Amplification Method against Current Code and Northridge Observations

5.9 Summary of Horizontal Acceleration Demands

This chapter has examined the horizontal acceleration demands on nonstructural components for a small sample of ductile moment frame buildings. The parameters that influence the horizontal acceleration response of nonstructural components were identified and discussed. The results of the IDA study presented in Chapter 4 were used to identify trends and support recommendations for alternative simplified equations. Currently, the code approximations are independent of the building properties, which is convenient for manufacturers of widely used generic nonstructural components. However, the results of this study along with several others mentioned demonstrate that the responses of the nonstructural components within a building are not independent of the dynamic characteristics of the supporting structure. With this observation two different alternatives are provided in which only the fundamental period of the building is required to obtain an improved estimate of the acceleration demands on nonstructural components. These alternative methods offer a more simplified analysis procedure than the modal analysis method provided in the code. These suggested improvements were based on the results of the analytical study but checked against data observed in the field during the 1994 Northridge earthquake. In total this chapter has performed a comprehensive investigation of the horizontal acceleration demands on nonstructural components mounted in ductile steel special moment frame buildings. It must be emphasized that the recommendation presented in this chapter must be confirmed for a wide range of building types, sizes, and configurations before being adopted by any code. These recommendations simply offer a starting point for additional work.

SECTION 6

VERTICAL ACCELERATION DEMANDS ON NONSTRUCTURAL COMPONENTS

6.1 Introduction

There are several nonstructural components in a building such as suspended ceiling systems, piping systems, and building contents which are vulnerable to vertical accelerations as well as horizontal accelerations. Thus, the study of vertical acceleration demands on the nonstructural components is critical. This chapter explores the influence of relative height within the building, level of yielding, and out-of-plane flexibility of the floor system on the vertical acceleration demands on nonstructural components as well as assesses the current code estimation of these demands.

6.2 Factors Influencing the Vertical Acceleration Response of Nonstructural Components

6.2.1 Relative Height of Mounting Location

The vertical acceleration excitation from the ground motion is transmitted to each floor of the building through the axial rigidity of columns and walls. In most SMRF buildings the axial stiffness of the columns far exceeds their lateral stiffness. As a result the vertical fundamental frequency of the floors at column joints is typically very high. Therefore, it is commonly assumed that the columns are axially rigid and that the vertical acceleration of each of the floors at the column joints is equal to the vertical ground acceleration. A recent study by Reinhorn et al. (2010) uses a similar argument to support its recommendation for a proposed code vertical required response spectrum without amplification along the height of the building.

6.2.2 Nonlinear Response of the Supporting Structure

While the influence of yielding on the horizontal acceleration response of nonstructural components has been the topic of several recent studies, as mentioned in Section 5.2.4 its effect on the vertical response of nonstructural components has not been studied. Typically, vertical floor accelerations have been examined for analysis of machinery, footfall, and other non-seismic excitations. Consequently, because structural yielding is not expected under vibration service loads, this effect is not well known.

6.2.3 Plan Location of Nonstructural Components

Floor systems consist of a collection of columns, beams, and secondary beams supporting a slab of reinforced concrete. At any given location on the floor the vertical dynamic characteristics vary according to the out-of-plane rigidity of the floor. Floors are vertically restrained at the location of columns and are free to vibrate near the center of the bay spanning four corner columns. As a result, the vertical acceleration demands on nonstructural components mounted at different locations on the floor will also vary. Quantifying the vertical acceleration demand envelops (minimum and maximum) of nonstructural components is one of the primary objectives of this investigation.

6.2.4 Dynamic Characteristics of Floor Slab System

The out-of-plane dynamic characteristics of floor systems have been investigated for service vibration. These studies identify natural frequencies of floor systems in order to assess the probability of exciting the floor through human activity. A survey of previous research is provided in the following paragraphs.

The AISC Design Guide Series 11 Floor Vibration Due to Human Activity written by Murray, Allen, and Ungar (1997) has provided a commonly used reference of design criteria of floor systems to reduce floor vibrations. It states that "most steel-framed floor systems in North American office buildings have first natural frequencies in the 5-9 Hz range."

Allen and Pernica (1998) described the nature of floor vibration and presented design and retrofit solutions to avoid significant floor vibrations. This research states that "a steel floor with a concrete deck usually has a natural frequency of between 3 Hz and 10 Hz."

Boice (2003) studied the vertical dynamic characteristics of 103 steel-framed floor systems for the purpose of improving the prediction of vibration due to human activity. The studied floors were classified into four categories: hot-rolled beams, hot-rolled girders with joists, hot-rolled girders with castellated beams, and joist girders with joists. An FFT analyzer with an accuracy of 0.25 Hz was used to determine the in-situ dynamic characteristics of each floor system. It was found that the fundamental frequencies of the 103 floor system studied ranged from 3 Hz to 13.5 Hz.

Barrett (2006) investigated the response of three multi-bay in-situ steel composite floors. Extensive dynamic testing using an electrodynamic shaker was performed to estimate their dynamic response and calibrate a set of finite element models. Dominant frequencies of these floors ranged from 4.85 Hz to 9 Hz.

It can be concluded that properly designed steel-framed floor systems will have a vertical fundamental frequency of vibration between 3 Hz and 13.5 Hz. Comparing this conclusion with the fundamental frequencies of the modeled floor systems in this investigation it is observed that the floor and roof systems of each of the buildings fall within this range with an exception of the roof of Building B20. Table 6-1 presents the fundamental vertical floor frequencies for each of the four buildings in this study. Building B20 has larger spans than the other buildings thus it is expected that this building has a slightly lower frequency than the others.

Table 6-1 Dominant Vertical Floor Frequencies

Building	**Floor**	**Period** *sec*	**Frequency** *Hz*
B3	Floor	0.224	4.464
B3	Roof	0.269	3.717
H3	Floor	0.226	4.425
H3	Roof	0.277	3.610
B9	Floor	0.220	4.545
B9	Roof	0.264	3.788
B20	Floor	0.278	3.597
B20	Roof	0.377	2.653

6.3 Current Code Approach

The ASCE 7-10 (ASCE, 2010) requires that in addition to the horizontal force determined by (5-7) that nonstructural components be concurrently subjected to a vertical force determined by (6-1)

$$F_p = \pm 0.2 S_{DS} W_p \tag{6-1}$$

In which S_{DS} = the short period design spectral acceleration, and W_p = the weight of the nonstructural component. This requirement suggests that the expected vertical acceleration demand on nonstructural components throughout the building, regardless of the relative height within the building, is equal to 50% of the peak horizontal ground acceleration. Moreover, the code assumes that there is no vertical acceleration amplification in the structure which suggests two conditions are satisfied. First, the columns of the building are sufficiently stiff axially to transfer the vertical ground acceleration to each floor with negligible amplification. Second, the vertical fundamental frequencies (due to out-of-plane flexibility) of the floor systems do not resonate with the vertical fundamental frequencies of the nonstructural component.

It should be noted that there is no vertical acceleration spectra required by ASCE 7 due to the reluctance of engineers to have to analyze the floor diaphragms for dynamic motion. To study the vertical seismic excitation of floors is rare as strong motion instruments are not typically located in the middle of a floor bay. Though ASCE 7 does not provide a vertical acceleration spectrum, the 2009 NEHRP provisions have included a unique vertical acceleration spectrum.

The AC 156 document specifies that the vertical required response spectrum be equal to two-thirds of the horizontal required response spectrum defined by Figure 5-1. This two-thirds rule was carried over from the optional provisions of the old UBC. The value of z in (5-9) and (5-10) may be taken as zero for the evaluation of the vertical required response spectrum. This stipulation also implies that there is no vertical acceleration amplification expected throughout the height of the building. The vertical required response spectrum is broken down into common acceleration terms in (6-2) and (6-3)

$$2/3A_{RIG} = 2/3(0.4S_{DS}) = 2/3PGA_h = PGA_v \tag{6-2}$$

$$2/3A_{FLX} = 2/3(0.4S_{DS}a_p) = 2/3\frac{FSA}{PFA}PGA_h = \frac{FSA}{PFA}PGA_v \tag{6-3}$$

where, A_{RIG} = spectral acceleration of rigid nonstructural components, A_{FLX} = spectral acceleration of flexible nonstructural components, S_{DS} = the design short period ground spectral acceleration, FSA = floor spectral acceleration which is the same a A_{FLX} or A_{RIG} depending on the period of the nonstructural component, PFA = peak floor acceleration, PGA_h = the horizontal peak ground acceleration, which is approximated as 40% of S_{DS}, and PGA_v = the vertical peak ground acceleration which is approximated as 2/3 of the horizontal peak ground acceleration.

For the 21 motions used in this investigation, the median and 84% fractile PGA_v/PGA_h ratios are equal to 0.425 and 0.697, respectively. Therefore the ground motions fall conservatively within the code expectations. A scatter plot of the peak vertical ground acceleration versus the peak horizontal ground motion is shown in Figure 3-4.

6.4 Results and Discussion

As described in Chapter 2, the floor systems of each building were modeled using a mesh of nine area elements per bay. Consequently, the vertical acceleration response of the floor was recorded at 247, 247, 256, and 304 nodes on each floor of buildings B3, H3, B9, and B20, respectively. With this information the influence of parameters including relative mounting height along the height of the structure, level of structural yielding, and location within the plan of the floor was identified.

Conservative representations of the vertical acceleration demands were selected by dividing the recorded responses into four categories, namely columns (points located at the intersection of a column and the floor), x-beams (points on beams oriented along the x-axis), y-beams (points on beams oriented along the y-axis), and open-bay (points within a bay of the floor) then selecting the record with the maximum peak vertical acceleration from each category. With four representative acceleration records per floor the peak vertical accelerations along with the vertical floor acceleration spectra were calculated.

6.4.1 Effect of Relative Height of Mounting Location

To demonstrate the effect of the mounting location along the height of the structure, the peak acceleration amplification factor (PFA_v/PGA_h) and the normalized floor acceleration spectra (FSA_v/PGA_h) were monitored for column locations and open-bay locations of the floors.

6.4.1.1 Rigid Nonstructural Components

Two versions of the peak vertical acceleration amplification profiles were generated. The first, in Figure 6-1, plots the median peak vertical floor acceleration (PFA_v) normalized by the peak vertical ground acceleration (PGA_v) against the relative height of the building for the column and open-bay locations. Whereas the second, in Figure 6-2, plots the median peak vertical floor acceleration (PFA_v) normalized by the peak horizontal ground acceleration (PGA_h) against the relative height of the building for the column and open-bay locations. The first plot in a clear and direct manner shows the vertical acceleration amplification ($PFAv/PGAv$) along the height of the building.

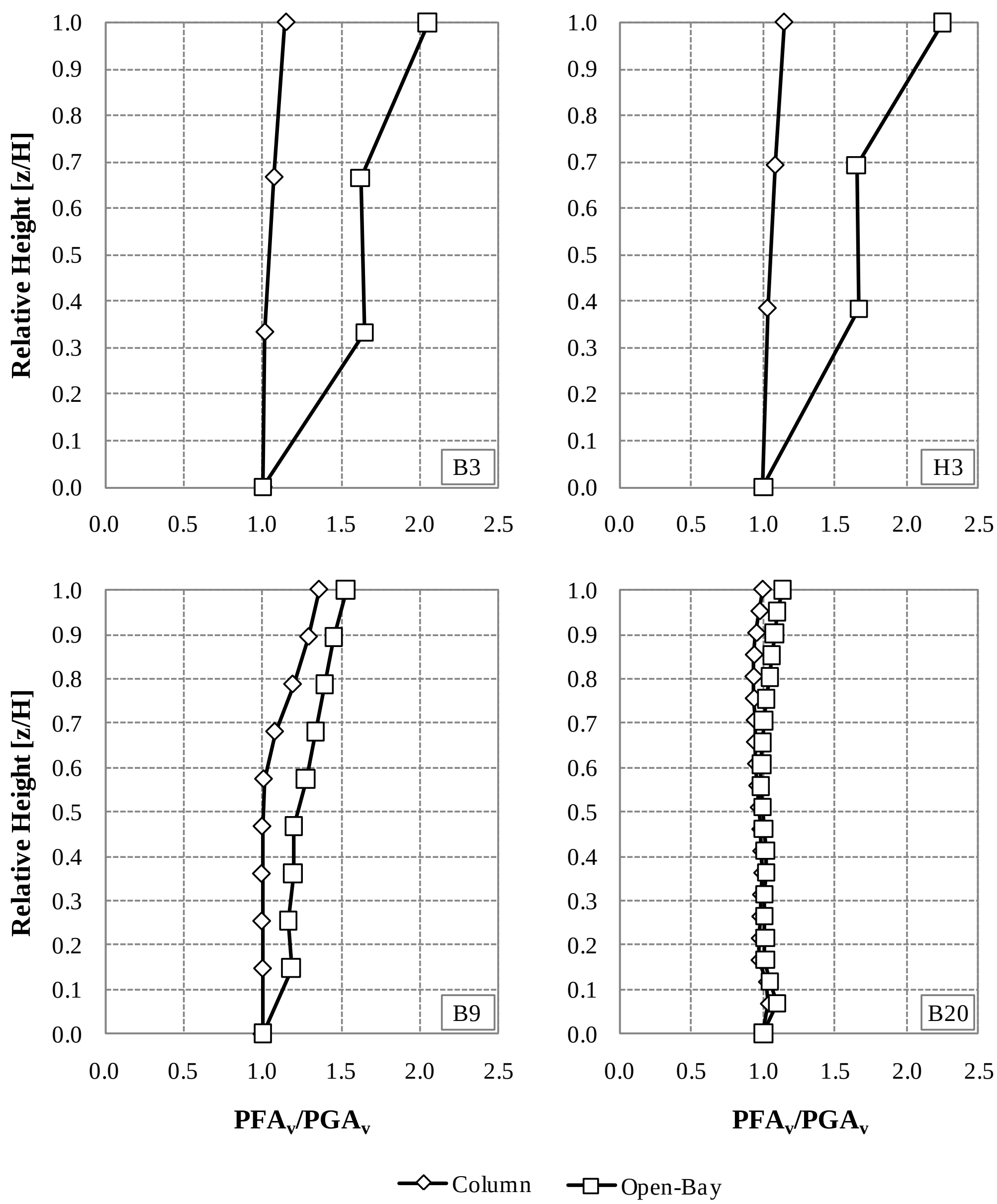

Figure 6-1 Influence of Relative Height on Vertical Peak Acceleration Amplification [B3, H3, B9, B20]

There is negligible amplification of the vertical floor acceleration at the column locations for buildings B3, H3, and B20 while building B9 shows some level of amplification between the mid height and roof of the building. Buildings B3, H3, and B20 confirm the assumption that the column axial stiffness is sufficiently great to provide essentially rigid body motion in the vertical direction. The amplification shown by building B9 can be attributed to a 22% reduction in the stiffness of the columns at the 6^{th} story column splice. This reduction of stiffness is thought to have increased the vertical period into the excitable range of most ground motions. The reason building B20, which also contains column splices does not show similar amplifications is because the reduction of column stiffness is not sufficient to shift the period due to the lighter floors of the building.

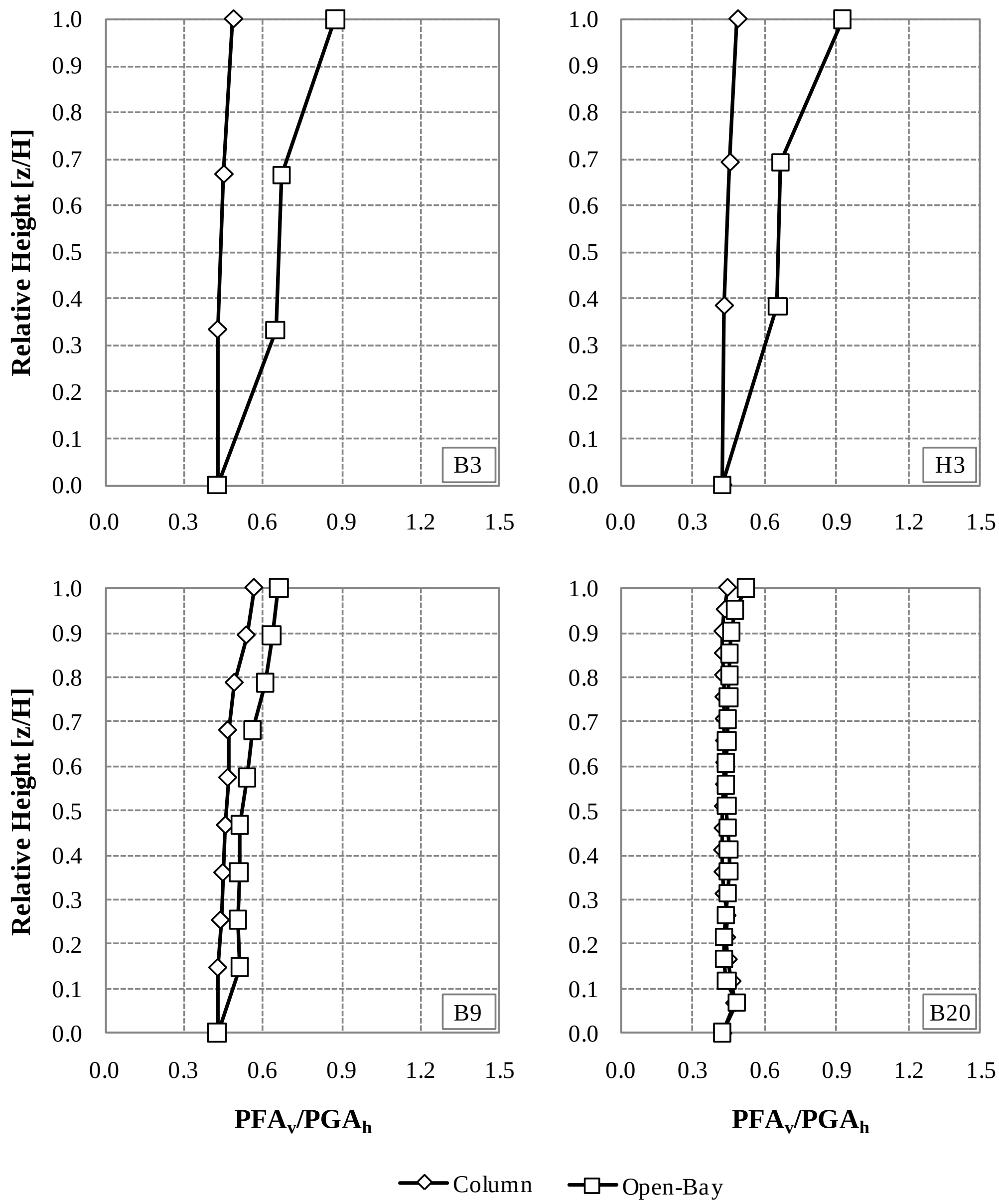

Figure 6-2 Influence of Relative Height on Vertical Peak Acceleration Amplification [B3, H3, B9, B20]

The open-bay locations of the floors show significantly greater amplification than the column locations. This observation was expected when considering the fundamental vertical frequencies of the floor systems (Table 6-1) in comparison with the vertical acceleration spectra (Figure 3-5). The vertical floor frequencies are clearly within the excited range of the ground motions. While all of the buildings show greater amplification at the open-bay nodes than the column nodes, the amount of increase in the vertical acceleration amplification is greater for the shorter buildings compared to the taller buildings. A larger increase in vertical acceleration amplification is noted at the roof of each building. This is attributed to the difference in floor and roof fundamental frequencies. The difference in these frequencies in shown in Figure 6-1 and comes from the variation in floor properties explained in Section 2.3.4.2.

The second set of vertical peak acceleration amplification profiles (Figure 6-2) compares the vertical floor acceleration response to the horizontal ground acceleration. The profiles show similar trends to the previous set; however the magnitude of the amplification is less. The value of the PFA_v/PGA_h ratio at the ground (z/H = 0) corresponds to the median PGA_v/PGA_h ratio which is equal to 0.425 for the investigated suite of ground motions. This ratio is carried throughout the height of the profile which causes the reduced amplification magnitude. The reason for presenting this version of the peak acceleration amplification profile is to show the conservative nature of the two-thirds rule specified by the AC 156.

6.4.1.2 Flexible Nonstructural Components

The normalized vertical floor acceleration spectra for each building are shown in Figure 6-3 through Figure 6-6. These plots compare the vertical floor acceleration spectra at the column and open-bay locations of three particular floors (z/H ≈ 0.33, 0.67, and 1.00) of each building. From these relationships a few observations are obtained.

Relative height is found to have little influence on the vertical floor acceleration spectra at the column locations. This is expected is the columns are assumed to be axially rigid. However, there is a noticeable difference in the vertical acceleration spectra of the roofs of the buildings compared to the lower floors at the open-bay location. This too is expected because of the difference in fundamental frequencies. Due to the roofs increased flexibility made it more susceptible to excitation by the ground motion.

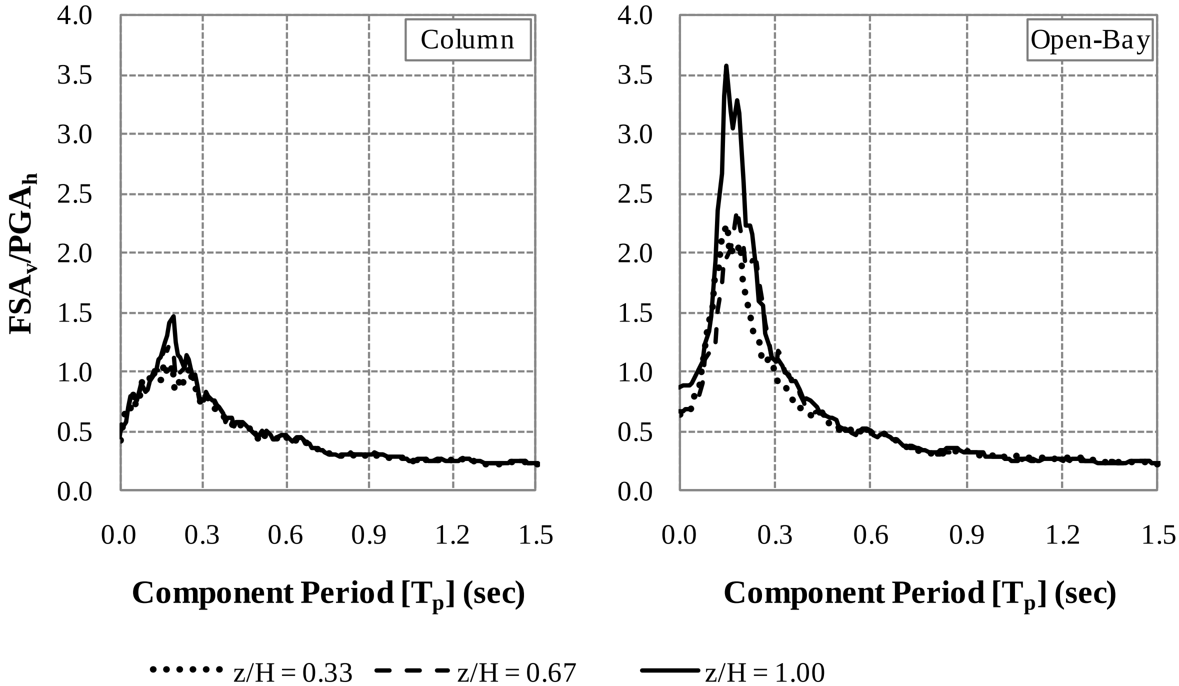

Figure 6-3 Influence of Relative Height on Normalized Vertical Acceleration Spectra [B3]

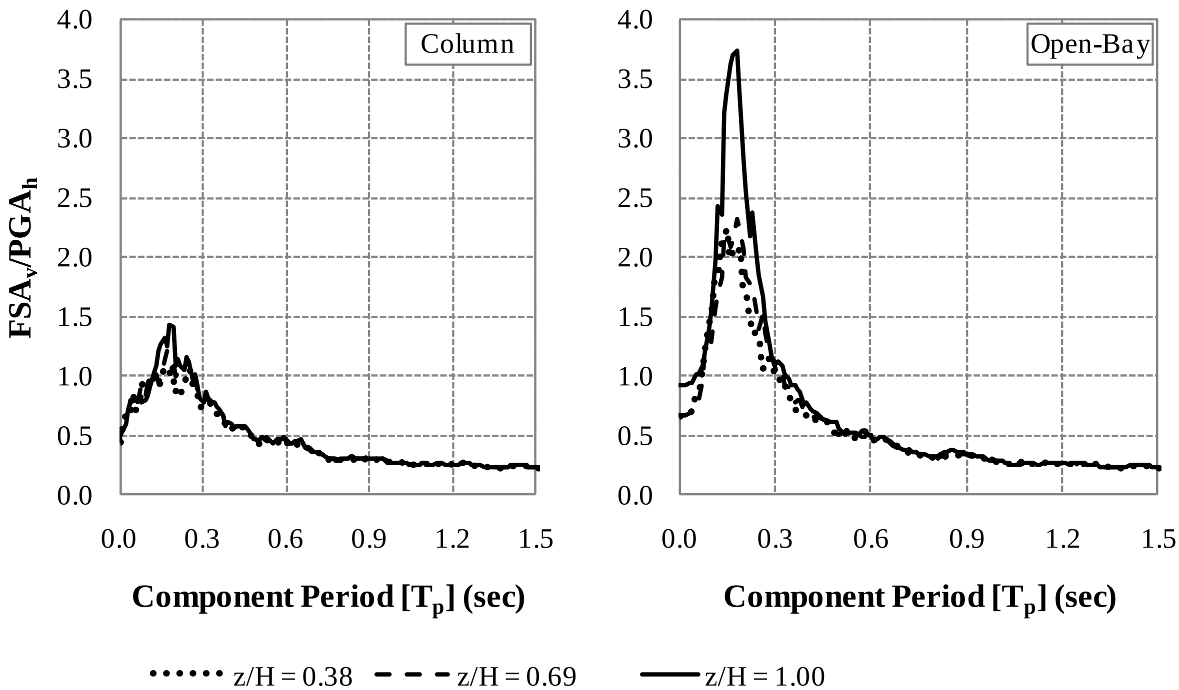

Figure 6-4 Influence of Relative Height on Normalized Vertical Acceleration Spectra [H3]

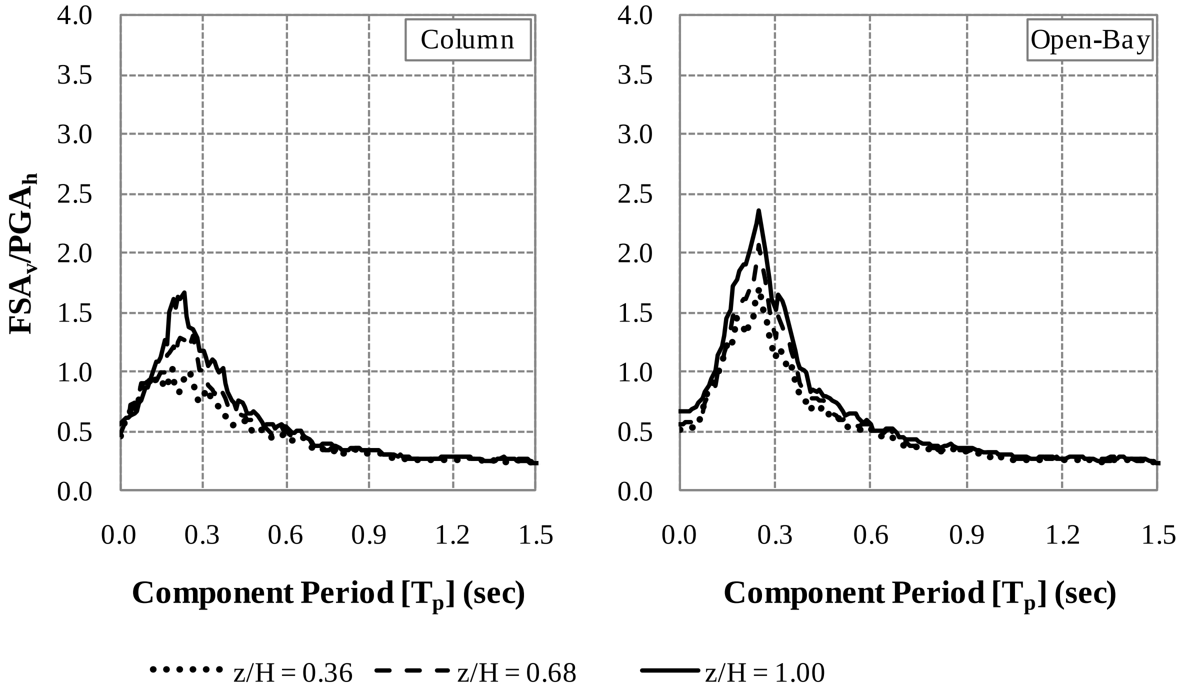

Figure 6-5 Influence of Relative Height on Normalized Vertical Acceleration Spectra [B9]

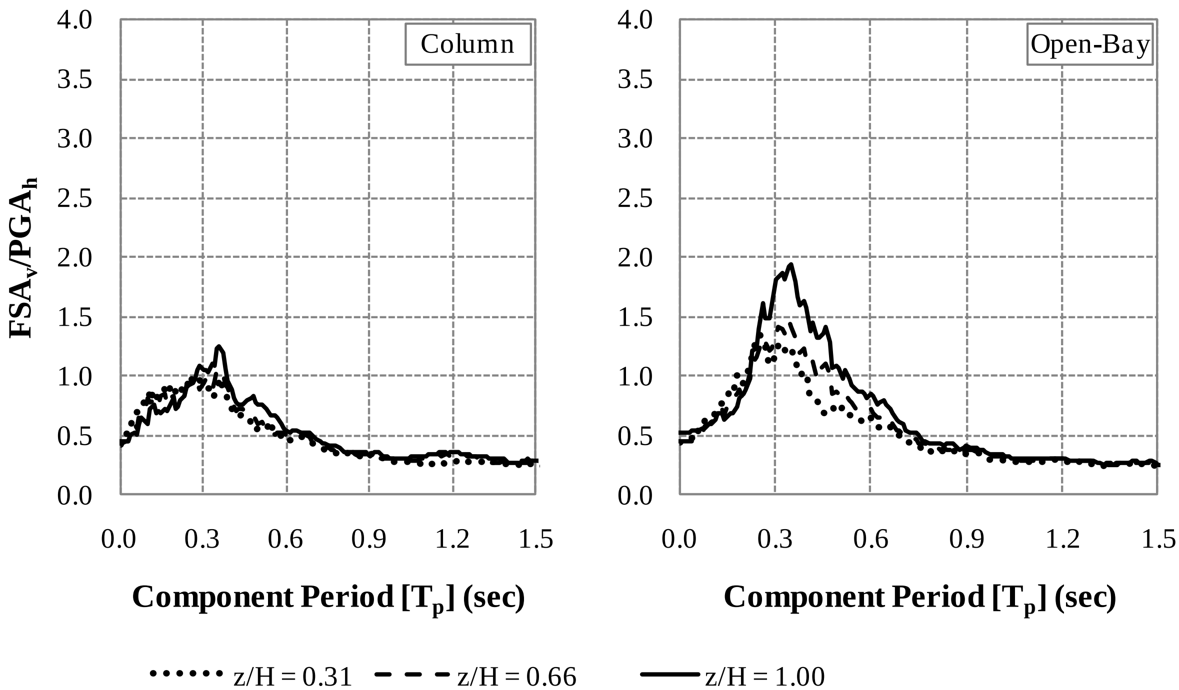

Figure 6-6 Influence of Relative Height on Normalized Vertical Acceleration Spectra [B20]

In comparing the floor acceleration spectra of each building, it is obvious that the open-bay locations of the shorter buildings impose a significantly greater vertical acceleration demand on nonstructural components tuned with the fundamental vertical frequency of the floor than the taller buildings. This is believed to be due to the increased interaction between floors in the taller buildings. The greater number of floors provides a greater potential for out-of-phase interaction of floor vibrations which act as a tuned mass damper. This theory is supported by the increased range of frequencies excited by the floors of the taller buildings compared to the shorter buildings. The increased range of frequencies shows that slight variations in resonant frequencies of floor systems due to slight changes in column stiffness or support beam stiffness result in a reduced acceleration demand on the nonstructural components.

6.4.2 Effect of Structural Yielding

The influence of lateral yielding of the structure on the vertical acceleration demands has not been studied as rigorously as horizontal acceleration, since most research on vertical floor response is in reference to floor vibration studies as opposed to seismic performance. The results presented in this section demonstrate the influence of nonlinear response of the SMRF frame on the vertical floor acceleration response. It should be noted that the results presented are somewhat limited by the modeling assumption that the concrete floors and gravity load-carrying systems remain elastic under all levels of seismic loads.

6.4.2.1 Rigid Nonstructural Components

The effect of structural yielding on the peak vertical floor acceleration response was illustrated by plotting the PFA_v/PGA_h ratio as a function of global ductility in Figure 6-7 through Figure 6-10. It is obvious that unlike in the horizontal direction the vertical acceleration demands are not influenced by yielding in the SMRFs. It is noted that the vertical peak acceleration amplification of the roof at both column and open-bay joints is constant for all levels of ground motion intensity. Also, that the dispersion in the data is greater for the open-bay locations of the floor than the column locations.

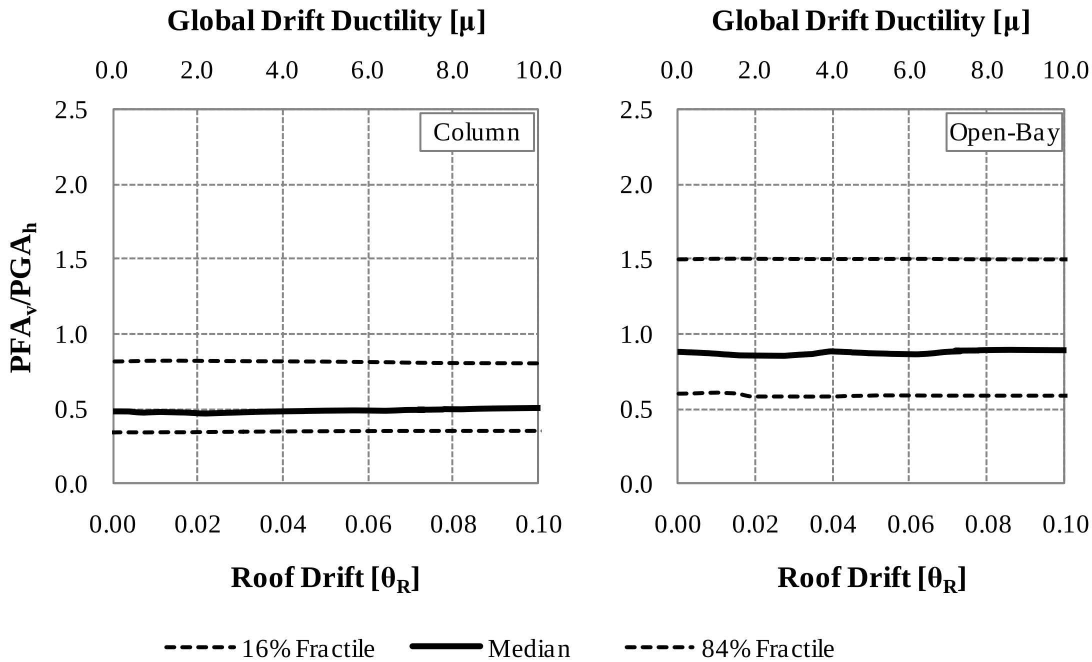

Figure 6-7 Influence of Ductility on Vertical Roof Acceleration Amplification [B3]

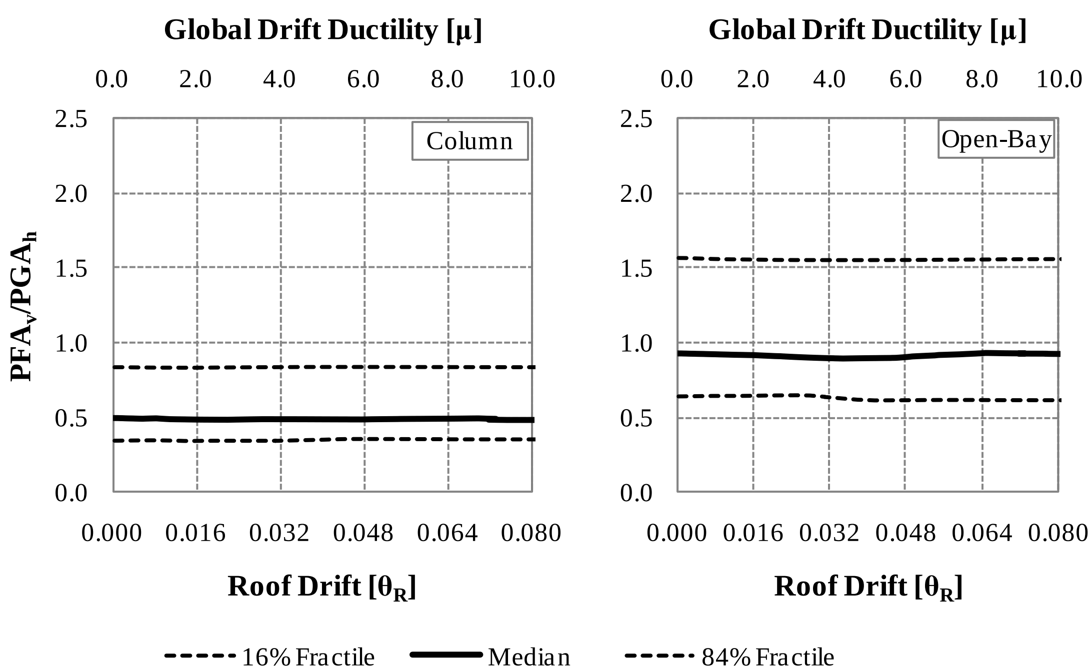

Figure 6-8 Influence of Ductility on Vertical Roof Acceleration Amplification [H3]

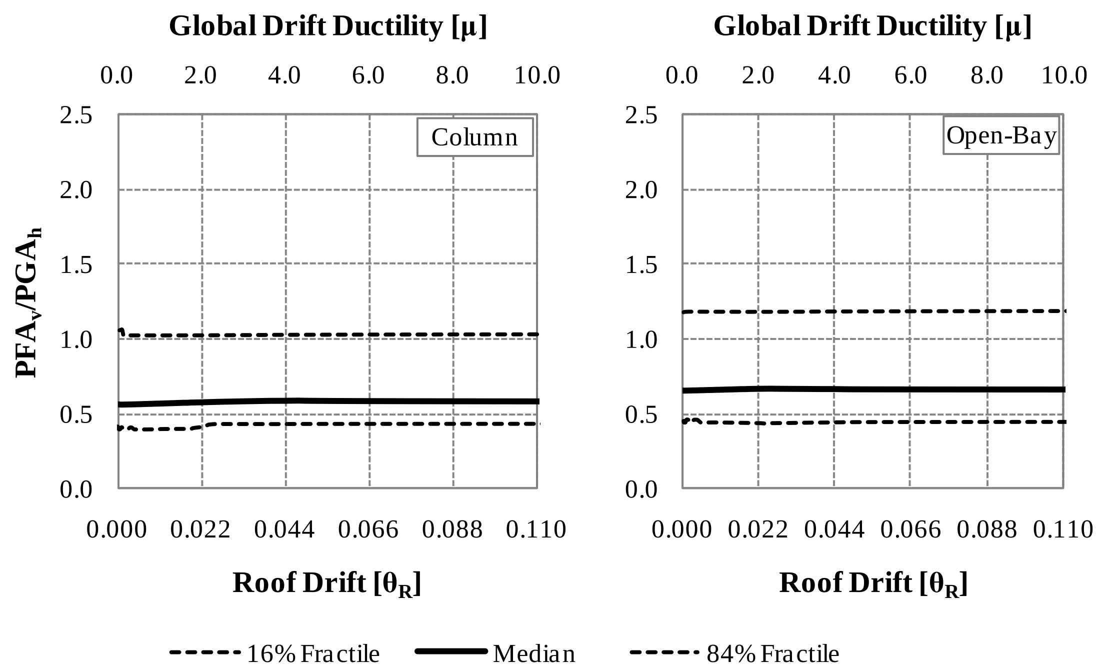

Figure 6-9 Influence of Ductility on Vertical Roof Acceleration Amplification [B9]

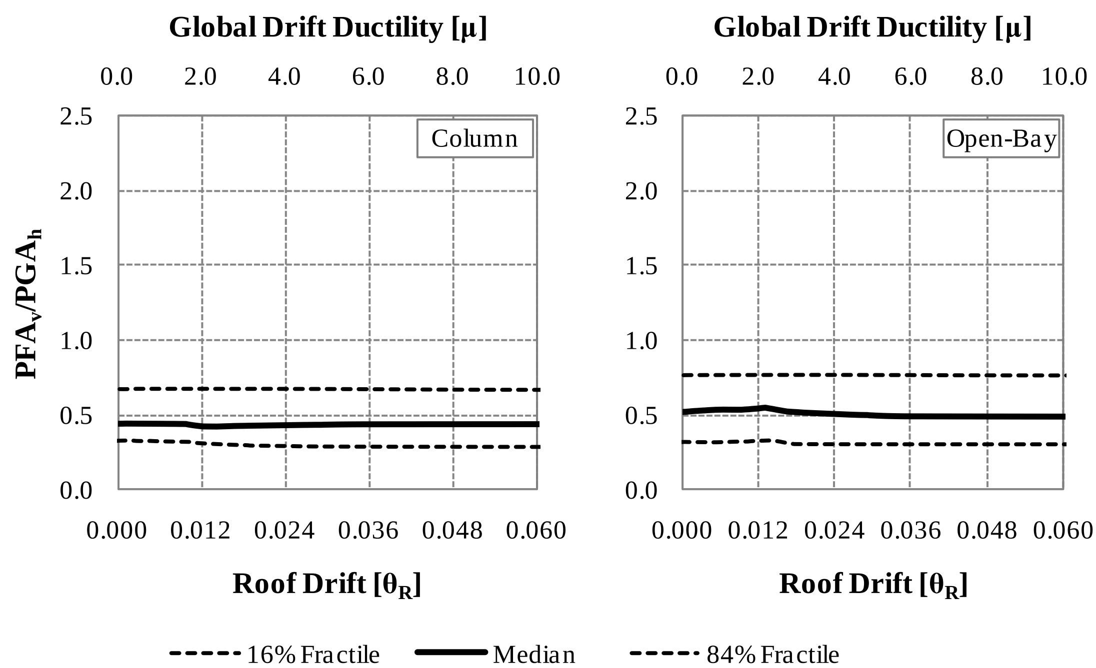

Figure 6-10 Influence of Ductility on Vertical Roof Acceleration Amplification [B20]

6.4.2.2 Flexible Nonstructural Components

The normalized vertical roof acceleration spectra (FSA_v/ PGA_h) for four ductility levels of each building are presented in Figure 6-11 through Figure 6-14. The plots show little dependency on the level of ductility. This means that increased levels of ductility have no influence on the vertical acceleration demands on nonstructural components regardless of the period or location of the nonstructural component.

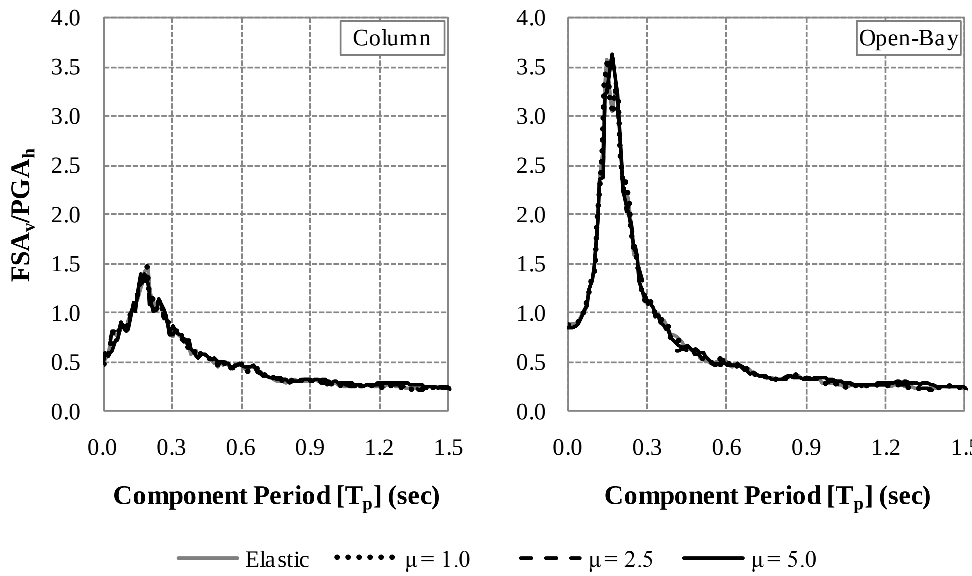

Figure 6-11 Influence of Ductility on Vertical Roof Acceleration Spectra [B3]

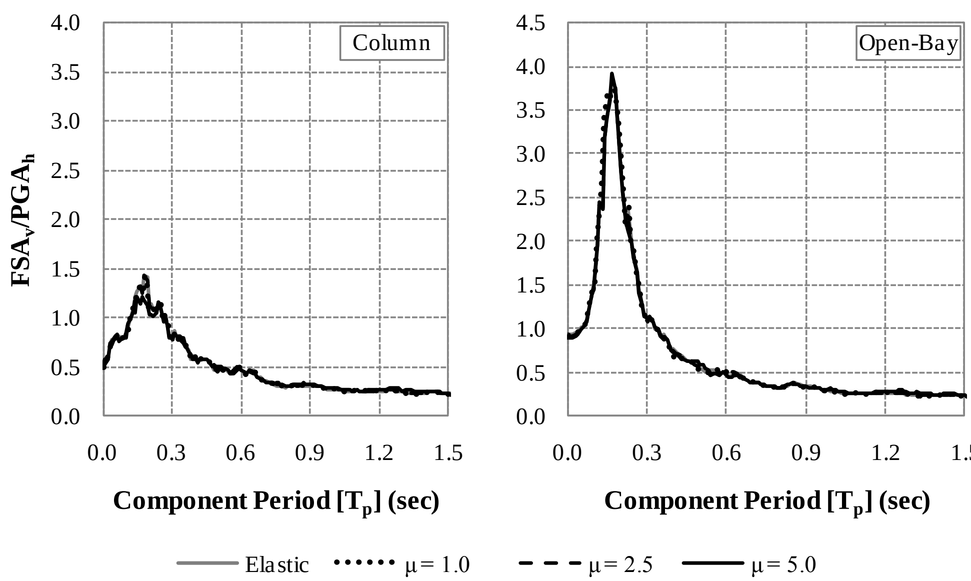

Figure 6-12 Influence of Ductility on Vertical Roof Acceleration Spectra [H3]

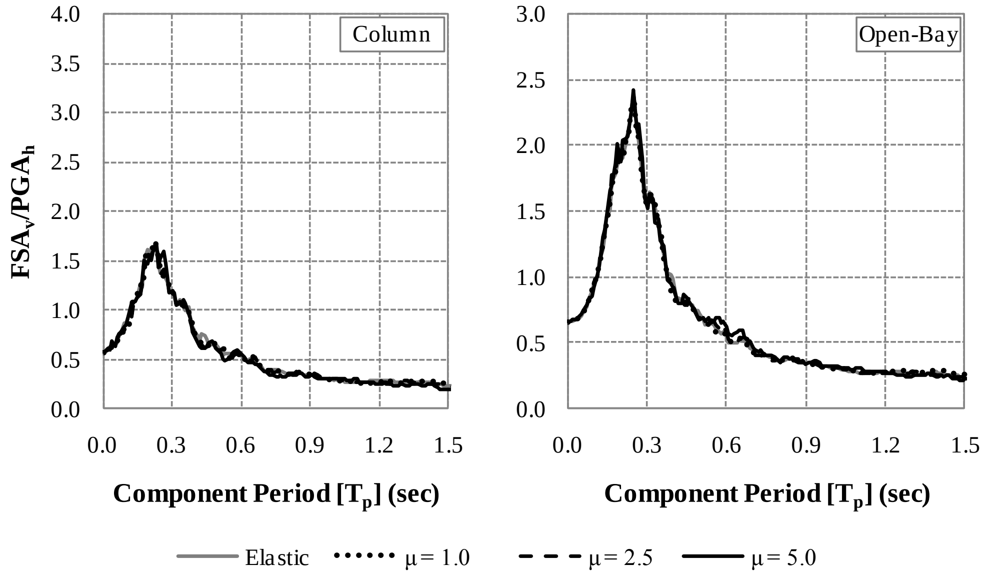

Figure 6-13 Influence of Ductility on Vertical Roof Acceleration Spectra [B9]

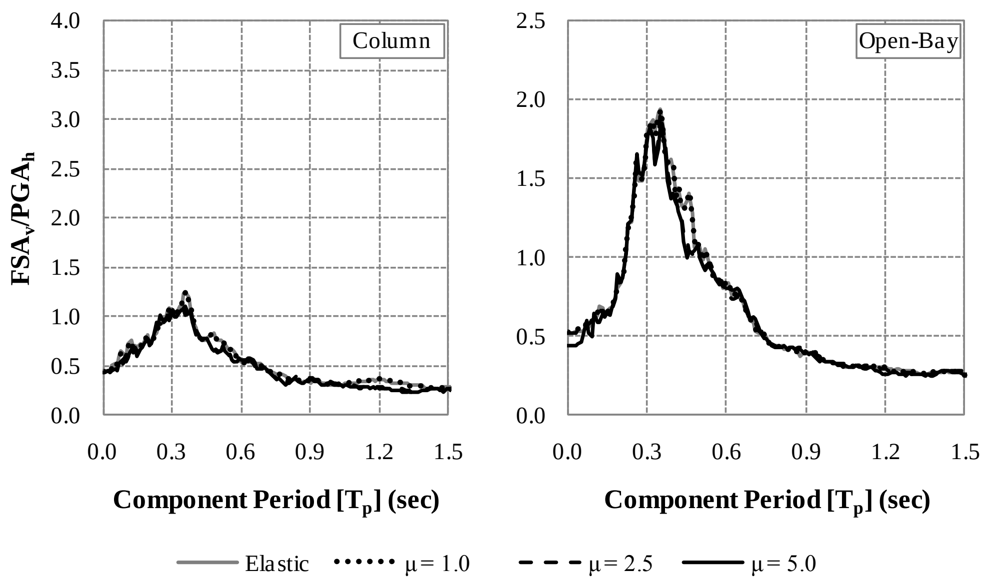

Figure 6-14 Influence of Ductility on Vertical Roof Acceleration Spectra [B20]

6.4.3 Effect of Plan Position of Mounting Location

The dynamic amplification of floor systems vary depending on the location within the plan dimensions of the floor. Near the column locations the floor is most stiff and as the distance from the columns increase the floor becomes more flexible. With several closely spaced natural frequencies of multi-bay floor systems the influence of the frequency content of the ground motion is credible.

The influence of the ground motion (frequency content) on the vertical acceleration amplification (PFAv/PGAv) at the roof of each building is presented in Figure 6-15 through Figure 6-18. In these figures, contour and surface representations of the vertical acceleration amplification factor of each recorded point on the roof were plotted over the plan area for three selected ground motions.

The contour plots make it easy to identify the location of the support columns, and the surface plots provide a better perspective of the amount of amplification throughout the roof. Together one can gather a large quantity of information. From these graphs a number of observations were made.

First, the amplification of the roof due to each ground motion is different. The frequency content of each ground motion excites different modes of vibration in the floor thus creating a unique vertical acceleration response. Because there are several modes of vibration of the floor/roof systems with similar natural frequencies it is possible that slight variations in the ground motion frequency content will excite completely different modes of vibration. This makes it very difficult to predict the location on the floor/roof which is most susceptible to excitation during seismic events.

Second, the column locations provide the most consistent amplification. Again due to their axial stiffness the acceleration amplification at column locations is often very small ($PFA_v/PGA_v \approx 1.0$). However, the amplitude of vertical acceleration amplification throughout the floor ranges from 0.4 to 3.7. This also makes it challenging to formulate an efficient and simple relationship for estimating the vertical acceleration response of typical floor/roof systems.

Third, each floor system is different in that span between columns, the number of adjoining bays, and the effect of one-way or two-way transmission of the vertical load have a profound effect on the vertical vibration of the floor/roof systems. In comparing, the distribution of acceleration amplification between buildings it is noted that typically longer spans generate a larger excited region (Building B20). Adjoining bays do not necessarily experience similar levels of acceleration amplification. And one-way slabs may produce a wave effect in the vertical acceleration response as shown in Event 12 in buildings B3 and H3 as well as Event 7 in building B20.

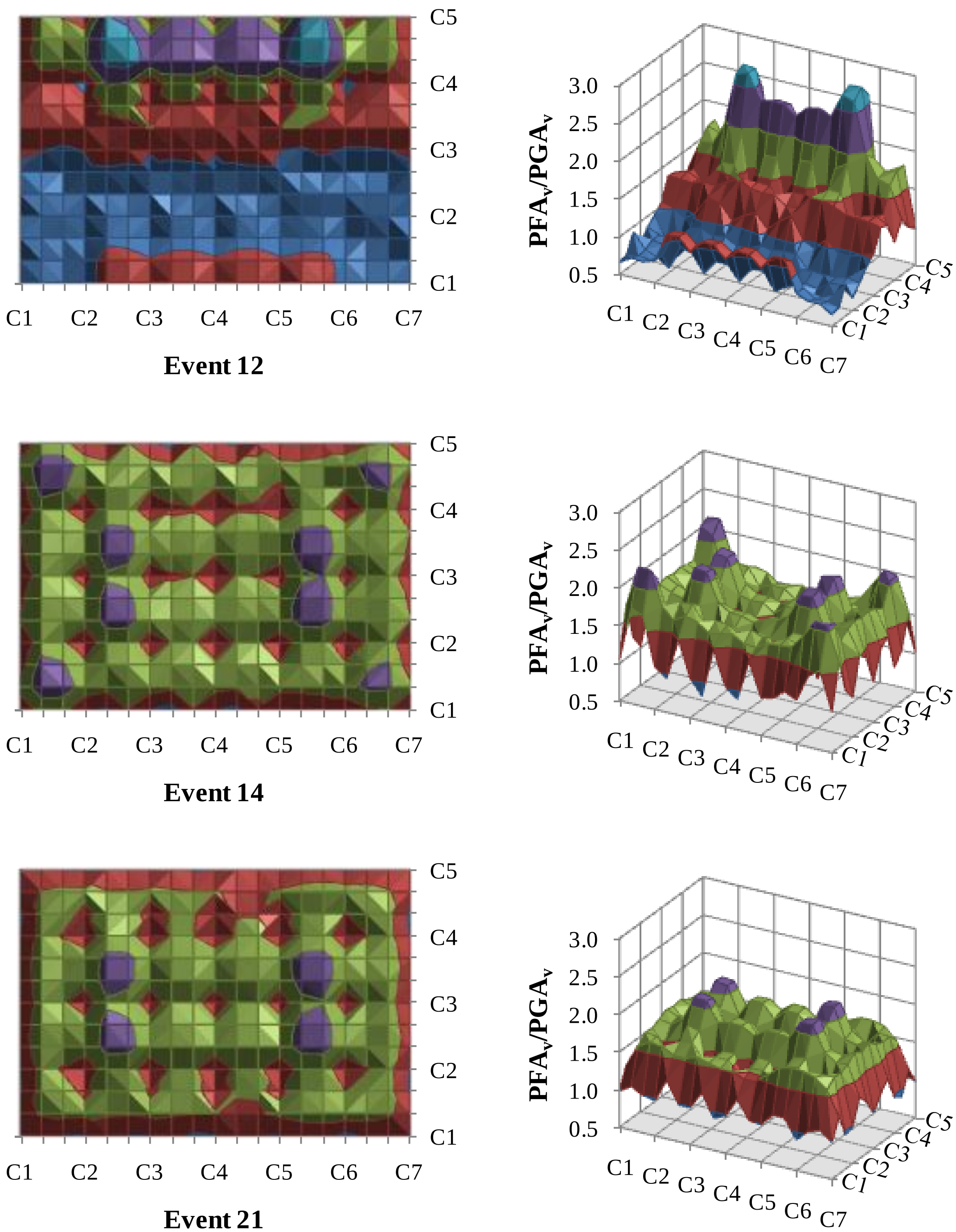

Figure 6-15 Influence of Ground Motion on Vertical Roof Acceleration Amplification [B3]

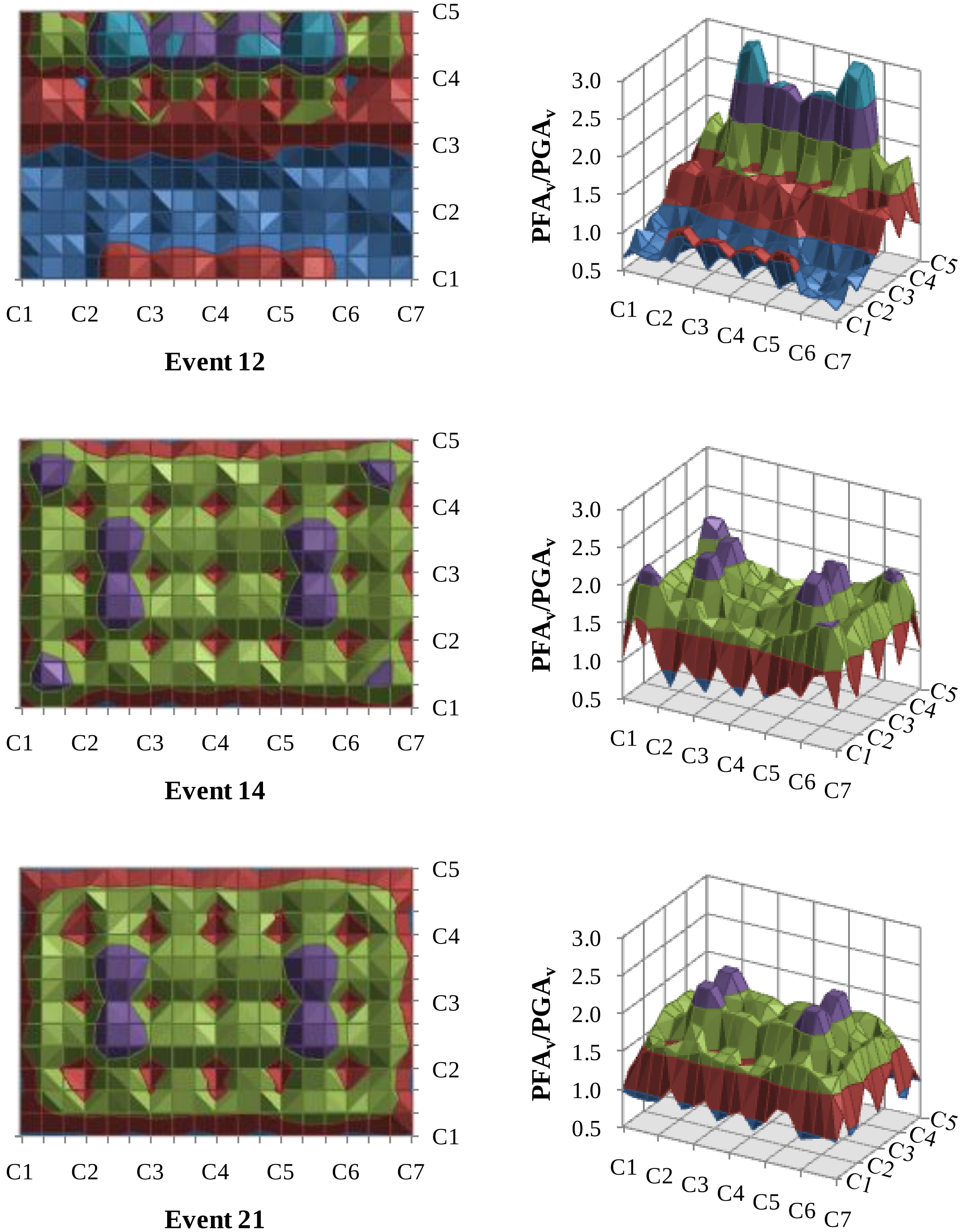

Figure 6-16 Influence of Ground Motion on Vertical Roof Acceleration Amplification [H3]

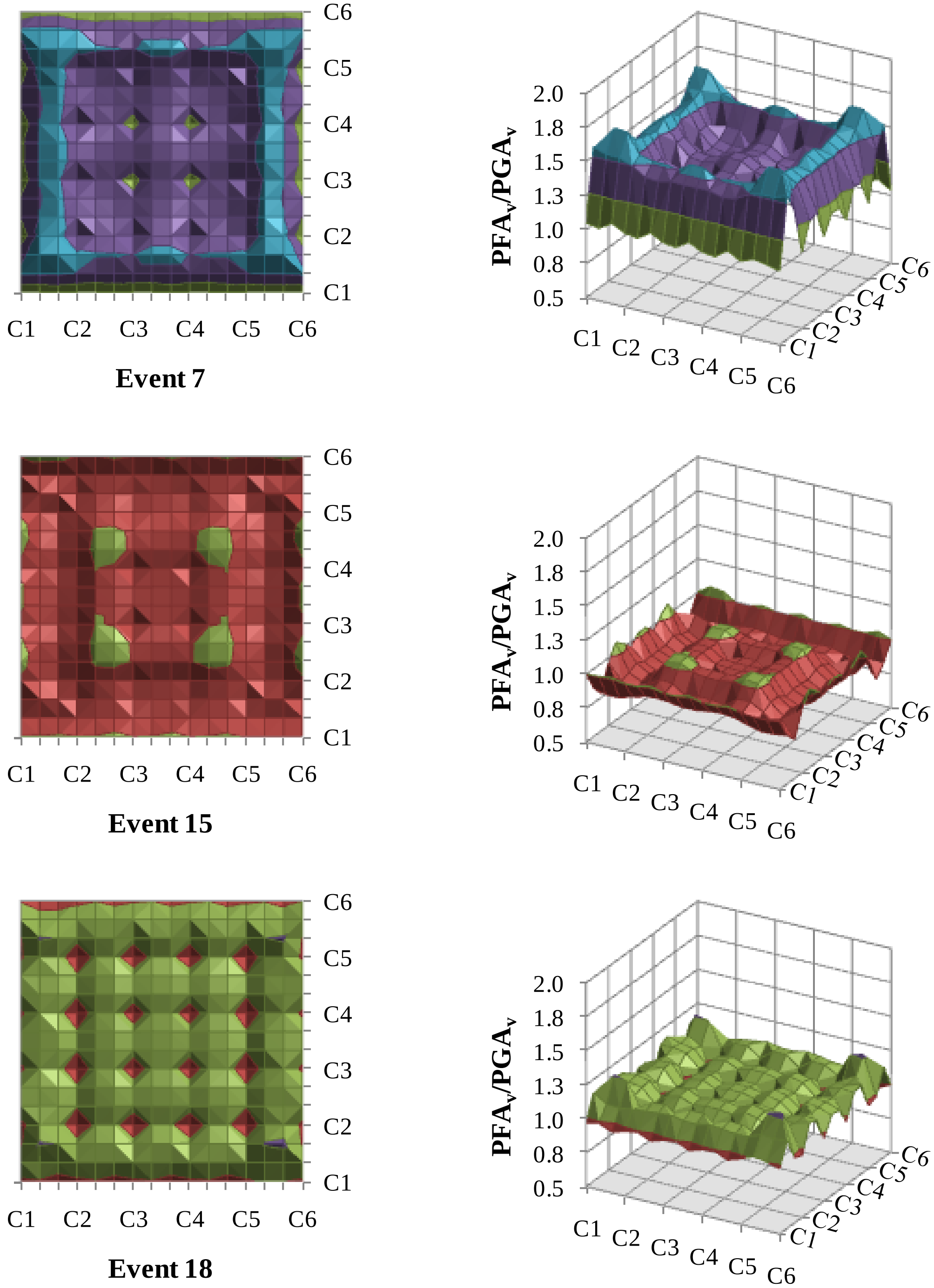

Figure 6-17 Influence of Ground Motion on Vertical Roof Acceleration Amplification [B9]

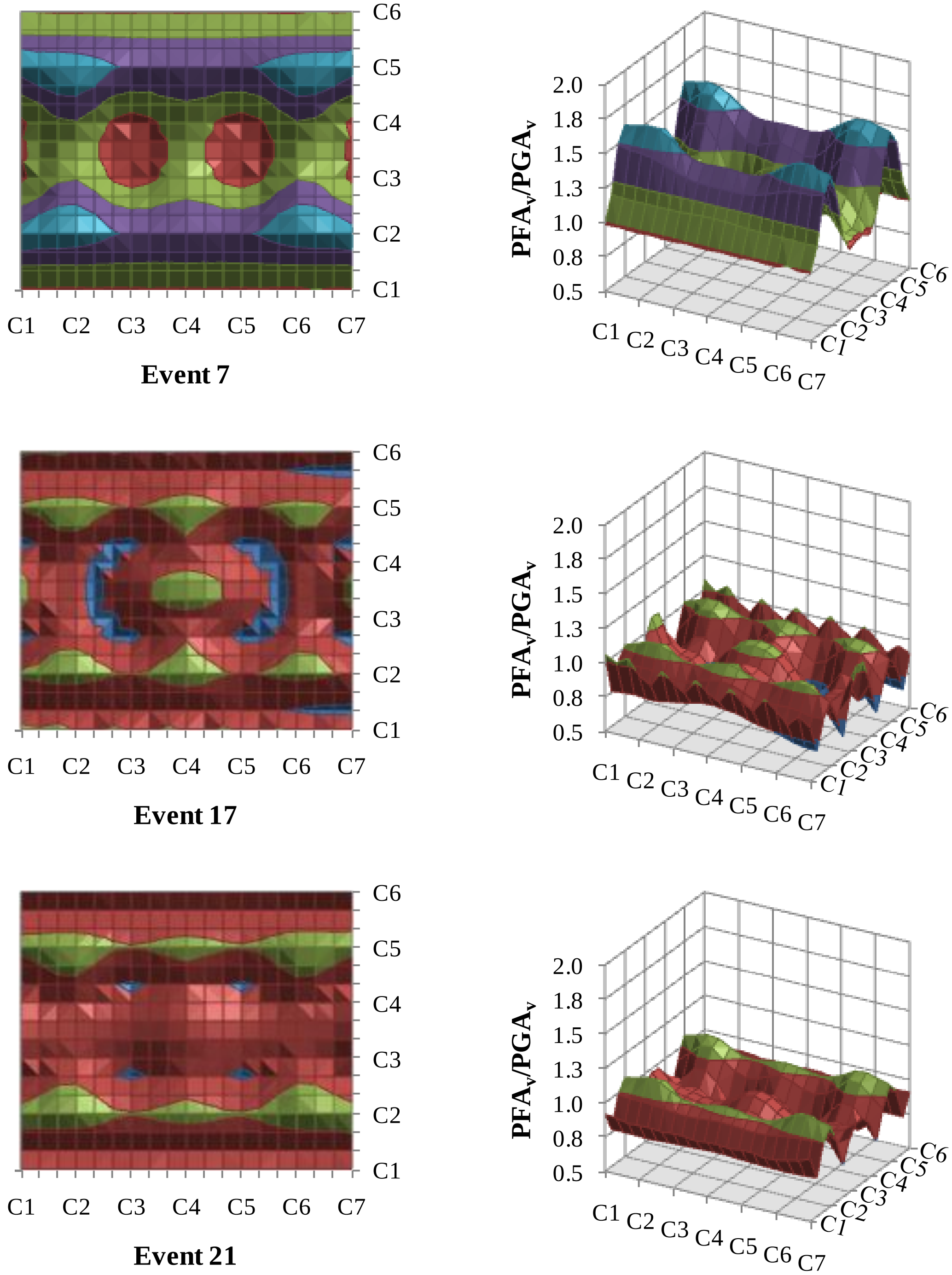

Figure 6-18 Influence of Ground Motion on Vertical Roof Acceleration Amplification [B20]

6.5 Assessment of Current Code Provisions

Having investigated the influence of the relative height, structural yielding, and plan location on the vertical acceleration response of floor/roof systems in earthquakes it is possible to assess the code estimation of such response. Section 6.3 has illustrated the approach of two standards that are adopted by the building code, the ASCE 7-10 (ASCE, 2010) and the AC 156 (ICC, 2006). These code provisions were compared to the results of this study in Figure 6-19 through Figure 6-22. These plots represent the median floor acceleration spectra of the column and open-bay locations with the greatest peak vertical acceleration on the roof level of each building. The ground motion intensity provides a structural response with global ductility, $\mu = 1$, which symbolizes the onset of inelastic structural response. This level of ground motion is close to, yet slightly less than the design level earthquake of the building. The S_{DS} used to calculate the ASCE 7-10 required vertical acceleration as well as the vertical required response spectrum specified in the AC 156 document was selected as the median horizontal spectral acceleration of the ground inducing a $\mu = 1$ response at period of 0.2 seconds. The following sections will discuss the comparison of these provisions with the results from this study.

6.5.1 ASCE 7-10 Provisions

The vertical acceleration required by the ASCE 7-10 depends simply on the short period design spectral acceleration, S_{DS}. Its simplicity is convenient for design but unfortunately provides a poor estimation of the vertical acceleration demands on nonstructural components, as shown by Figure 6-19 through Figure 6-22. This requirement suggests that the vertical acceleration of all nonstructural components within the building, regardless of their natural period of location within the structure, is equal to 50% of the horizontal peak ground acceleration.

First of all, the median and 84% fractile peak vertical ground accelerations were found to be 0.425 and 0.697 times the peak horizontal ground acceleration. Therefore, the ASCE 7-10 correctly estimates the peak vertical ground acceleration less than 84% of the time. Second, the results of this Section 6.2.1 show that significant amplification is induced at different points on the floor due to resonance with the dominant out-of-plane frequencies of the floor. The ASCE 7-10 does not consider this effect in its estimation, thus it can be unconservative for a large portion of the floor (away from the columns). Third, this equation does not incorporate the period of the nonstructural component and therefore is unconservative for flexible nonstructural components resonating with the floor acceleration response.

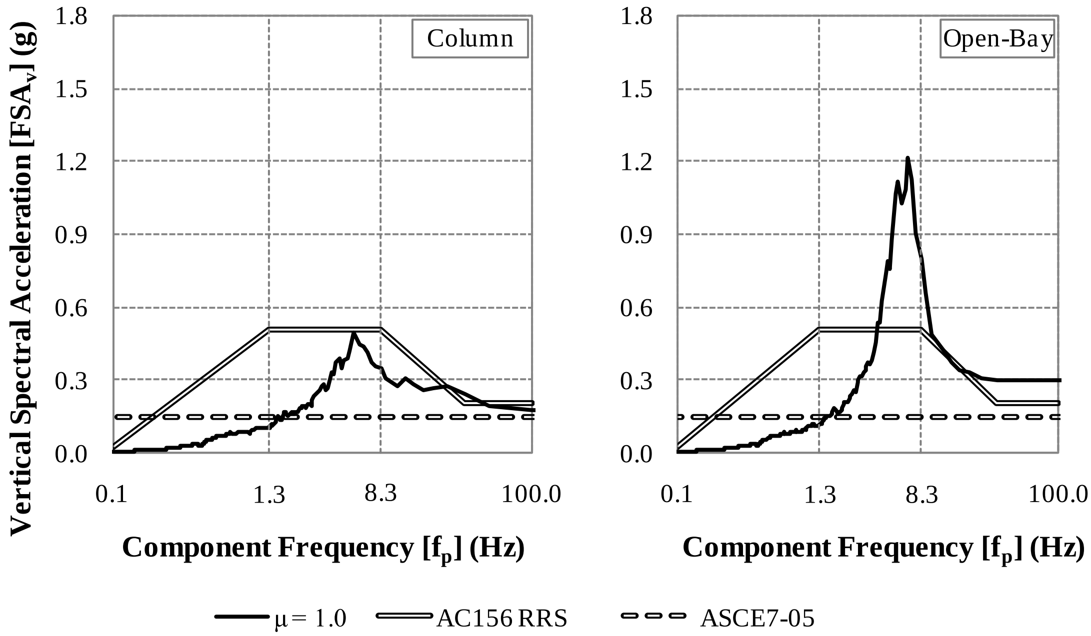

Figure 6-19 Comparison of AC 156 Vertical Required Response Spectrum vs. Vertical Roof Acceleration Spectrum (μ = 1.0) [B3]

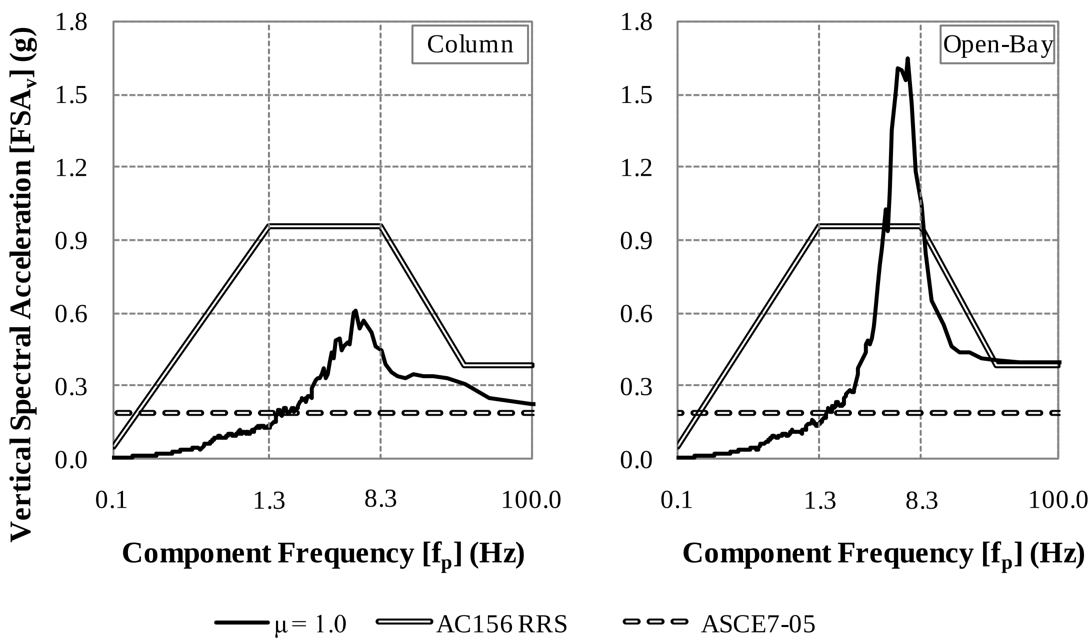

Figure 6-20 Comparison of AC 156 Vertical Required Response Spectrum vs. Vertical Roof Acceleration Spectrum (μ = 1.0) [H3]

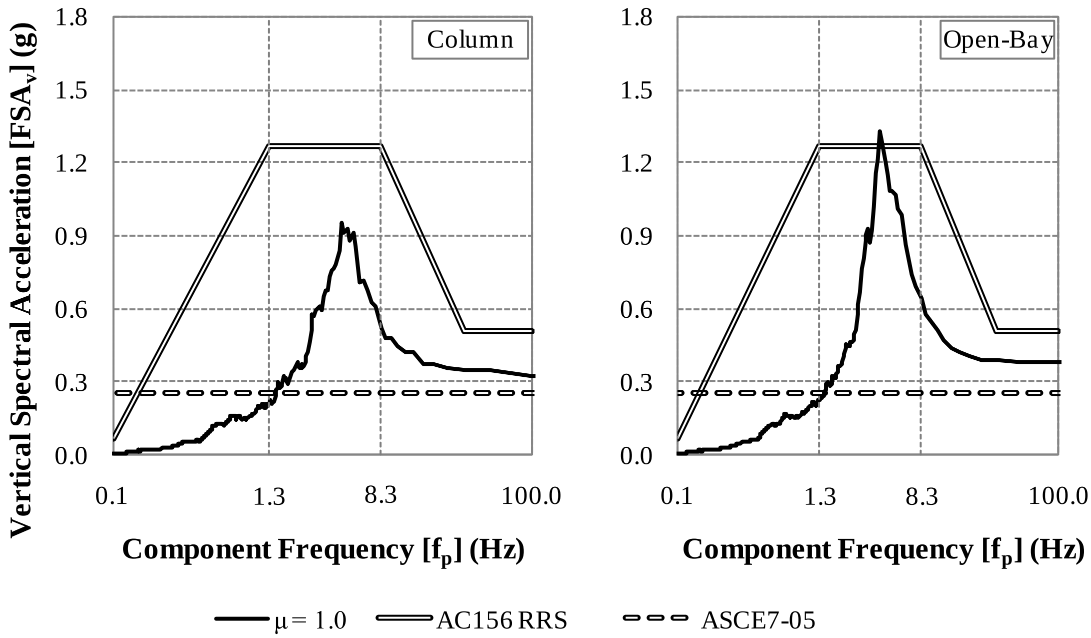

Figure 6-21 Comparison of AC 156 Vertical Required Response Spectrum vs. Vertical Roof Acceleration Spectrum (μ = 1.0) [B9]

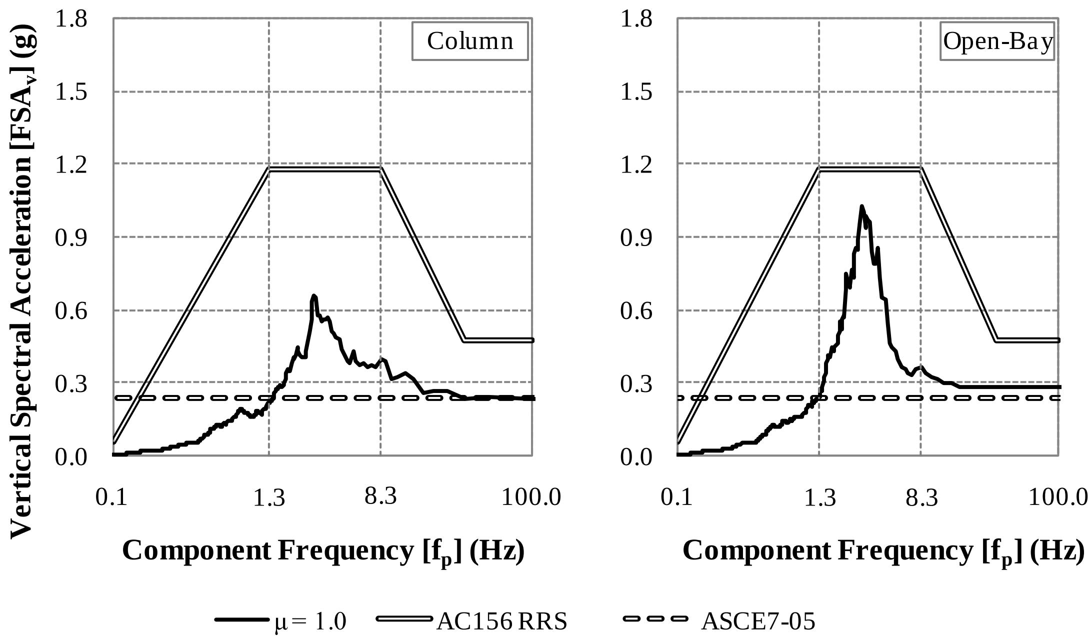

Figure 6-22 Comparison of AC 156 Vertical Required Response Spectrum vs. Vertical Roof Acceleration Spectrum (μ = 1.0) [B20]

6.5.2 AC 156 Provisions

In the AC 156 provisions, the vertical required response spectrum is defined as 2/3 times the horizontal required response spectrum. In addition, the amplification along the height of the structure is neglected. At the column locations of the floors this is justified, however vertical accelerations maybe amplified by a factor ranging between 0.4 and 3.7 on average at open-bay locations due to resonance of the floor/roof system with the vertical ground excitation. This amplification is significant and is currently overlooked in the derivation of the vertical required response spectrum. On the other hand, the effect of the period of the nonstructural component is accounted for and does capture the amplification due to resonance of the nonstructural component with the floor. The range of excited frequencies between 1.3 Hz and 8.3 Hz specified by the required response spectrum seems to adequately cover the range of frequencies excited in this study. Figure 6-19 through Figure 6-22 demonstrate that for the column locations the vertical required response spectrum is conservative. However, for open-bay locations of the floor/roof systems it may be significantly underestimating the vertical acceleration demands.

6.6 Summary

The results and discussion of this chapter have established that the vertical acceleration demands on nonstructural components is dependent on the period of the nonstructural component, and the location of the nonstructural component in the floor plan, specifically in relation to the columns and open-bays of the floor. The vertical acceleration demands on nonstructural components are independent of relative height within the structure, and yielding of the SMRF. The estimation of vertical acceleration demands on nonstructural components specified by the ASCE 7-10 is unrealistically simplistic and unconservative. The vertical required response spectrum defined by the AC 156 conservatively estimates the vertical acceleration demands on nonstructural components attached near the columns of the building, but fails to account for acceleration amplification due to the out-of-plane flexibility of the floors away from the columns. This influence has been shown to increase the vertical acceleration of the open-bay locations of the floors up to 4 times that of points near the columns.

These conclusions are based on the small sample of building structures with flexible diaphragms included in this investigation. While the analysis provided is assumed to identify important trends and possible deficiencies in the code, significantly more research is needed before broad conclusions can be drawn. For example, the floor systems studied herein represent a small portion of the possible configurations, types, and frequencies of floor systems. Future research on vertical response of flooring systems to seismic excitation should include generating vertical motions compatible with the new vertical acceleration spectra presented in the 2009 NEHRP provisions. Nonetheless, the observations of this and future studies should be validated by physical observations either in the field or in the laboratory before entering into the code requirements.

SECTION 7
FEASIBILITY OF USING FLOOR MOTION DATABASE FOR SHAKE TABLE STUDIES

7.1 Introduction

A database of substantial size of floor motion responses was generated in the course of this study. This database contains acceleration, velocity, and displacement time history records of each floor of every building for over 1,000 nonlinear earthquake analyses obtained from incremental dynamic analyses. These floor motions can be used to examine the performance of nonstructural components exposed to typical nonlinear floor motions. This database has the potential of providing the drive motions for shake table testing of nonstructural components. This chapter explores the feasibility of using motions from this database as potential shake table input motions.

7.2 Description of Floor Motion Database

The accumulated nonlinear floor motion database contains floor acceleration, velocity, and displacement time history records. The records are organized by seismic event, ground acceleration intensity, floor level, and direction. A series of MATLAB data structures were created to store the information in a logical easy to access database.

Using this database as a foundation, other response parameters such as maximum interstory drift, average interstory drift, roof drift, global ductility, and floor acceleration, velocity, and displacement spectra were calculated to classify the floor motions by building performance or expected elastic nonstructural component response. A building performance level was assigned to each motion in order to group motions induced by similar levels of inelastic building response. Four building performance levels were defined based on the level of ductility of the structure as defined in Section 4.2.2.3. PL 1 corresponds to elastic building responses ($\mu < 1.0$); PL 2 corresponds to the initiation of yielding ($1.0 < \mu \leq 2.5$); PL 3 corresponds to moderate yielding within the structure ($2.5 < \mu \leq 5.0$); and PL 4 corresponds to extensive yielding and near collapse response of the structure ($\mu > 5.0$).

A summary sheet was generated in Excel (Microsoft, 2007) to facilitate the identification and selection of time history records based on desired motion and building performance characteristics. Figure 7-1 shows the layout of the summary sheet. The summary sheet can be used to identify records based on criteria such as, event, floor level, direction, peak acceleration, peak velocity, peak displacement, and building performance level. Once the desired motions are identified from the summary sheet, the time history records, spectral information, and building performance information can be extracted from the MATLAB database. This multi-step procedure was implemented to enable the user to navigate the database. A data CD is included as Appendix A of this report that includes the time history responses of the analyzed building.

FLOOR MOTION SUMMARY SHEET

Selection Criteria		
Criteria	**Min**	**Max**
Event	1	21
Floor	1	4
Direction	1	2
PFA	0.200	1.000
PFV	0.0	50.0
PFD		
PL	1	4

Number of Qualified Records		
Count	**Total**	**% of Total**
2901	11098	26.14%

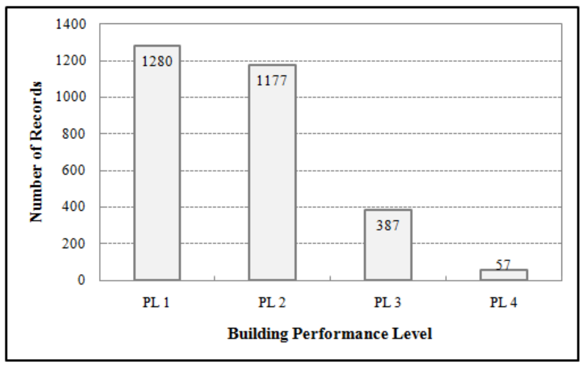

No.	Building	Event	Intensity	Floor	Direction	PFA	PFV	PFD	θ_{max}	θ_{avg}	θ_R	μ	PL
1	1	1	3	4	1	0.241	15.4	16.3	0.006	0.005	0.006	0.6	1
2	1	1	3	4	2	0.248	17.1	8.4	0.006	0.006	0.006	0.5	1
3	1	1	4	1	1	0.205	0.0	31.4	0.012	0.011	0.011	1.1	2
4	1	1	4	3	1	0.306	18.3	30.1	0.012	0.011	0.011	1.1	2
5	1	1	4	4	1	0.410	27.6	30.9	0.012	0.011	0.011	1.1	2

Figure 7-1 Database Summary Sheet

7.3 UNR Shake Table Limitations

The Large Scale Structures Laboratory (LSSL) at the University of Nevada, Reno is home to three 50-ton biaxial shake tables and one 20-ton six degree of freedom shake table. As one of fifteen experimental facilities in the George E. Brown, Jr. Network for Earthquake Engineering and Simulation (NEES), the LSSL is funded by the National Science Foundation (NSF) to maintain a state-of-the-art earthquake simulation laboratory. Primarily founded as a bridge engineering research facility, the LSSL has recently expanded the scope of its research to include building, and nonstructural systems. The addition of the 6DOF shake table in 2008 enabled the

LSSL to perform seismic qualification testing of nonstructural components which requires vertical excitation per the AC 156.

Potentially, the floor motions from the database developed in this study may be used for shake table testing of nonstructural components under realistic floor accelerations of yielding building structures. To determine the feasibility of their use in shake table testing, first the physical limitations of the shake tables must be understood. The nominal shake table capacities for the biaxial and 6DOF shake tables at UNR are presented in Table 7-1 and Table 7-2, respectively. It should be noted that the limitation on acceleration increases as the payload decreases and since typically nonstructural components are light weight, accelerations greater than 1 g may be possible. On the other hand, the limitations on peak velocity are not as flexible. As the velocity approaches the limitations of the hydraulic actuators the ability to control the performance of the shake table is diminished. One of the primary limitations to using floor motions directly as shake table input motions is the inherent large displacements due to sway of the building. The dynamic stroke of the shake tables is a limit that physically cannot be exceeded.

Table 7-1 Nominal Capacities of UNR Biaxial Shake Tables

Biaxial Shake Tables	
Table Size:	14.0 ft x 14.6 ft
Nominal Payload:	50 ton
Maximum Payload:	150 kip
Maximum Force:	165 kip
Maximum Pitch Moment:	1000 kip-ft
Maximum Yaw Moment:	400 kip-ft
Maximum Roll Moment:	400 kip-ft
Maximum Acceleration:	1 g with 100 kip
Maximum Velocity:	50 in/sec
Maximum Displacement:	+/- 12 in
Operating Frequency:	0 - 50 Hz

Table 7-2 Nominal Capacities of UNR 6DOF Shake Table

6DOF Shake Table		
	Table Size: Nominal Payload:	9.3 ft x 9.3 ft 20 ton
X-Axis	Maximum Acceleration: Maximum Velocity: Maximum Displacement:	1 g with 40 kip 50 in/sec +/- 12 in
Y-Axis	Maximum Acceleration: Maximum Velocity: Maximum Displacement:	1 g with 95 kip 35 in/sec +/- 3 in
Z-Axis	Maximum Acceleration: Maximum Velocity: Maximum Displacement:	1 g with 125 kip 55 in/sec +/- 4 in

7.4 Potential Shake Table Input Motions

Considering both the characteristics of the motions within the database along with the limitations of the shake tables in the UNR LSSL, a set of floor response motions was generated for potential use in shake table experiments on nonstructural components. The set of motions contains records from a variety of events and building performances whose characteristics are within the limitations of the shake tables. The set of motions summarized in Table 7-3 provides 12 motions at the roof of Building B3. The set offers pairs of motions in the X and Y directions that may be applied biaxially as well as are produced from a variety of earthquakes producing arrange of ductilities in the building. This would facilitate the experimental verification of the performance of nonstructural components located on the roof of buildings experiencing various levels of yielding.

7.5 Filtering

Many of the floor motions in this database contain large displacements which come from the sway of the building. As a result these motions are not suitable for shake table use because they exceed the stroke limitations of the shake tables. In addition to large displacements generated by the sway of the building, low frequency content of the ground motion may also generate significant displacements in the record. These displacements may be filtered out negligible effect on the acceleration records. An example of the effectiveness of filtering the motion is discussed below.

Table 7-3 Proposed Shake Table Motions

No	EQ	Database Indices (Building B3)				Motion Characteristics				Building Response Characteristics				
		Event	Int	Fl	Dir	PGA g	PFA g	PFV in/sec	PFD in	θ_{max} in/in	θ_{avg} in/in	θ_{roof} in/in	Duct	PL
1	Northridge	2	6	4	1	0.454	0.598	32.5	7.2	0.018	0.016	0.009	0.9	1
2	Northridge	2	6	4	2	0.454	0.597	32.6	7.3	0.011	0.009	0.009	0.8	1
3	Kobe	8	5	4	1	0.310	0.513	28.8	8.2	0.015	0.013	0.010	1.0	1
4	Kobe	8	5	4	2	0.311	0.511	28.9	8.7	0.011	0.010	0.010	0.9	1
5	Duzce	3	7	4	1	0.607	0.514	40.7	8.3	0.025	0.023	0.012	1.2	2
6	Duzce	3	7	4	2	0.606	0.512	40.7	8.0	0.014	0.012	0.012	1.1	2
7	Imperial Valley	6	7	4	1	0.616	0.571	31.2	6.4	0.014	0.012	0.012	1.2	2
8	Imperial Valley	6	7	4	2	0.613	0.567	31.0	6.2	0.013	0.012	0.012	1.1	2
9	Landers	11	7	4	1	0.558	0.529	42.3	11.6	0.053	0.050	0.030	3.0	3
10	Landers	11	7	4	2	0.561	0.537	41.0	10.2	0.031	0.030	0.030	2.7	3
11	Cape Menocino	17	10	4	1	1.245	0.943	45.8	7.7	0.031	0.025	0.043	4.3	3
12	Cape Menocino	17	10	4	2	1.242	0.945	45.9	7.5	0.045	0.044	0.043	3.9	3

For the purpose of demonstration, a motion from the roof of building B3 which has a peak acceleration of 0.725 g, peak velocity of 50.8 in/sec, and peak displacement of 22.8 in was selected from the database. This particular roof motion corresponds highly inelastic response, $\mu = 5.1$. The unfiltered motion exceeds the displacement capacity of the shake table. However, by applying a high pass 4^{th} order Butterworth filter (Mathworks, 2004) with a cut-off frequency of 0.25 Hz to the acceleration record; the large displacements due to the sway of the building were reduced from 22.8 in to 9.3 in, as shown in Figure 7-2 and Figure 7-3.

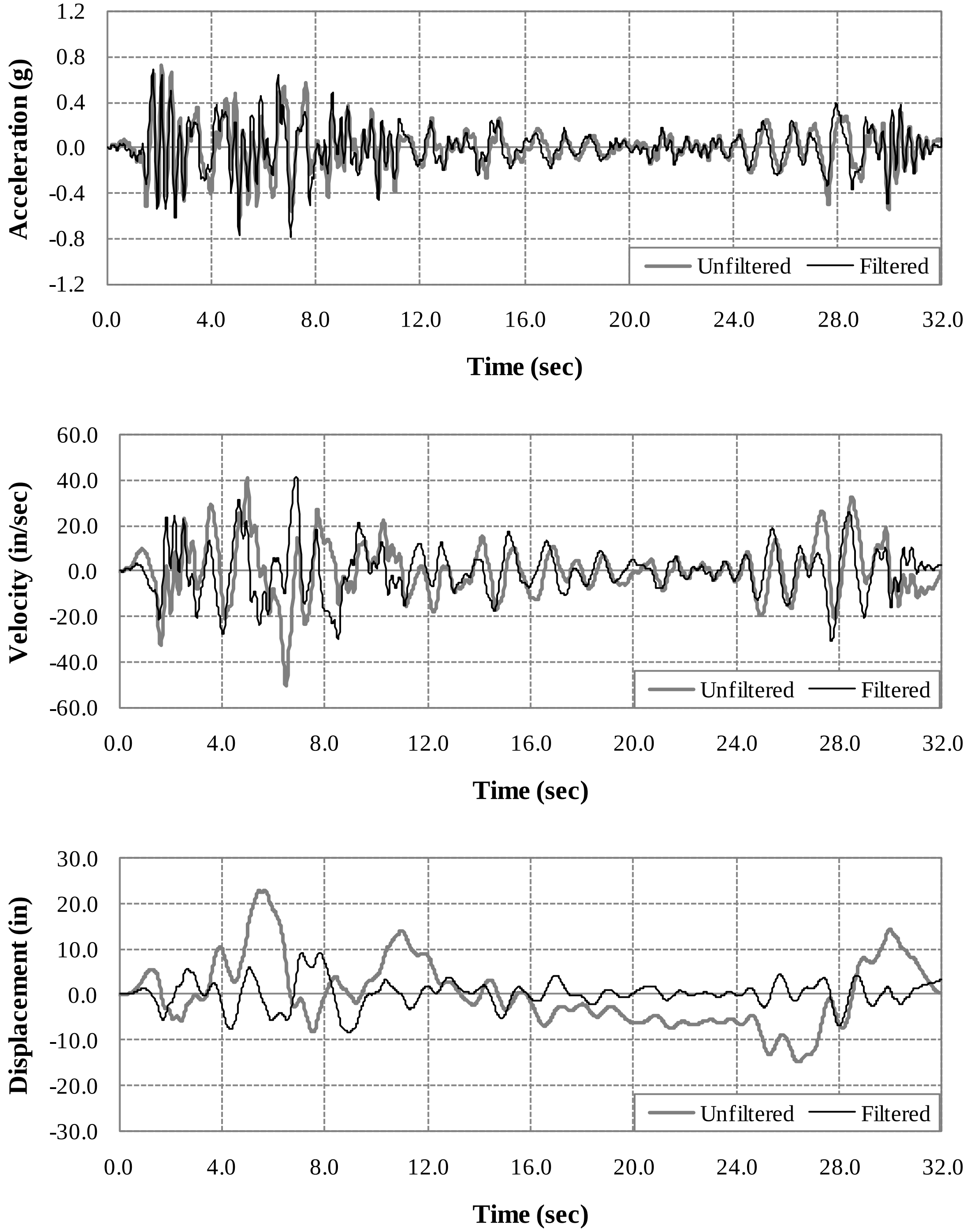

Figure 7-2 Effect of High Pass Filter on Floor Response of Building B3

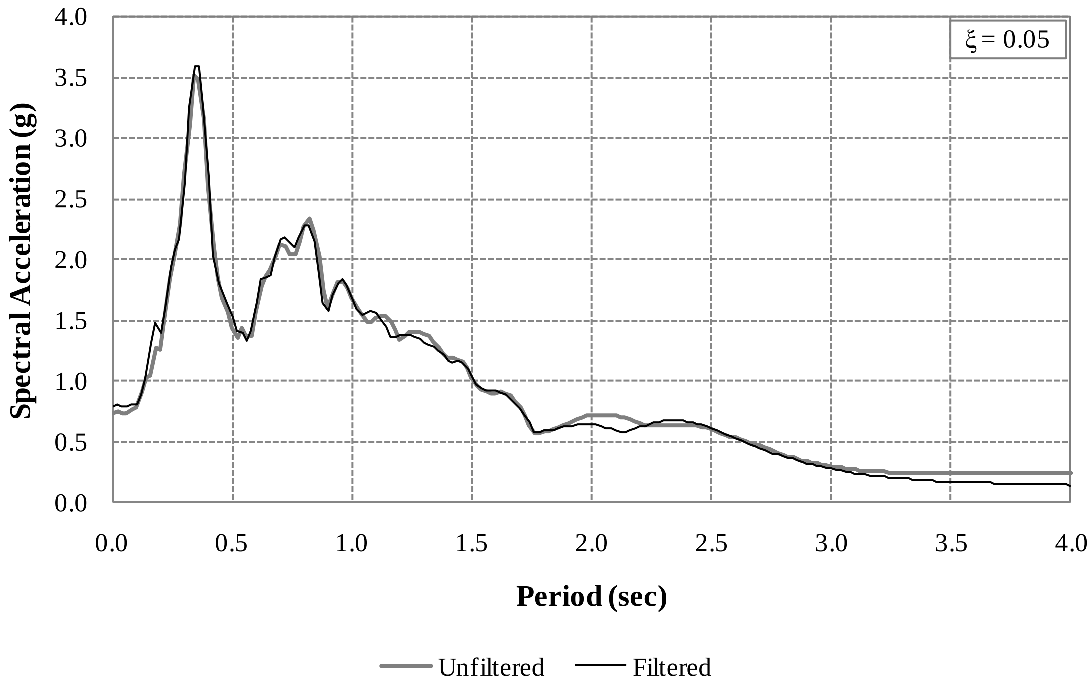

Figure 7-3 Effect of Filtering on Acceleration Spectrum

The critical decision in applying the filter is determining an appropriate cut-off frequency. If the cut-off frequency is too low then the large displacements may be insufficiently reduced. Conversely, if the cut-off frequency is too high then the acceleration record may be significantly altered. In order to quantify the influence of the filter on the acceleration record, the acceleration response spectra of the filtered motion is compared with the unfiltered motion in the period range of interest (0.06 sec to 0.8 sec for most nonstructural components). Figure 7-4 presents the influence of the cut-off frequency on the resulting filtered motion. Due to the uniqueness of each motion, the iterative procedure of selecting an appropriate cut-off frequency must be done for each record individually. If the cut-off frequency required to keep the acceleration spectra equivalent does not provide sufficient reduction in displacement demands then it may not be feasible to use that particular motion for shake table input.

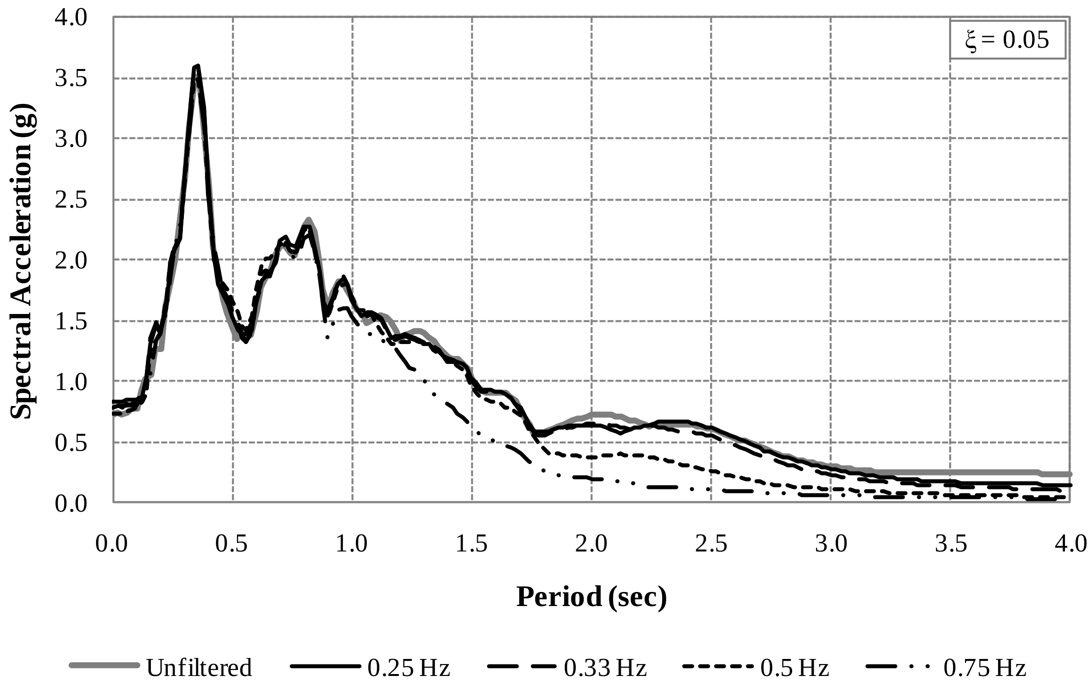

Figure 7-4 Influence of Filter Cut-Off Frequency on Acceleration Spectrum

Overall this chapter has shown that the database of floor response motions does provide representative acceleration records to be used directly or after high-pass filtering as shake table input motions for experimental evaluations of nonstructural seismic performance.

SECTION 8
SUMMARY AND CONCLUSIONS

8.1 Summary

Damage to the nonstructural components of a building interrupts operation and can result in injuries. Recent earthquakes have shown that damage to nonstructural components can occur at lower levels of ground motion intensity than required to inflict structural damage. Due to the dynamic amplification of ground accelerations throughout the height of the building, nonstructural components may be subjected to high accelerations even in low intensity seismic events. Damage to nonstructural components during earthquakes has been shown to be expensive. There is a profound need to improve the understanding of seismic demands on nonstructural components attached to buildings and develop simple design methodologies applicable to ordinary buildings that minimize the damage to nonstructural components.

This study has performed an evaluation of the acceleration demands on nonstructural components in typical steel moment frame structures. A comparison of the current seismic design practice of nonstructural components with the results of this investigation was carried out. The 3-story office building, 3-story hospital, 9-story office building, and 20-story office building structures were subjected to all three components suite of 21 ground motions using the incremental dynamic analysis method. A database of floor response motions was generated and used to identify the effect of variables such as structural period, structural yielding, relative height within the structure, nonstructural component damping ratio, and out-of-plane flexibility of the floor system on acceleration demands on nonstructural components. An empirical multi-linear spectral amplification function which amplifies the ground acceleration response spectrum to achieve a nonstructural component design response spectrum has been proposed. Also the feasibility of using floor response motions from the accumulated database as drive motions for shake table testing of nonstructural components was assessed.

8.2 Observations

Some critical observations were made and are listed below:

- Peak ground accelerations are amplified by both the building and the nonstructural components. Horizontal acceleration amplification occurs due to the lateral flexibility of the building and vertical acceleration amplification occurs due to the out-of-plane flexibility of the floor systems.
- The peak horizontal floor accelerations decrease with increasing structural period.
- The peak horizontal floor accelerations of elastic buildings increase along the height of the structure due to the shape of the dominant dynamic mode.
- The peak horizontal floor accelerations decrease with increasing levels of yielding in the structure due to the added damping and the elongation of period of vibration.
- The component amplification factor, a_p, is found to be a function of the period ratio, relative height within the supporting structure, and level of yielding in the supporting structure.
- The horizontal acceleration response of nonstructural components increases with decreasing nonstructural component damping ratios.
- An increase in the level of yielding in the structure significantly reduces the acceleration response of nonstructural components tuned with the fundamental period of the building. This effect is not observed for nonstructural components tuned with higher modes of the building.
- In comparing the bidirectional horizontal accelerations of this investigation with the unidirectional horizontal accelerations of previous studies, the trends are the same. Therefore, for the purpose of generating horizontal accelerations of nonstructural components, three-dimensional models are not required.

- Amplification of vertical accelerations along the height of the structure is negligible near the columns of the building.
- Significant amplification of the vertical acceleration is present in the middle of floor bays. This amplification is a result of the out-of-plane flexibility of the floor systems.
- The location of the peak vertical acceleration of a multi-bay floor system is dependent on the frequency content of the ground motion.
- The current vertical acceleration required response spectrum underestimates the vertical acceleration in the middle of floor bays.

8.3 Conclusions

The most significant conclusions as related to the objectives of the study are as follows:

- Including the effects of nonlinearity is critical to the development of a database of realistic floor motions.
- The horizontal floor accelerations are dependent on the period, ductility, and relative height of the floor. The vertical accelerations are independent of period, ductility, and relative height, but are dependent on the out-of-plane flexibility of the floor system.
- The current code estimates of floor accelerations are over conservative in many cases because they do not account for the period of the structure. The component amplification factor of $a_p = 2.5$ currently in the code fails to account for the critical parameter of period ratio, T_p/T_1. A direct method of developing a floor response spectrum offers an alternative method of designing nonstructural components.
- The current code limit on component acceleration of 4 times the peak ground acceleration may be unconservative for peak cases.

- The developed database has the potential for providing shake table input motions for the experimental evaluation of nonstructural components in yielding buildings.

It should be noted that the observations and conclusions presented herein are applicable to flexible ductile steel moment frame structures subjected to ground motions with similar characteristics to those presented in Section 3. The recommendations provided within this document are based on these observations and conclusions, thus they may not be valid for situations outside the scope of this investigation.

8.4 Recommendations for Future Investigations

Future work in this area should incorporate the influence of accidental torsion into the three-dimensional models. The models developed in this investigation could be modified to account for this effect. Additional floor systems should be investigated to collect a broader envelope of their effects. A larger set of ground motions of various frequency content and duration should be investigated as well as the influence of near fault ground motions. This investigation focused primarily on moment frame buildings. In order to broaden the assessment of the current code provisions and provide improvements, other lateral load-resisting systems should be included.

SECTION 9
REFERENCES

ACI. (2008). ACI 318-08. *Building Code Requirements for Structural Concrete and Commentary* . American Concrete Institue.

AISC. (2005). Steel Construction Manual. *13th Edition*. American Institute of Steel Construction Inc.

Allen, D., & Pernica, G. (1998). Control of Floor Vibration. *Constructurion Technology Update, No. 22* . NRC Institue for Research in Construction, National Research Council Canada.

Amin, M., Hall, W., Newmark, N., & Kassawara, R. (1971). Earthquake Response of Multiply Connected Light Secondary Systems by Spectrum Methods. *Proc. ASME 1st National Congress on Pressure Vessels and Piping* (pp. 103-129). New York, NY: American Society of Mechanical Engineers (ASME).

Arias, A. (1970). A Measure of Earthquake Intensity. In *Seismic Design for Nuclear Power Plants* (pp. 438–483). Cambridge, MA: MIT Press.

ASCE. (1987). *Seismic Analysis of Safety Related Nuclear Structures and Commentary on Standard for Seismic Analysis of Safety Related Nuclear Structures* . New York, NY: American Society of Civil Engineers.

ASCE. (2005). ASCE 7-05. *Minimum Design Loads for Buildings and Other Structures* . American Society of Civil Engineers.

Barrett, A. (2006). *Dynamic Testing of In-Situ Composite Floors and Evaluation of Vibration Serviceability Using the Finite Element Method.* Ph.D Dissertation, Virginia Polytechnic Institute and State University, Department of Civil Engineering, Blacksburg, Virginia.

Biggs, J., & Roesset, J. (1970). Seismic Analysis of Equipment Mounted on a Massive Structure. In R. Hansen (Ed.), *Seismic Design for Nuclear Power Plants* (pp. 319-343). Cambridge, MA: MIT Press.

Boice, M. (2003). *Study to Improve the Predicted Response of Floor Systems due to Walking.* MS Thesis, Virginia Polytechnic Institute and State University, Department of Civil Engineering, Blacksburg, Virginia.

Bommer, J., & Martinez-Pereira, A. (1999). The Effective Duration of Earthquake Strong Motion. *Journal of Earthquake Engineering , 3* (2), 127-172.

Chen, Y., & Soong, T. (1988). State-of-the-Art-Review: Seismic Resposne of Secondary Systems. *Engineering Structures , 10* (4), 218-228.

Chopra, A. K. (2007). *Dynamics of Structures* (3rd Edition ed.). Upper Saddle River, NJ: Prentice Hall.

CSI. (2007). SAP 2000. *CSI Analysis Reference Manual* . Computers and Structures Inc.

FEMA. (1995). FEMA 267. *Interim Guidelines: Evaluation, Repair, Modification and Design of Welded Steel Moment Frame Structures* . Federal Emergency Management Agency.

FEMA. (1997a). FEMA 267A. *Interim Guidelines Advisory No. 1* . Federal Emergency Management Agency.

FEMA. (1997b). FEMA 273. *NEHRP Guidelines for the Seismic Rehabilitation of Buildings* . Federal Emergency Management Agency.

FEMA. (2000). FEMA 350. *Recommended Seismic Design Criteria for New Steel Moment Frame Buildings* . Federal Emergency Management Agency.

FEMA. (2009). FEMA P695. *Quantification of Building Seismic Performance Factors* . Federal Emergency Management Agency.

FEMA. (2009). FEMA P750. *NEHRP Recommended Seismic Provisions for New Buildings and Other Structures*. Federal Emergency Management Agency.

Foutch, D., & Seung-Yul, Y. (2001). Modeling of Steel Moment Frames for Seismic Loads. *Journal of Constructional Steel Research , 58*, 529-564.

Gupta, A., & Krawinkler, H. (1999). *Seismic Demands for Performance Evaluation of Steel Moment Resisting Frame Structures.* John A. Blume Earthquake Engineering Research Center Report No. 132, Stanford University, Department of Civil Engineering.

ICBO. (1994). 1994 Uniform Building Code. *Structural Engineering Design Provisions , 2* . International Conference of Building Officials.

ICC. (2006). 2006 International Building Code. International Code Council.

ICC. (2006). AC 156. *Acceptance Criteria for Seismic Qualification by Shake Table Testing of Nonstructural Components and Systems* . ICC Evaluation Service, Inc.

Igusa, T., & Der Kiureghian, A. (1985). Dynamic Characterization of Two-Degree-of-Freedom Equipment-Structure Systems. *Journal of Engineering Mechanics , 111*, 1-19.

Igusa, T., & Der Kiureghian, A. (1985). Generation of Floor Response Spectra Including Ocillator-Structure Interaction. *Earthquake Engineering and Structural Dynamics , 13*, 661-676.

Lin, J., & Mahin, S. A. (1985). Seismic Response of Light Subsystems on Inelastic Structures. *Journal of Strucutrla Engineering , 111* (2), 400-417.

Mackie, K., & Stojadinovic, B. (2002). Relation Between Probabilistic Seismic Demand Analysis and Incremental Dynamic Analysis. *7th US National Conference on Earthquake Engineering.* Boston, MA.

Maragakis, E. (2007). NEESR-GC: Simulation of the Seismic Performance of Nonstructural Systems. *Proposal for NEESR-GC project funded by the US National Science Foundation* .

Mathworks Inc. (2004). MATLAB. *The Language of Technical Computing: Version 7* . Natick, MA: Mathworks Inc.

Mazzoni, S., McKenna, F., Scott, M., & Fenves, G. (2009). *Open System for Earthquake Engineering Simulation User Command Language Manual.* Pacific Earthquake Engineering Research Center, University of California, Berkeley.

Medina, R. A., & Krawinkler, H. (2003). *Seismic Demands for Nondeteriorating Strucutres and Their Dependence on Ground Motions.* John A. Blume Earthquake Engineering Center Report No. TR-144, Stanford University, Department of Civil and Environmental Engineering, Stanford, CA.

Medina, R. A., Sankaranarayanan, R., & Kingston, K. M. (2006). Floor response spectra for light components mounted on regular moment-resisting frame structures. *Engineering Structures , 28*, 1927–1940.

Microsoft. (2007). Excel. *Windows Office 2007 .*

Miranda, E., & Taghavi, S. (2009). A Comprehensive Study of Floor Acceleration Demands in Multi-Story Buildings. *ATC & SEI 2009 Conference on Improving the Seismic Performance of Existing Buildings and Other Strucutures*, (pp. 616-626).

Murray, T., Allen, D., & Ungar, E. (1997). Floor Vibrations Due to Human Activity. *AISC Steel Design Guide Series 11 .*

Naeim, F. (1997). *Performance of Extensively Instrumented Buildings During the January 17, 1994 Northridge Earthquake.* Los Angeles, CA: John A. Martin and Associates, Inc.

OpenSees. (2010). *OpenSees*. Retrieved from http://opensees.berkeley.edu

PEER. (2006). *PEER NGA Database*. Retrieved from http://peer.berkeley.edu/nga/

Pekcan, G., Itani, A., & Staehlin, W. (2003). Nonstructural System Response to Vertical Excitation and Implications for Seismic Design and Qualification. *ATC-29-2 Seminar on Seismic Design, Performance, and Retrofit of Nonstructural Components inCritical Facilities.* Los Angeles, CA: Applied Technology Council.

Reinhorn, A. M., Ryu, K.-P., & Maddaloni, G. (2010). *Modeling and Seismic Evaluation of Nonstructural Components: Testing Frame for Experimental Evaluation of Suspended Ceiling Systems.* Technical Report MCEER-10-0004.

Reitherman, R., & Sabol, T. (1995). Northridge Earthquake of January 17, 1994: Reconnaissance Report Nonstructural Damage. *Earthquake Spectra , 11*, 453-514.

Rodriguez, M. E., Restrepo, J. I., & Carr, A. J. (2002). Earthquake-Induced Floor Horizontal Accelerations in Buildings. *Earthquake Engineering and Structural Dynamics , 31*, 693-718.

Singh, A., & Ang, A.-S. (1974). Stochastic Prediction of Maximum Seismic Resposne of Light Secondary Systems. *Nuclear Engineering Design , 29*, 218-230.

Taghavi, S., & Miranda, E. (2006). *Probabilistic Seismic Assessment of Floor Acceleration Demands in Multi-Story Buildings.* John A. Blume Earthquake Engineering Center Report No. 162, Stanford University, Department of Civil and Environmental Engineering, Stanford, CA.

U.S. Nuclear Regulatory Commission. (1978). U.S. NRC Regulatory Guide 1.122. *Development of Floor Design Spectra for Seismic Design of Floor-Supported Equipment or Components* .

USGS. (2002). *2002 Seismic Design Maps*. Retrieved from United States Geologic Survey: http://earthquake.usgs.gov/hazards/designmaps/

Vamvatsikos, D., & Cornell, C. (2004). Applied Incremental Dynamic Analysis. *Earthquake Spectra , 20* (2), 523-553.

Vamvatsikos, D., & Cornell, C. (2002). Incremental Dynamic Analysis. *Earthquake Engineering Structural Dynamics* .

Villaverde, R. (2004). Seismic Analysis and Design of Nonstrucutral Elements. In Y. Bozorgnia, & V. V. Bertero (Eds.), *Earthquake Engineering: From Engineering Seismology to Performance-Based Engineering.* Bocca Raton, FL: CRC Press LLC.

Villaverde, R. (1997). Seismic Design of Secondary Structures: State of the Art. *Journal of Structural Engineering , 123* (8), 1011-1019.

Villaverde, R. (1987). Simplified Approach for the Seismic Analysis of Equipment Attached to Elastoplastic Structures. *Nuclear Engineering and Design , 103*, 267-279.

MCEER Technical Reports

MCEER publishes technical reports on a variety of subjects written by authors funded through MCEER. These reports are available from both MCEER Publications and the National Technical Information Service (NTIS). Requests for reports should be directed to MCEER Publications, MCEER, University at Buffalo, State University of New York, 133A Ketter Hall, Buffalo, New York 14260. Reports can also be requested through NTIS, P.O. Box 1425, Springfield, Virginia 22151. NTIS accession numbers are shown in parenthesis, if available.

NCEER-87-0001 "First-Year Program in Research, Education and Technology Transfer," 3/5/87, (PB88-134275, A04, MF-A01).

NCEER-87-0002 "Experimental Evaluation of Instantaneous Optimal Algorithms for Structural Control," by R.C. Lin, T.T. Soong and A.M. Reinhorn, 4/20/87, (PB88-134341, A04, MF-A01).

NCEER-87-0003 "Experimentation Using the Earthquake Simulation Facilities at University at Buffalo," by A.M. Reinhorn and R.L. Ketter, not available.

NCEER-87-0004 "The System Characteristics and Performance of a Shaking Table," by J.S. Hwang, K.C. Chang and G.C. Lee, 6/1/87, (PB88-134259, A03, MF-A01). This report is available only through NTIS (see address given above).

NCEER-87-0005 "A Finite Element Formulation for Nonlinear Viscoplastic Material Using a Q Model," by O. Gyebi and G. Dasgupta, 11/2/87, (PB88-213764, A08, MF-A01).

NCEER-87-0006 "Symbolic Manipulation Program (SMP) - Algebraic Codes for Two and Three Dimensional Finite Element Formulations," by X. Lee and G. Dasgupta, 11/9/87, (PB88-218522, A05, MF-A01).

NCEER-87-0007 "Instantaneous Optimal Control Laws for Tall Buildings Under Seismic Excitations," by J.N. Yang, A. Akbarpour and P. Ghaemmaghami, 6/10/87, (PB88-134333, A06, MF-A01). This report is only available through NTIS (see address given above).

NCEER-87-0008 "IDARC: Inelastic Damage Analysis of Reinforced Concrete Frame - Shear-Wall Structures," by Y.J. Park, A.M. Reinhorn and S.K. Kunnath, 7/20/87, (PB88-134325, A09, MF-A01). This report is only available through NTIS (see address given above).

NCEER-87-0009 "Liquefaction Potential for New York State: A Preliminary Report on Sites in Manhattan and Buffalo," by M. Budhu, V. Vijayakumar, R.F. Giese and L. Baumgras, 8/31/87, (PB88-163704, A03, MF-A01). This report is available only through NTIS (see address given above).

NCEER-87-0010 "Vertical and Torsional Vibration of Foundations in Inhomogeneous Media," by A.S. Veletsos and K.W. Dotson, 6/1/87, (PB88-134291, A03, MF-A01). This report is only available through NTIS (see address given above).

NCEER-87-0011 "Seismic Probabilistic Risk Assessment and Seismic Margins Studies for Nuclear Power Plants," by Howard H.M. Hwang, 6/15/87, (PB88-134267, A03, MF-A01). This report is only available through NTIS (see address given above).

NCEER-87-0012 "Parametric Studies of Frequency Response of Secondary Systems Under Ground-Acceleration Excitations," by Y. Yong and Y.K. Lin, 6/10/87, (PB88-134309, A03, MF-A01). This report is only available through NTIS (see address given above).

NCEER-87-0013 "Frequency Response of Secondary Systems Under Seismic Excitation," by J.A. HoLung, J. Cai and Y.K. Lin, 7/31/87, (PB88-134317, A05, MF-A01). This report is only available through NTIS (see address given above).

NCEER-87-0014 "Modelling Earthquake Ground Motions in Seismically Active Regions Using Parametric Time Series Methods," by G.W. Ellis and A.S. Cakmak, 8/25/87, (PB88-134283, A08, MF-A01). This report is only available through NTIS (see address given above).

NCEER-87-0015 "Detection and Assessment of Seismic Structural Damage," by E. DiPasquale and A.S. Cakmak, 8/25/87, (PB88-163712, A05, MF-A01). This report is only available through NTIS (see address given above).

NCEER-87-0016 "Pipeline Experiment at Parkfield, California," by J. Isenberg and E. Richardson, 9/15/87, (PB88-163720, A03, MF-A01). This report is available only through NTIS (see address given above).

NCEER-87-0017 "Digital Simulation of Seismic Ground Motion," by M. Shinozuka, G. Deodatis and T. Harada, 8/31/87, (PB88-155197, A04, MF-A01). This report is available only through NTIS (see address given above).

NCEER-87-0018 "Practical Considerations for Structural Control: System Uncertainty, System Time Delay and Truncation of Small Control Forces," J.N. Yang and A. Akbarpour, 8/10/87, (PB88-163738, A08, MF-A01). This report is only available through NTIS (see address given above).

NCEER-87-0019 "Modal Analysis of Nonclassically Damped Structural Systems Using Canonical Transformation," by J.N. Yang, S. Sarkani and F.X. Long, 9/27/87, (PB88-187851, A04, MF-A01).

NCEER-87-0020 "A Nonstationary Solution in Random Vibration Theory," by J.R. Red-Horse and P.D. Spanos, 11/3/87, (PB88-163746, A03, MF-A01).

NCEER-87-0021 "Horizontal Impedances for Radially Inhomogeneous Viscoelastic Soil Layers," by A.S. Veletsos and K.W. Dotson, 10/15/87, (PB88-150859, A04, MF-A01).

NCEER-87-0022 "Seismic Damage Assessment of Reinforced Concrete Members," by Y.S. Chung, C. Meyer and M. Shinozuka, 10/9/87, (PB88-150867, A05, MF-A01). This report is available only through NTIS (see address given above).

NCEER-87-0023 "Active Structural Control in Civil Engineering," by T.T. Soong, 11/11/87, (PB88-187778, A03, MF-A01).

NCEER-87-0024 "Vertical and Torsional Impedances for Radially Inhomogeneous Viscoelastic Soil Layers," by K.W. Dotson and A.S. Veletsos, 12/87, (PB88-187786, A03, MF-A01).

NCEER-87-0025 "Proceedings from the Symposium on Seismic Hazards, Ground Motions, Soil-Liquefaction and Engineering Practice in Eastern North America," October 20-22, 1987, edited by K.H. Jacob, 12/87, (PB88-188115, A23, MF-A01). This report is available only through NTIS (see address given above).

NCEER-87-0026 "Report on the Whittier-Narrows, California, Earthquake of October 1, 1987," by J. Pantelic and A. Reinhorn, 11/87, (PB88-187752, A03, MF-A01). This report is available only through NTIS (see address given above).

NCEER-87-0027 "Design of a Modular Program for Transient Nonlinear Analysis of Large 3-D Building Structures," by S. Srivastav and J.F. Abel, 12/30/87, (PB88-187950, A05, MF-A01). This report is only available through NTIS (see address given above).

NCEER-87-0028 "Second-Year Program in Research, Education and Technology Transfer," 3/8/88, (PB88-219480, A04, MF-A01).

NCEER-88-0001 "Workshop on Seismic Computer Analysis and Design of Buildings With Interactive Graphics," by W. McGuire, J.F. Abel and C.H. Conley, 1/18/88, (PB88-187760, A03, MF-A01). This report is only available through NTIS (see address given above).

NCEER-88-0002 "Optimal Control of Nonlinear Flexible Structures," by J.N. Yang, F.X. Long and D. Wong, 1/22/88, (PB88-213772, A06, MF-A01).

NCEER-88-0003 "Substructuring Techniques in the Time Domain for Primary-Secondary Structural Systems," by G.D. Manolis and G. Juhn, 2/10/88, (PB88-213780, A04, MF-A01).

NCEER-88-0004 "Iterative Seismic Analysis of Primary-Secondary Systems," by A. Singhal, L.D. Lutes and P.D. Spanos, 2/23/88, (PB88-213798, A04, MF-A01).

NCEER-88-0005 "Stochastic Finite Element Expansion for Random Media," by P.D. Spanos and R. Ghanem, 3/14/88, (PB88-213806, A03, MF-A01).

NCEER-88-0006 "Combining Structural Optimization and Structural Control," by F.Y. Cheng and C.P. Pantelides, 1/10/88, (PB88-213814, A05, MF-A01).

NCEER-88-0007 "Seismic Performance Assessment of Code-Designed Structures," by H.H-M. Hwang, J-W. Jaw and H-J. Shau, 3/20/88, (PB88-219423, A04, MF-A01). This report is only available through NTIS (see address given above).

NCEER-88-0008 "Reliability Analysis of Code-Designed Structures Under Natural Hazards," by H.H-M. Hwang, H. Ushiba and M. Shinozuka, 2/29/88, (PB88-229471, A07, MF-A01). This report is only available through NTIS (see address given above).

NCEER-88-0009 "Seismic Fragility Analysis of Shear Wall Structures," by J-W Jaw and H.H-M. Hwang, 4/30/88, (PB89-102867, A04, MF-A01).

NCEER-88-0010 "Base Isolation of a Multi-Story Building Under a Harmonic Ground Motion - A Comparison of Performances of Various Systems," by F-G Fan, G. Ahmadi and I.G. Tadjbakhsh, 5/18/88, (PB89-122238, A06, MF-A01). This report is only available through NTIS (see address given above).

NCEER-88-0011 "Seismic Floor Response Spectra for a Combined System by Green's Functions," by F.M. Lavelle, L.A. Bergman and P.D. Spanos, 5/1/88, (PB89-102875, A03, MF-A01).

NCEER-88-0012 "A New Solution Technique for Randomly Excited Hysteretic Structures," by G.Q. Cai and Y.K. Lin, 5/16/88, (PB89-102883, A03, MF-A01).

NCEER-88-0013 "A Study of Radiation Damping and Soil-Structure Interaction Effects in the Centrifuge," by K. Weissman, supervised by J.H. Prevost, 5/24/88, (PB89-144703, A06, MF-A01).

NCEER-88-0014 "Parameter Identification and Implementation of a Kinematic Plasticity Model for Frictional Soils," by J.H. Prevost and D.V. Griffiths, not available.

NCEER-88-0015 "Two- and Three- Dimensional Dynamic Finite Element Analyses of the Long Valley Dam," by D.V. Griffiths and J.H. Prevost, 6/17/88, (PB89-144711, A04, MF-A01).

NCEER-88-0016 "Damage Assessment of Reinforced Concrete Structures in Eastern United States," by A.M. Reinhorn, M.J. Seidel, S.K. Kunnath and Y.J. Park, 6/15/88, (PB89-122220, A04, MF-A01). This report is only available through NTIS (see address given above).

NCEER-88-0017 "Dynamic Compliance of Vertically Loaded Strip Foundations in Multilayered Viscoelastic Soils," by S. Ahmad and A.S.M. Israil, 6/17/88, (PB89-102891, A04, MF-A01).

NCEER-88-0018 "An Experimental Study of Seismic Structural Response With Added Viscoelastic Dampers," by R.C. Lin, Z. Liang, T.T. Soong and R.H. Zhang, 6/30/88, (PB89-122212, A05, MF-A01). This report is available only through NTIS (see address given above).

NCEER-88-0019 "Experimental Investigation of Primary - Secondary System Interaction," by G.D. Manolis, G. Juhn and A.M. Reinhorn, 5/27/88, (PB89-122204, A04, MF-A01).

NCEER-88-0020 "A Response Spectrum Approach For Analysis of Nonclassically Damped Structures," by J.N. Yang, S. Sarkani and F.X. Long, 4/22/88, (PB89-102909, A04, MF-A01).

NCEER-88-0021 "Seismic Interaction of Structures and Soils: Stochastic Approach," by A.S. Veletsos and A.M. Prasad, 7/21/88, (PB89-122196, A04, MF-A01). This report is only available through NTIS (see address given above).

NCEER-88-0022 "Identification of the Serviceability Limit State and Detection of Seismic Structural Damage," by E. DiPasquale and A.S. Cakmak, 6/15/88, (PB89-122188, A05, MF-A01). This report is available only through NTIS (see address given above).

NCEER-88-0023 "Multi-Hazard Risk Analysis: Case of a Simple Offshore Structure," by B.K. Bhartia and E.H. Vanmarcke, 7/21/88, (PB89-145213, A05, MF-A01).

NCEER-88-0024 "Automated Seismic Design of Reinforced Concrete Buildings," by Y.S. Chung, C. Meyer and M. Shinozuka, 7/5/88, (PB89-122170, A06, MF-A01). This report is available only through NTIS (see address given above).

NCEER-88-0025 "Experimental Study of Active Control of MDOF Structures Under Seismic Excitations," by L.L. Chung, R.C. Lin, T.T. Soong and A.M. Reinhorn, 7/10/88, (PB89-122600, A04, MF-A01).

NCEER-88-0026 "Earthquake Simulation Tests of a Low-Rise Metal Structure," by J.S. Hwang, K.C. Chang, G.C. Lee and R.L. Ketter, 8/1/88, (PB89-102917, A04, MF-A01).

NCEER-88-0027 "Systems Study of Urban Response and Reconstruction Due to Catastrophic Earthquakes," by F. Kozin and H.K. Zhou, 9/22/88, (PB90-162348, A04, MF-A01).

NCEER-88-0028 "Seismic Fragility Analysis of Plane Frame Structures," by H.H-M. Hwang and Y.K. Low, 7/31/88, (PB89-131445, A06, MF-A01).

NCEER-88-0029 "Response Analysis of Stochastic Structures," by A. Kardara, C. Bucher and M. Shinozuka, 9/22/88, (PB89-174429, A04, MF-A01).

NCEER-88-0030 "Nonnormal Accelerations Due to Yielding in a Primary Structure," by D.C.K. Chen and L.D. Lutes, 9/19/88, (PB89-131437, A04, MF-A01).

NCEER-88-0031 "Design Approaches for Soil-Structure Interaction," by A.S. Veletsos, A.M. Prasad and Y. Tang, 12/30/88, (PB89-174437, A03, MF-A01). This report is available only through NTIS (see address given above).

NCEER-88-0032 "A Re-evaluation of Design Spectra for Seismic Damage Control," by C.J. Turkstra and A.G. Tallin, 11/7/88, (PB89-145221, A05, MF-A01).

NCEER-88-0033 "The Behavior and Design of Noncontact Lap Splices Subjected to Repeated Inelastic Tensile Loading," by V.E. Sagan, P. Gergely and R.N. White, 12/8/88, (PB89-163737, A08, MF-A01).

NCEER-88-0034 "Seismic Response of Pile Foundations," by S.M. Mamoon, P.K. Banerjee and S. Ahmad, 11/1/88, (PB89-145239, A04, MF-A01).

NCEER-88-0035 "Modeling of R/C Building Structures With Flexible Floor Diaphragms (IDARC2)," by A.M. Reinhorn, S.K. Kunnath and N. Panahshahi, 9/7/88, (PB89-207153, A07, MF-A01).

NCEER-88-0036 "Solution of the Dam-Reservoir Interaction Problem Using a Combination of FEM, BEM with Particular Integrals, Modal Analysis, and Substructuring," by C-S. Tsai, G.C. Lee and R.L. Ketter, 12/31/88, (PB89-207146, A04, MF-A01).

NCEER-88-0037 "Optimal Placement of Actuators for Structural Control," by F.Y. Cheng and C.P. Pantelides, 8/15/88, (PB89-162846, A05, MF-A01).

NCEER-88-0038 "Teflon Bearings in Aseismic Base Isolation: Experimental Studies and Mathematical Modeling," by A. Mokha, M.C. Constantinou and A.M. Reinhorn, 12/5/88, (PB89-218457, A10, MF-A01). This report is available only through NTIS (see address given above).

NCEER-88-0039 "Seismic Behavior of Flat Slab High-Rise Buildings in the New York City Area," by P. Weidlinger and M. Ettouney, 10/15/88, (PB90-145681, A04, MF-A01).

NCEER-88-0040 "Evaluation of the Earthquake Resistance of Existing Buildings in New York City," by P. Weidlinger and M. Ettouney, 10/15/88, not available.

NCEER-88-0041 "Small-Scale Modeling Techniques for Reinforced Concrete Structures Subjected to Seismic Loads," by W. Kim, A. El-Attar and R.N. White, 11/22/88, (PB89-189625, A05, MF-A01).

NCEER-88-0042 "Modeling Strong Ground Motion from Multiple Event Earthquakes," by G.W. Ellis and A.S. Cakmak, 10/15/88, (PB89-174445, A03, MF-A01).

NCEER-88-0043 "Nonstationary Models of Seismic Ground Acceleration," by M. Grigoriu, S.E. Ruiz and E. Rosenblueth, 7/15/88, (PB89-189617, A04, MF-A01).

NCEER-88-0044 "SARCF User's Guide: Seismic Analysis of Reinforced Concrete Frames," by Y.S. Chung, C. Meyer and M. Shinozuka, 11/9/88, (PB89-174452, A08, MF-A01).

NCEER-88-0045 "First Expert Panel Meeting on Disaster Research and Planning," edited by J. Pantelic and J. Stoyle, 9/15/88, (PB89-174460, A05, MF-A01).

NCEER-88-0046 "Preliminary Studies of the Effect of Degrading Infill Walls on the Nonlinear Seismic Response of Steel Frames," by C.Z. Chrysostomou, P. Gergely and J.F. Abel, 12/19/88, (PB89-208383, A05, MF-A01).

NCEER-88-0047 "Reinforced Concrete Frame Component Testing Facility - Design, Construction, Instrumentation and Operation," by S.P. Pessiki, C. Conley, T. Bond, P. Gergely and R.N. White, 12/16/88, (PB89-174478, A04, MF-A01).

NCEER-89-0001 "Effects of Protective Cushion and Soil Compliancy on the Response of Equipment Within a Seismically Excited Building," by J.A. HoLung, 2/16/89, (PB89-207179, A04, MF-A01).

NCEER-89-0002 "Statistical Evaluation of Response Modification Factors for Reinforced Concrete Structures," by H.H-M. Hwang and J-W. Jaw, 2/17/89, (PB89-207187, A05, MF-A01).

NCEER-89-0003 "Hysteretic Columns Under Random Excitation," by G-Q. Cai and Y.K. Lin, 1/9/89, (PB89-196513, A03, MF-A01).

NCEER-89-0004 "Experimental Study of `Elephant Foot Bulge' Instability of Thin-Walled Metal Tanks," by Z-H. Jia and R.L. Ketter, 2/22/89, (PB89-207195, A03, MF-A01).

NCEER-89-0005 "Experiment on Performance of Buried Pipelines Across San Andreas Fault," by J. Isenberg, E. Richardson and T.D. O'Rourke, 3/10/89, (PB89-218440, A04, MF-A01). This report is available only through NTIS (see address given above).

NCEER-89-0006 "A Knowledge-Based Approach to Structural Design of Earthquake-Resistant Buildings," by M. Subramani, P. Gergely, C.H. Conley, J.F. Abel and A.H. Zaghw, 1/15/89, (PB89-218465, A06, MF-A01).

NCEER-89-0007 "Liquefaction Hazards and Their Effects on Buried Pipelines," by T.D. O'Rourke and P.A. Lane, 2/1/89, (PB89-218481, A09, MF-A01).

NCEER-89-0008 "Fundamentals of System Identification in Structural Dynamics," by H. Imai, C-B. Yun, O. Maruyama and M. Shinozuka, 1/26/89, (PB89-207211, A04, MF-A01).

NCEER-89-0009 "Effects of the 1985 Michoacan Earthquake on Water Systems and Other Buried Lifelines in Mexico," by A.G. Ayala and M.J. O'Rourke, 3/8/89, (PB89-207229, A06, MF-A01).

NCEER-89-R010 "NCEER Bibliography of Earthquake Education Materials," by K.E.K. Ross, Second Revision, 9/1/89, (PB90-125352, A05, MF-A01). This report is replaced by NCEER-92-0018.

NCEER-89-0011 "Inelastic Three-Dimensional Response Analysis of Reinforced Concrete Building Structures (IDARC-3D), Part I - Modeling," by S.K. Kunnath and A.M. Reinhorn, 4/17/89, (PB90-114612, A07, MF-A01). This report is available only through NTIS (see address given above).

NCEER-89-0012 "Recommended Modifications to ATC-14," by C.D. Poland and J.O. Malley, 4/12/89, (PB90-108648, A15, MF-A01).

NCEER-89-0013 "Repair and Strengthening of Beam-to-Column Connections Subjected to Earthquake Loading," by M. Corazao and A.J. Durrani, 2/28/89, (PB90-109885, A06, MF-A01).

NCEER-89-0014 "Program EXKAL2 for Identification of Structural Dynamic Systems," by O. Maruyama, C-B. Yun, M. Hoshiya and M. Shinozuka, 5/19/89, (PB90-109877, A09, MF-A01).

NCEER-89-0015 "Response of Frames With Bolted Semi-Rigid Connections, Part I - Experimental Study and Analytical Predictions," by P.J. DiCorso, A.M. Reinhorn, J.R. Dickerson, J.B. Radziminski and W.L. Harper, 6/1/89, not available.

NCEER-89-0016 "ARMA Monte Carlo Simulation in Probabilistic Structural Analysis," by P.D. Spanos and M.P. Mignolet, 7/10/89, (PB90-109893, A03, MF-A01).

NCEER-89-P017 "Preliminary Proceedings from the Conference on Disaster Preparedness - The Place of Earthquake Education in Our Schools," Edited by K.E.K. Ross, 6/23/89, (PB90-108606, A03, MF-A01).

NCEER-89-0017 "Proceedings from the Conference on Disaster Preparedness - The Place of Earthquake Education in Our Schools," Edited by K.E.K. Ross, 12/31/89, (PB90-207895, A012, MF-A02). This report is available only through NTIS (see address given above).

NCEER-89-0018 "Multidimensional Models of Hysteretic Material Behavior for Vibration Analysis of Shape Memory Energy Absorbing Devices, by E.J. Graesser and F.A. Cozzarelli, 6/7/89, (PB90-164146, A04, MF-A01).

NCEER-89-0019 "Nonlinear Dynamic Analysis of Three-Dimensional Base Isolated Structures (3D-BASIS)," by S. Nagarajaiah, A.M. Reinhorn and M.C. Constantinou, 8/3/89, (PB90-161936, A06, MF-A01). This report has been replaced by NCEER-93-0011.

NCEER-89-0020 "Structural Control Considering Time-Rate of Control Forces and Control Rate Constraints," by F.Y. Cheng and C.P. Pantelides, 8/3/89, (PB90-120445, A04, MF-A01).

NCEER-89-0021 "Subsurface Conditions of Memphis and Shelby County," by K.W. Ng, T-S. Chang and H-H.M. Hwang, 7/26/89, (PB90-120437, A03, MF-A01).

NCEER-89-0022 "Seismic Wave Propagation Effects on Straight Jointed Buried Pipelines," by K. Elhmadi and M.J. O'Rourke, 8/24/89, (PB90-162322, A10, MF-A02).

NCEER-89-0023 "Workshop on Serviceability Analysis of Water Delivery Systems," edited by M. Grigoriu, 3/6/89, (PB90-127424, A03, MF-A01).

NCEER-89-0024 "Shaking Table Study of a 1/5 Scale Steel Frame Composed of Tapered Members," by K.C. Chang, J.S. Hwang and G.C. Lee, 9/18/89, (PB90-160169, A04, MF-A01).

NCEER-89-0025 "DYNA1D: A Computer Program for Nonlinear Seismic Site Response Analysis - Technical Documentation," by Jean H. Prevost, 9/14/89, (PB90-161944, A07, MF-A01). This report is available only through NTIS (see address given above).

NCEER-89-0026 "1:4 Scale Model Studies of Active Tendon Systems and Active Mass Dampers for Aseismic Protection," by A.M. Reinhorn, T.T. Soong, R.C. Lin, Y.P. Yang, Y. Fukao, H. Abe and M. Nakai, 9/15/89, (PB90-173246, A10, MF-A02). This report is available only through NTIS (see address given above).

NCEER-89-0027 "Scattering of Waves by Inclusions in a Nonhomogeneous Elastic Half Space Solved by Boundary Element Methods," by P.K. Hadley, A. Askar and A.S. Cakmak, 6/15/89, (PB90-145699, A07, MF-A01).

NCEER-89-0028 "Statistical Evaluation of Deflection Amplification Factors for Reinforced Concrete Structures," by H.H.M. Hwang, J-W. Jaw and A.L. Ch'ng, 8/31/89, (PB90-164633, A05, MF-A01).

NCEER-89-0029 "Bedrock Accelerations in Memphis Area Due to Large New Madrid Earthquakes," by H.H.M. Hwang, C.H.S. Chen and G. Yu, 11/7/89, (PB90-162330, A04, MF-A01).

NCEER-89-0030 "Seismic Behavior and Response Sensitivity of Secondary Structural Systems," by Y.Q. Chen and T.T. Soong, 10/23/89, (PB90-164658, A08, MF-A01).

NCEER-89-0031 "Random Vibration and Reliability Analysis of Primary-Secondary Structural Systems," by Y. Ibrahim, M. Grigoriu and T.T. Soong, 11/10/89, (PB90-161951, A04, MF-A01).

NCEER-89-0032 "Proceedings from the Second U.S. - Japan Workshop on Liquefaction, Large Ground Deformation and Their Effects on Lifelines, September 26-29, 1989," Edited by T.D. O'Rourke and M. Hamada, 12/1/89, (PB90-209388, A22, MF-A03).

NCEER-89-0033 "Deterministic Model for Seismic Damage Evaluation of Reinforced Concrete Structures," by J.M. Bracci, A.M. Reinhorn, J.B. Mander and S.K. Kunnath, 9/27/89, (PB91-108803, A06, MF-A01).

NCEER-89-0034 "On the Relation Between Local and Global Damage Indices," by E. DiPasquale and A.S. Cakmak, 8/15/89, (PB90-173865, A05, MF-A01).

NCEER-89-0035 "Cyclic Undrained Behavior of Nonplastic and Low Plasticity Silts," by A.J. Walker and H.E. Stewart, 7/26/89, (PB90-183518, A10, MF-A01).

NCEER-89-0036 "Liquefaction Potential of Surficial Deposits in the City of Buffalo, New York," by M. Budhu, R. Giese and L. Baumgrass, 1/17/89, (PB90-208455, A04, MF-A01).

NCEER-89-0037 "A Deterministic Assessment of Effects of Ground Motion Incoherence," by A.S. Veletsos and Y. Tang, 7/15/89, (PB90-164294, A03, MF-A01).

NCEER-89-0038 "Workshop on Ground Motion Parameters for Seismic Hazard Mapping," July 17-18, 1989, edited by R.V. Whitman, 12/1/89, (PB90-173923, A04, MF-A01).

NCEER-89-0039 "Seismic Effects on Elevated Transit Lines of the New York City Transit Authority," by C.J. Costantino, C.A. Miller and E. Heymsfield, 12/26/89, (PB90-207887, A06, MF-A01).

NCEER-89-0040 "Centrifugal Modeling of Dynamic Soil-Structure Interaction," by K. Weissman, Supervised by J.H. Prevost, 5/10/89, (PB90-207879, A07, MF-A01).

NCEER-89-0041 "Linearized Identification of Buildings With Cores for Seismic Vulnerability Assessment," by I-K. Ho and A.E. Aktan, 11/1/89, (PB90-251943, A07, MF-A01).

NCEER-90-0001 "Geotechnical and Lifeline Aspects of the October 17, 1989 Loma Prieta Earthquake in San Francisco," by T.D. O'Rourke, H.E. Stewart, F.T. Blackburn and T.S. Dickerman, 1/90, (PB90-208596, A05, MF-A01).

NCEER-90-0002 "Nonnormal Secondary Response Due to Yielding in a Primary Structure," by D.C.K. Chen and L.D. Lutes, 2/28/90, (PB90-251976, A07, MF-A01).

NCEER-90-0003 "Earthquake Education Materials for Grades K-12," by K.E.K. Ross, 4/16/90, (PB91-251984, A05, MF-A05). This report has been replaced by NCEER-92-0018.

NCEER-90-0004 "Catalog of Strong Motion Stations in Eastern North America," by R.W. Busby, 4/3/90, (PB90-251984, A05, MF-A01).

NCEER-90-0005 "NCEER Strong-Motion Data Base: A User Manual for the GeoBase Release (Version 1.0 for the Sun3)," by P. Friberg and K. Jacob, 3/31/90 (PB90-258062, A04, MF-A01).

NCEER-90-0006 "Seismic Hazard Along a Crude Oil Pipeline in the Event of an 1811-1812 Type New Madrid Earthquake," by H.H.M. Hwang and C-H.S. Chen, 4/16/90, (PB90-258054, A04, MF-A01).

NCEER-90-0007 "Site-Specific Response Spectra for Memphis Sheahan Pumping Station," by H.H.M. Hwang and C.S. Lee, 5/15/90, (PB91-108811, A05, MF-A01).

NCEER-90-0008 "Pilot Study on Seismic Vulnerability of Crude Oil Transmission Systems," by T. Ariman, R. Dobry, M. Grigoriu, F. Kozin, M. O'Rourke, T. O'Rourke and M. Shinozuka, 5/25/90, (PB91-108837, A06, MF-A01).

NCEER-90-0009 "A Program to Generate Site Dependent Time Histories: EQGEN," by G.W. Ellis, M. Srinivasan and A.S. Cakmak, 1/30/90, (PB91-108829, A04, MF-A01).

NCEER-90-0010 "Active Isolation for Seismic Protection of Operating Rooms," by M.E. Talbott, Supervised by M. Shinozuka, 6/8/9, (PB91-110205, A05, MF-A01).

NCEER-90-0011 "Program LINEARID for Identification of Linear Structural Dynamic Systems," by C-B. Yun and M. Shinozuka, 6/25/90, (PB91-110312, A08, MF-A01).

NCEER-90-0012 "Two-Dimensional Two-Phase Elasto-Plastic Seismic Response of Earth Dams," by A.N. Yiagos, Supervised by J.H. Prevost, 6/20/90, (PB91-110197, A13, MF-A02).

NCEER-90-0013 "Secondary Systems in Base-Isolated Structures: Experimental Investigation, Stochastic Response and Stochastic Sensitivity," by G.D. Manolis, G. Juhn, M.C. Constantinou and A.M. Reinhorn, 7/1/90, (PB91-110320, A08, MF-A01).

NCEER-90-0014 "Seismic Behavior of Lightly-Reinforced Concrete Column and Beam-Column Joint Details," by S.P. Pessiki, C.H. Conley, P. Gergely and R.N. White, 8/22/90, (PB91-108795, A11, MF-A02).

NCEER-90-0015 "Two Hybrid Control Systems for Building Structures Under Strong Earthquakes," by J.N. Yang and A. Danielians, 6/29/90, (PB91-125393, A04, MF-A01).

NCEER-90-0016 "Instantaneous Optimal Control with Acceleration and Velocity Feedback," by J.N. Yang and Z. Li, 6/29/90, (PB91-125401, A03, MF-A01).

NCEER-90-0017 "Reconnaissance Report on the Northern Iran Earthquake of June 21, 1990," by M. Mehrain, 10/4/90, (PB91-125377, A03, MF-A01).

NCEER-90-0018 "Evaluation of Liquefaction Potential in Memphis and Shelby County," by T.S. Chang, P.S. Tang, C.S. Lee and H. Hwang, 8/10/90, (PB91-125427, A09, MF-A01).

NCEER-90-0019 "Experimental and Analytical Study of a Combined Sliding Disc Bearing and Helical Steel Spring Isolation System," by M.C. Constantinou, A.S. Mokha and A.M. Reinhorn, 10/4/90, (PB91-125385, A06, MF-A01). This report is available only through NTIS (see address given above).

NCEER-90-0020 "Experimental Study and Analytical Prediction of Earthquake Response of a Sliding Isolation System with a Spherical Surface," by A.S. Mokha, M.C. Constantinou and A.M. Reinhorn, 10/11/90, (PB91-125419, A05, MF-A01).

NCEER-90-0021 "Dynamic Interaction Factors for Floating Pile Groups," by G. Gazetas, K. Fan, A. Kaynia and E. Kausel, 9/10/90, (PB91-170381, A05, MF-A01).

NCEER-90-0022 "Evaluation of Seismic Damage Indices for Reinforced Concrete Structures," by S. Rodriguez-Gomez and A.S. Cakmak, 9/30/90, PB91-171322, A06, MF-A01).

NCEER-90-0023 "Study of Site Response at a Selected Memphis Site," by H. Desai, S. Ahmad, E.S. Gazetas and M.R. Oh, 10/11/90, (PB91-196857, A03, MF-A01).

NCEER-90-0024 "A User's Guide to Strongmo: Version 1.0 of NCEER's Strong-Motion Data Access Tool for PCs and Terminals," by P.A. Friberg and C.A.T. Susch, 11/15/90, (PB91-171272, A03, MF-A01).

NCEER-90-0025 "A Three-Dimensional Analytical Study of Spatial Variability of Seismic Ground Motions," by L-L. Hong and A.H.-S. Ang, 10/30/90, (PB91-170399, A09, MF-A01).

NCEER-90-0026 "MUMOID User's Guide - A Program for the Identification of Modal Parameters," by S. Rodriguez-Gomez and E. DiPasquale, 9/30/90, (PB91-171298, A04, MF-A01).

NCEER-90-0027 "SARCF-II User's Guide - Seismic Analysis of Reinforced Concrete Frames," by S. Rodriguez-Gomez, Y.S. Chung and C. Meyer, 9/30/90, (PB91-171280, A05, MF-A01).

NCEER-90-0028 "Viscous Dampers: Testing, Modeling and Application in Vibration and Seismic Isolation," by N. Makris and M.C. Constantinou, 12/20/90 (PB91-190561, A06, MF-A01).

NCEER-90-0029 "Soil Effects on Earthquake Ground Motions in the Memphis Area," by H. Hwang, C.S. Lee, K.W. Ng and T.S. Chang, 8/2/90, (PB91-190751, A05, MF-A01).

NCEER-91-0001 "Proceedings from the Third Japan-U.S. Workshop on Earthquake Resistant Design of Lifeline Facilities and Countermeasures for Soil Liquefaction, December 17-19, 1990," edited by T.D. O'Rourke and M. Hamada, 2/1/91, (PB91-179259, A99, MF-A04).

NCEER-91-0002 "Physical Space Solutions of Non-Proportionally Damped Systems," by M. Tong, Z. Liang and G.C. Lee, 1/15/91, (PB91-179242, A04, MF-A01).

NCEER-91-0003 "Seismic Response of Single Piles and Pile Groups," by K. Fan and G. Gazetas, 1/10/91, (PB92-174994, A04, MF-A01).

NCEER-91-0004 "Damping of Structures: Part 1 - Theory of Complex Damping," by Z. Liang and G. Lee, 10/10/91, (PB92-197235, A12, MF-A03).

NCEER-91-0005 "3D-BASIS - Nonlinear Dynamic Analysis of Three Dimensional Base Isolated Structures: Part II," by S. Nagarajaiah, A.M. Reinhorn and M.C. Constantinou, 2/28/91, (PB91-190553, A07, MF-A01). This report has been replaced by NCEER-93-0011.

NCEER-91-0006 "A Multidimensional Hysteretic Model for Plasticity Deforming Metals in Energy Absorbing Devices," by E.J. Graesser and F.A. Cozzarelli, 4/9/91, (PB92-108364, A04, MF-A01).

NCEER-91-0007 "A Framework for Customizable Knowledge-Based Expert Systems with an Application to a KBES for Evaluating the Seismic Resistance of Existing Buildings," by E.G. Ibarra-Anaya and S.J. Fenves, 4/9/91, (PB91-210930, A08, MF-A01).

NCEER-91-0008 "Nonlinear Analysis of Steel Frames with Semi-Rigid Connections Using the Capacity Spectrum Method," by G.G. Deierlein, S-H. Hsieh, Y-J. Shen and J.F. Abel, 7/2/91, (PB92-113828, A05, MF-A01).

NCEER-91-0009 "Earthquake Education Materials for Grades K-12," by K.E.K. Ross, 4/30/91, (PB91-212142, A06, MF-A01). This report has been replaced by NCEER-92-0018.

NCEER-91-0010 "Phase Wave Velocities and Displacement Phase Differences in a Harmonically Oscillating Pile," by N. Makris and G. Gazetas, 7/8/91, (PB92-108356, A04, MF-A01).

NCEER-91-0011 "Dynamic Characteristics of a Full-Size Five-Story Steel Structure and a 2/5 Scale Model," by K.C. Chang, G.C. Yao, G.C. Lee, D.S. Hao and Y.C. Yeh," 7/2/91, (PB93-116648, A06, MF-A02).

NCEER-91-0012 "Seismic Response of a 2/5 Scale Steel Structure with Added Viscoelastic Dampers," by K.C. Chang, T.T. Soong, S-T. Oh and M.L. Lai, 5/17/91, (PB92-110816, A05, MF-A01).

NCEER-91-0013 "Earthquake Response of Retaining Walls; Full-Scale Testing and Computational Modeling," by S. Alampalli and A-W.M. Elgamal, 6/20/91, not available.

NCEER-91-0014 "3D-BASIS-M: Nonlinear Dynamic Analysis of Multiple Building Base Isolated Structures," by P.C. Tsopelas, S. Nagarajaiah, M.C. Constantinou and A.M. Reinhorn, 5/28/91, (PB92-113885, A09, MF-A02).

NCEER-91-0015 "Evaluation of SEAOC Design Requirements for Sliding Isolated Structures," by D. Theodossiou and M.C. Constantinou, 6/10/91, (PB92-114602, A11, MF-A03).

NCEER-91-0016 "Closed-Loop Modal Testing of a 27-Story Reinforced Concrete Flat Plate-Core Building," by H.R. Somaprasad, T. Toksoy, H. Yoshiyuki and A.E. Aktan, 7/15/91, (PB92-129980, A07, MF-A02).

NCEER-91-0017 "Shake Table Test of a 1/6 Scale Two-Story Lightly Reinforced Concrete Building," by A.G. El-Attar, R.N. White and P. Gergely, 2/28/91, (PB92-222447, A06, MF-A02).

NCEER-91-0018 "Shake Table Test of a 1/8 Scale Three-Story Lightly Reinforced Concrete Building," by A.G. El-Attar, R.N. White and P. Gergely, 2/28/91, (PB93-116630, A08, MF-A02).

NCEER-91-0019 "Transfer Functions for Rigid Rectangular Foundations," by A.S. Veletsos, A.M. Prasad and W.H. Wu, 7/31/91, not available.

NCEER-91-0020 "Hybrid Control of Seismic-Excited Nonlinear and Inelastic Structural Systems," by J.N. Yang, Z. Li and A. Danielians, 8/1/91, (PB92-143171, A06, MF-A02).

NCEER-91-0021 "The NCEER-91 Earthquake Catalog: Improved Intensity-Based Magnitudes and Recurrence Relations for U.S. Earthquakes East of New Madrid," by L. Seeber and J.G. Armbruster, 8/28/91, (PB92-176742, A06, MF-A02).

NCEER-91-0022 "Proceedings from the Implementation of Earthquake Planning and Education in Schools: The Need for Change - The Roles of the Changemakers," by K.E.K. Ross and F. Winslow, 7/23/91, (PB92-129998, A12, MF-A03).

NCEER-91-0023 "A Study of Reliability-Based Criteria for Seismic Design of Reinforced Concrete Frame Buildings," by H.H.M. Hwang and H-M. Hsu, 8/10/91, (PB92-140235, A09, MF-A02).

NCEER-91-0024 "Experimental Verification of a Number of Structural System Identification Algorithms," by R.G. Ghanem, H. Gavin and M. Shinozuka, 9/18/91, (PB92-176577, A18, MF-A04).

NCEER-91-0025 "Probabilistic Evaluation of Liquefaction Potential," by H.H.M. Hwang and C.S. Lee," 11/25/91, (PB92-143429, A05, MF-A01).

NCEER-91-0026 "Instantaneous Optimal Control for Linear, Nonlinear and Hysteretic Structures - Stable Controllers," by J.N. Yang and Z. Li, 11/15/91, (PB92-163807, A04, MF-A01).

NCEER-91-0027 "Experimental and Theoretical Study of a Sliding Isolation System for Bridges," by M.C. Constantinou, A. Kartoum, A.M. Reinhorn and P. Bradford, 11/15/91, (PB92-176973, A10, MF-A03).

NCEER-92-0001 "Case Studies of Liquefaction and Lifeline Performance During Past Earthquakes, Volume 1: Japanese Case Studies," Edited by M. Hamada and T. O'Rourke, 2/17/92, (PB92-197243, A18, MF-A04).

NCEER-92-0002 "Case Studies of Liquefaction and Lifeline Performance During Past Earthquakes, Volume 2: United States Case Studies," Edited by T. O'Rourke and M. Hamada, 2/17/92, (PB92-197250, A20, MF-A04).

NCEER-92-0003 "Issues in Earthquake Education," Edited by K. Ross, 2/3/92, (PB92-222389, A07, MF-A02).

NCEER-92-0004 "Proceedings from the First U.S. - Japan Workshop on Earthquake Protective Systems for Bridges," Edited by I.G. Buckle, 2/4/92, (PB94-142239, A99, MF-A06).

NCEER-92-0005 "Seismic Ground Motion from a Haskell-Type Source in a Multiple-Layered Half-Space," A.P. Theoharis, G. Deodatis and M. Shinozuka, 1/2/92, not available.

NCEER-92-0006 "Proceedings from the Site Effects Workshop," Edited by R. Whitman, 2/29/92, (PB92-197201, A04, MF-A01).

NCEER-92-0007 "Engineering Evaluation of Permanent Ground Deformations Due to Seismically-Induced Liquefaction," by M.H. Baziar, R. Dobry and A-W.M. Elgamal, 3/24/92, (PB92-222421, A13, MF-A03).

NCEER-92-0008 "A Procedure for the Seismic Evaluation of Buildings in the Central and Eastern United States," by C.D. Poland and J.O. Malley, 4/2/92, (PB92-222439, A20, MF-A04).

NCEER-92-0009 "Experimental and Analytical Study of a Hybrid Isolation System Using Friction Controllable Sliding Bearings," by M.Q. Feng, S. Fujii and M. Shinozuka, 5/15/92, (PB93-150282, A06, MF-A02).

NCEER-92-0010 "Seismic Resistance of Slab-Column Connections in Existing Non-Ductile Flat-Plate Buildings," by A.J. Durrani and Y. Du, 5/18/92, (PB93-116812, A06, MF-A02).

NCEER-92-0011 "The Hysteretic and Dynamic Behavior of Brick Masonry Walls Upgraded by Ferrocement Coatings Under Cyclic Loading and Strong Simulated Ground Motion," by H. Lee and S.P. Prawel, 5/11/92, not available.

NCEER-92-0012 "Study of Wire Rope Systems for Seismic Protection of Equipment in Buildings," by G.F. Demetriades, M.C. Constantinou and A.M. Reinhorn, 5/20/92, (PB93-116655, A08, MF-A02).

NCEER-92-0013 "Shape Memory Structural Dampers: Material Properties, Design and Seismic Testing," by P.R. Witting and F.A. Cozzarelli, 5/26/92, (PB93-116663, A05, MF-A01).

NCEER-92-0014 "Longitudinal Permanent Ground Deformation Effects on Buried Continuous Pipelines," by M.J. O'Rourke, and C. Nordberg, 6/15/92, (PB93-116671, A08, MF-A02).

NCEER-92-0015 "A Simulation Method for Stationary Gaussian Random Functions Based on the Sampling Theorem," by M. Grigoriu and S. Balopoulou, 6/11/92, (PB93-127496, A05, MF-A01).

NCEER-92-0016 "Gravity-Load-Designed Reinforced Concrete Buildings: Seismic Evaluation of Existing Construction and Detailing Strategies for Improved Seismic Resistance," by G.W. Hoffmann, S.K. Kunnath, A.M. Reinhorn and J.B. Mander, 7/15/92, (PB94-142007, A08, MF-A02).

NCEER-92-0017 "Observations on Water System and Pipeline Performance in the Limón Area of Costa Rica Due to the April 22, 1991 Earthquake," by M. O'Rourke and D. Ballantyne, 6/30/92, (PB93-126811, A06, MF-A02).

NCEER-92-0018 "Fourth Edition of Earthquake Education Materials for Grades K-12," Edited by K.E.K. Ross, 8/10/92, (PB93-114023, A07, MF-A02).

NCEER-92-0019 "Proceedings from the Fourth Japan-U.S. Workshop on Earthquake Resistant Design of Lifeline Facilities and Countermeasures for Soil Liquefaction," Edited by M. Hamada and T.D. O'Rourke, 8/12/92, (PB93-163939, A99, MF-E11).

NCEER-92-0020 "Active Bracing System: A Full Scale Implementation of Active Control," by A.M. Reinhorn, T.T. Soong, R.C. Lin, M.A. Riley, Y.P. Wang, S. Aizawa and M. Higashino, 8/14/92, (PB93-127512, A06, MF-A02).

NCEER-92-0021 "Empirical Analysis of Horizontal Ground Displacement Generated by Liquefaction-Induced Lateral Spreads," by S.F. Bartlett and T.L. Youd, 8/17/92, (PB93-188241, A06, MF-A02).

NCEER-92-0022 "IDARC Version 3.0: Inelastic Damage Analysis of Reinforced Concrete Structures," by S.K. Kunnath, A.M. Reinhorn and R.F. Lobo, 8/31/92, (PB93-227502, A07, MF-A02).

NCEER-92-0023 "A Semi-Empirical Analysis of Strong-Motion Peaks in Terms of Seismic Source, Propagation Path and Local Site Conditions, by M. Kamiyama, M.J. O'Rourke and R. Flores-Berrones, 9/9/92, (PB93-150266, A08, MF-A02).

NCEER-92-0024 "Seismic Behavior of Reinforced Concrete Frame Structures with Nonductile Details, Part I: Summary of Experimental Findings of Full Scale Beam-Column Joint Tests," by A. Beres, R.N. White and P. Gergely, 9/30/92, (PB93-227783, A05, MF-A01).

NCEER-92-0025 "Experimental Results of Repaired and Retrofitted Beam-Column Joint Tests in Lightly Reinforced Concrete Frame Buildings," by A. Beres, S. El-Borgi, R.N. White and P. Gergely, 10/29/92, (PB93-227791, A05, MF-A01).

NCEER-92-0026 "A Generalization of Optimal Control Theory: Linear and Nonlinear Structures," by J.N. Yang, Z. Li and S. Vongchavalitkul, 11/2/92, (PB93-188621, A05, MF-A01).

NCEER-92-0027 "Seismic Resistance of Reinforced Concrete Frame Structures Designed Only for Gravity Loads: Part I - Design and Properties of a One-Third Scale Model Structure," by J.M. Bracci, A.M. Reinhorn and J.B. Mander, 12/1/92, (PB94-104502, A08, MF-A02).

NCEER-92-0028 "Seismic Resistance of Reinforced Concrete Frame Structures Designed Only for Gravity Loads: Part II - Experimental Performance of Subassemblages," by L.E. Aycardi, J.B. Mander and A.M. Reinhorn, 12/1/92, (PB94-104510, A08, MF-A02).

NCEER-92-0029 "Seismic Resistance of Reinforced Concrete Frame Structures Designed Only for Gravity Loads: Part III - Experimental Performance and Analytical Study of a Structural Model," by J.M. Bracci, A.M. Reinhorn and J.B. Mander, 12/1/92, (PB93-227528, A09, MF-A01).

NCEER-92-0030 "Evaluation of Seismic Retrofit of Reinforced Concrete Frame Structures: Part I - Experimental Performance of Retrofitted Subassemblages," by D. Choudhuri, J.B. Mander and A.M. Reinhorn, 12/8/92, (PB93-198307, A07, MF-A02).

NCEER-92-0031 "Evaluation of Seismic Retrofit of Reinforced Concrete Frame Structures: Part II - Experimental Performance and Analytical Study of a Retrofitted Structural Model," by J.M. Bracci, A.M. Reinhorn and J.B. Mander, 12/8/92, (PB93-198315, A09, MF-A03).

NCEER-92-0032 "Experimental and Analytical Investigation of Seismic Response of Structures with Supplemental Fluid Viscous Dampers," by M.C. Constantinou and M.D. Symans, 12/21/92, (PB93-191435, A10, MF-A03). This report is available only through NTIS (see address given above).

NCEER-92-0033 "Reconnaissance Report on the Cairo, Egypt Earthquake of October 12, 1992," by M. Khater, 12/23/92, (PB93-188621, A03, MF-A01).

NCEER-92-0034 "Low-Level Dynamic Characteristics of Four Tall Flat-Plate Buildings in New York City," by H. Gavin, S. Yuan, J. Grossman, E. Pekelis and K. Jacob, 12/28/92, (PB93-188217, A07, MF-A02).

NCEER-93-0001 "An Experimental Study on the Seismic Performance of Brick-Infilled Steel Frames With and Without Retrofit," by J.B. Mander, B. Nair, K. Wojtkowski and J. Ma, 1/29/93, (PB93-227510, A07, MF-A02).

NCEER-93-0002 "Social Accounting for Disaster Preparedness and Recovery Planning," by S. Cole, E. Pantoja and V. Razak, 2/22/93, (PB94-142114, A12, MF-A03).

NCEER-93-0003 "Assessment of 1991 NEHRP Provisions for Nonstructural Components and Recommended Revisions," by T.T. Soong, G. Chen, Z. Wu, R-H. Zhang and M. Grigoriu, 3/1/93, (PB93-188639, A06, MF-A02).

NCEER-93-0004 "Evaluation of Static and Response Spectrum Analysis Procedures of SEAOC/UBC for Seismic Isolated Structures," by C.W. Winters and M.C. Constantinou, 3/23/93, (PB93-198299, A10, MF-A03).

NCEER-93-0005 "Earthquakes in the Northeast - Are We Ignoring the Hazard? A Workshop on Earthquake Science and Safety for Educators," edited by K.E.K. Ross, 4/2/93, (PB94-103066, A09, MF-A02).

NCEER-93-0006 "Inelastic Response of Reinforced Concrete Structures with Viscoelastic Braces," by R.F. Lobo, J.M. Bracci, K.L. Shen, A.M. Reinhorn and T.T. Soong, 4/5/93, (PB93-227486, A05, MF-A02).

NCEER-93-0007 "Seismic Testing of Installation Methods for Computers and Data Processing Equipment," by K. Kosar, T.T. Soong, K.L. Shen, J.A. HoLung and Y.K. Lin, 4/12/93, (PB93-198299, A07, MF-A02).

NCEER-93-0008 "Retrofit of Reinforced Concrete Frames Using Added Dampers," by A. Reinhorn, M. Constantinou and C. Li, not available.

NCEER-93-0009 "Seismic Behavior and Design Guidelines for Steel Frame Structures with Added Viscoelastic Dampers," by K.C. Chang, M.L. Lai, T.T. Soong, D.S. Hao and Y.C. Yeh, 5/1/93, (PB94-141959, A07, MF-A02).

NCEER-93-0010 "Seismic Performance of Shear-Critical Reinforced Concrete Bridge Piers," by J.B. Mander, S.M. Waheed, M.T.A. Chaudhary and S.S. Chen, 5/12/93, (PB93-227494, A08, MF-A02).

NCEER-93-0011 "3D-BASIS-TABS: Computer Program for Nonlinear Dynamic Analysis of Three Dimensional Base Isolated Structures," by S. Nagarajaiah, C. Li, A.M. Reinhorn and M.C. Constantinou, 8/2/93, (PB94-141819, A09, MF-A02).

NCEER-93-0012 "Effects of Hydrocarbon Spills from an Oil Pipeline Break on Ground Water," by O.J. Helweg and H.H.M. Hwang, 8/3/93, (PB94-141942, A06, MF-A02).

NCEER-93-0013 "Simplified Procedures for Seismic Design of Nonstructural Components and Assessment of Current Code Provisions," by M.P. Singh, L.E. Suarez, E.E. Matheu and G.O. Maldonado, 8/4/93, (PB94-141827, A09, MF-A02).

NCEER-93-0014 "An Energy Approach to Seismic Analysis and Design of Secondary Systems," by G. Chen and T.T. Soong, 8/6/93, (PB94-142767, A11, MF-A03).

NCEER-93-0015 "Proceedings from School Sites: Becoming Prepared for Earthquakes - Commemorating the Third Anniversary of the Loma Prieta Earthquake," Edited by F.E. Winslow and K.E.K. Ross, 8/16/93, (PB94-154275, A16, MF-A02).

NCEER-93-0016 "Reconnaissance Report of Damage to Historic Monuments in Cairo, Egypt Following the October 12, 1992 Dahshur Earthquake," by D. Sykora, D. Look, G. Croci, E. Karaesmen and E. Karaesmen, 8/19/93, (PB94-142221, A08, MF-A02).

NCEER-93-0017 "The Island of Guam Earthquake of August 8, 1993," by S.W. Swan and S.K. Harris, 9/30/93, (PB94-141843, A04, MF-A01).

NCEER-93-0018 "Engineering Aspects of the October 12, 1992 Egyptian Earthquake," by A.W. Elgamal, M. Amer, K. Adalier and A. Abul-Fadl, 10/7/93, (PB94-141983, A05, MF-A01).

NCEER-93-0019 "Development of an Earthquake Motion Simulator and its Application in Dynamic Centrifuge Testing," by I. Krstelj, Supervised by J.H. Prevost, 10/23/93, (PB94-181773, A-10, MF-A03).

NCEER-93-0020 "NCEER-Taisei Corporation Research Program on Sliding Seismic Isolation Systems for Bridges: Experimental and Analytical Study of a Friction Pendulum System (FPS)," by M.C. Constantinou, P. Tsopelas, Y-S. Kim and S. Okamoto, 11/1/93, (PB94-142775, A08, MF-A02).

NCEER-93-0021 "Finite Element Modeling of Elastomeric Seismic Isolation Bearings," by L.J. Billings, Supervised by R. Shepherd, 11/8/93, not available.

NCEER-93-0022 "Seismic Vulnerability of Equipment in Critical Facilities: Life-Safety and Operational Consequences," by K. Porter, G.S. Johnson, M.M. Zadeh, C. Scawthorn and S. Eder, 11/24/93, (PB94-181765, A16, MF-A03).

NCEER-93-0023 "Hokkaido Nansei-oki, Japan Earthquake of July 12, 1993, by P.I. Yanev and C.R. Scawthorn, 12/23/93, (PB94-181500, A07, MF-A01).

NCEER-94-0001 "An Evaluation of Seismic Serviceability of Water Supply Networks with Application to the San Francisco Auxiliary Water Supply System," by I. Markov, Supervised by M. Grigoriu and T. O'Rourke, 1/21/94, (PB94-204013, A07, MF-A02).

NCEER-94-0002 "NCEER-Taisei Corporation Research Program on Sliding Seismic Isolation Systems for Bridges: Experimental and Analytical Study of Systems Consisting of Sliding Bearings, Rubber Restoring Force Devices and Fluid Dampers," Volumes I and II, by P. Tsopelas, S. Okamoto, M.C. Constantinou, D. Ozaki and S. Fujii, 2/4/94, (PB94-181740, A09, MF-A02 and PB94-181757, A12, MF-A03).

NCEER-94-0003 "A Markov Model for Local and Global Damage Indices in Seismic Analysis," by S. Rahman and M. Grigoriu, 2/18/94, (PB94-206000, A12, MF-A03).

NCEER-94-0004 "Proceedings from the NCEER Workshop on Seismic Response of Masonry Infills," edited by D.P. Abrams, 3/1/94, (PB94-180783, A07, MF-A02).

NCEER-94-0005 "The Northridge, California Earthquake of January 17, 1994: General Reconnaissance Report," edited by J.D. Goltz, 3/11/94, (PB94-193943, A10, MF-A03).

NCEER-94-0006 "Seismic Energy Based Fatigue Damage Analysis of Bridge Columns: Part I - Evaluation of Seismic Capacity," by G.A. Chang and J.B. Mander, 3/14/94, (PB94-219185, A11, MF-A03).

NCEER-94-0007 "Seismic Isolation of Multi-Story Frame Structures Using Spherical Sliding Isolation Systems," by T.M. Al-Hussaini, V.A. Zayas and M.C. Constantinou, 3/17/94, (PB94-193745, A09, MF-A02).

NCEER-94-0008 "The Northridge, California Earthquake of January 17, 1994: Performance of Highway Bridges," edited by I.G. Buckle, 3/24/94, (PB94-193851, A06, MF-A02).

NCEER-94-0009 "Proceedings of the Third U.S.-Japan Workshop on Earthquake Protective Systems for Bridges," edited by I.G. Buckle and I. Friedland, 3/31/94, (PB94-195815, A99, MF-A06).

NCEER-94-0010 "3D-BASIS-ME: Computer Program for Nonlinear Dynamic Analysis of Seismically Isolated Single and Multiple Structures and Liquid Storage Tanks," by P.C. Tsopelas, M.C. Constantinou and A.M. Reinhorn, 4/12/94, (PB94-204922, A09, MF-A02).

NCEER-94-0011 "The Northridge, California Earthquake of January 17, 1994: Performance of Gas Transmission Pipelines," by T.D. O'Rourke and M.C. Palmer, 5/16/94, (PB94-204989, A05, MF-A01).

NCEER-94-0012 "Feasibility Study of Replacement Procedures and Earthquake Performance Related to Gas Transmission Pipelines," by T.D. O'Rourke and M.C. Palmer, 5/25/94, (PB94-206638, A09, MF-A02).

NCEER-94-0013 "Seismic Energy Based Fatigue Damage Analysis of Bridge Columns: Part II - Evaluation of Seismic Demand," by G.A. Chang and J.B. Mander, 6/1/94, (PB95-18106, A08, MF-A02).

NCEER-94-0014 "NCEER-Taisei Corporation Research Program on Sliding Seismic Isolation Systems for Bridges: Experimental and Analytical Study of a System Consisting of Sliding Bearings and Fluid Restoring Force/Damping Devices," by P. Tsopelas and M.C. Constantinou, 6/13/94, (PB94-219144, A10, MF-A03).

NCEER-94-0015 "Generation of Hazard-Consistent Fragility Curves for Seismic Loss Estimation Studies," by H. Hwang and J-R. Huo, 6/14/94, (PB95-181996, A09, MF-A02).

NCEER-94-0016 "Seismic Study of Building Frames with Added Energy-Absorbing Devices," by W.S. Pong, C.S. Tsai and G.C. Lee, 6/20/94, (PB94-219136, A10, A03).

NCEER-94-0017 "Sliding Mode Control for Seismic-Excited Linear and Nonlinear Civil Engineering Structures," by J. Yang, J. Wu, A. Agrawal and Z. Li, 6/21/94, (PB95-138483, A06, MF-A02).

NCEER-94-0018 "3D-BASIS-TABS Version 2.0: Computer Program for Nonlinear Dynamic Analysis of Three Dimensional Base Isolated Structures," by A.M. Reinhorn, S. Nagarajaiah, M.C. Constantinou, P. Tsopelas and R. Li, 6/22/94, (PB95-182176, A08, MF-A02).

NCEER-94-0019 "Proceedings of the International Workshop on Civil Infrastructure Systems: Application of Intelligent Systems and Advanced Materials on Bridge Systems," Edited by G.C. Lee and K.C. Chang, 7/18/94, (PB95-252474, A20, MF-A04).

NCEER-94-0020 "Study of Seismic Isolation Systems for Computer Floors," by V. Lambrou and M.C. Constantinou, 7/19/94, (PB95-138533, A10, MF-A03).

NCEER-94-0021 "Proceedings of the U.S.-Italian Workshop on Guidelines for Seismic Evaluation and Rehabilitation of Unreinforced Masonry Buildings," Edited by D.P. Abrams and G.M. Calvi, 7/20/94, (PB95-138749, A13, MF-A03).

NCEER-94-0022 "NCEER-Taisei Corporation Research Program on Sliding Seismic Isolation Systems for Bridges: Experimental and Analytical Study of a System Consisting of Lubricated PTFE Sliding Bearings and Mild Steel Dampers," by P. Tsopelas and M.C. Constantinou, 7/22/94, (PB95-182184, A08, MF-A02).

NCEER-94-0023 "Development of Reliability-Based Design Criteria for Buildings Under Seismic Load," by Y.K. Wen, H. Hwang and M. Shinozuka, 8/1/94, (PB95-211934, A08, MF-A02).

NCEER-94-0024 "Experimental Verification of Acceleration Feedback Control Strategies for an Active Tendon System," by S.J. Dyke, B.F. Spencer, Jr., P. Quast, M.K. Sain, D.C. Kaspari, Jr. and T.T. Soong, 8/29/94, (PB95-212320, A05, MF-A01).

NCEER-94-0025 "Seismic Retrofitting Manual for Highway Bridges," Edited by I.G. Buckle and I.F. Friedland, published by the Federal Highway Administration (PB95-212676, A15, MF-A03).

NCEER-94-0026 "Proceedings from the Fifth U.S.-Japan Workshop on Earthquake Resistant Design of Lifeline Facilities and Countermeasures Against Soil Liquefaction," Edited by T.D. O'Rourke and M. Hamada, 11/7/94, (PB95-220802, A99, MF-E08).

NCEER-95-0001 "Experimental and Analytical Investigation of Seismic Retrofit of Structures with Supplemental Damping: Part 1 - Fluid Viscous Damping Devices," by A.M. Reinhorn, C. Li and M.C. Constantinou, 1/3/95, (PB95-266599, A09, MF-A02).

NCEER-95-0002 "Experimental and Analytical Study of Low-Cycle Fatigue Behavior of Semi-Rigid Top-And-Seat Angle Connections," by G. Pekcan, J.B. Mander and S.S. Chen, 1/5/95, (PB95-220042, A07, MF-A02).

NCEER-95-0003 "NCEER-ATC Joint Study on Fragility of Buildings," by T. Anagnos, C. Rojahn and A.S. Kiremidjian, 1/20/95, (PB95-220026, A06, MF-A02).

NCEER-95-0004 "Nonlinear Control Algorithms for Peak Response Reduction," by Z. Wu, T.T. Soong, V. Gattulli and R.C. Lin, 2/16/95, (PB95-220349, A05, MF-A01).

NCEER-95-0005 "Pipeline Replacement Feasibility Study: A Methodology for Minimizing Seismic and Corrosion Risks to Underground Natural Gas Pipelines," by R.T. Eguchi, H.A. Seligson and D.G. Honegger, 3/2/95, (PB95-252326, A06, MF-A02).

NCEER-95-0006 "Evaluation of Seismic Performance of an 11-Story Frame Building During the 1994 Northridge Earthquake," by F. Naeim, R. DiSulio, K. Benuska, A. Reinhorn and C. Li, not available.

NCEER-95-0007 "Prioritization of Bridges for Seismic Retrofitting," by N. Basöz and A.S. Kiremidjian, 4/24/95, (PB95-252300, A08, MF-A02).

NCEER-95-0008 "Method for Developing Motion Damage Relationships for Reinforced Concrete Frames," by A. Singhal and A.S. Kiremidjian, 5/11/95, (PB95-266607, A06, MF-A02).

NCEER-95-0009 "Experimental and Analytical Investigation of Seismic Retrofit of Structures with Supplemental Damping: Part II - Friction Devices," by C. Li and A.M. Reinhorn, 7/6/95, (PB96-128087, A11, MF-A03).

NCEER-95-0010 "Experimental Performance and Analytical Study of a Non-Ductile Reinforced Concrete Frame Structure Retrofitted with Elastomeric Spring Dampers," by G. Pekcan, J.B. Mander and S.S. Chen, 7/14/95, (PB96-137161, A08, MF-A02).

NCEER-95-0011 "Development and Experimental Study of Semi-Active Fluid Damping Devices for Seismic Protection of Structures," by M.D. Symans and M.C. Constantinou, 8/3/95, (PB96-136940, A23, MF-A04).

NCEER-95-0012 "Real-Time Structural Parameter Modification (RSPM): Development of Innervated Structures," by Z. Liang, M. Tong and G.C. Lee, 4/11/95, (PB96-137153, A06, MF-A01).

NCEER-95-0013 "Experimental and Analytical Investigation of Seismic Retrofit of Structures with Supplemental Damping: Part III - Viscous Damping Walls," by A.M. Reinhorn and C. Li, 10/1/95, (PB96-176409, A11, MF-A03).

NCEER-95-0014 "Seismic Fragility Analysis of Equipment and Structures in a Memphis Electric Substation," by J-R. Huo and H.H.M. Hwang, 8/10/95, (PB96-128087, A09, MF-A02).

NCEER-95-0015 "The Hanshin-Awaji Earthquake of January 17, 1995: Performance of Lifelines," Edited by M. Shinozuka, 11/3/95, (PB96-176383, A15, MF-A03).

NCEER-95-0016 "Highway Culvert Performance During Earthquakes," by T.L. Youd and C.J. Beckman, available as NCEER-96-0015.

NCEER-95-0017 "The Hanshin-Awaji Earthquake of January 17, 1995: Performance of Highway Bridges," Edited by I.G. Buckle, 12/1/95, not available.

NCEER-95-0018 "Modeling of Masonry Infill Panels for Structural Analysis," by A.M. Reinhorn, A. Madan, R.E. Valles, Y. Reichmann and J.B. Mander, 12/8/95, (PB97-110886, MF-A01, A06).

NCEER-95-0019 "Optimal Polynomial Control for Linear and Nonlinear Structures," by A.K. Agrawal and J.N. Yang, 12/11/95, (PB96-168737, A07, MF-A02).

NCEER-95-0020 "Retrofit of Non-Ductile Reinforced Concrete Frames Using Friction Dampers," by R.S. Rao, P. Gergely and R.N. White, 12/22/95, (PB97-133508, A10, MF-A02).

NCEER-95-0021 "Parametric Results for Seismic Response of Pile-Supported Bridge Bents," by G. Mylonakis, A. Nikolaou and G. Gazetas, 12/22/95, (PB97-100242, A12, MF-A03).

NCEER-95-0022 "Kinematic Bending Moments in Seismically Stressed Piles," by A. Nikolaou, G. Mylonakis and G. Gazetas, 12/23/95, (PB97-113914, MF-A03, A13).

NCEER-96-0001 "Dynamic Response of Unreinforced Masonry Buildings with Flexible Diaphragms," by A.C. Costley and D.P. Abrams," 10/10/96, (PB97-133573, MF-A03, A15).

NCEER-96-0002 "State of the Art Review: Foundations and Retaining Structures," by I. Po Lam, not available.

NCEER-96-0003 "Ductility of Rectangular Reinforced Concrete Bridge Columns with Moderate Confinement," by N. Wehbe, M. Saiidi, D. Sanders and B. Douglas, 11/7/96, (PB97-133557, A06, MF-A02).

NCEER-96-0004 "Proceedings of the Long-Span Bridge Seismic Research Workshop," edited by I.G. Buckle and I.M. Friedland, not available.

NCEER-96-0005 "Establish Representative Pier Types for Comprehensive Study: Eastern United States," by J. Kulicki and Z. Prucz, 5/28/96, (PB98-119217, A07, MF-A02).

NCEER-96-0006 "Establish Representative Pier Types for Comprehensive Study: Western United States," by R. Imbsen, R.A. Schamber and T.A. Osterkamp, 5/28/96, (PB98-118607, A07, MF-A02).

NCEER-96-0007 "Nonlinear Control Techniques for Dynamical Systems with Uncertain Parameters," by R.G. Ghanem and M.I. Bujakov, 5/27/96, (PB97-100259, A17, MF-A03).

NCEER-96-0008 "Seismic Evaluation of a 30-Year Old Non-Ductile Highway Bridge Pier and Its Retrofit," by J.B. Mander, B. Mahmoodzadegan, S. Bhadra and S.S. Chen, 5/31/96, (PB97-110902, MF-A03, A10).

NCEER-96-0009 "Seismic Performance of a Model Reinforced Concrete Bridge Pier Before and After Retrofit," by J.B. Mander, J.H. Kim and C.A. Ligozio, 5/31/96, (PB97-110910, MF-A02, A10).

NCEER-96-0010 "IDARC2D Version 4.0: A Computer Program for the Inelastic Damage Analysis of Buildings," by R.E. Valles, A.M. Reinhorn, S.K. Kunnath, C. Li and A. Madan, 6/3/96, (PB97-100234, A17, MF-A03).

NCEER-96-0011 "Estimation of the Economic Impact of Multiple Lifeline Disruption: Memphis Light, Gas and Water Division Case Study," by S.E. Chang, H.A. Seligson and R.T. Eguchi, 8/16/96, (PB97-133490, A11, MF-A03).

NCEER-96-0012 "Proceedings from the Sixth Japan-U.S. Workshop on Earthquake Resistant Design of Lifeline Facilities and Countermeasures Against Soil Liquefaction, Edited by M. Hamada and T. O'Rourke, 9/11/96, (PB97-133581, A99, MF-A06).

NCEER-96-0013 "Chemical Hazards, Mitigation and Preparedness in Areas of High Seismic Risk: A Methodology for Estimating the Risk of Post-Earthquake Hazardous Materials Release," by H.A. Seligson, R.T. Eguchi, K.J. Tierney and K. Richmond, 11/7/96, (PB97-133565, MF-A02, A08).

NCEER-96-0014 "Response of Steel Bridge Bearings to Reversed Cyclic Loading," by J.B. Mander, D-K. Kim, S.S. Chen and G.J. Premus, 11/13/96, (PB97-140735, A12, MF-A03).

NCEER-96-0015 "Highway Culvert Performance During Past Earthquakes," by T.L. Youd and C.J. Beckman, 11/25/96, (PB97-133532, A06, MF-A01).

NCEER-97-0001 "Evaluation, Prevention and Mitigation of Pounding Effects in Building Structures," by R.E. Valles and A.M. Reinhorn, 2/20/97, (PB97-159552, A14, MF-A03).

NCEER-97-0002 "Seismic Design Criteria for Bridges and Other Highway Structures," by C. Rojahn, R. Mayes, D.G. Anderson, J. Clark, J.H. Hom, R.V. Nutt and M.J. O'Rourke, 4/30/97, (PB97-194658, A06, MF-A03).

NCEER-97-0003 “Proceedings of the U.S.-Italian Workshop on Seismic Evaluation and Retrofit,” Edited by D.P. Abrams and G.M. Calvi, 3/19/97, (PB97-194666, A13, MF-A03).

NCEER-97-0004 "Investigation of Seismic Response of Buildings with Linear and Nonlinear Fluid Viscous Dampers," by A.A. Seleemah and M.C. Constantinou, 5/21/97, (PB98-109002, A15, MF-A03).

NCEER-97-0005 "Proceedings of the Workshop on Earthquake Engineering Frontiers in Transportation Facilities," edited by G.C. Lee and I.M. Friedland, 8/29/97, (PB98-128911, A25, MR-A04).

NCEER-97-0006 "Cumulative Seismic Damage of Reinforced Concrete Bridge Piers," by S.K. Kunnath, A. El-Bahy, A. Taylor and W. Stone, 9/2/97, (PB98-108814, A11, MF-A03).

NCEER-97-0007 "Structural Details to Accommodate Seismic Movements of Highway Bridges and Retaining Walls," by R.A. Imbsen, R.A. Schamber, E. Thorkildsen, A. Kartoum, B.T. Martin, T.N. Rosser and J.M. Kulicki, 9/3/97, (PB98-108996, A09, MF-A02).

NCEER-97-0008 "A Method for Earthquake Motion-Damage Relationships with Application to Reinforced Concrete Frames," by A. Singhal and A.S. Kiremidjian, 9/10/97, (PB98-108988, A13, MF-A03).

NCEER-97-0009 "Seismic Analysis and Design of Bridge Abutments Considering Sliding and Rotation," by K. Fishman and R. Richards, Jr., 9/15/97, (PB98-108897, A06, MF-A02).

NCEER-97-0010 "Proceedings of the FHWA/NCEER Workshop on the National Representation of Seismic Ground Motion for New and Existing Highway Facilities," edited by I.M. Friedland, M.S. Power and R.L. Mayes, 9/22/97, (PB98-128903, A21, MF-A04).

NCEER-97-0011 "Seismic Analysis for Design or Retrofit of Gravity Bridge Abutments," by K.L. Fishman, R. Richards, Jr. and R.C. Divito, 10/2/97, (PB98-128937, A08, MF-A02).

NCEER-97-0012 "Evaluation of Simplified Methods of Analysis for Yielding Structures," by P. Tsopelas, M.C. Constantinou, C.A. Kircher and A.S. Whittaker, 10/31/97, (PB98-128929, A10, MF-A03).

NCEER-97-0013 "Seismic Design of Bridge Columns Based on Control and Repairability of Damage," by C-T. Cheng and J.B. Mander, 12/8/97, (PB98-144249, A11, MF-A03).

NCEER-97-0014 "Seismic Resistance of Bridge Piers Based on Damage Avoidance Design," by J.B. Mander and C-T. Cheng, 12/10/97, (PB98-144223, A09, MF-A02).

NCEER-97-0015 “Seismic Response of Nominally Symmetric Systems with Strength Uncertainty,” by S. Balopoulou and M. Grigoriu, 12/23/97, (PB98-153422, A11, MF-A03).

NCEER-97-0016 “Evaluation of Seismic Retrofit Methods for Reinforced Concrete Bridge Columns,” by T.J. Wipf, F.W. Klaiber and F.M. Russo, 12/28/97, (PB98-144215, A12, MF-A03).

NCEER-97-0017 “Seismic Fragility of Existing Conventional Reinforced Concrete Highway Bridges,” by C.L. Mullen and A.S. Cakmak, 12/30/97, (PB98-153406, A08, MF-A02).

NCEER-97-0018 “Loss Asssessment of Memphis Buildings,” edited by D.P. Abrams and M. Shinozuka, 12/31/97, (PB98-144231, A13, MF-A03).

NCEER-97-0019 “Seismic Evaluation of Frames with Infill Walls Using Quasi-static Experiments,” by K.M. Mosalam, R.N. White and P. Gergely, 12/31/97, (PB98-153455, A07, MF-A02).

NCEER-97-0020 “Seismic Evaluation of Frames with Infill Walls Using Pseudo-dynamic Experiments,” by K.M. Mosalam, R.N. White and P. Gergely, 12/31/97, (PB98-153430, A07, MF-A02).

NCEER-97-0021 “Computational Strategies for Frames with Infill Walls: Discrete and Smeared Crack Analyses and Seismic Fragility,” by K.M. Mosalam, R.N. White and P. Gergely, 12/31/97, (PB98-153414, A10, MF-A02).

NCEER-97-0022 "Proceedings of the NCEER Workshop on Evaluation of Liquefaction Resistance of Soils," edited by T.L. Youd and I.M. Idriss, 12/31/97, (PB98-155617, A15, MF-A03).

MCEER-98-0001 "Extraction of Nonlinear Hysteretic Properties of Seismically Isolated Bridges from Quick-Release Field Tests," by Q. Chen, B.M. Douglas, E.M. Maragakis and I.G. Buckle, 5/26/98, (PB99-118838, A06, MF-A01).

MCEER-98-0002 "Methodologies for Evaluating the Importance of Highway Bridges," by A. Thomas, S. Eshenaur and J. Kulicki, 5/29/98, (PB99-118846, A10, MF-A02).

MCEER-98-0003 "Capacity Design of Bridge Piers and the Analysis of Overstrength," by J.B. Mander, A. Dutta and P. Goel, 6/1/98, (PB99-118853, A09, MF-A02).

MCEER-98-0004 "Evaluation of Bridge Damage Data from the Loma Prieta and Northridge, California Earthquakes," by N. Basoz and A. Kiremidjian, 6/2/98, (PB99-118861, A15, MF-A03).

MCEER-98-0005 "Screening Guide for Rapid Assessment of Liquefaction Hazard at Highway Bridge Sites," by T. L. Youd, 6/16/98, (PB99-118879, A06, not available on microfiche).

MCEER-98-0006 "Structural Steel and Steel/Concrete Interface Details for Bridges," by P. Ritchie, N. Kauhl and J. Kulicki, 7/13/98, (PB99-118945, A06, MF-A01).

MCEER-98-0007 "Capacity Design and Fatigue Analysis of Confined Concrete Columns," by A. Dutta and J.B. Mander, 7/14/98, (PB99-118960, A14, MF-A03).

MCEER-98-0008 "Proceedings of the Workshop on Performance Criteria for Telecommunication Services Under Earthquake Conditions," edited by A.J. Schiff, 7/15/98, (PB99-118952, A08, MF-A02).

MCEER-98-0009 "Fatigue Analysis of Unconfined Concrete Columns," by J.B. Mander, A. Dutta and J.H. Kim, 9/12/98, (PB99-123655, A10, MF-A02).

MCEER-98-0010 "Centrifuge Modeling of Cyclic Lateral Response of Pile-Cap Systems and Seat-Type Abutments in Dry Sands," by A.D. Gadre and R. Dobry, 10/2/98, (PB99-123606, A13, MF-A03).

MCEER-98-0011 "IDARC-BRIDGE: A Computational Platform for Seismic Damage Assessment of Bridge Structures," by A.M. Reinhorn, V. Simeonov, G. Mylonakis and Y. Reichman, 10/2/98, (PB99-162919, A15, MF-A03).

MCEER-98-0012 "Experimental Investigation of the Dynamic Response of Two Bridges Before and After Retrofitting with Elastomeric Bearings," by D.A. Wendichansky, S.S. Chen and J.B. Mander, 10/2/98, (PB99-162927, A15, MF-A03).

MCEER-98-0013 "Design Procedures for Hinge Restrainers and Hinge Sear Width for Multiple-Frame Bridges," by R. Des Roches and G.L. Fenves, 11/3/98, (PB99-140477, A13, MF-A03).

MCEER-98-0014 "Response Modification Factors for Seismically Isolated Bridges," by M.C. Constantinou and J.K. Quarshie, 11/3/98, (PB99-140485, A14, MF-A03).

MCEER-98-0015 "Proceedings of the U.S.-Italy Workshop on Seismic Protective Systems for Bridges," edited by I.M. Friedland and M.C. Constantinou, 11/3/98, (PB2000-101711, A22, MF-A04).

MCEER-98-0016 "Appropriate Seismic Reliability for Critical Equipment Systems: Recommendations Based on Regional Analysis of Financial and Life Loss," by K. Porter, C. Scawthorn, C. Taylor and N. Blais, 11/10/98, (PB99-157265, A08, MF-A02).

MCEER-98-0017 "Proceedings of the U.S. Japan Joint Seminar on Civil Infrastructure Systems Research," edited by M. Shinozuka and A. Rose, 11/12/98, (PB99-156713, A16, MF-A03).

MCEER-98-0018 "Modeling of Pile Footings and Drilled Shafts for Seismic Design," by I. PoLam, M. Kapuskar and D. Chaudhuri, 12/21/98, (PB99-157257, A09, MF-A02).

MCEER-99-0001 "Seismic Evaluation of a Masonry Infilled Reinforced Concrete Frame by Pseudodynamic Testing," by S.G. Buonopane and R.N. White, 2/16/99, (PB99-162851, A09, MF-A02).

MCEER-99-0002 "Response History Analysis of Structures with Seismic Isolation and Energy Dissipation Systems: Verification Examples for Program SAP2000," by J. Scheller and M.C. Constantinou, 2/22/99, (PB99-162869, A08, MF-A02).

MCEER-99-0003 "Experimental Study on the Seismic Design and Retrofit of Bridge Columns Including Axial Load Effects," by A. Dutta, T. Kokorina and J.B. Mander, 2/22/99, (PB99-162877, A09, MF-A02).

MCEER-99-0004 "Experimental Study of Bridge Elastomeric and Other Isolation and Energy Dissipation Systems with Emphasis on Uplift Prevention and High Velocity Near-source Seismic Excitation," by A. Kasalanati and M. C. Constantinou, 2/26/99, (PB99-162885, A12, MF-A03).

MCEER-99-0005 "Truss Modeling of Reinforced Concrete Shear-flexure Behavior," by J.H. Kim and J.B. Mander, 3/8/99, (PB99-163693, A12, MF-A03).

MCEER-99-0006 "Experimental Investigation and Computational Modeling of Seismic Response of a 1:4 Scale Model Steel Structure with a Load Balancing Supplemental Damping System," by G. Pekcan, J.B. Mander and S.S. Chen, 4/2/99, (PB99-162893, A11, MF-A03).

MCEER-99-0007 "Effect of Vertical Ground Motions on the Structural Response of Highway Bridges," by M.R. Button, C.J. Cronin and R.L. Mayes, 4/10/99, (PB2000-101411, A10, MF-A03).

MCEER-99-0008 "Seismic Reliability Assessment of Critical Facilities: A Handbook, Supporting Documentation, and Model Code Provisions," by G.S. Johnson, R.E. Sheppard, M.D. Quilici, S.J. Eder and C.R. Scawthorn, 4/12/99, (PB2000-101701, A18, MF-A04).

MCEER-99-0009 "Impact Assessment of Selected MCEER Highway Project Research on the Seismic Design of Highway Structures," by C. Rojahn, R. Mayes, D.G. Anderson, J.H. Clark, D'Appolonia Engineering, S. Gloyd and R.V. Nutt, 4/14/99, (PB99-162901, A10, MF-A02).

MCEER-99-0010 "Site Factors and Site Categories in Seismic Codes," by R. Dobry, R. Ramos and M.S. Power, 7/19/99, (PB2000-101705, A08, MF-A02).

MCEER-99-0011 "Restrainer Design Procedures for Multi-Span Simply-Supported Bridges," by M.J. Randall, M. Saiidi, E. Maragakis and T. Isakovic, 7/20/99, (PB2000-101702, A10, MF-A02).

MCEER-99-0012 "Property Modification Factors for Seismic Isolation Bearings," by M.C. Constantinou, P. Tsopelas, A. Kasalanati and E. Wolff, 7/20/99, (PB2000-103387, A11, MF-A03).

MCEER-99-0013 "Critical Seismic Issues for Existing Steel Bridges," by P. Ritchie, N. Kauhl and J. Kulicki, 7/20/99, (PB2000-101697, A09, MF-A02).

MCEER-99-0014 "Nonstructural Damage Database," by A. Kao, T.T. Soong and A. Vender, 7/24/99, (PB2000-101407, A06, MF-A01).

MCEER-99-0015 "Guide to Remedial Measures for Liquefaction Mitigation at Existing Highway Bridge Sites," by H.G. Cooke and J. K. Mitchell, 7/26/99, (PB2000-101703, A11, MF-A03).

MCEER-99-0016 "Proceedings of the MCEER Workshop on Ground Motion Methodologies for the Eastern United States," edited by N. Abrahamson and A. Becker, 8/11/99, (PB2000-103385, A07, MF-A02).

MCEER-99-0017 "Quindío, Colombia Earthquake of January 25, 1999: Reconnaissance Report," by A.P. Asfura and P.J. Flores, 10/4/99, (PB2000-106893, A06, MF-A01).

MCEER-99-0018 "Hysteretic Models for Cyclic Behavior of Deteriorating Inelastic Structures," by M.V. Sivaselvan and A.M. Reinhorn, 11/5/99, (PB2000-103386, A08, MF-A02).

MCEER-99-0019 "Proceedings of the 7th U.S.- Japan Workshop on Earthquake Resistant Design of Lifeline Facilities and Countermeasures Against Soil Liquefaction," edited by T.D. O'Rourke, J.P. Bardet and M. Hamada, 11/19/99, (PB2000-103354, A99, MF-A06).

MCEER-99-0020 "Development of Measurement Capability for Micro-Vibration Evaluations with Application to Chip Fabrication Facilities," by G.C. Lee, Z. Liang, J.W. Song, J.D. Shen and W.C. Liu, 12/1/99, (PB2000-105993, A08, MF-A02).

MCEER-99-0021 "Design and Retrofit Methodology for Building Structures with Supplemental Energy Dissipating Systems," by G. Pekcan, J.B. Mander and S.S. Chen, 12/31/99, (PB2000-105994, A11, MF-A03).

MCEER-00-0001 "The Marmara, Turkey Earthquake of August 17, 1999: Reconnaissance Report," edited by C. Scawthorn; with major contributions by M. Bruneau, R. Eguchi, T. Holzer, G. Johnson, J. Mander, J. Mitchell, W. Mitchell, A. Papageorgiou, C. Scaethorn, and G. Webb, 3/23/00, (PB2000-106200, A11, MF-A03).

MCEER-00-0002 "Proceedings of the MCEER Workshop for Seismic Hazard Mitigation of Health Care Facilities," edited by G.C. Lee, M. Ettouney, M. Grigoriu, J. Hauer and J. Nigg, 3/29/00, (PB2000-106892, A08, MF-A02).

MCEER-00-0003 "The Chi-Chi, Taiwan Earthquake of September 21, 1999: Reconnaissance Report," edited by G.C. Lee and C.H. Loh, with major contributions by G.C. Lee, M. Bruneau, I.G. Buckle, S.E. Chang, P.J. Flores, T.D. O'Rourke, M. Shinozuka, T.T. Soong, C-H. Loh, K-C. Chang, Z-J. Chen, J-S. Hwang, M-L. Lin, G-Y. Liu, K-C. Tsai, G.C. Yao and C-L. Yen, 4/30/00, (PB2001-100980, A10, MF-A02).

MCEER-00-0004 "Seismic Retrofit of End-Sway Frames of Steel Deck-Truss Bridges with a Supplemental Tendon System: Experimental and Analytical Investigation," by G. Pekcan, J.B. Mander and S.S. Chen, 7/1/00, (PB2001-100982, A10, MF-A02).

MCEER-00-0005 "Sliding Fragility of Unrestrained Equipment in Critical Facilities," by W.H. Chong and T.T. Soong, 7/5/00, (PB2001-100983, A08, MF-A02).

MCEER-00-0006 "Seismic Response of Reinforced Concrete Bridge Pier Walls in the Weak Direction," by N. Abo-Shadi, M. Saiidi and D. Sanders, 7/17/00, (PB2001-100981, A17, MF-A03).

MCEER-00-0007 "Low-Cycle Fatigue Behavior of Longitudinal Reinforcement in Reinforced Concrete Bridge Columns," by J. Brown and S.K. Kunnath, 7/23/00, (PB2001-104392, A08, MF-A02).

MCEER-00-0008 "Soil Structure Interaction of Bridges for Seismic Analysis," I. PoLam and H. Law, 9/25/00, (PB2001-105397, A08, MF-A02).

MCEER-00-0009 "Proceedings of the First MCEER Workshop on Mitigation of Earthquake Disaster by Advanced Technologies (MEDAT-1), edited by M. Shinozuka, D.J. Inman and T.D. O'Rourke, 11/10/00, (PB2001-105399, A14, MF-A03).

MCEER-00-0010 "Development and Evaluation of Simplified Procedures for Analysis and Design of Buildings with Passive Energy Dissipation Systems, Revision 01," by O.M. Ramirez, M.C. Constantinou, C.A. Kircher, A.S. Whittaker, M.W. Johnson, J.D. Gomez and C. Chrysostomou, 11/16/01, (PB2001-105523, A23, MF-A04).

MCEER-00-0011 "Dynamic Soil-Foundation-Structure Interaction Analyses of Large Caissons," by C-Y. Chang, C-M. Mok, Z-L. Wang, R. Settgast, F. Waggoner, M.A. Ketchum, H.M. Gonnermann and C-C. Chin, 12/30/00, (PB2001-104373, A07, MF-A02).

MCEER-00-0012 "Experimental Evaluation of Seismic Performance of Bridge Restrainers," by A.G. Vlassis, E.M. Maragakis and M. Saiid Saiidi, 12/30/00, (PB2001-104354, A09, MF-A02).

MCEER-00-0013 "Effect of Spatial Variation of Ground Motion on Highway Structures," by M. Shinozuka, V. Saxena and G. Deodatis, 12/31/00, (PB2001-108755, A13, MF-A03).

MCEER-00-0014 "A Risk-Based Methodology for Assessing the Seismic Performance of Highway Systems," by S.D. Werner, C.E. Taylor, J.E. Moore, II, J.S. Walton and S. Cho, 12/31/00, (PB2001-108756, A14, MF-A03).

MCEER-01-0001 "Experimental Investigation of P-Delta Effects to Collapse During Earthquakes," by D. Vian and M. Bruneau, 6/25/01, (PB2002-100534, A17, MF-A03).

MCEER-01-0002 "Proceedings of the Second MCEER Workshop on Mitigation of Earthquake Disaster by Advanced Technologies (MEDAT-2)," edited by M. Bruneau and D.J. Inman, 7/23/01, (PB2002-100434, A16, MF-A03).

MCEER-01-0003 "Sensitivity Analysis of Dynamic Systems Subjected to Seismic Loads," by C. Roth and M. Grigoriu, 9/18/01, (PB2003-100884, A12, MF-A03).

MCEER-01-0004 "Overcoming Obstacles to Implementing Earthquake Hazard Mitigation Policies: Stage 1 Report," by D.J. Alesch and W.J. Petak, 12/17/01, (PB2002-107949, A07, MF-A02).

MCEER-01-0005 "Updating Real-Time Earthquake Loss Estimates: Methods, Problems and Insights," by C.E. Taylor, S.E. Chang and R.T. Eguchi, 12/17/01, (PB2002-107948, A05, MF-A01).

MCEER-01-0006 "Experimental Investigation and Retrofit of Steel Pile Foundations and Pile Bents Under Cyclic Lateral Loadings," by A. Shama, J. Mander, B. Blabac and S. Chen, 12/31/01, (PB2002-107950, A13, MF-A03).

MCEER-02-0001 "Assessment of Performance of Bolu Viaduct in the 1999 Duzce Earthquake in Turkey" by P.C. Roussis, M.C. Constantinou, M. Erdik, E. Durukal and M. Dicleli, 5/8/02, (PB2003-100883, A08, MF-A02).

MCEER-02-0002 "Seismic Behavior of Rail Counterweight Systems of Elevators in Buildings," by M.P. Singh, Rildova and L.E. Suarez, 5/27/02. (PB2003-100882, A11, MF-A03).

MCEER-02-0003 "Development of Analysis and Design Procedures for Spread Footings," by G. Mylonakis, G. Gazetas, S. Nikolaou and A. Chauncey, 10/02/02, (PB2004-101636, A13, MF-A03, CD-A13).

MCEER-02-0004 "Bare-Earth Algorithms for Use with SAR and LIDAR Digital Elevation Models," by C.K. Huyck, R.T. Eguchi and B. Houshmand, 10/16/02, (PB2004-101637, A07, CD-A07).

MCEER-02-0005 "Review of Energy Dissipation of Compression Members in Concentrically Braced Frames," by K.Lee and M. Bruneau, 10/18/02, (PB2004-101638, A10, CD-A10).

MCEER-03-0001 "Experimental Investigation of Light-Gauge Steel Plate Shear Walls for the Seismic Retrofit of Buildings" by J. Berman and M. Bruneau, 5/2/03, (PB2004-101622, A10, MF-A03, CD-A10).

MCEER-03-0002 "Statistical Analysis of Fragility Curves," by M. Shinozuka, M.Q. Feng, H. Kim, T. Uzawa and T. Ueda, 6/16/03, (PB2004-101849, A09, CD-A09).

MCEER-03-0003 "Proceedings of the Eighth U.S.-Japan Workshop on Earthquake Resistant Design f Lifeline Facilities and Countermeasures Against Liquefaction," edited by M. Hamada, J.P. Bardet and T.D. O'Rourke, 6/30/03, (PB2004-104386, A99, CD-A99).

MCEER-03-0004 "Proceedings of the PRC-US Workshop on Seismic Analysis and Design of Special Bridges," edited by L.C. Fan and G.C. Lee, 7/15/03, (PB2004-104387, A14, CD-A14).

MCEER-03-0005 "Urban Disaster Recovery: A Framework and Simulation Model," by S.B. Miles and S.E. Chang, 7/25/03, (PB2004-104388, A07, CD-A07).

MCEER-03-0006 "Behavior of Underground Piping Joints Due to Static and Dynamic Loading," by R.D. Meis, M. Maragakis and R. Siddharthan, 11/17/03, (PB2005-102194, A13, MF-A03, CD-A00).

MCEER-04-0001 "Experimental Study of Seismic Isolation Systems with Emphasis on Secondary System Response and Verification of Accuracy of Dynamic Response History Analysis Methods," by E. Wolff and M. Constantinou, 1/16/04 (PB2005-102195, A99, MF-E08, CD-A00).

MCEER-04-0002 "Tension, Compression and Cyclic Testing of Engineered Cementitious Composite Materials," by K. Kesner and S.L. Billington, 3/1/04, (PB2005-102196, A08, CD-A08).

MCEER-04-0003 "Cyclic Testing of Braces Laterally Restrained by Steel Studs to Enhance Performance During Earthquakes," by O.C. Celik, J.W. Berman and M. Bruneau, 3/16/04, (PB2005-102197, A13, MF-A03, CD-A00).

MCEER-04-0004 "Methodologies for Post Earthquake Building Damage Detection Using SAR and Optical Remote Sensing: Application to the August 17, 1999 Marmara, Turkey Earthquake," by C.K. Huyck, B.J. Adams, S. Cho, R.T. Eguchi, B. Mansouri and B. Houshmand, 6/15/04, (PB2005-104888, A10, CD-A00).

MCEER-04-0005 "Nonlinear Structural Analysis Towards Collapse Simulation: A Dynamical Systems Approach," by M.V. Sivaselvan and A.M. Reinhorn, 6/16/04, (PB2005-104889, A11, MF-A03, CD-A00).

MCEER-04-0006 "Proceedings of the Second PRC-US Workshop on Seismic Analysis and Design of Special Bridges," edited by G.C. Lee and L.C. Fan, 6/25/04, (PB2005-104890, A16, CD-A00).

MCEER-04-0007 "Seismic Vulnerability Evaluation of Axially Loaded Steel Built-up Laced Members," by K. Lee and M. Bruneau, 6/30/04, (PB2005-104891, A16, CD-A00).

MCEER-04-0008 "Evaluation of Accuracy of Simplified Methods of Analysis and Design of Buildings with Damping Systems for Near-Fault and for Soft-Soil Seismic Motions," by E.A. Pavlou and M.C. Constantinou, 8/16/04, (PB2005-104892, A08, MF-A02, CD-A00).

MCEER-04-0009 "Assessment of Geotechnical Issues in Acute Care Facilities in California," by M. Lew, T.D. O'Rourke, R. Dobry and M. Koch, 9/15/04, (PB2005-104893, A08, CD-A00).

MCEER-04-0010 "Scissor-Jack-Damper Energy Dissipation System," by A.N. Sigaher-Boyle and M.C. Constantinou, 12/1/04 (PB2005-108221).

MCEER-04-0011 "Seismic Retrofit of Bridge Steel Truss Piers Using a Controlled Rocking Approach," by M. Pollino and M. Bruneau, 12/20/04 (PB2006-105795).

MCEER-05-0001 "Experimental and Analytical Studies of Structures Seismically Isolated with an Uplift-Restraint Isolation System," by P.C. Roussis and M.C. Constantinou, 1/10/05 (PB2005-108222).

MCEER-05-0002 "A Versatile Experimentation Model for Study of Structures Near Collapse Applied to Seismic Evaluation of Irregular Structures," by D. Kusumastuti, A.M. Reinhorn and A. Rutenberg, 3/31/05 (PB2006-101523).

MCEER-05-0003 "Proceedings of the Third PRC-US Workshop on Seismic Analysis and Design of Special Bridges," edited by L.C. Fan and G.C. Lee, 4/20/05, (PB2006-105796).

MCEER-05-0004 "Approaches for the Seismic Retrofit of Braced Steel Bridge Piers and Proof-of-Concept Testing of an Eccentrically Braced Frame with Tubular Link," by J.W. Berman and M. Bruneau, 4/21/05 (PB2006-101524).

MCEER-05-0005 "Simulation of Strong Ground Motions for Seismic Fragility Evaluation of Nonstructural Components in Hospitals," by A. Wanitkorkul and A. Filiatrault, 5/26/05 (PB2006-500027).

MCEER-05-0006 "Seismic Safety in California Hospitals: Assessing an Attempt to Accelerate the Replacement or Seismic Retrofit of Older Hospital Facilities," by D.J. Alesch, L.A. Arendt and W.J. Petak, 6/6/05 (PB2006-105794).

MCEER-05-0007 "Development of Seismic Strengthening and Retrofit Strategies for Critical Facilities Using Engineered Cementitious Composite Materials," by K. Kesner and S.L. Billington, 8/29/05 (PB2006-111701).

MCEER-05-0008 "Experimental and Analytical Studies of Base Isolation Systems for Seismic Protection of Power Transformers," by N. Murota, M.Q. Feng and G-Y. Liu, 9/30/05 (PB2006-111702).

MCEER-05-0009 "3D-BASIS-ME-MB: Computer Program for Nonlinear Dynamic Analysis of Seismically Isolated Structures," by P.C. Tsopelas, P.C. Roussis, M.C. Constantinou, R. Buchanan and A.M. Reinhorn, 10/3/05 (PB2006-111703).

MCEER-05-0010 "Steel Plate Shear Walls for Seismic Design and Retrofit of Building Structures," by D. Vian and M. Bruneau, 12/15/05 (PB2006-111704).

MCEER-05-0011 "The Performance-Based Design Paradigm," by M.J. Astrella and A. Whittaker, 12/15/05 (PB2006-111705).

MCEER-06-0001 "Seismic Fragility of Suspended Ceiling Systems," H. Badillo-Almaraz, A.S. Whittaker, A.M. Reinhorn and G.P. Cimellaro, 2/4/06 (PB2006-111706).

MCEER-06-0002 "Multi-Dimensional Fragility of Structures," by G.P. Cimellaro, A.M. Reinhorn and M. Bruneau, 3/1/06 (PB2007-106974, A09, MF-A02, CD A00).

MCEER-06-0003 "Built-Up Shear Links as Energy Dissipators for Seismic Protection of Bridges," by P. Dusicka, A.M. Itani and I.G. Buckle, 3/15/06 (PB2006-111708).

MCEER-06-0004 "Analytical Investigation of the Structural Fuse Concept," by R.E. Vargas and M. Bruneau, 3/16/06 (PB2006-111709).

MCEER-06-0005 "Experimental Investigation of the Structural Fuse Concept," by R.E. Vargas and M. Bruneau, 3/17/06 (PB2006-111710).

MCEER-06-0006 "Further Development of Tubular Eccentrically Braced Frame Links for the Seismic Retrofit of Braced Steel Truss Bridge Piers," by J.W. Berman and M. Bruneau, 3/27/06 (PB2007-105147).

MCEER-06-0007 "REDARS Validation Report," by S. Cho, C.K. Huyck, S. Ghosh and R.T. Eguchi, 8/8/06 (PB2007-106983).

MCEER-06-0008 "Review of Current NDE Technologies for Post-Earthquake Assessment of Retrofitted Bridge Columns," by J.W. Song, Z. Liang and G.C. Lee, 8/21/06 (PB2007-106984).

MCEER-06-0009 "Liquefaction Remediation in Silty Soils Using Dynamic Compaction and Stone Columns," by S. Thevanayagam, G.R. Martin, R. Nashed, T. Shenthan, T. Kanagalingam and N. Ecemis, 8/28/06 (PB2007-106985).

MCEER-06-0010 "Conceptual Design and Experimental Investigation of Polymer Matrix Composite Infill Panels for Seismic Retrofitting," by W. Jung, M. Chiewanichakorn and A.J. Aref, 9/21/06 (PB2007-106986).

MCEER-06-0011 "A Study of the Coupled Horizontal-Vertical Behavior of Elastomeric and Lead-Rubber Seismic Isolation Bearings," by G.P. Warn and A.S. Whittaker, 9/22/06 (PB2007-108679).

MCEER-06-0012 "Proceedings of the Fourth PRC-US Workshop on Seismic Analysis and Design of Special Bridges: Advancing Bridge Technologies in Research, Design, Construction and Preservation," Edited by L.C. Fan, G.C. Lee and L. Ziang, 10/12/06 (PB2007-109042).

MCEER-06-0013 "Cyclic Response and Low Cycle Fatigue Characteristics of Plate Steels," by P. Dusicka, A.M. Itani and I.G. Buckle, 11/1/06 06 (PB2007-106987).

MCEER-06-0014 "Proceedings of the Second US-Taiwan Bridge Engineering Workshop," edited by W.P. Yen, J. Shen, J-Y. Chen and M. Wang, 11/15/06 (PB2008-500041).

MCEER-06-0015 "User Manual and Technical Documentation for the REDARS^{TM} Import Wizard," by S. Cho, S. Ghosh, C.K. Huyck and S.D. Werner, 11/30/06 (PB2007-114766).

MCEER-06-0016 "Hazard Mitigation Strategy and Monitoring Technologies for Urban and Infrastructure Public Buildings: Proceedings of the China-US Workshops," edited by X.Y. Zhou, A.L. Zhang, G.C. Lee and M. Tong, 12/12/06 (PB2008-500018).

MCEER-07-0001 "Static and Kinetic Coefficients of Friction for Rigid Blocks," by C. Kafali, S. Fathali, M. Grigoriu and A.S. Whittaker, 3/20/07 (PB2007-114767).

MCEER-07-0002 "Hazard Mitigation Investment Decision Making: Organizational Response to Legislative Mandate," by L.A. Arendt, D.J. Alesch and W.J. Petak, 4/9/07 (PB2007-114768).

MCEER-07-0003 "Seismic Behavior of Bidirectional-Resistant Ductile End Diaphragms with Unbonded Braces in Straight or Skewed Steel Bridges," by O. Celik and M. Bruneau, 4/11/07 (PB2008-105141).

MCEER-07-0004 “Modeling Pile Behavior in Large Pile Groups Under Lateral Loading,” by A.M. Dodds and G.R. Martin, 4/16/07(PB2008-105142).

MCEER-07-0005 “Experimental Investigation of Blast Performance of Seismically Resistant Concrete-Filled Steel Tube Bridge Piers,” by S. Fujikura, M. Bruneau and D. Lopez-Garcia, 4/20/07 (PB2008-105143).

MCEER-07-0006 “Seismic Analysis of Conventional and Isolated Liquefied Natural Gas Tanks Using Mechanical Analogs,” by I.P. Christovasilis and A.S. Whittaker, 5/1/07, not available.

MCEER-07-0007 “Experimental Seismic Performance Evaluation of Isolation/Restraint Systems for Mechanical Equipment – Part 1: Heavy Equipment Study,” by S. Fathali and A. Filiatrault, 6/6/07 (PB2008-105144).

MCEER-07-0008 “Seismic Vulnerability of Timber Bridges and Timber Substructures,” by A.A. Sharma, J.B. Mander, I.M. Friedland and D.R. Allicock, 6/7/07 (PB2008-105145).

MCEER-07-0009 “Experimental and Analytical Study of the XY-Friction Pendulum (XY-FP) Bearing for Bridge Applications,” by C.C. Marin-Artieda, A.S. Whittaker and M.C. Constantinou, 6/7/07 (PB2008-105191).

MCEER-07-0010 “Proceedings of the PRC-US Earthquake Engineering Forum for Young Researchers,” Edited by G.C. Lee and X.Z. Qi, 6/8/07 (PB2008-500058).

MCEER-07-0011 “Design Recommendations for Perforated Steel Plate Shear Walls,” by R. Purba and M. Bruneau, 6/18/07, (PB2008-105192).

MCEER-07-0012 “Performance of Seismic Isolation Hardware Under Service and Seismic Loading,” by M.C. Constantinou, A.S. Whittaker, Y. Kalpakidis, D.M. Fenz and G.P. Warn, 8/27/07, (PB2008-105193).

MCEER-07-0013 “Experimental Evaluation of the Seismic Performance of Hospital Piping Subassemblies,” by E.R. Goodwin, E. Maragakis and A.M. Itani, 9/4/07, (PB2008-105194).

MCEER-07-0014 “A Simulation Model of Urban Disaster Recovery and Resilience: Implementation for the 1994 Northridge Earthquake,” by S. Miles and S.E. Chang, 9/7/07, (PB2008-106426).

MCEER-07-0015 “Statistical and Mechanistic Fragility Analysis of Concrete Bridges,” by M. Shinozuka, S. Banerjee and S-H. Kim, 9/10/07, (PB2008-106427).

MCEER-07-0016 “Three-Dimensional Modeling of Inelastic Buckling in Frame Structures,” by M. Schachter and AM. Reinhorn, 9/13/07, (PB2008-108125).

MCEER-07-0017 “Modeling of Seismic Wave Scattering on Pile Groups and Caissons,” by I. Po Lam, H. Law and C.T. Yang, 9/17/07 (PB2008-108150).

MCEER-07-0018 “Bridge Foundations: Modeling Large Pile Groups and Caissons for Seismic Design,” by I. Po Lam, H. Law and G.R. Martin (Coordinating Author), 12/1/07 (PB2008-111190).

MCEER-07-0019 “Principles and Performance of Roller Seismic Isolation Bearings for Highway Bridges,” by G.C. Lee, Y.C. Ou, Z. Liang, T.C. Niu and J. Song, 12/10/07 (PB2009-110466).

MCEER-07-0020 “Centrifuge Modeling of Permeability and Pinning Reinforcement Effects on Pile Response to Lateral Spreading,” by L.L Gonzalez-Lagos, T. Abdoun and R. Dobry, 12/10/07 (PB2008-111191).

MCEER-07-0021 “Damage to the Highway System from the Pisco, Perú Earthquake of August 15, 2007,” by J.S. O’Connor, L. Mesa and M. Nykamp, 12/10/07, (PB2008-108126).

MCEER-07-0022 “Experimental Seismic Performance Evaluation of Isolation/Restraint Systems for Mechanical Equipment – Part 2: Light Equipment Study,” by S. Fathali and A. Filiatrault, 12/13/07 (PB2008-111192).

MCEER-07-0023 “Fragility Considerations in Highway Bridge Design,” by M. Shinozuka, S. Banerjee and S.H. Kim, 12/14/07 (PB2008-111193).

MCEER-07-0024 "Performance Estimates for Seismically Isolated Bridges," by G.P. Warn and A.S. Whittaker, 12/30/07 (PB2008-112230).

MCEER-08-0001 "Seismic Performance of Steel Girder Bridge Superstructures with Conventional Cross Frames," by L.P. Carden, A.M. Itani and I.G. Buckle, 1/7/08, (PB2008-112231).

MCEER-08-0002 "Seismic Performance of Steel Girder Bridge Superstructures with Ductile End Cross Frames with Seismic Isolators," by L.P. Carden, A.M. Itani and I.G. Buckle, 1/7/08 (PB2008-112232).

MCEER-08-0003 "Analytical and Experimental Investigation of a Controlled Rocking Approach for Seismic Protection of Bridge Steel Truss Piers," by M. Pollino and M. Bruneau, 1/21/08 (PB2008-112233).

MCEER-08-0004 "Linking Lifeline Infrastructure Performance and Community Disaster Resilience: Models and Multi-Stakeholder Processes," by S.E. Chang, C. Pasion, K. Tatebe and R. Ahmad, 3/3/08 (PB2008-112234).

MCEER-08-0005 "Modal Analysis of Generally Damped Linear Structures Subjected to Seismic Excitations," by J. Song, Y-L. Chu, Z. Liang and G.C. Lee, 3/4/08 (PB2009-102311).

MCEER-08-0006 "System Performance Under Multi-Hazard Environments," by C. Kafali and M. Grigoriu, 3/4/08 (PB2008-112235).

MCEER-08-0007 "Mechanical Behavior of Multi-Spherical Sliding Bearings," by D.M. Fenz and M.C. Constantinou, 3/6/08 (PB2008-112236).

MCEER-08-0008 "Post-Earthquake Restoration of the Los Angeles Water Supply System," by T.H.P. Tabucchi and R.A. Davidson, 3/7/08 (PB2008-112237).

MCEER-08-0009 "Fragility Analysis of Water Supply Systems," by A. Jacobson and M. Grigoriu, 3/10/08 (PB2009-105545).

MCEER-08-0010 "Experimental Investigation of Full-Scale Two-Story Steel Plate Shear Walls with Reduced Beam Section Connections," by B. Qu, M. Bruneau, C-H. Lin and K-C. Tsai, 3/17/08 (PB2009-106368).

MCEER-08-0011 "Seismic Evaluation and Rehabilitation of Critical Components of Electrical Power Systems," S. Ersoy, B. Feizi, A. Ashrafi and M. Ala Saadeghvaziri, 3/17/08 (PB2009-105546).

MCEER-08-0012 "Seismic Behavior and Design of Boundary Frame Members of Steel Plate Shear Walls," by B. Qu and M. Bruneau, 4/26/08 . (PB2009-106744).

MCEER-08-0013 "Development and Appraisal of a Numerical Cyclic Loading Protocol for Quantifying Building System Performance," by A. Filiatrault, A. Wanitkorkul and M. Constantinou, 4/27/08 (PB2009-107906).

MCEER-08-0014 "Structural and Nonstructural Earthquake Design: The Challenge of Integrating Specialty Areas in Designing Complex, Critical Facilities," by W.J. Petak and D.J. Alesch, 4/30/08 (PB2009-107907).

MCEER-08-0015 "Seismic Performance Evaluation of Water Systems," by Y. Wang and T.D. O'Rourke, 5/5/08 (PB2009-107908).

MCEER-08-0016 "Seismic Response Modeling of Water Supply Systems," by P. Shi and T.D. O'Rourke, 5/5/08 (PB2009-107910).

MCEER-08-0017 "Numerical and Experimental Studies of Self-Centering Post-Tensioned Steel Frames," by D. Wang and A. Filiatrault, 5/12/08 (PB2009-110479).

MCEER-08-0018 "Development, Implementation and Verification of Dynamic Analysis Models for Multi-Spherical Sliding Bearings," by D.M. Fenz and M.C. Constantinou, 8/15/08 (PB2009-107911).

MCEER-08-0019 "Performance Assessment of Conventional and Base Isolated Nuclear Power Plants for Earthquake Blast Loadings," by Y.N. Huang, A.S. Whittaker and N. Luco, 10/28/08 (PB2009-107912).

MCEER-08-0020 "Remote Sensing for Resilient Multi-Hazard Disaster Response – Volume I: Introduction to Damage Assessment Methodologies," by B.J. Adams and R.T. Eguchi, 11/17/08 (PB2010-102695).

MCEER-08-0021 "Remote Sensing for Resilient Multi-Hazard Disaster Response – Volume II: Counting the Number of Collapsed Buildings Using an Object-Oriented Analysis: Case Study of the 2003 Bam Earthquake," by L. Gusella, C.K. Huyck and B.J. Adams, 11/17/08 (PB2010-100925).

MCEER-08-0022 "Remote Sensing for Resilient Multi-Hazard Disaster Response – Volume III: Multi-Sensor Image Fusion Techniques for Robust Neighborhood-Scale Urban Damage Assessment," by B.J. Adams and A. McMillan, 11/17/08 (PB2010-100926).

MCEER-08-0023 "Remote Sensing for Resilient Multi-Hazard Disaster Response – Volume IV: A Study of Multi-Temporal and Multi-Resolution SAR Imagery for Post-Katrina Flood Monitoring in New Orleans," by A. McMillan, J.G. Morley, B.J. Adams and S. Chesworth, 11/17/08 (PB2010-100927).

MCEER-08-0024 "Remote Sensing for Resilient Multi-Hazard Disaster Response – Volume V: Integration of Remote Sensing Imagery and VIEWS^{TM} Field Data for Post-Hurricane Charley Building Damage Assessment," by J.A. Womble, K. Mehta and B.J. Adams, 11/17/08 (PB2009-115532).

MCEER-08-0025 "Building Inventory Compilation for Disaster Management: Application of Remote Sensing and Statistical Modeling," by P. Sarabandi, A.S. Kiremidjian, R.T. Eguchi and B. J. Adams, 11/20/08 (PB2009-110484).

MCEER-08-0026 "New Experimental Capabilities and Loading Protocols for Seismic Qualification and Fragility Assessment of Nonstructural Systems," by R. Retamales, G. Mosqueda, A. Filiatrault and A. Reinhorn, 11/24/08 (PB2009-110485).

MCEER-08-0027 "Effects of Heating and Load History on the Behavior of Lead-Rubber Bearings," by I.V. Kalpakidis and M.C. Constantinou, 12/1/08 (PB2009-115533).

MCEER-08-0028 "Experimental and Analytical Investigation of Blast Performance of Seismically Resistant Bridge Piers," by S.Fujikura and M. Bruneau, 12/8/08 (PB2009-115534).

MCEER-08-0029 "Evolutionary Methodology for Aseismic Decision Support," by Y. Hu and G. Dargush, 12/15/08.

MCEER-08-0030 "Development of a Steel Plate Shear Wall Bridge Pier System Conceived from a Multi-Hazard Perspective," by D. Keller and M. Bruneau, 12/19/08 (PB2010-102696).

MCEER-09-0001 "Modal Analysis of Arbitrarily Damped Three-Dimensional Linear Structures Subjected to Seismic Excitations," by Y.L. Chu, J. Song and G.C. Lee, 1/31/09 (PB2010-100922).

MCEER-09-0002 "Air-Blast Effects on Structural Shapes," by G. Ballantyne, A.S. Whittaker, A.J. Aref and G.F. Dargush, 2/2/09 (PB2010-102697).

MCEER-09-0003 "Water Supply Performance During Earthquakes and Extreme Events," by A.L. Bonneau and T.D. O'Rourke, 2/16/09 (PB2010-100923).

MCEER-09-0004 "Generalized Linear (Mixed) Models of Post-Earthquake Ignitions," by R.A. Davidson, 7/20/09 (PB2010-102698).

MCEER-09-0005 "Seismic Testing of a Full-Scale Two-Story Light-Frame Wood Building: NEESWood Benchmark Test," by I.P. Christovasilis, A. Filiatrault and A. Wanitkorkul, 7/22/09 (PB2012-102401).

MCEER-09-0006 "IDARC2D Version 7.0: A Program for the Inelastic Damage Analysis of Structures," by A.M. Reinhorn, H. Roh, M. Sivaselvan, S.K. Kunnath, R.E. Valles, A. Madan, C. Li, R. Lobo and Y.J. Park, 7/28/09 (PB2010-103199).

MCEER-09-0007 "Enhancements to Hospital Resiliency: Improving Emergency Planning for and Response to Hurricanes," by D.B. Hess and L.A. Arendt, 7/30/09 (PB2010-100924).

MCEER-09-0008 "Assessment of Base-Isolated Nuclear Structures for Design and Beyond-Design Basis Earthquake Shaking," by Y.N. Huang, A.S. Whittaker, R.P. Kennedy and R.L. Mayes, 8/20/09 (PB2010-102699).

MCEER-09-0009 "Quantification of Disaster Resilience of Health Care Facilities," by G.P. Cimellaro, C. Fumo, A.M Reinhorn and M. Bruneau, 9/14/09 (PB2010-105384).

MCEER-09-0010 "Performance-Based Assessment and Design of Squat Reinforced Concrete Shear Walls," by C.K. Gulec and A.S. Whittaker, 9/15/09 (PB2010-102700).

MCEER-09-0011 "Proceedings of the Fourth US-Taiwan Bridge Engineering Workshop," edited by W.P. Yen, J.J. Shen, T.M. Lee and R.B. Zheng, 10/27/09 (PB2010-500009).

MCEER-09-0012 "Proceedings of the Special International Workshop on Seismic Connection Details for Segmental Bridge Construction," edited by W. Phillip Yen and George C. Lee, 12/21/09 (PB2012-102402).

MCEER-10-0001 "Direct Displacement Procedure for Performance-Based Seismic Design of Multistory Woodframe Structures," by W. Pang and D. Rosowsky, 4/26/10 (PB2012-102403).

MCEER-10-0002 "Simplified Direct Displacement Design of Six-Story NEESWood Capstone Building and Pre-Test Seismic Performance Assessment," by W. Pang, D. Rosowsky, J. van de Lindt and S. Pei, 5/28/10 (PB2012-102404).

MCEER-10-0003 "Integration of Seismic Protection Systems in Performance-Based Seismic Design of Woodframed Structures," by J.K. Shinde and M.D. Symans, 6/18/10 (PB2012-102405).

MCEER-10-0004 "Modeling and Seismic Evaluation of Nonstructural Components: Testing Frame for Experimental Evaluation of Suspended Ceiling Systems," by A.M. Reinhorn, K.P. Ryu and G. Maddaloni, 6/30/10 (PB2012-102406).

MCEER-10-0005 "Analytical Development and Experimental Validation of a Structural-Fuse Bridge Pier Concept," by S. El-Bahey and M. Bruneau, 10/1/10 (PB2012-102407).

MCEER-10-0006 "A Framework for Defining and Measuring Resilience at the Community Scale: The PEOPLES Resilience Framework," by C.S. Renschler, A.E. Frazier, L.A. Arendt, G.P. Cimellaro, A.M. Reinhorn and M. Bruneau, 10/8/10 (PB2012-102408).

MCEER-10-0007 "Impact of Horizontal Boundary Elements Design on Seismic Behavior of Steel Plate Shear Walls," by R. Purba and M. Bruneau, 11/14/10 (PB2012-102409).

MCEER-10-0008 "Seismic Testing of a Full-Scale Mid-Rise Building: The NEESWood Capstone Test," by S. Pei, J.W. van de Lindt, S.E. Pryor, H. Shimizu, H. Isoda and D.R. Rammer, 12/1/10 (PB2012-102410).

MCEER-10-0009 "Modeling the Effects of Detonations of High Explosives to Inform Blast-Resistant Design," by P. Sherkar, A.S. Whittaker and A.J. Aref, 12/1/10 (PB2012-102411).

MCEER-10-0010 "L'Aquila Earthquake of April 6, 2009 in Italy: Rebuilding a Resilient City to Withstand Multiple Hazards," by G.P. Cimellaro, I.P. Christovasilis, A.M. Reinhorn, A. De Stefano and T. Kirova, 12/29/10.

MCEER-11-0001 "Numerical and Experimental Investigation of the Seismic Response of Light-Frame Wood Structures," by I.P. Christovasilis and A. Filiatrault, 8/8/11 (PB2012-102412).

MCEER-11-0002 "Seismic Design and Analysis of a Precast Segmental Concrete Bridge Model," by M. Anagnostopoulou, A. Filiatrault and A. Aref, 9/15/11.

MCEER-11-0003 'Proceedings of the Workshop on Improving Earthquake Response of Substation Equipment," Edited by A.M. Reinhorn, 9/19/11 (PB2012-102413).

MCEER-11-0004 "LRFD-Based Analysis and Design Procedures for Bridge Bearings and Seismic Isolators," by M.C. Constantinou, I. Kalpakidis, A. Filiatrault and R.A. Ecker Lay, 9/26/11.

MCEER-11-0005 “Experimental Seismic Evaluation, Model Parameterization, and Effects of Cold-Formed Steel-Framed Gypsum Partition Walls on the Seismic Performance of an Essential Facility,” by R. Davies, R. Retamales, G. Mosqueda and A. Filiatrault, 10/12/11.

MCEER-11-0006 “Modeling and Seismic Performance Evaluation of High Voltage Transformers and Bushings,” by A.M. Reinhorn, K. Oikonomou, H. Roh, A. Schiff and L. Kempner, Jr., 10/3/11.

MCEER-11-0007 “Extreme Load Combinations: A Survey of State Bridge Engineers,” by G.C. Lee, Z. Liang, J.J. Shen and J.S. O’Connor, 10/14/11.

MCEER-12-0001 “Simplified Analysis Procedures in Support of Performance Based Seismic Design,” by Y.N. Huang and A.S. Whittaker.

MCEER-12-0002 “Seismic Protection of Electrical Transformer Bushing Systems by Stiffening Techniques,” by M. Koliou, A. Filiatrault, A.M. Reinhorn and N. Oliveto, 6/1/12.

MCEER-12-0003 “Post-Earthquake Bridge Inspection Guidelines,” by J.S. O’Connor and S. Alampalli, 6/8/12.

MCEER-12-0004 “Integrated Design Methodology for Isolated Floor Systems in Single-Degree-of-Freedom Structural Fuse Systems,” by S. Cui, M. Bruneau and M.C. Constantinou, 6/13/12.

MCEER-12-0005 “Characterizing the Rotational Components of Earthquake Ground Motion,” by D. Basu, A.S. Whittaker and M.C. Constantinou, 6/15/12.

MCEER-12-0006 “Bayesian Fragility for Nonstructural Systems,” by C.H. Lee and M.D. Grigoriu, 9/12/12.

MCEER-12-0007 “A Numerical Model for Capturing the In-Plane Seismic Response of Interior Metal Stud Partition Walls,” by R.L. Wood and T.C. Hutchinson, 9/12/12.

MCEER-12-0008 “Assessment of Floor Accelerations in Yielding Buildings,” by J.D. Wieser, G. Pekcan, A.E. Zaghi, A.M. Itani and E. Maragakis, 10/5/12.

MCEER

EARTHQUAKE ENGINEERING TO EXTREME EVENTS

University at Buffalo, The State University of New York

133A Ketter Hall ▪ Buffalo, New York 14260-4300

Phone: (716) 645-3391 ▪ Fax: (716) 645-3399

Email: *mceer@buffalo.edu* ▪ Web: *http://mceer.buffalo.edu*

University at Buffalo *The State University of New York*

ISSN 1520-295X